INVESTIGATION OF NOISE AND VIBRATION WITHIN AN OIL FLOODED SLIDING VANE ROTARY AIR COMPRESSOR

NEIL LIONEL GROSS

Master of Philosophy

THE UNIVERSITY OF ASTON IN BIRMINGHAM

August 1990

The University of Aston in Birmingham

Investigation of noise and vibration within an oil flooded sliding vane rotary air compressor

Neil Lionel Gross

Master of Philosophy
1990

Summary

The Sound Power Level and tonal character of the noise generated by all types of machinery is of significant importance to both manufacturer and consumer.

The present investigation has analysed all the major sources of noise and vibration within an oil flooded sliding vane compressor mechanism and also considered the effect of the drive motor and cooling fan in relation to overall compressor noise levels. The sliding vane compressor has minimal out of balance and relatively low running speeds and therefore the potential to be a quiet machine.

It has been shown that both mechanical vibration sources and aerodynamically generated noise contribute to the radiated noise spectrum in different frequency bands; mechanical vibration sources dominate below 2.5 kHz but in the range between 2.5 kHz and 5 kHz the sources are predominately aerodynamic.

The elimination of the sealing arc bore within the compression mechanism to leave a purely circular bore significantly reduced vibration levels. The use of a specially designed reactive silencer reduced the impact that noise, generated at the discharge port, had on the compressor shell. Finally the cooling fan was identified as the major noise source and recommendations are made for its redesign.

Keywords: **Noise** **Vibration** **Air compressors**

Acknowledgements

The present project would not have been possible without the invaluable help of the following people. Hydrovane and in particular Mr M Williams for all the necessary information and equipment in relation to air compressors. Dr S Garvey who had access to the necessary computer facilities for the theoretical modelling of compressor components and finally Mr W Flint for his continual guidance and moral support throughout the whole research program.

List of Contents

List of Tables

List of Figures

1.0 Introduction to the research project

The reduction of noise generated by almost all forms of machinery is of major importance in the environment conscious society in which we now live. Not only does EEC legislation dictate the maximum noise levels which machinery may generate but the new "Noise at Work Regulations 1989" restrict the amount of sound energy to which an employee may be exposed either by reducing noise levels or exposure times. Since a reduction in exposure time by imposing extended break periods is equivelant to a loss in overall efficiency lower noise levels which can lead to increased exposure times and therefore increased efficiency are now an essential part of any design brief and an important marketing factor.

The earliest use of air compressors was to create a partial vacuum. Von Guerricke used a vacuum pump in the renound Magdeburg hemisphere experiment and his later use of a vacuum in a lifting device was the first application of air as an energy transfer medium. Early pumps and compressors were hand operated positive displacement devices. Linear motion positive displacement compressors are still common today in the form of reciprocating machines typically driven by electric motors or internal combustion engines. The positive displacement rotary compressor avoids the need to transfer between rotary and linear motion and two main forms have developed. In the screw compressor, a modern development of the lobed rotor machine, the meshing of helically contoured rotors entraps, transports and compresses the medium. In the sliding vane machine compression is achieved by the motion of vanes in a slotted rotor turning in an eccentrically mounted stator. The turbo-compressor, in which compression is achieved by aerodynamic action, overcomes the inherent mass flow limitations of positive displacement devices but is not the concern of the present investigation.

Analysis of the three main types of positive displacement compression mechanisms: reciprocating, screw and rotary vane reveals that their major noise generation processes are slightly different depending on the manner in which compression is achieved and the noise generated by each type of compressor has a particular character. Motor noise can be considered as a separate noise source for most compressors.

Reciprocating compressors contain the greatest out of balance rotating masses and these generate considerable vibration within the structure which is then radiated as noise. Large pulsations due to the abrupt intake and exhaust of gases and actual valve operation also dominate the noise profile. Screw compressor noise is generally an annoying whine produced by the very high rotational speeds of the two screws. Rotary vane compressors can be split into further sub sections-: the rolling piston and sliding vane arrangements. Rotational speeds are relatively low, both types show a degree of out of balance and some models are fitted with valves whose action increases the possibility of gas pulsations. The rotary sliding vane arrangement exhibits all the noise sources discussed above but to a lesser degree than the reciprocating or screw type compressor and it is therefore fundamentally quieter. The extensive use of small rotary compressors in a domestic market which demands quiet equipment has naturally led to a reduction in noise levels for similar compressors utilised in the industrial market. Increased competition from abroad, new stringent European legislation and the continual strive to produce British products which are market leaders has generated a need for further research into air compressor noise.

Hydrovane have produced air compressors based on the oil-flooded sliding vane principle for approximately thirty years. Until recently performance and reliability have been the most important factors on which research has been based and Hydrovane have been fortunate that noise levels from their rotary compressors have been

generally lower than the reciprocating and screw compressors produced by their competitors. For commercial, environmental and legislative reasons Hydrovane have steadily increased their interest in compressor noise and consequently vibration and their needs were well suited to the research programme.

Previous analysis concerned with Hydrovane compressors has identified the rotor vane passage frequency and its harmonics as the main cause of noise as they appear strongly in all noise and vibration spectra. There has been no investigation into all the possible internal forces that exist during a compression cycle and therefore no definite conclusion as to the main source of vibration generation. The present project was instigated to increase the knowledge of the noise generation process within an oil flooded sliding vane compressor.

It was first necessary to survey the available literature to discover the present understanding of compressor noise. This was followed by an investigation into the noise and vibration characteristics of a standard production compressor to determine the major noise sources and dominant frequencies. Cooling fan noise was known to be a problem with the particular high speed model tested and is discussed in some detail in Chapter 8. However, the main project objectives were concerned with noise and vibration from the "air-end" which houses the sliding vane mechanism common to all Hydrovane compressors and it is this aspect of research that dominates the bulk of the thesis, starting at Chapter 3. To investigate potential resonance problems arising from compressor components it was essential to complete both theoretical (using finite element analysis) and experimental modal testing and this is detailed in Chapter 4. It was considered that noise radiation from the air-end could be attributed to casing vibration which in turn was considered to be due to both transmission of vibration from the compression unit through the structure and direct aerodynamic excitation from the internal cavity into which the compression unit

discharges. An extensive experimental investigation was pursued to assess these sources and is discussed in Chapter 5. These two sources can be further sub-divided into the generation of noise and vibration from the fundamental compressor operations and Chapters 6 and 7 detail both the mathematical model and complementary experimental programme which were necessary to fully comprehend their relative importance. From this foundation level it was hoped to make recommendations to reduce the noise levels of all Hydrovane compressors. Ideally this would be achieved at source by improved design, but if this was not feasable then the transmission of noise from source to radiating surface would be evaluated and reduced where practical.

It was hoped that improving the acoustic design would eliminate the need for expensive enclosures which may have adverse effects on the cooling, increase the space required to house the unit, make maintenance awkward and possibly spoil aesthetics.

Acoustics was one of the earlier branches of science to be studied. Both the Greeks and Romans investigated acoustic effects in order to enhance theatrical performances by improving auditorium acoustics, while the modern theory of sound can be attributed to Lord Rayleigh in his account published in 1894. Since the beginning of this century much time and effort has been expended by researchers in producing a comprehensive theoretical and practical foundation. Beyond this foundation, which can be applied to all noise and vibration problems, lie phenomena that relate to only one particular source of noise or vibration generation. For this reason there is extensive research into noise and vibration.

The best definition of noise is probably "unwanted sound". The measure of noise is therefore subjective, since sound unwanted by certain persons may not be unwanted by others. From a scientific viewpoint sound must be defined and quantified before noise can be

measured.

A sound will be heard if the fluctuations in air pressure at the entrance to the human ear satisfy two constraints: the magnitude of pressure fluctuations are above a certain threshold and the frequency of fluctuation is in a certain range. For a single pressure fluctuation a "thud" or "click" would be heard, sound is the continual generation of these fluctuations.

To reach the human ear the air must be able to transmit these fluctuations in pressure. Since air is an elastic medium a pressure variation in an elemental volume will produce an identical pressure variation in a neighbouring elemental volume. The sound travels through the air in the form of a longitudinal pressure wave.

The point at which the pressure fluctuations are generated is termed the sound source. Sound sources fall into two categories; firstly the forced vibration of a structure that excites the neighbouring air molecules; for example a drum or cymbal; and secondly the direct excitation of air molecules by air flow processes as produced by a fan or jet. The compression of air within a sliding vane compressor will cause excitation of the compressor structure due to internal forces and pressure fluctuations. In the typical industrial compressor the compression unit operates in conjunction with an electric motor and cooling fan, therefore both types of sound source exist.

This first chapter reviews relevant literature concerned with other compressor mechanisms, outlines the project objectives, deals with the fundamentals of sound and vibration and also details the operation of a Hydrovane oil flooded sliding vane compressor.

1.1 Literature review of compressor noise

The study of compressor noise has focussed mainly on reciprocating compressors. In particular, in recent years, there has been extensive study into small, hermetically sealed refrigeration compressors typical of those used in domestic refrigerators, freezers and automobile air-conditioning systems. Significant noise reduction has been achieved through various techniques that include reducing the out of balance forces by the use of counterweights, reducing or eliminating transmission paths from the source to receiver and altering the dynamic characteristics of the outer casing. Because it is impossible to remove the fundamental out of balance force that exists in a reciprocating compressor mechanism without using expensive elements there will always be a potential for vibration and therefore noise.

In many domestic products the compressor is a hermetically sealed unit, therefore all the noise is radiated from the outer casing. A great deal of research has analysed the dynamic characteristics of the hermetically sealed casing as this is the last barrier between source and receiver. Possible modifications to reduce the radiated noise from the casing include the shifting of casing natural frequencies, alteration of local casing stiffness, relocation of the internal suspension system or any other connections between compressor mechanism and casing, alteration of cavity shapes and the application of acoustic damping materials. Many papers have considered and evaluated these aspects and each drawn different conclusions as to the most suitable. This variety of problems faces the acoustic engineer and makes each compressor design a unique case.

Apart from the legislative restrictions which have been introduced in recent years, manufacturers now appreciate that low noise levels in a domestic product are an essential marketing factor. This is one reason why attention has been transferred to other types of

compressor mechanisms, for example, the rolling piston compressor arrangement which has a lower fundamental out of balance force and therefore the potential to be a quieter compressor. However as outlined in the following review the noise problems and methods of reduction are very similar in both types of compressor mechanism.

Waser and Hamilton (1984) evaluated all these aspects for a reciprocating compressor. They used a modal analysis technique to determine shell natural frequencies and produce a deformation pattern of the troubled modes for a running compressor. Such a deformation pattern revealed the position of the nodes and antinodes at each particular frequency. Waser and Hamilton showed that the relocation of the suspension from anti-nodal points to nodal points reduced the vibration transmission significantly at certain design frequencies. Inevitably the vibration transmission increased at other frequencies but these can be chosen to be of reduced importance in relation to the noise spectrum.

They showed that the application of local stiffening to reduce the modal deflection at the input locations was possible when the input force was applied through the suspension system. However, this solution was not appropiate if the force was due to gas pressures that act over the whole internal surface. As the majority of energy was transmitted through the mechanical path the possible suspension point locations reduced to a small number.

In their particular work Waser and Hamilton showed that a specific harmonic of the forcing frequency clashed with the natural frequency of a troubled casing mode of vibration. They decided against an adjustment of the natural frequency by altering casing stiffness, as in mass production there are always slight changes in material properties and assembly techniques that can lead to slight changes in stiffness. Since the forcing function had a very high harmonic density any change in

stiffness could lead to difficulties in other modes. However, this technique can be an extremely effective method of reducing the radiated noise emission from a particular installation.

Waser and Hamilton concluded that all the aforementioned techniques require careful evaluation if they are not to have any adverse effects at other frequencies. For the most cost effective noise reduction they suggested it was "safer" to apply damping to the complete shell structure. Analysis of the shell deformation pattern revealed the areas of high vibratory amplitude and the application of additional damping at these locations was shown to be very effective.

Imaichi (1984) showed for a rolling piston refrigeration compressor that the provision of a more symmetrical hermetic shell of increased stiffness and with a greater area of internal mechanism support reduced vibration levels on the shell above 2 kHz, but increased vibration levels between 1 kHz and 1.5 kHz. This type of problem had been forecast by Waser and Hamilton (1984) who specifically avoided this technique to reduce noise levels.

Saito et al (1980) showed, perhaps conversely, that a more asymmetric shell reduced the surface vibration magnitudes. In a symmetric shell the direction of the inertia principal axis is not fixed. For this reason all forced vibration close to the resonance frequency is amplified. For an asymmetric shell the direction of the inertia principal axis is fixed, therefore the node of the vibration normal mode is fixed and only a limited number of forced vibrations, close to resonant frequencies, are amplified.

All the above authors altered the mode of vibration and the natural frequencies of the compressor structure to avoid coincidence with a harmonic of the forcing frequency. The problem with this type of approach was highlighted by Imaichi (1984). He discovered, as stated

above, that alteration of the shell stiffness to reduce vibration levels at higher frequencies had increased noise in the 1 kHz - 1.5 kHz frequency range. This was shown to be related to cavity resonance. The dynamic characteristics of the original shell had successfully damped this excitation whereas the modified shell had moved a resonance frequency into the 1 kHz - 1.5 kHz region and any excitation of the shell in that frequency range was more readily amplified. The solution was to reduce the excitation at source, which was achieved using an internal muffler.

Other studies have tackled the transmission path between source and receiver in order to reduce noise. They have shown that the mounting of the motor and compressor mechanism within the hermetic shell critically affects vibration transmission to the shell and the noise radiated from it. Kjeldsen and Madsen (1978) analysed the motion of a single cylinder reciprocating compressor mechanism. The internal horizontal vibration levels were minimised by first calculating the optimum position of the counterweight and then the location of supporting springs. Their paper showed that there is only one plane, at right angles to the axis of motion, where the vibrations are a minimum. To minimise the external vibration levels the supporting springs were then attached between locations on this plane of the compressor mechanism and the shell. No quantitative figures were quoted but a marked reduction of the vibration level in relation to other known designs was achieved.

Sisson and Simpson (1984) analysed an air conditioning / heat pump hermetic compressor and showed that there was significant transmission of vibrational energy from the internal mechanism to the shell via structural paths. The inclusion of anti-vibration mounts rather than spring connections reduced vibration transmission. These anti-vibration mounts had similar stiffness characteristics but improved damping properties. Sisson and Simpson also replaced the standard all-metal discharge tube with a length of rubber hose. This modification

increased the flexibility of the discharge system and reduced the vibration transmission to the shell. However, they showed that the application of constrained layer damping to the shell was the most effective method of reducing the radiated noise.

Soedel (1980) produced a mathematical model that analysed the effect of changes in gas pulsations in the inlet and discharge tubing on the vibration transmission between the compressor mechanism and hermetic shell. It is important to mention this noise generation process as one possible explanation for the different noise levels generated by a compressor at slightly different operating conditions. The pressure difference across the tubing wall determines its radial stiffness; a change in pressure difference will alter the stiffness and hence the natural frequency. Since the tubes are rigidly fixed between the compressor body and hermetic shell any change in natural frequency will affect the transmission of vibration. If operating conditions allow the tubing to vibrate at a natural frequency then significantly increased vibration transmission will arise.

Tojo et al (1980) showed that there were two paths, one air-borne the other structure-borne by which the hermetically sealed shell of a refrigeration compressor was excited. In the 500 Hz region cavity resonance due to gas pulsations in the suction system produced solid body motion of the shell which radiated noise. In the 2 kHz region noise was generated by local deformation of the shell due to vibration transmission via the internal connections from the compressor mechanism. Gas pulsations in the cylinder were also shown to excite the compressor mechanism.

Tojo concluded that the transmission could be reduced by altering the natural frequency of the discharge tubing by the provision of a sharp bend and a more flexible material. To reduce the cavity resonance problem a Helmholtz style reactive silencer was incorporated into the

suction line. However the most significant improvement was achieved by altering the shell stiffness where third order resonance of the shell coincided with the high noise levels in the 2 kHz region. An increase in shell stiffness by altering the shape to a near perfect sphere and the inclusion of circular stiffeners increased the natural frequency of the shell and consequently the harmonics which eliminated the third order frequency clash.

Tree and Shryock (1976) showed that the hermetic shell of a rotary vane compressor which was solidly mounted to the compression mechanism provides a low resistance mechanical transmission path. They analysed sound spectra from two identical compression mechanisms one was enclosed in its standard shell the other remained open. They showed that the shell and/or mounting system was just transmitting the even harmonics but amplifying the odd harmonics to an extent that overall sound levels were increased by 5 dB. It was assumed in this study that the shell had negligible energy feedback to the compressor mechanism and therefore no effect on the sound generation process.

Probably the single most important paper relating to noise in rotary sliding vane compressors is the noise study of a twin vane fractional horsepower refrigerant compressor by Johnson and Hamilton (1972a). The sound spectrum showed peaks at the pumping frequency (115 Hz to 118 Hz) and harmonics to approximately 4 kHz. The highest peaks were in the 1.8 kHz to 2.4 kHz region where human hearing characteristics are most sensitive.

Johnson and Hamilton considered the source of compressor shell excitation was structure-borne transmission from the stator, which in turn had two sources of excitation: fluctuating internal pressures and centrifugal forces due to rotor unbalance. Since stator vibration measurement had revealed peaks to the 43^{rd} harmonic, forces due to

rotor unbalance could be neglected as they oscillate sinusoidally and would not generate vibration at the higher harmonics. This paper also introduced cavity resonance as a source of casing excitation. It was shown that the casing vibration levels at the fourth harmonic of the pumping frequency were related to internal gas temperature. Ensuring the gas temperature does not reach the critical value, or changing the cavity shape would reduce the problem at this specific frequency. However, care must be taken to avoid an undesirable clash at another frequency.

A further paper by Hamilton and Tree (1974) investigated the two paths through which excitation of the shell was possible; firstly the gas pressures within the shell and secondly the suspension system and tubing connections between mechanism and shell. A comparison of stator vibration to radiated noise showed close correlation, indicating that gas forces and journal bearing film pressure forces within the stator are predominant. They showed that the only significant difference between the stator vibration spectrum and radiated noise spectrum was a peak at 460 Hz in the latter. Predictions confirmed that this was attributed to cavity resonance. Other authors have also recognised the cavity resonance phenomenon which is discussed further in Chapter 7.

The papers discussed to date have been concerned with refrigeration compressors which exist in domestic environments where noise levels are critical. However, the majority of air compressors are used in industrial enviroments where noise levels from ancillary equipment are generally higher, or the compressors are situated in a separate room away from employees, where they are not an annoyance. For this reason there is very little relevant published work on air compressors and this is especially the case for sliding vane compressors, no doubt because they are fundamentally quieter. The sliding vane compressor has only one major moving part and there is much less out of balance mass than is associated with reciprocating compressors.

However as statutory regulations concerning maximum noise levels have become more stringent and noise has come to be considered an enviromental pollutant, low noise levels are now a strong selling point.

The present research program examined a Hydrovane oil flooded rotary compressor with eight sliding vanes. Previous investigations of Hydrovane compressors of similar design have all revealed one major fact: The noise and vibration problem is related to the harmonics of the fundamental rotational frequency.

A report on a prototype 25hp Hydrovane sliding vane compressor completed by the Institute of Sound and Vibration Research (1985) utilised a lead shielding technique to determine the relative strengths of the various noise sources. Initially the complete compressor was carefully surrounded with a series of lead and foam panels which covered each of the possible noise sources. As each section of shielding was removed the change in sound pressure was measured and the contribution of the exposed area to the overall sound level was calculated. These results showed the compressor casing and the cooling fan to be the major noise sources. Narrow band frequency analysis showed that the noise peaks were related to the rotor vane passage frequency and the cooling fan blade passage frequency. The air intake was also shown to contribute to the noise but was not considered a major source.

Structural vibration characteristics measured at various locations on the prototype compressor structure showed maximum vibration levels on the compressor casing in the 600 Hz to 6 kHz region and on the oil cooler fins in the 250 Hz to 600 Hz region. The casing vibration patterns were seen to be typical complex ring type mode shapes with peaks at all harmonics of the rotor vane passage frequency.

A further report by Sound Research Laboratories (1986) on

another prototype Type 25 compressor in accordance with BS 4196:1967 drew identical conclusions. The rotor vane passage frequency and harmonics were shown to be the major cause of noise, the cooling fan blade passage frequency and its harmonics were also significant, particularly the "hunting" that occurred at the coincident harmonics. It was suggested that alteration of the number of rotor vanes or fan blades to prime numbers would prevent the harmonics clashing.

Other improvements recommended were: The use of backward curved blades rather than radial blades and a reduction in fan diameter to reduce cooling fan noise; the use of an internal reactive silencer to reduce the excitation of the casing. However with no accurate knowledge of the internal enviroment, this could not be designed with confidence.

The foregoing review has indicated that most noise problems are unique and each must be tackled as an individual project. A number of papers have provided useful ideas and highlighted different techniques and assumptions many of which have been adapted and used in the present project.

1.2 Fundamentals of noise and vibration

The fundamental principles of acoustics are detailed in all text books dealing with noise and vibration. Textbooks by Beranek (1971), Harris (1978), White and Walker (1982), Bell (1982) and Sharland (1972) deal with all aspects of sound and vibration and include details of measurement, analysis and particular applications. They provide an introduction to many subjects and include references if further details are required. However for the sake of clarity some of the more common terms and definitions used in the present thesis are quoted below.

1.2.1 Common definitions in noise and vibration

The Bel is defined as the logarithm to the base 10 of the ratio of a measured quantity to a known standard reference quantity. The decibel (dB) is simply this scale split into ten divisions. In acoustics the "quantity" is either a sound pressure, sound power or sound intensity, in vibration a vibratory acceleration level, vibratory velocity level or vibratory displacement level.

$$dB = 10 \log \frac{\text{Measured quantity}}{\text{Reference quantity}}$$

A microphone is capable of detecting small pressure fluctuations above and below atmospheric pressure. If the r.m.s pressure value or sound pressure is donated by (p) then the Sound Pressure Level (SPL) which is measured in decibels is defined as;

$$SPL\ (dB) = 10\ \log \frac{p^2}{p_{ref}^2}$$

where p_{ref} is the reference r.m.s pressure taken as the threshhold of hearing (2×10^{-5} N/m^2).

The sound intensity (I) is defined as

$$I = \left[\frac{p^2}{\rho c} \right]$$

where

ρ = density of the medium

c = speed of sound in the medium

If the sound pressure is identical over a spherical surface of radius r surrounding a noise source, the surface area is $4\pi r^2$ and the sound power (W) emitted by the source is defined as;

$$W = I \times 4 \pi r^2 \qquad \text{therefore}$$

$$W = \left[\frac{p^2}{\rho c}\right] 4 \pi r^2$$

and the sound power level (SWL) is defined by

$$SWL\,(dB) = 10 \log \left[\frac{W}{W_{ref}}\right]$$

where the reference power level $W_{ref} = 1 \times 10^{-12}$ Watts.

The sound power value is unique and a fundamental property of the source. Figures 1.1 & 1.2 show typical SWL and SPL values for various noise sources.

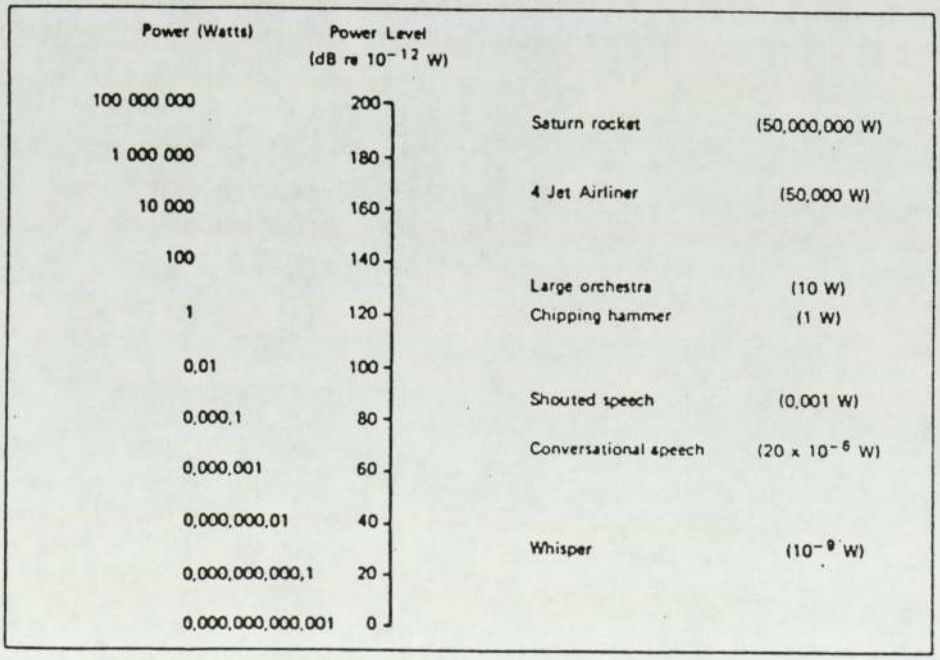

Figure 1.1 Sound Power Level of typical noise sources

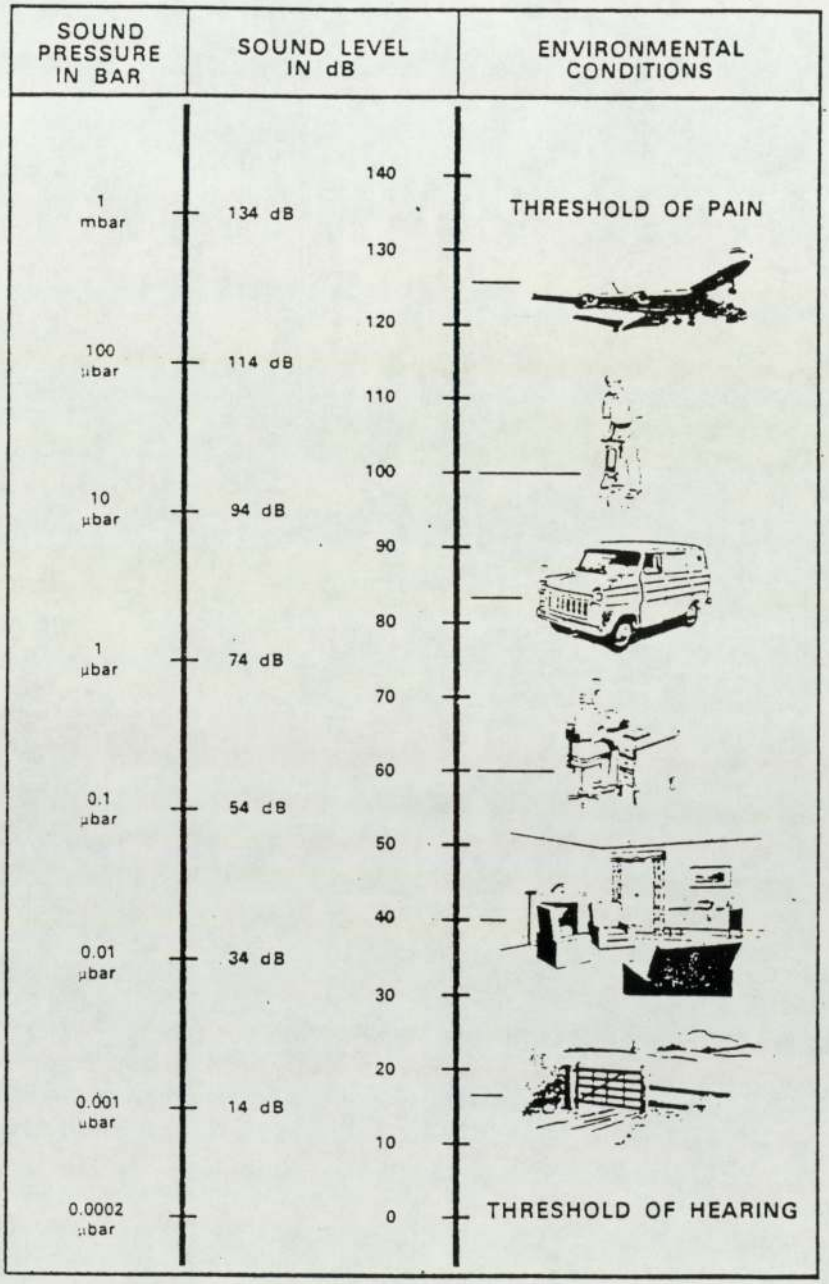

Figure 1.2 Sound Pressure Level of typical noise sources

The sound radiated from all noise sources is a combinaion of noise at various magnitudes and frequencies. To aid the acoustic engineer in identifying the possible noise sources these frequencies must be determined and their relative magnitudes assessed. The fast fourier transform basically transforms the overall noise signal, which is a function of time, into a frequency spectrum that contains the magnitude and frequency of its constituents. For general noise measurement the information can be displayed in octave bandwidths that split the overall signal into the noise level in 11 bands. If greater accuracy is required the bandwidth must be reduced to a one-third octave bandwidth which uses 32 bands or for maximum accuracy to narrow bandwidth analysis. The bandwidth available depends on the frequency range of interest and the accuracy of the analyser. Narrow bandwidth analysis has been used throughout the present investigation.

The human ear does not respond in a linear manner to either the magnitude or frequency of sound and the hearing characteristics of every healthy ear are slightly different. A typical healthy ear is most sensitive in the 2 kHz to 5 kHz region. The further away from this range the poorer the response. This information is shown graphically in Fig.1.3 and it is apparent that for two noise sources at different frequencies it is possible that the source which is physically quieter can be heard as being louder. To overcome this problem a weighting method is employed which simulates the hearing characteristics of the human ear. This is defined as "A-weighting" and is shown in Fig.1.4. This weighting gives a more accurate interpretation of the character of the noise source and the relative importance of various frequency components. Any signal that receives this weighting is measured as "dB(A)".

Vibration, like sound, has also been studied extensively. The vibration of a system involves the alternating transfer of energy between its potential (or strain) and kinetic forms. The displacaement, velocity

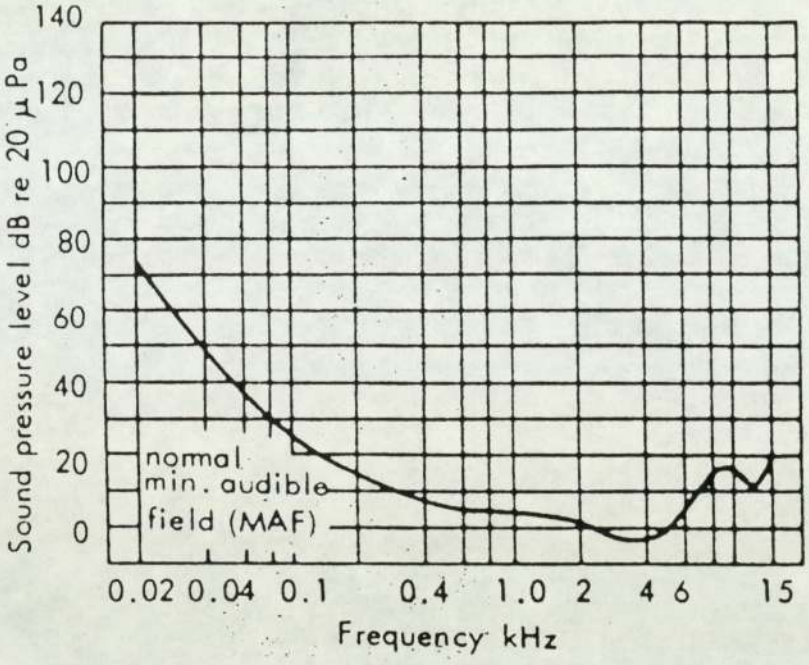

Figure1.3 Normal binaural minimum audible field (MAF) at different frequencies

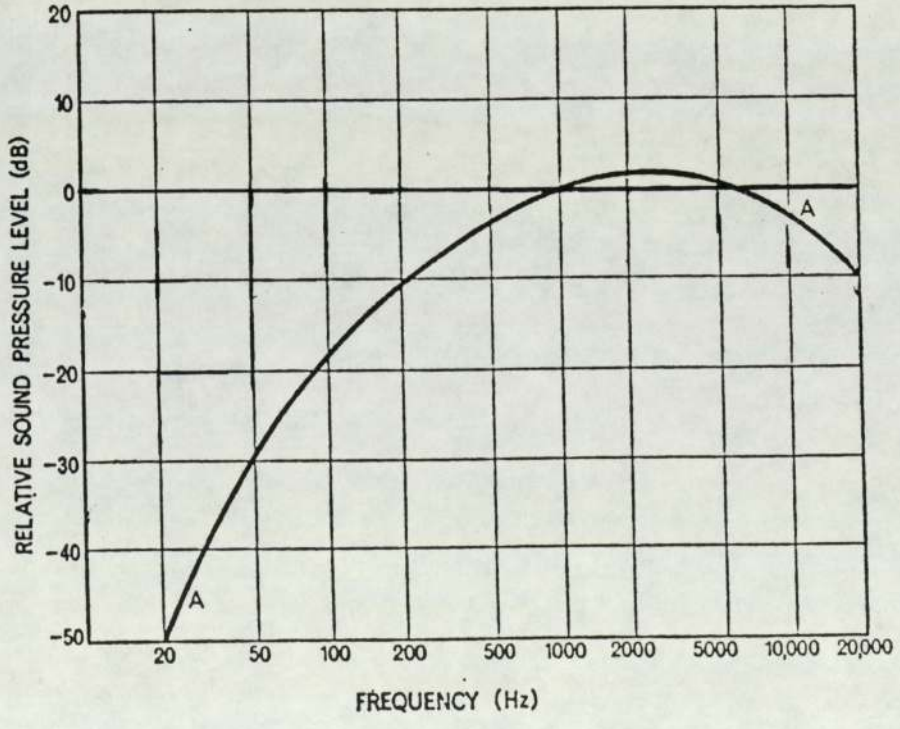

Figure1.4 Standard A weighting spectrum

and acceleration of a surface are related and measurable quantities. Since the motion is assumed to be made up of sinusoidal motion at various frequencies, magnitudes and phases it is possible to determine any of the three motions from measurement of one, either by differentiation or integration. The most common form of measurement transducer is an accelerometer, fixed rigidly to the surface of interest: implicitly the accelerometer output signal is proportional to the acceleration of the surface. Integration will provide velocity and further integration the displacement.

Terms used for vibration measurement are as follows, the suffix 0 refers to the reference quantity;

Vibratory acceleration level	$(La) = 20 \log a/a_0$	$a_0=1 \times 10^{-5}$ m/s^2
Vibratory velocity level	$(Lv) = 20 \log v/v_0$	$v_0=1 \times 10^{-8}$ m/s
Vibratory displacement level	$(Ld) = 20 \log d/d_0$	$d_0=1 \times 10^{-11}$ m

Most vibration has a mechanical origin, although structural vibration can be generated by unsteady fluid flow, vortex shedding or by high noise levels impinging on the structure. Conversely, structural vibration will radiate noise. The amount of energy transferred from vibration to sound is dependent on the geometric and dynamic properties of the structure, the physical properties of the surrounding medium and the radiation efficiency (σ) of the surface. The radiated acoustic power (W) is defined as

$$W = \rho c S \sigma \langle v_n^2 \rangle$$

where

$[v_n^2]$ = spatial average of the mean square normal vibration velocity and

S = the surface area.

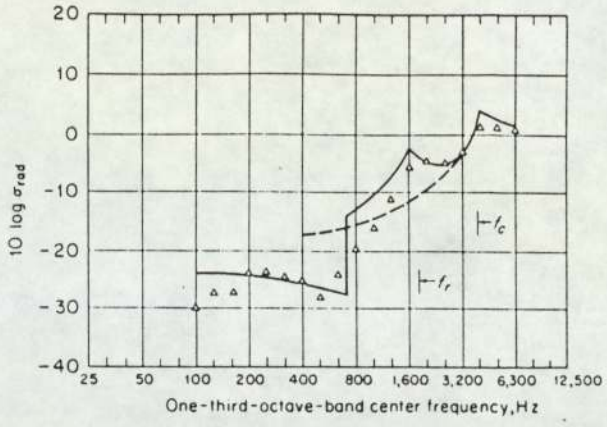

Figure 1.5 Radiation efficiency of a cylindrical shell

The noise radiation efficiency of a short uniform cylindrical shell is shown in Fig.1.5. This illustrates that radiation efficiency is a complex function of frequency. The frequency at which the efficiency becomes unity is known as the critical frequency and occurs when the speed of bending waves in the material is equal to the speed of sound in the surrounding medium. The speed of bending waves (C_L) within a material is given by

$$C_L^2 = \left[\frac{E}{\rho\left(1-\upsilon^2\right)} \right]$$

For example if it is assumed that the casing of a sliding vane compressor is a thin cast aluminimum cylinder then ($E = 70.2 \times 10^9$ N/m^2, $\rho = 2720$ kg/m^3 and $\upsilon = 0.33$) the speed of bending waves is calculated as 5385 m/s.

The critical frequency (f_c) of a thin cylindrical shell (Fahy 1988) is calculated as

$$f_c = c^2 \Big/ 1.8\, h\, C_L$$

where h is the shell wall thickness and c the speed of sound (340 m/s). For the compressor casing used in the present work h is 4mm and the critical frequency is calculated as 2981 Hz

Below the critical frequency the radiation efficiency is dependant on the function (ρc / Sf_c). As this function is increased the radiation efficiency increases.

The radiation of noise from source to receiver is also dependent on frequency. High frequency noise is more readily dissipated in the transmitting medium than low frequency noise. However, at the small distances used for measurement work in air this effect can be neglected.

1.3 Compressor details

The compressor used in the present study was a Hydrovane oil flooded rotary sliding vane machine consisting of three main components; the motor, the cooling fan and air-end (Fig.1.6). Air-end is the term used to describe the complete structure that houses the compression unit. The particular model was a "series 15, 10 bar, PUTS", which signifies an air-end that delivers at 10 bar and is driven at 2880 rpm by a 1.3 kW single phase motor mounted on a tripod.

1.4 Compressor operation

To aid the appreciation of the experimental procedures, the methods used to analyse results and the conclusions drawn from these results the operation of the air-end within an oil flooded sliding vane compressor is described.

Air-end operation can be split into two distinct fluid processes relating to the air and oil. Atmospheric air is drawn in, compressed and then discharged to a high pressure line. Oil is continually recirculated acting as a surface lubricant for shaft bearings and vanes and as a coolant following injection into the compression cells where it also acts as a sealant. The oil must then be separated from the high pressure air and cooled prior to recirculation.

The operation is discussed in four sections. The induction and compression of air, the injection and cooling of oil, the separation of air and oil and finally aspects of compressor control.

1.4.1 Air induction and compression

Compression is achieved by positive displacement with a fixed compression ratio for any given model. The compression unit consists of a cylinder or stator in which a rotor rotates concentrically to the "seal" bore and eccentrically to the "compression" bore.

In the model under investigation the rotor has eight radial slots parallel to the axis of rotation in which vanes are able to slide freely and are "thrown" by centrifugal action on to the cylindrical wall of the stator. As the rotor rotates, consecutive vanes pass the inlet port to form a cell. The air entrapped is compressed as the cell volume decreases, until the leading vane passes the outlet port where the air is discharged to the high pressure side of the air-end.

The compression cycle and subsequent control of the flow of compressed air can best be illustrated diagramatically (Fig.1.7).

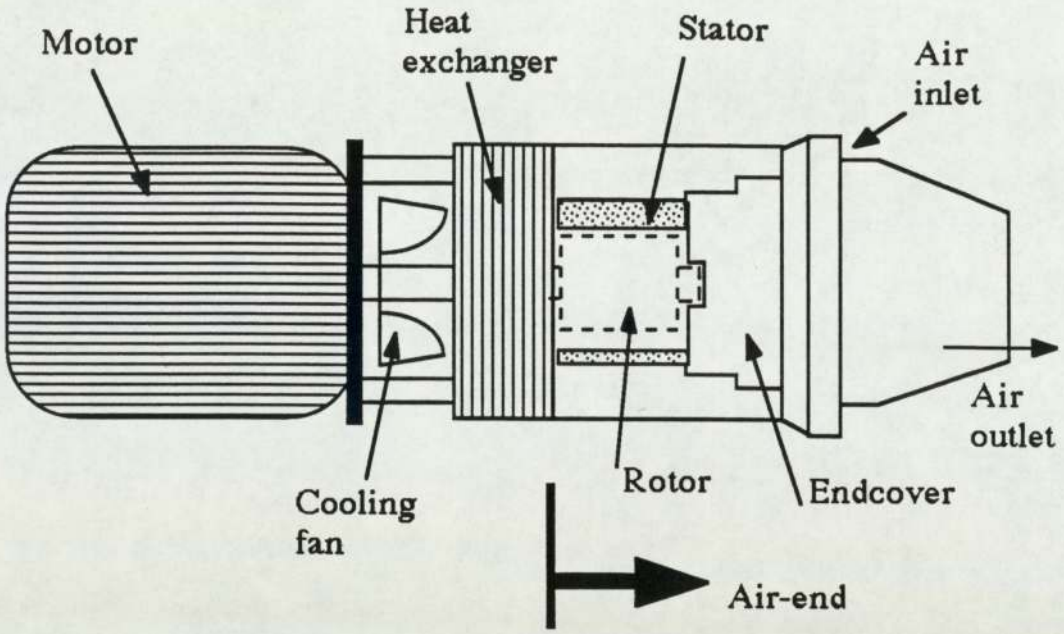

Figure 1.6 Main compressor components

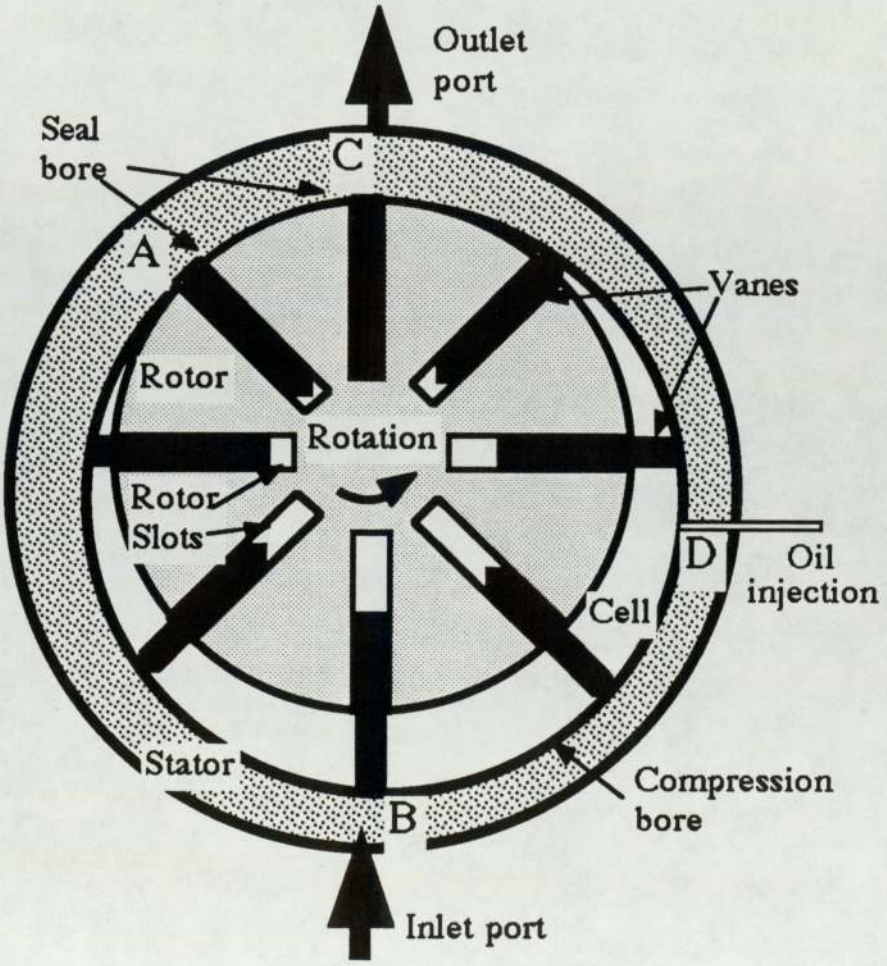

Figure 1.7 General arrangement of rotor and stator

With rotation clockwise from A to B, the volume between the vanes, the rotor and the stator increase. Consequently, the pressure drops and generates a partial vacuum to draw air in through the inlet port at B. With further rotation, cell volume decreases and as the cell approaches the outlet port at C, the volume reduces rapidly which produces a sharp rise in air pressure. Air cannot continue round with the rotor due to the seal formed between C and A. The concentricity and clearance of this seal are precisely controlled.

1.4.2 Oil injection and cooling

To improve the efficiency of the compressor, oil is injected during compression. This serves to

- seal each cell from it's neighbour,
- seal between the high pressure at outlet and partial vacuum at inlet,
- cool the air during compression.

Without oil injection to absorb part of the heat generated by compression, the air temperature would increase to approach adiabatic compression i.e. no heat transfer to the surroundings. If it were possible for the oil to absorb sufficient energy during compression then the process could be isothermal i.e. the air temperature remains constant. In practice the compression is approximately polytropic, falling between adiabatic and isothermal. The air temperature at final compressor discharge is approximately 35-40 °C above ambient.

The oil is also fed under pressure to the rotor bearings which are a plain white metal type located in the endcovers of the stator. Control of the oil flow is therefore, most important. Circulation is effected by utilising the high pressure air to induce the oil flow. To achieve this the compression unit is housed in a chamber which is half filled with oil.

When delivered from the rotor stator unit, the compressed air exerts its pressure on the surface of the oil collected in the bottom of the casing. The oil is then directed via a cooler and filter into the compression cycle at D. The full volume of oil within the compressor is circulated every thirty seconds.

Clearly the oil, which is used to seal, lubricate, cool and control the sliding vane compressor is critical to the efficient operation. The oils used have been developed by the industry and proved in exhaustive testing by the compressor manufacturers. They must retain their properties over a reasonable working life at temperatures between 80^0C and 100^0C. The recommended oils are a detergent type with anti-oxidant and dispersive additives. High viscosities are required to ensure adequate film thickness for sealing and coalescing.

1.4.3 Combination and separation of air and oil

As a result of oil injection the air delivered from the compression unit is saturated with oil which must be removed before the air is taken from the compressor. As the air and oil mixture leaves the discharge port it impinges on the casing endcover, which deliberately creates turbulence that allows mechanical separation of the heavier oil droplets. The droplets drain to the base of the chamber to join the bulk oil for continued re-circulation. This process is over 99% efficient, but further separation is still required.

Relatively clean air leaves the chamber to enter a separator in which special filters remove most of the remaining oil by coalescing action. The maximum amount of oil carried over will be five parts of oil to a million of air by weight. The pressure drop associated with oil separation is between 0.07 - 0.14 bar at normal working pressures.

1.4.4 Compressor control

A minimum pressure valve is used to ensure that sufficient pressure is maintained within the air-end to generate oil circulation before air is allowed to leave. This valve also has a secondary purpose, acting as a non-return valve when the compressor stops.

When the compressor stops the intake valve is automatically shut and pressure within the compressor is reduced gradually through the oil return valve, purging the compressor and separation media. Nevertheless it is possible to trap oil in the compression unit and an oil relief valve is fitted to the stator to prevent hydraulic locking and possible damage when the compressor is restarted. This consists of a spring loaded plate which is opened by the pressure generated within the cell to provide an outlet for the excess oil to return to bulk oil. An additional purpose served by this valve is to reduce the load on the prime mover at start-up by allowing air to pass through the outlet instead of being fully compressed. This will continue until the chamber pressure has increased sufficiently to force the valve shut.

Further automatic controls are required to assure safety of operation. A high pressure relief valve and high temperature cut-out switch are fitted, although these are effectively redundant if the compressor has been carefully selected for its intended application.

2.0 Instrumentation, calibration and measurement techniques

As stated in Chapter 1 noise is generated from both mechanical and aerodynamic vibrations within the compressor. In addition to the measurement of noise radiated from the compressor it was necessary to measure vibration magnitudes of the compressor structure, initially externally and eventually internally and also the magnitude of internal pressure fluctuations. This chapter aims to discuss the main experimental techniques, instrumentation and calibration procedures. Where special circumstances have required any changes in the experimental procedures from those described in this chapter: these will be discussed at the appropriate point in later chapters. All the equipment used during the experimental work and specific details of calibration methods and values are detailed in Appendix A.

Figure 2.1 shows a circuit diagram of the various instrumentation and interactions used throughout the present research program. Briefly the appropiate transducers (Microphones, Accelerometers, Pressure Sensors) were coupled via signal conditioning equipment (Sound Level Meters, Charge Amplifiers, Wheatstone Bridges) to Oscilloscopes for observation, to Magnetic Tape Recorders for recording and storage, then finally to Spectrum Analysers for frequency analysis.

2.1 Noise measurement

Various methods of noise measurement are available to the acoustic engineer. The best technique in a particular situation depends greatly on the product itself as well as the available testing facilities. If accurate SWL measurements are required, then the product can either be analysed in a completely anechoic chamber, or in a room whose reverberant properties have been calculated. This requires only the use

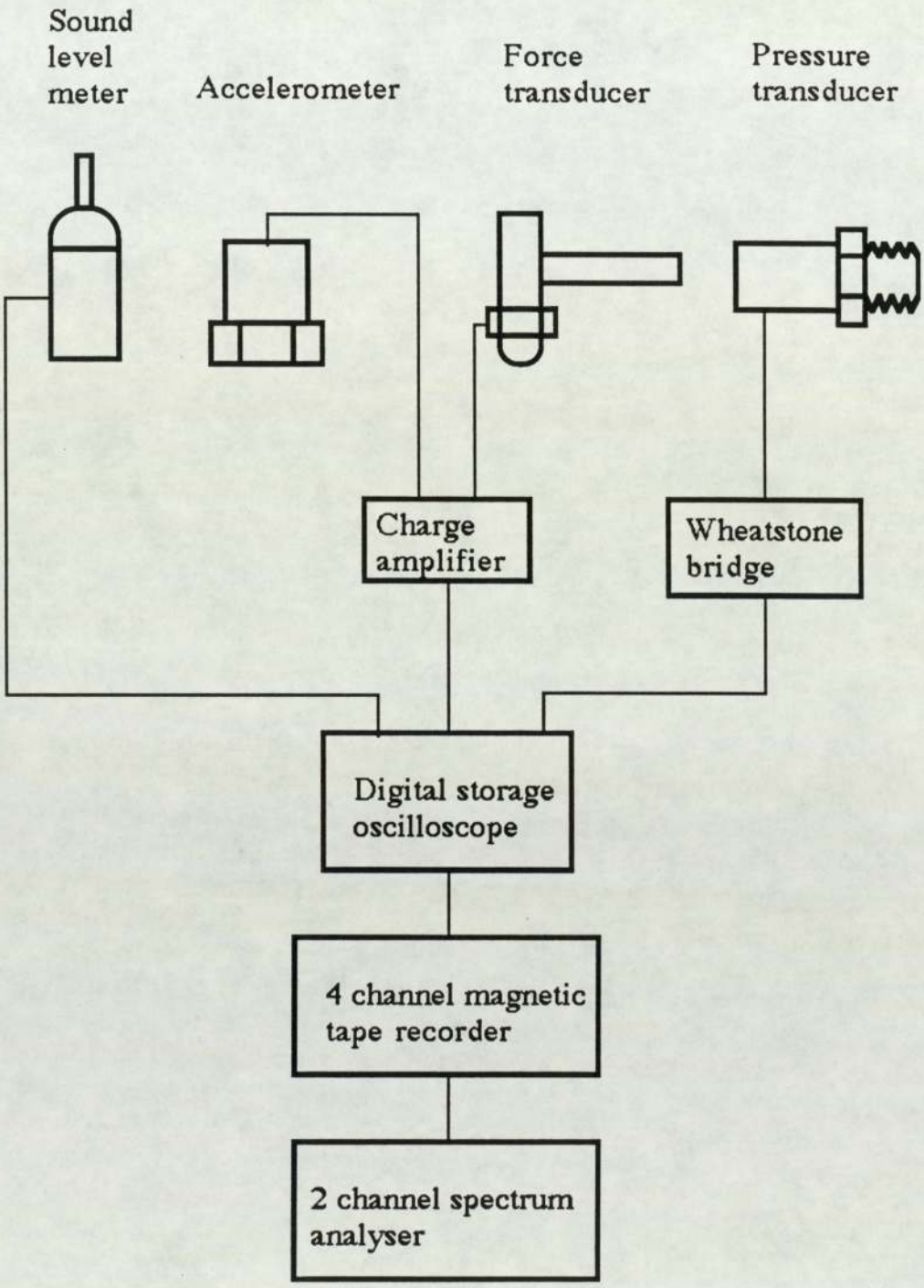

Figure 2.1 Circuit diagram of instumentation

of conventional microphones and sound level meters. In many cases the product is too large or requires ancillary equipment that may also be noisy; it must therefore be analysed in situ using a sound intensity technique (Lyon 1987). This technique measures the net flow of energy through a defined region. If sound intensity measurements are made over a region which completely encloses the noise source then any background noise from outside the defined region will be eliminated in the intensity calculation.

Once a particular machine has been isolated for measurement then it is essential to determine the major source of noise. Ranking of sources by shielding techniques is a useful method. The machine is enclosed in a lead cabinet and SPL's are recorded. Particular panels can then be removed in turn to reveal the possible noise sources i.e. discharge ports, motors or fans. The new SPL's are recorded and the exposure that produced the largest reduction in SPL is ranked as the noisiest source. This technique was used successfully by the Institute of Sound and Vibration Research on a Hydrovane compressor as outlined in Chapter 1 and also by Simonitsch and Robinet (1978) who showed that intake noise was the dominant noise source of a 35 cfm reciprocating air compressor, followed by fan noise and then noise radiated from the casing.

It is not completely satisfactory to base acoustic results on pure linear measurement. Acoustic assessment must be made subjectively since very strong tonal content might produce a lower SPL than a broadband noise but is in fact perceived as more annoying. Similarly, identical noise levels at different frequencies can be heard as quite different.

This type of problem has lead to the definition of scales other than the A-weighted scale mentioned in Chapter 1 that go some way to balancing the frequency and SPL combination. Each method of assessment is best suited to particular noise problems. The different scales are discussed in Beranek (1971) or Sharland (1972).

The Phon scale, for example was designed to give a measure of equal loudness with frequency and is the product of the SPL and a loudness factor. Fig 2.2 shows the relationship between frequency and SPL. The SPL scale and Phon scale are identical at 1 kHz. Single-number ratings, for example Noise Criteria (NC) curves (Fig. 2.3) are also used to measure noise levels which include a frequency weighting. Rather than stipulate a maximum overall noise level the levels are recorded in octave bandwidths. To satisfy a particular NC rating the noise levels must be below the stipulated levels in every bandwidth. The A-weighted scale is probably the best weighting because it correlates reasonably well with all the single-number ratings. It is for this reason that it is most common and is readily available on almost all sound measuring equipment.

SPL measurement in conjunction with the A-weighted scale was used throughout the experimental work of the present program as it is an efficient measure of the audible reduction achieved, rather than the physical reduction, at a particular location. If uniform hemispherical radiation is assumed then the SPL change is directly related to the SWL change. This technique gave adequate guidance in assessing the acoustic performance of any modifications. However, the final criterion in any noise reduction project must be the subjective opinion of a group of people who will all have slightly different hearing characteristics and will react to any particularly strong and annoying tonal content.

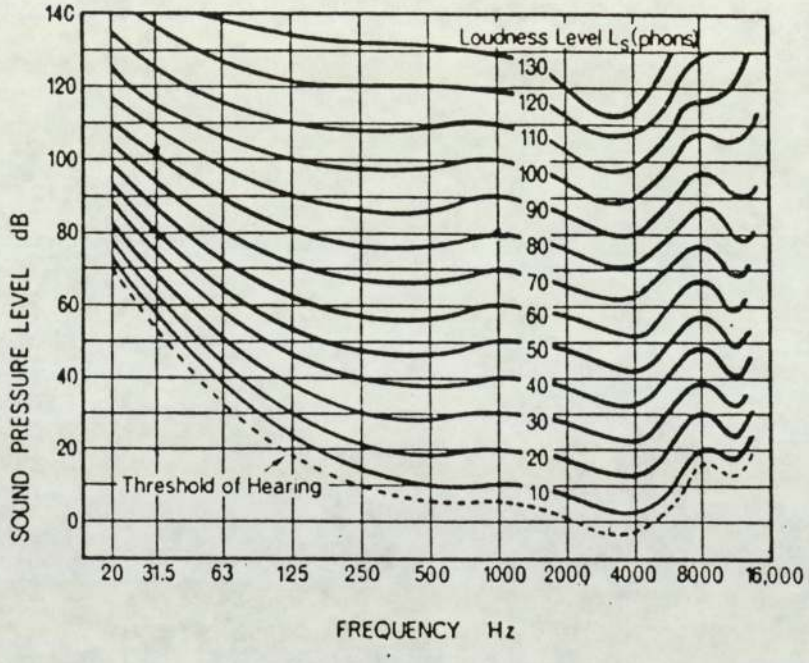

Figure 2.2 Equal loudness contours (phons)

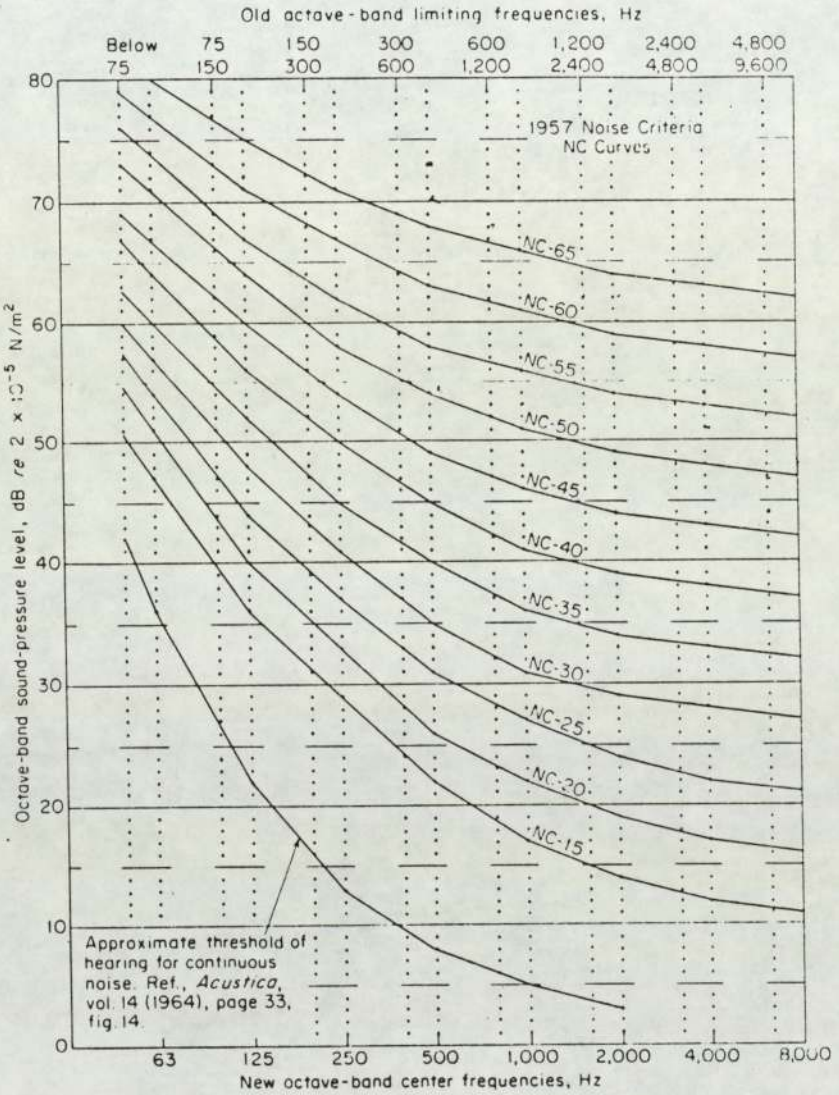

Figure 2.3 Noise criteria (NC) curves

and was used to determine the SWL of the standard compressor. Experimental work completed in the anechoic chamber involved recording the noise signal from the microphone directly on magnetic tape and similtaneously measuring either the linear SPL or an A-weighted SPL using a separate Bruel and Kjaer sound level meter outside the anechoic chamber. This meant there was no human interference within the anechoic chamber during measurements.

The technique used outside the anechoic chamber, ie in reverberant rooms, was to measure the noise signal directly using a CEL precision sound level meter. The signal was automatically A-weighted by the meter and the SPL displayed. The A-weighted output from the sound level meter was also recorded on magnetic tape.

For each particular set of experiments the standard component was always analysed to provide a datum level. A direct comparison of signals at each measurement location allowed changes in noise levels due to modifications of compressor components to be determined. The actual location of microphones and reverberation properties of the room were therefore not significant in relation to SWL changes.

During all experimental work the sound level meter was adjusted to ensure the highest signal to noise ratio. The meter has an option of two standard response modes, fast and slow. When the meter was operated in conjunction with the tape recorder the "fast mode" was used to ensure any sudden changes in noise were recorded. To increase signal damping when measuring overall noise levels the longer averaging time of the "slow mode" was employed.

The microphones and sound level meter were calibrated as one unit in accordance with British standard procedures (BS 4196 : Part 5) using a pistonphone which produces a constant A-weighted SPL of 113 dB ± 0.2 dB at 250 Hz. The output from the sound level meter when

recording the pistonphone signal was measured as 764 mV compared to a theoretical of 767 mV; this error of 0.4% will be introduced into the tape recorder.

2.2 Vibration measurement

Meaningful vibration measurement depends greatly on the positioning of the accelerometers. To describe completely the dynamics of a structure, accelerometer measurements would be necessary over the entire surface without the accelerometer actually affecting the dynamic characteristics of the surface. This is obviously impractical and the number of accelerometer positions must be reduced to a level at which the accuracy is acceptable.

Certain physical conditions can cause measurement problems, for example: in the case of a very light structure the mass of the accelerometer will affect the dynamic behaviour of the structure and natural frequencies will be altered. This error becomes more significant as the frequency is increased. Also high temperature surfaces prevent the use of standard accelerometers. In these cases laser measurement techniques must be employed (Bruel and Kjaer Laser set application notes). A laser beam is split; one part is aimed at reflective tape on the surface of interest the other is reflected from a rotating disc in the unit. The laser beam aimed at the location of interest will undergo a frequency shift proportional to the surface velocity. This is compared to the beam returned from the rotating disc to determine absolute velocity levels. Differentiation of this signal will provide the surface acceleration levels and integration will provide the dispacement levels. All the vibratory information is therefore available.

For the present program vibration measurement was achieved with piezoelectric type accelerometers in conjunction with charge

amplifiers. The mass of the accelerometers were considered negligible in relation to the compressor components to which they were attached. The accelerometers were fixed to the vibrating surface using a fast setting Araldite adhesive. Since the vibrating surface was hot, thin and under an internal pressure, the use of either wax or a stud was not possible and a hard adhesive which gives similar mounting characteristics was considered the most appropiate method. Care was taken to ensure that a similar quantity of adhesive was used for each accelerometer and that a suitable curing time elapsed before measurements were taken. The handbook "Measuring vibration" (Bruel and Kjaer 1982) indicates that this type of epoxy adhesive will give uniform response below 7 kHz. Above this frequency the dynamic behaviour of the adhesive will increasingly affect the response of the accelerometer with mounting resonance occuring at approximately 28 kHz.

The sensitivity of each charge amplifier was adjusted for the various experiments to compensate for changes in surface temperature which affected the operating response of the accelerometer. A table of amplification factors is shown in Appendix A.2. The output signal from the charge amplifiers was recorded directly on magnetic tape.

A reference method was used to calibrate this equipment using a vibrating table and reference accelerometer. The voltage output from the charge amplifier was compared for each accelerometer (Appendix A.3). All accelerometers registered within 3% of the reference accelerometer between 50 Hz and 6.5 kHz.

The skill involved in vibration analysis is in interpreting the dynamic behaviour of the system from accelerometer measurements. The characteristics of regular shapes i.e. plates and shells are now well documented: Blevin (1985) provides a summary of formulae for natural frequencies and mode shapes. Once a measurement at one location has

been compared favourably to the theoretical then the dynamic behaviour at all other locations can be predicted with a high degree of confidence. However, as a shape becomes more irregular the computation becomes more complex. Finite element techniques have improved the modelling capabilities enormously by building irregular shapes from a number of regularly shaped elements and as computers become more powerful the number of regular shapes used can be increased for the same analysis time, which increases the accuracy of prediction.

2.3 Magnetic Tape recording

To minimise experiment running times most noise and vibration data was stored on magnetic tape. Various analyses could then be performed if and when required. The four channel tape recorder was run at a speed of 60 inches per second which enabled frequency measurement up to 20 kHz to be recorded with a signal to noise ratio better than 48 dB.

The magnetic tape recorder was equiped with switchable input attenuation to provide a wide voltage range over which input signals could be measured. For each group of experiments the input attenuator setting was adjusted to to the lowest value that prevented overload, so as to give the best signal to noise ratio. With fixed attenuation all the results from a particular experiment could be directly compared. Consequently, when the results from different experiments are presented graphically they require the dB datum to be adjusted to accomodate this change. Where this has been necessary actual acceleration levels have been provided.

The tape recorder was calibrated by providing a series of known rms input voltages from an oscillator and measuring the rms output voltage from the tape recorder during replay to obtain the calibration

correction factor (Appendix A.4), which was determined as 1.1 ± 0.07.

2.4 Spectral or frequency analysis

For the assessment of a continuous noise signal i.e. the type of signal generated by a compressor operating steadily, a spectrum analyser is probably the most useful "tool" available since it is capable of converting a complex time signal into its magnitude and frequency components using an algorithm termed as the Fast Fourier Transform (FFT). It is this information which is essential to evaluate the relative importance of the various noise sources which comprise the complete noise signal and provide guidance for the most suitable noise control procedures. The Hewlett Packard spectrum analyser operated between 0 Hz and 25 kHz and a feature of the more expensive analysers only is its capability to measure over the following ranges 2.5 Hz, 10 Hz, 25Hz.... 25 kHz starting at any frequency.

The Hewlett Packard spectrum analyser was operated in a similar manner whether connected directly to the various signal conditioning equipment or used in conjunction with the tape recorder. Three types of signal filter were available, Uniform, Hanning and Flat top. The choice of filter depends on the type of input signal and also the information required; For transient signals the uniform window must be used and for random or periodic signals accurate amplitude information requires the use of the flat top filter which may not discriminate between close frequency components therefore the Hanning filter was used as this provides an amplitude / frequency compromise most suitable for general noise and vibration measurement. The rms averaging mode was used as this results in a smoothing of the signal but does not reduce the level and 64 averages were taken to produce each spectrum. The only function altered was the frequency span. The analyser uses a dBV scale which measures any voltage signal relative to 1 volt. It is defined as

follows:

$$dBV = 20 \log \frac{\text{Measured voltage}}{1 \text{ volt}}$$

Since the calibration correction factor for the tape recorder has been calculated a direct relationship exists between the dBV reading on the spectrum analyser and the input voltage to the tape recorder, which in turn is directly related to the acceleration level.

The calibration of the spectrum analyser was checked using the internal calibration test signal and by providing a signal of known magnitude and frequency from the sound level meter during pistonphone calibration. The frequency and magnitude of the resulting FFT analysis was compared to the actual input data. Fig.2.4 shows the frequency spectrum for the pistonphone. The rms output from the sound level meter was measured as 764 mV. The spectrum analyser indicates a peak at 250 Hz with a magnitude of -2.4 dBV. Converting this to a linear scale using the standard equation above gives a reading of 759 mV; an error of less than 0.5%.

This calibration had only confirmed the analyser operation at one frequency. An oscillator of 1% accuracy on the frequency scale was used to provide a signal across the frequency range from 10 Hz to 10 kHz. The magnitude of the input signal was measured using a Microvoltmeter. For a constant rms output of 500 mV the reading from the spectrum analyser remained linear at -6.1 dBV ±0.2 dBV (Fig.2.5).

The cumulative error at this stage (transducer to analyser) is at worst 6 %. This will introduce an error of up to 0.5 dBV on the screen. This information is then transferred to graph paper. The data is then interpolated to provide the necessary frequency and magnitude information. Human error in interpolation will introduce another

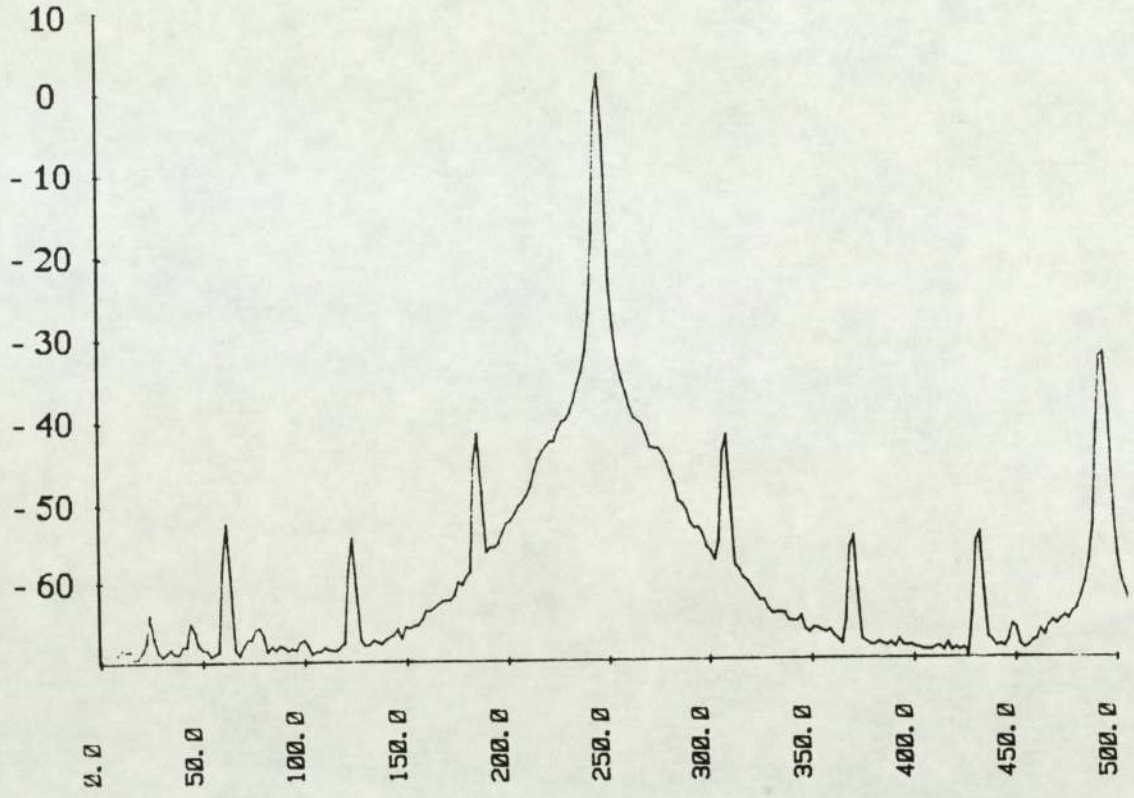

Figure 2.4 Pistonphone frequency spectrum

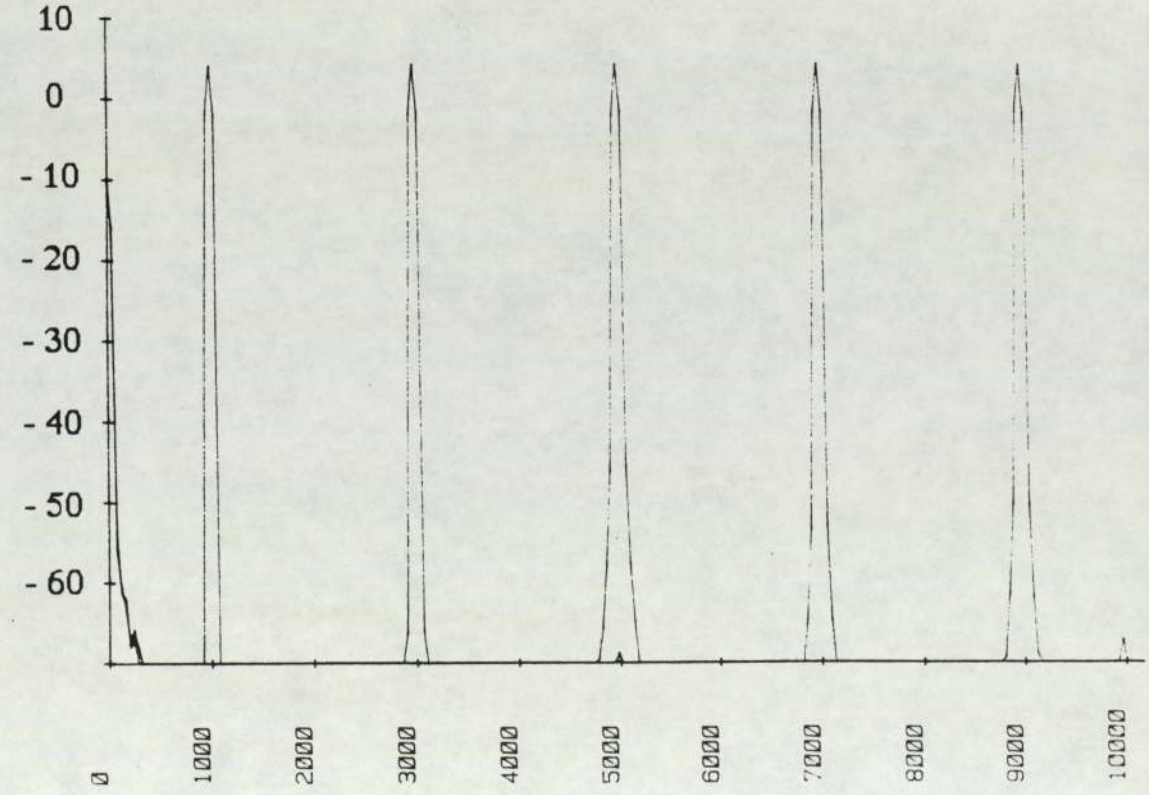

Figure 2.5 Oscillator output at different frequencies

0.3 dBV into the overall error resulting in a total of 0.8 dBV. Therefore only differences in measurement greater than 1 dBV were considered significant in predicting whether alterations to the compressor had made particular peaks larger or smaller. This criterion has been used throughout the experimental work.

2.5 Time analysis

The use of a digital storage oscilloscope enabled noise, vibration and pressure signals to be plotted against time. The time scale was adjusted to incorporate one complete revolution of the rotor. A trigger signal once per shaft revolution enabled accurate interpolation between transducer signal and rotor position. This unit was always calibrated in conjunction with either the sound level meter, accelerometer or pressure transducer and again the maximum error occurred when interpreting data from hard copies of graphs.

2.6 Modal Testing

Modal Testing is the theoretical or practical measurement of the natural vibrational characteristics of a structure. This section outlines the practical routine, which requires a known force to be applied to the structure and the acceleration response measured at various corresponding locations; the number and orientation is dependant on the accuracy required.

A Bruel and Kjaer impulse hammer which has a force transducer located in the hammer head was used to excite the compressor structure during modal analysis. The hammer impulse will excite all modes of vibration of the structure since it contains a force at every frequency below the frequency corresponding to the impulse duration. Three tips

are available so that the impulse from the hammer may be optimally suited to the frequency range of interest. A rubber tip is suitable below 500 Hz a nylon tip below 1 kHz and the steel tip below 6 kHz. The steel tip was used for all the experimental work.

The signals from the force transducer and accelerometer were both connected via charge amplifiers to the spectrum analyser. The transfer function, calculated instantaneously by the spectrum analyser, is the ratio of these signals and comprises magnitude and phase information. In this particular case the ratio of acceleration to force is termed the receptance.

The calibration of the impulse hammer and amplifier on an absolute scale was not necessary as these results were used for direct comparison only. The spectral analysis of a signal from the force transducer using the steel tip (Fig.2.6a) was compared to the standard spectrum provided in the handbook (Fig.2.6b) to confirm the satisfactory operation of the hammer.

2.7 Pressure measurement

A fast response gauge pressure transducer compensated to 93°C was used to measure pressure fluctuations within the compressor. The transducer was operated in conjunction with a full bridge amplifier and the ouput from the bridge was recorded on magnetic tape and then replayed through the digital storage oscilloscope enabling pressure fluctuations to be plotted against time as outlined above.

The pressure transducer, wheatstone bridge and digital storage oscilloscope were calibrated as one unit using a Budenburg dead weight pressure tester which calibrates to 0.05% of the operating pressure. The accuracy of the pressure transducer and digital storage scope introduced

a cumulative error of less than 1%. Further error occurs when interpreting data from the graphs (Fig.2.7). Using a ruler to measure fluctuations an accuracy of 0.5 mm was assumed over a scale of 150 mm (0.3%); the total error error was calculated as ± 1.3%. The pressure fluctuations measured during experimental work were in the range of 0.2 bar to 0.5 bar. The errors were therefore significantly lower than the accuracy required to determine whether changes in pressure fluctuations had occurred.

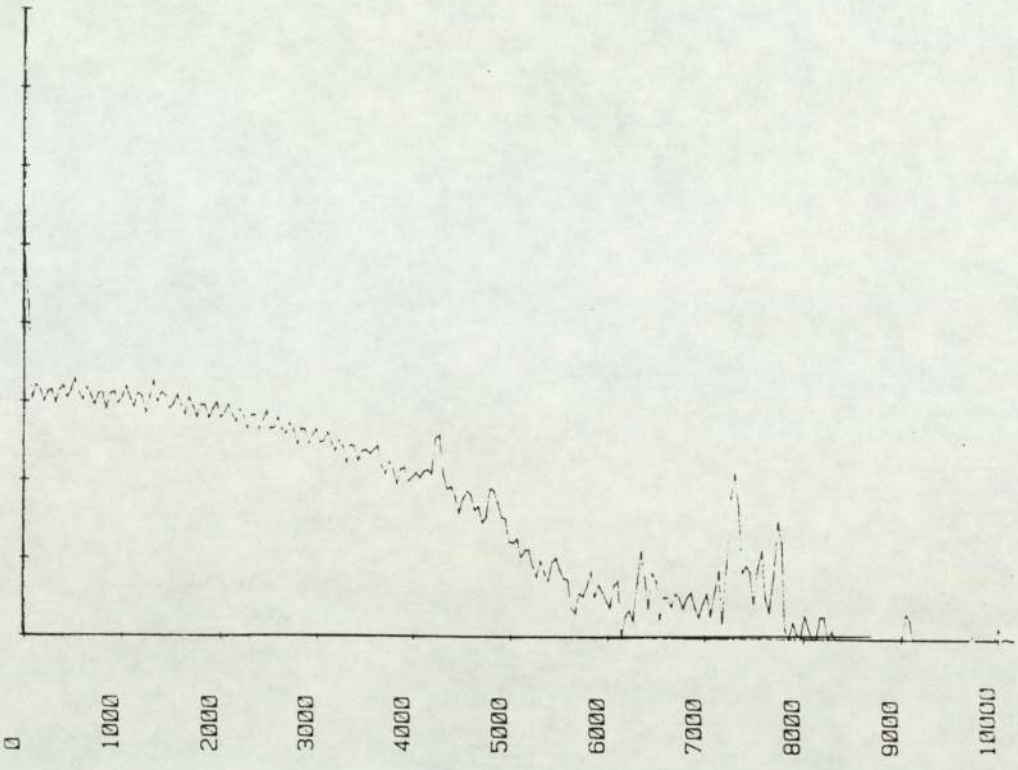

Figure 2.6a Measured force spectrum with steel tip

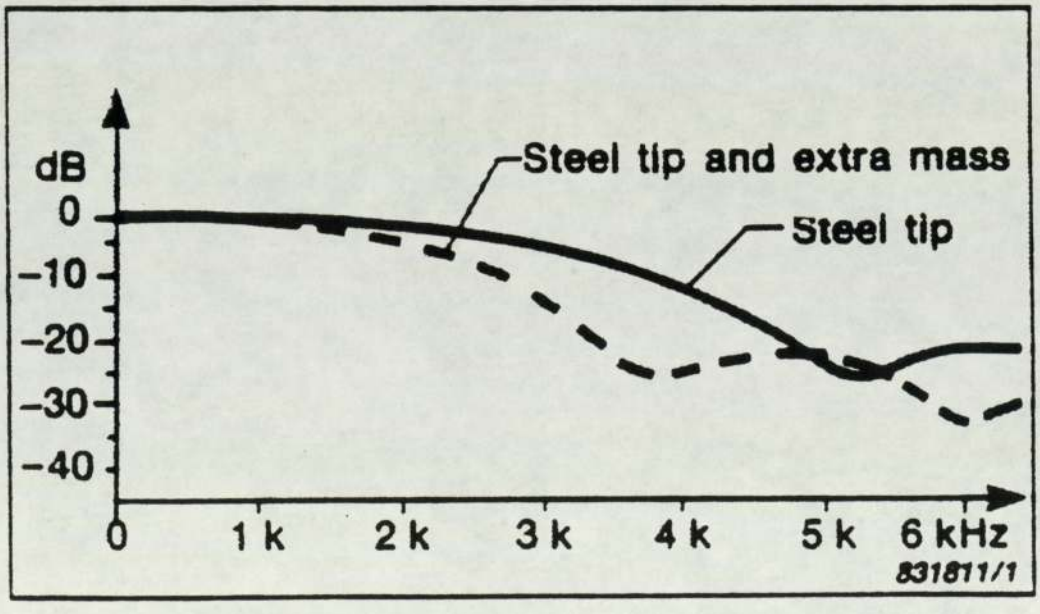

Figure 2.6b Standard force spectrum with steel tip

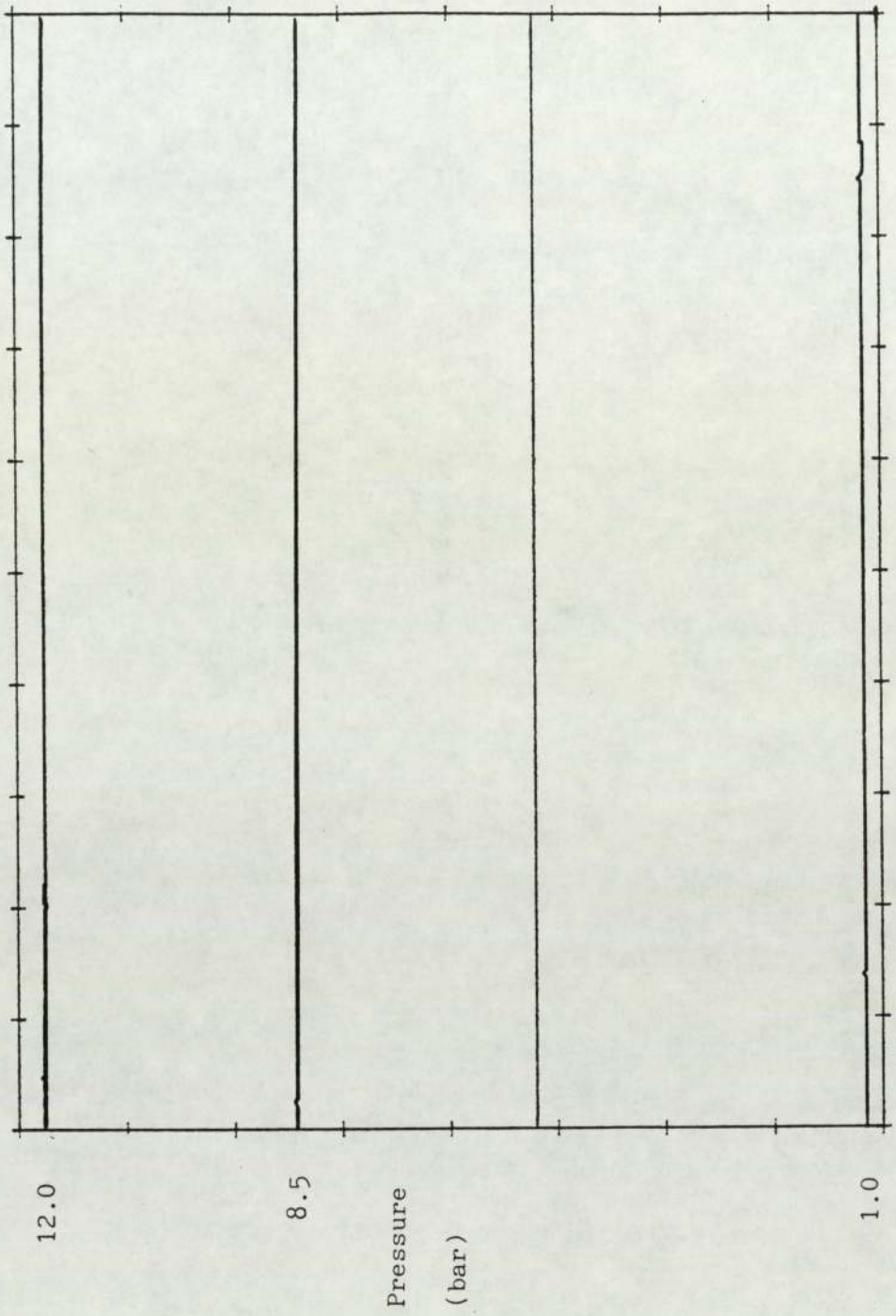

Figure 2.7 Pressure transducer output calibrated using Budenburg device

3.0 Initial noise and vibration survey

The following pages describe the initial noise and vibration survey on a standard Hydrovane series-15 compressor under normal operating conditions. Before any improvements or modifications can be made, it is essential that the main source of noise is determined and the noise or vibration generation process is fully understood. The starting point was therefore a complete investigation of the noise radiated from the compressor; this included an assessment of the noise from each of the three main components (motor, cooling fan and air-end). This preliminary noise investigation was completed in an anechoic chamber: an investigation into the vibratory characteristics of the compressor structure during normal operation was also necessary.

3.1 Noise investigation

The British standard test procedure which was followed, (BS 4196: Part 5:1981) refers to precision SWL determination in anechoic and semi anechoic chambers. The volume of the noise source must be less than 0.5% of the volume of the anechoic chamber. The dimensions of the available chamber (4m x 3.5m x 2.5m) were of sufficient magnitude to satisfy this requirement for the size of compressor under investigation. Using precision measuring equipment such as that described in Chapter 2, the SWL was calculated to an accuracy within 1.0 dB.

The compressor was mounted on a combination of foam blocks and chipboard to reduce vibration transmission to the grid metal floor of the chamber. A single microphone was supported using a retort stand and associated clamp, the retort stand was also separated from the floor with foam to reduce vibration transmission.

Before each experiment the compressor was allowed to "warm up" to reach an approximately steady state operating condition. To prevent a significant temperature increase and reduce background noise levels within the anechoic chamber, the air was discharged outside the chamber via a nylon pipe and exhaust silencer.

Four different operating modes were chosen for the initial investigation, namely:

1 Compressor inoperative in order to measure the background noise.
2 Casing pressure 6.5 bar: discharge valve fully open.
3 Casing pressure 10.5 bar: discharge valve partially open.
4 Recirculating: discharge valve fully closed.

In accordance with BS 4196: Part 5 SPL readings were recorded for each operating mode at ten microphone positions over a hemisphere which had its centre at the intersection of the planes which bisect the compressor by length and width, the third plane being the imaginary floor (Fig.3.1). The hemisphere radius (r) was taken as twice the major compressor dimension (2 x 0.7m = 1.4m). The actual microphone positions are stipulated in Table 3.1: the x axis runs parallel to the compressor's axis of rotation, the z axis is perpendicular to the chamber floor. The signals were also recorded on magnetic tape for later spectral analysis. This also allowed the possibility of applying various weightings to the sound data.

Since Hydrovane produce an almost identical compressor (slight alteration of stator bore and slower running speed) it was decided to repeat the complete experiment for the standard compressor air-end driven by the slower four pole (1420 rpm) motor. This would enable any components of noise generation not related to running speed to be detected and therefore confirm those which are speed related.

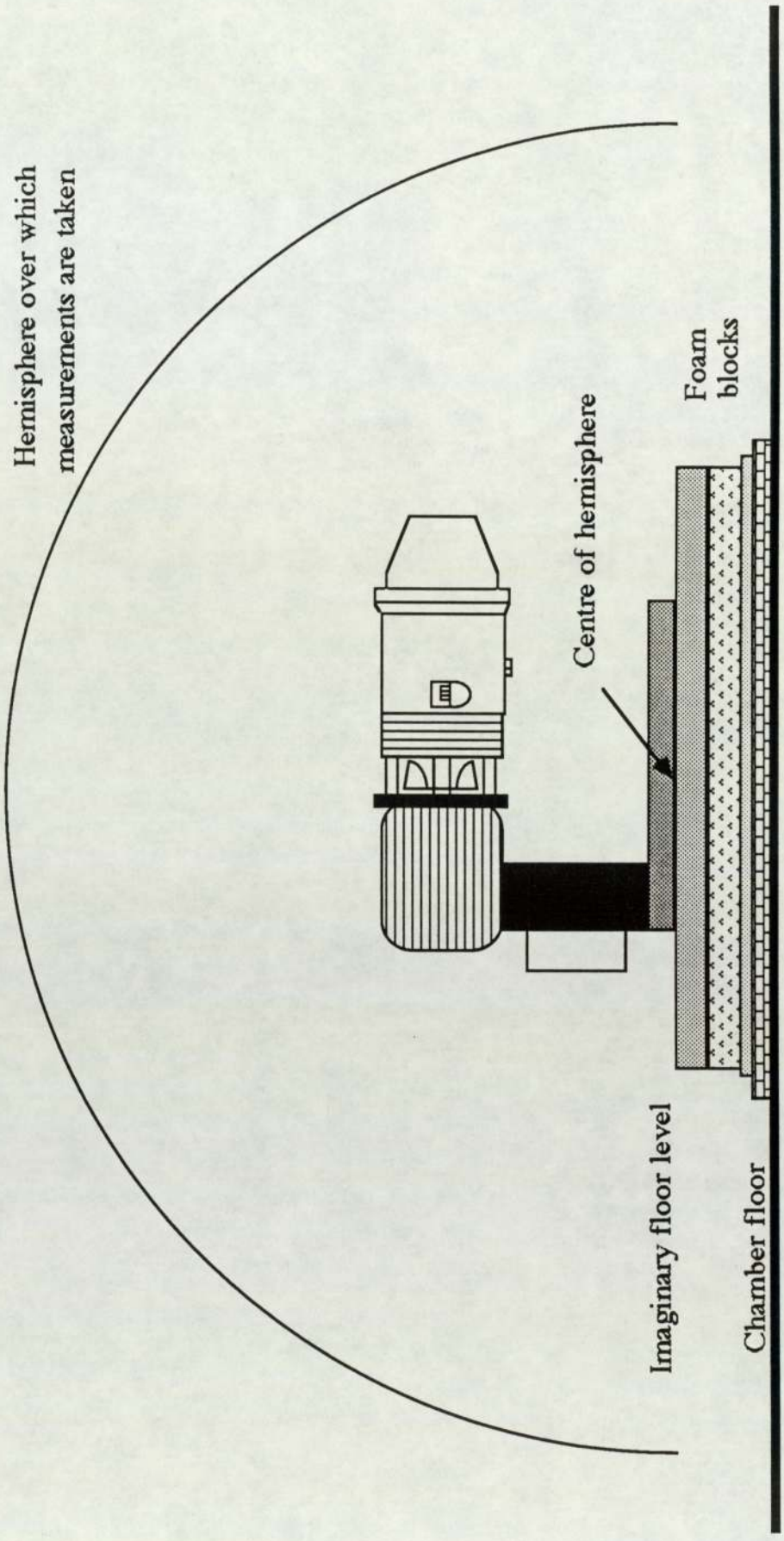

Figure 3.1 Compressor location in anechoic chamber

Table 3.1 Cartesian coordinates of microphone positions

Note : The z-axis is chosen perpendicularly upward from a horizontal plane z = 0 and r is the radius of the hemisphere

No.	$\frac{x}{r}$	$\frac{y}{r}$	$\frac{z}{r}$
1	− 0,99	0	0,15
2	0,50	− 0,86	0,15
3	0,50	0,86	0,15
4	− 0,45	0,77	0,45
5	− 0,45	− 0,77	0,45
6	0,89	0	0,45
7	0,33	0,57	0,75
8	− 0,66	0	0,75
9	0,33	− 0,57	0,75
10	0	0	1,0
11	0,99	0	− 0,15
12	− 0,50	0,86	− 0,15
13	− 0,50	− 0,86	− 0,15
14	0,45	− 0,77	− 0,45
15	0,45	0,77	− 0,45
16	− 0,89	0	− 0,45
17	− 0,33	− 0,57	− 0,75
18	0,66	0	− 0,75
19	− 0,33	0,57	− 0,75
20	0	0	− 1,0

Table 3.2 Distribution of Sound Pressure Levels

Location	SPL at various pressures dB(A)		
	6.5 bar	10.5 bar	Recirculating
1	67.6	69.7	70.9
2	68.4	69.4	70.1
3	67.7	70.1	70.6
4	69.6	71.1	71.7
5	69.0	70.1	70.6
6	67.4	68.9	70.2
7	69.3	70.1	70.3
8	69.2	71.1	72.9
9	68.6	69.9	70.5
10	70.0	70.7	71.5

3.1.1 Calculation of Sound Power Level

Table 3.2 above and Fig.3.18 show the distribution of SPL's for the two pole motor tests. The calculation of overall SWL is as follows.

The sound pressure (p) at each location can be determined from the SPL recorded.

$$SPL\ (dB) = 10\ \log\left[\frac{p^2}{p_{ref}^2}\right]$$

rearranging gives

$$p^2 = p_{ref}^2\left[10^{\frac{SPL}{10}}\right]$$

where $p_{ref} = 2 \times 10^{-5}\ N/m^2$

The intensity (I) at each location, the power per unit area is then calculated as.

$$I = \frac{p^2}{\rho c}$$

where ρc is the acoustic impedance.

It is assumed that these intensities exist over a surface area equal to the surface area of the hemisphere that surrounds the machine, divided by the number of microphone positions. The total power radiated in the hemisphere above the compressor is calculated as the sum of the intensities at all ten locations. It is assumed that only half the power flows through this hemisphere as the measurements were made in a full anechoic chamber (the sound energy radiated below the compressor is

completely absorbed by the chamber floor). Therefore the total intensity figure must be doubled before the sound power (W) is calculated. The sound power is defined as

$$W = 2\frac{4\pi r^2}{2.10}\sum_{1}^{10}\frac{p^2}{\rho c} \quad \text{watts}$$

The SWL is then calculated as

$$SWL\ (dB) = 10\ \log\frac{W}{W_{ref}}$$

where $W_{ref} = 1 \times 10^{-12}$ watts

Substituting the values for linear SPL mesurements into the equations the SWL for the standard compressor was calculated as 86.6 dB. Using the A-weighted SPL measurements the SWL was calculated as 83.6 dB(A). These two values will be used as a basis with which the success of any future modifications can be compared. A reduction in the linear figure of 86.6 dB will measure the physical attenuation achieved, but it is any change in the A-weighted figure of 83.6 dB(A) that signifies the improvement which will be perceived.

3.1.2 Results : Two pole motor

All spectra shown below contain no absolute A-weighted level in dB they simply show the relative dBV values calculated by the spectrum analyser at the different frequencies. Typical noise spectra taken at two microphone locations with the compressor operating at 10.5 bar are shown in Figs.3.2 & 3.3. It can be seen that the lower part of each spectrum (0 to 2 kHz) is dominated by peaks which are all harmonics of the rotational frequency (48 Hz). These include; peaks due to rotor and

motor unbalance (48 Hz) and their harmonics, peaks due to the vane passage frequency (8 x 48 = 384 Hz) and its harmonics and also peaks due to the cooling fan blade passage frequency (10 x 48 = 480 Hz) and its harmonics. A peak also exists at 100 Hz (twice mains frequency) due to magnetostriction i.e. electromagnetic forces on the motor rotor.

A typical spectrum including background noise and covering a larger frequency range (10 kHz) is shown in Fig.3.4. In the higher frequency range the peaks only exist at the harmonics of the vane passage frequency (384 Hz) and they occur strongly up to 8 kHz. To enable a more accurate comparison of noise levels between the different locations and operating modes spectra were plotted over a 5 kHz range. Noise spectra from four different microphone locations and at all three operating modes are shown in Figs.3.5 - 3.16 and are discussed below: the background noise spectrum within the anechoic chamber is shown in Fig.3.17.

Fig.3.18 shows a plot of the measured SPL's at the ten different microphone locations. A comparison of noise levels at 10.5 bar shows that the lowest SPL of 68.9 dB(A) was measured at location 6 and the highest SPL of 71.1 dB(A) at location 8. Since the harmonic peaks related to vane passage frequency must be generated within the air-end, the harmonic content is much stronger at location 8 (Fig.3.15) than at location 6 (Fig.3.12) location 8 being closer to the air-end and with no obstructions. The other interesting point particular to these locations is that there is no peak relating to the cooling fan blade passage frequency (480Hz). This is because the noise propagation path from the cooling fan is shielded by the motor at location 6 and the air-end at location 8.

The microphone positions 4 and 5 on either side of the compressor (Fig.3.18) have SPL's of 71.1 dB(A) and 70.1 dB(A) respectively. The cooling fan blade passage frequency is the most dominant peak at location 5 (Fig.3.9) and also occurs strongly at

location 4 (Fig.3.6). Other cooling fan harmonics (960 Hz and 1920 Hz) occur at both locations. Below 2 kHz the harmonic content from the air-end is slightly higher at location 5 and above 2 kHz it is higher at location 4. The asymmetry and increased stiffness of the casing due to the oil filler plug recess probably accounts for a difference in the noise radiated from opposite sides of the casing.

Slight variation was discovered in the SPL's between the different operating conditions. In all positions, as the casing pressure increased, the SPL increased. The spectra all show an increase in the magnitude of the harmonic peaks. The change in overall SWL as the pressure was increased from 6.5 bar to 10.5 bar was calculated as 82.4 dB(A) to 83.6 dB(A). The increase in SPL at each location level varied between 0.7 dB(A) and 2.2 dB(A). It can be seen that the largest increases in noise levels occur nearer the air-end of the compressor. This was expected since this is the only region where there is any significant change in those operating parameters which affect the noise level.

3.1.3 Results : Four pole motor

Figure 3.19 shows a typical noise spectrum (over 10 kHz) for the compressor operating at 10.5 bar and driven by the four pole motor (1420 rpm). The noise level diminishes rapidly with frequency and there is no significant noise radiation above 4 kHz. The overall SWL was calculated as 76.4 dB(A) ie 7.2 dB(A) lower than when the compressor was driven by the two pole motor. Below 4 kHz the spectrum is dominated by peaks relating to the fundamental rotational frequency (23.7 Hz) and particularly the vane passage frequency (190 Hz). These peaks are very dominant below 2.5 kHz. At two and four pole operating speeds the peaks diminish in the region beyond the 20th harmonic. Comparing a 10 kHz spectrum for the compressor driven by the two pole motor (Fig 3.4) with a 5 kHz spectrum for the compressor driven

by the four pole motor (Fig.3.20), i.e. the same range of harmonics, shows the general shape to be very similar. These results indicate that the noise generation process is identical in both compressors. With the two pole motor the rotational frequency is twice that of the four pole motor and corresponding vibrations are forced at twice the frequency (half the time period) even though they may not be significantly larger in magnitude. An important consequence is that the forcing function is therefore more impulsive which gives rise to the stronger harmonic content exhibited by the spectra.

Spectra from the compressor recorded at the four locations used for the four pole motor are shown in Figs.3.21 - 3.32. In a similar manner to the two pole results, as the delivery pressure increased so did the overall noise level and the magnitude of the harmonic peaks. One major difference is that the compressor driven by the four pole motor showed no significant peaks corresponding to the cooling fan blade passage frequency (240 Hz).

Table 3.3 is a summary of the frequencies at which peaks exist and suggests the probable cause. One important calculation that was necessary at this stage was to determine the relative importance of the peaks and the white noise. This is best shown with a simple example.

For a continuous spectrum in the 100 Hz frequency range shown in Fig.3.33a the white noise is at a level of 70 dB. The corresponding intensity is calculated as 1×10^{-5} W/m^2 (assuming $\rho c = 400$ kg/m^{2}s). If the range is split into one hundred 1 Hz bandwidths the overall intensity is calculated as

$$\text{Total Intensity} = 100 \times 1 \times 10^{-5} = 1 \times 10^{-3} \text{ W/m}^2$$

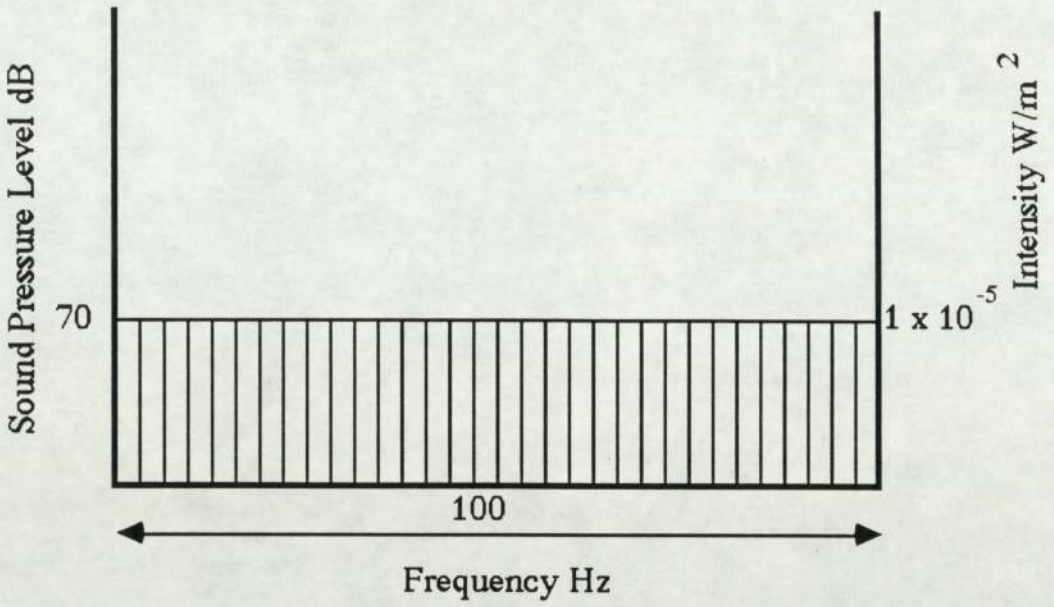

Figure 3.33a Flat spectrum

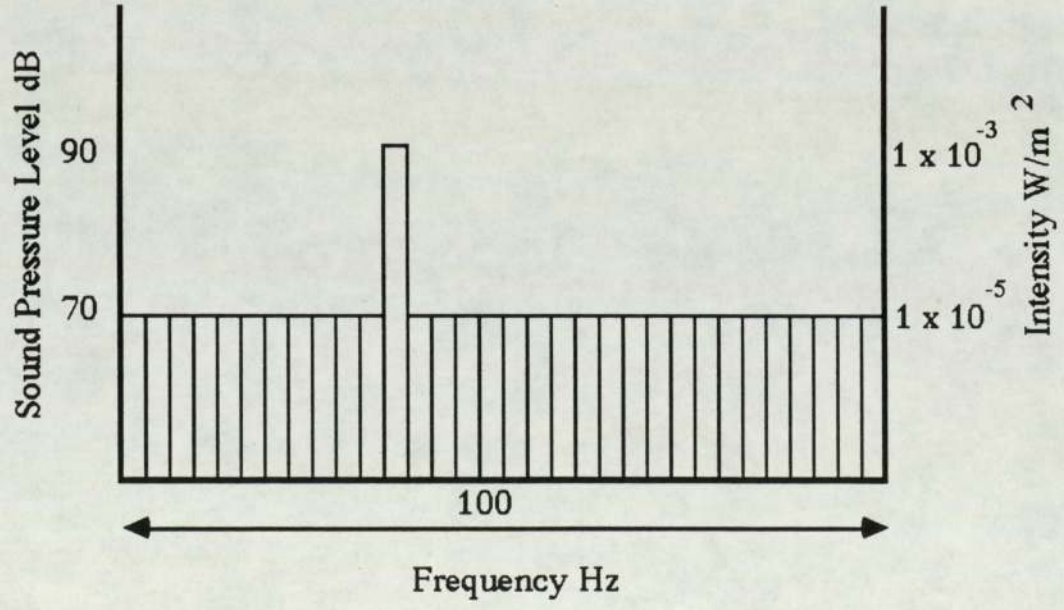

Figure 3.33b Spectrum with single peak

If, now, a single peak of amplitude 20 dB is added over just a 1 Hz bandwidth (Fig.3.33b) the intensity corresponding to this peak is 1×10^{-3} W/m^2 and the new overall intensity is calculated as

$$\text{Total Intensity} = 99 \times 1 \times 10^{-5} + 1 \times 1 \times 10^{-3} = 1.99 \times 10^{-3} \text{ W/m}^2$$

As can be seen this is almost double the original amount and equivalent to a 3 dB increase in white noise across the whole 100 Hz range. However, as mentioned earlier noise reduction is not simply a case of obtaining the lowest physical SWL measurement. Pure tones are considered to be more annoying than broadband white noise that may have a higher overall intensity. This indicates that even though the white noise must not be neglected it is important to concentrate on the individual peaks, since they are tonal and their source will be related to a specific noise generation process.

3.1.4 Noise investigation : Conclusions

The results of this noise investigation are similar to those found by earlier investigations into larger compressors, as outlined in the literature review. They indicate that the noise generation process within the air-end is common to all compressor sizes and powers and dominated by vane passage frequency harmonics. The physical characteristics of the compressor structure and the noise generated by the motor and cooling fan will determine the relative importance of air-end noise for each model.

3.2 Experiments to determine major noise source

The preliminary noise survey reviewed above has shown that the noise spectra are dominated by peaks related to the fundamental

rotational frequency: in particular, harmonics of the vane passage frequency and cooling fan blade passage frequency. In order to achieve a significant reduction in overall noise levels it was necessary to identify the component which contributes most to compressor noise since any improvements must first be applied to this component. The lead shielding technique is difficult to apply successfully to an air compressor as gaps must be provided for the inlet air to the air-end and cooling air for the fan and motor. Therefore, a slightly different technique was used which involved noise measurement for various configurations of the standard compressor components.

The series 15 compressor was split into three main components, the two pole motor, cooling fan and air-end. SPL measurements were taken at the two locations shown in Fig.3.34 for the configurations below-:

1) motor alone,
2) motor and fan,
3) motor and air-end,
4) complete compressor.

The results are shown below in Table 3.4.

Table 3.4 Results of noise measurements

Configuration	SPL dB(A)	SPL dB(A)	SPL(average) dB(A)
Motor (off load)	69.5	70.6	70.1
Motor and Fan	75.4	76.8	76.2
Motor and Air-end	73.7	74.8	74.3
Complete Compressor	77.2	78.5	77.9

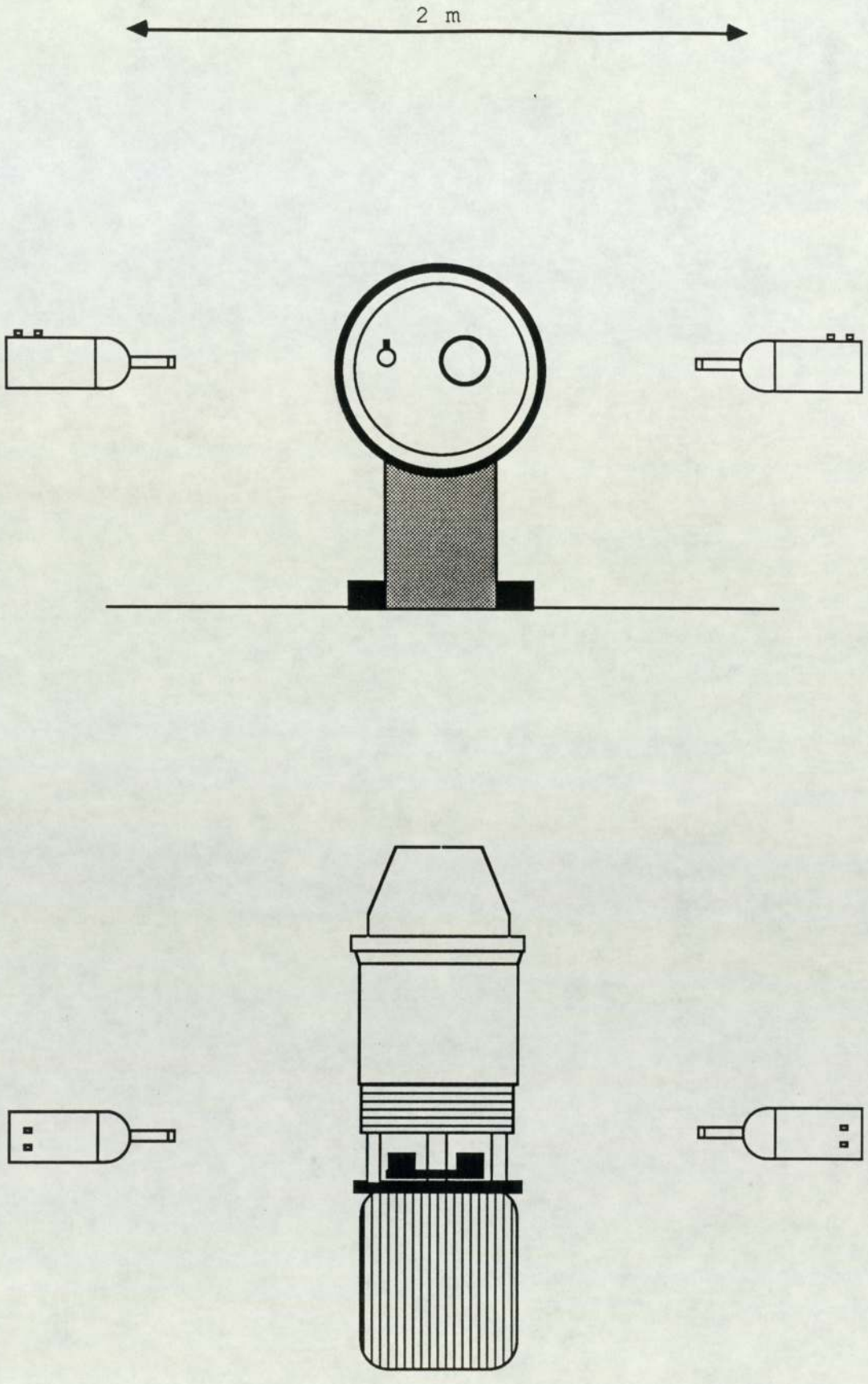

Figure 3.34 Microphone locations either side of compressor

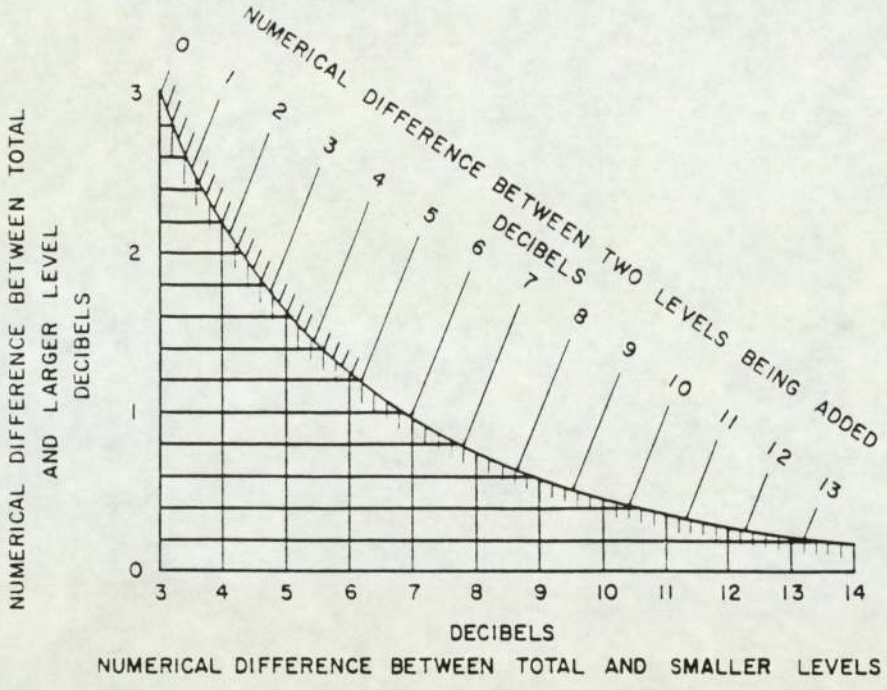

Figure 3.35 Graph showing addition of noise sources

Referring to Fig.3.35 which shows graphically how to calculate the overall SPL when combining two sources of known SPL, it was possible to calculate the contribution from the two pole motor, cooling fan and air-end respectively. It must be emphasised that the motor noise was measured under no load conditions and this figure could be misleading. White and Walker 1986 suggest that a difference of up to 3 dB(A) could be measured between on-load and off-load conditions.

Using the figure of 70.1 dB(A) for the motor and 76.2 dB(A) for the motor and fan combined indicates that the contribution from the fan to be 75.0 dB(A) since the motor is off-load. The motor and air-end combined was measured as 74.3 dB(A) since the motor is operating on-load the contribution of the air-end was calculated in the range 68.2 dB(A) to 72.2 dB(A) based on the 3 dB(A) fluctuation in motor noise quoted above. Summing these three individual components gives an overall SPL of 77.7 dB(A), which, when compared to the measured value of 77.9 dB(A) indicates that approximately 0.2 dB(A) is generated simply by their combination, i.e. noise generated in one part of the

compressor transmitted to another and then radiated more effectively. This quantity is insignificant and could also be accounted for by experimental error and the unknown behaviour of the motor.

This experiment highlighted the fact that in this particular compressor the fan is the dominant noise source. An A-weighted spectrum from the motor and cooling fan is shown in Fig.3.36. The harmonic content and the broadband noise content are significant below 2 kHz and both diminish at higher frequencies. Fan noise is discussed in greater detail in Chapter 8.

3.3 Vibration measurement to determine the dynamic behaviour of compressor structure

An analysis of the dynamic behaviour of the compressor structure during normal operation was necessary to provide more information on the noise generation process. Ten accelerometer locations (Fig.3.37) were used in the experimental program; five were equispaced around the casing and five in identical radial planes on the motor flange. In a similar manner to the noise experiments the compressor was allowed to reach normal operating temperature before measurements were taken. Vibration levels were recorded at the two motor speeds and at each of the operating conditions employed in previous tests, viz.

1) Casing pressure 6.5 bar, discharge valve fully open.
2) Casing pressure 10.5 bar, discharge valve partially open.
3) Recirculating, discharge valve fully closed.

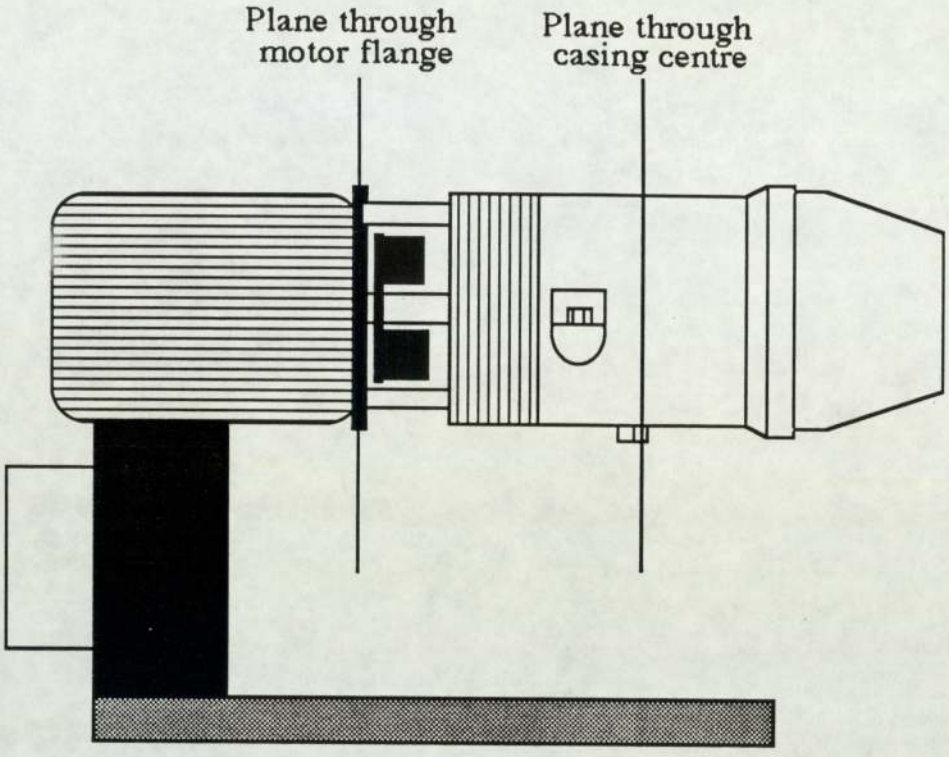

Five equispaced locations in both planes shown above

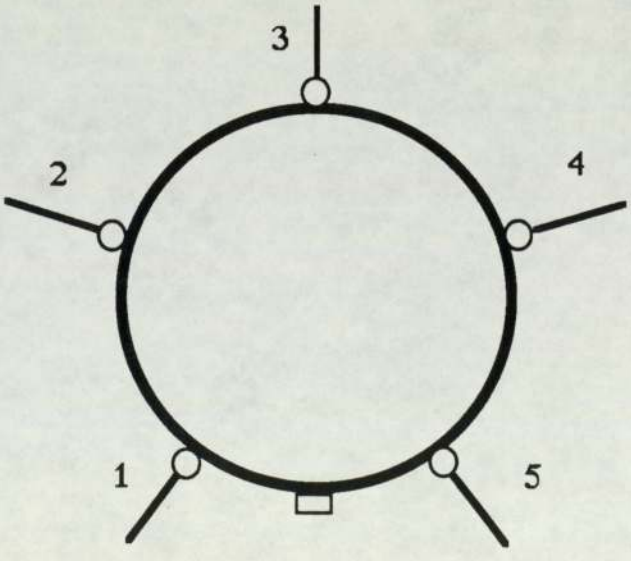

Figure 3.37 Casing and motor accelerometer locations

3.3.1 Casing vibration : Results and discussion

The vibration tests results using the two pole motor are shown for two different operating pressures and at four different locations; two on the casing and two on the motor flange (Figs.3.38 - 3.45)

The spectra are shown over 10 kHz and contain prominent peaks in the range up to 8 kHz that are harmonically related to the vane passage frequency. A comparison between casing and motor spectra (Figs.3.41 & 3.43 respectively) show that below 1 kHz the vibration levels are similar. Above 1 kHz the vibration levels on the motor flange are significantly lower than those on the casing. This is mainly due to the higher stiffness of the motor flange and partly due to the increase in path length from the source of vibration. The increased transmission path length will damp the vibrations particularly at higher frequencies.

For the motor flange there is a fluctuation in the base vibration level but no overall increase with frequency. For the casing spectrum there is a steady increase in the base vibration level with frequency that reaches a maximum at approximately 7 kHz. The height of the peaks above this base level is determined by the location of the transducer and the mode shape of the casing at that particular frequency. If the measurement location is at a nodal point no peak will exist; if the measurement location is at an anti-nodal point then the peak will be a maximum. This is the reason why all the spectra are slightly different in frequency content even though the general shapes are very similar.

The frequency spectra for the casing of the compressor driven by the four pole motor are shown over 10 kHz for the same casing locations and operating modes used previously (Figs.3.46 - 3.49). The peaks at harmonics of the vane passage frequency are particularly dominant below 2.5 kHz. Between 2.5 kHz and 4 kHz peaks can be identified when the casing is at the higher pressure and above 4 kHz no peaks were

visible. These vibration results coincide with the conclusions drawn from the initial noise survey which showed the noise level above 4 kHz had dropped to the background level.

The general shape of the spectra for the compressor driven by the four pole motor did not rise to a maximum at approximately 7 kHz, as had been shown by the two pole motor, but remained relatively level. This indicates that above 4 kHz, there is little forced excitation within the compressor and no substantial vibration transmission to the casing.

In both two and four pole cases there was a slight increase in vibration levels as casing pressure was increased. The magnitude of the harmonic peaks was increased and there was a slight increase in the base vibration level at higher frequencies. This was identical to the results produced earlier by the preliminary noise investigation.

These results have indicated that radiation from the casing is the main source of noise from the compressor air-end. Further proof was required to show whether or not this was the case over the complete frequency spectrum.

The radiation of noise from any surface is a function of frequency. The two factors related to frequency which determine the radiated noise are the surface vibratory velocity levels and the radiation efficiency of the surface. The surface vibration levels are dependant on the forcing function and the dynamic characterictics of the structure. To determine the surface vibratory velocity levels as a function of frequency it is necessary to integrate the acceleration signal. For a frequency spectrum of the vibratory acceleration levels this is equivelant to dividing the magnitude at each frequency by the frequency. When the casing was driven by the two pole motor the prediction of vibratory velocity levels had the effect of flattening out the base vibration levels and reducing the magnitude of the peaks.

The radiation efficiency is also a function of frequency. It is unity above the critical frequency of the surface and reduces from unity below the critical frequency. The critical frequency of the surface depends on the geometrical properties of the vibrating medium and the material properties of both vibrating medium and the medium that surrounds it.

Assuming the casing to be a thin cylinder the critical frequency was calculated in Chapter 1 as 2.9 kHz. If the casing is the major source of noise radiation then a spectrum obtained by subtracting the effects that an increase of frequency has on a surface's radiation efficiency from a casing vibratory velocity spectrum should show a similar pattern to a noise spectrum.

This has been done manually for two casing vibration spectra and the result is shown in Figs.3.50 & 3.51. A comparison of this spectrum to a noise spectrum (Fig.3.4) shows that the harmonic content of the actual radiated noise is very similar to the expected noise levels calculated and clearly indicates that casing vibration is the main source of noise. However, below 2 kHz the white noise content of these spectra are not at all similar. The higher levels on the actual spectrum are probably due to cooling fan turbulence, which generates a high broadband noise level in the 1 kHz to 2 kHz region. A cooling fan noise spectrum is shown in Fig.3.36 which shows the high noise levels in this frequency range.

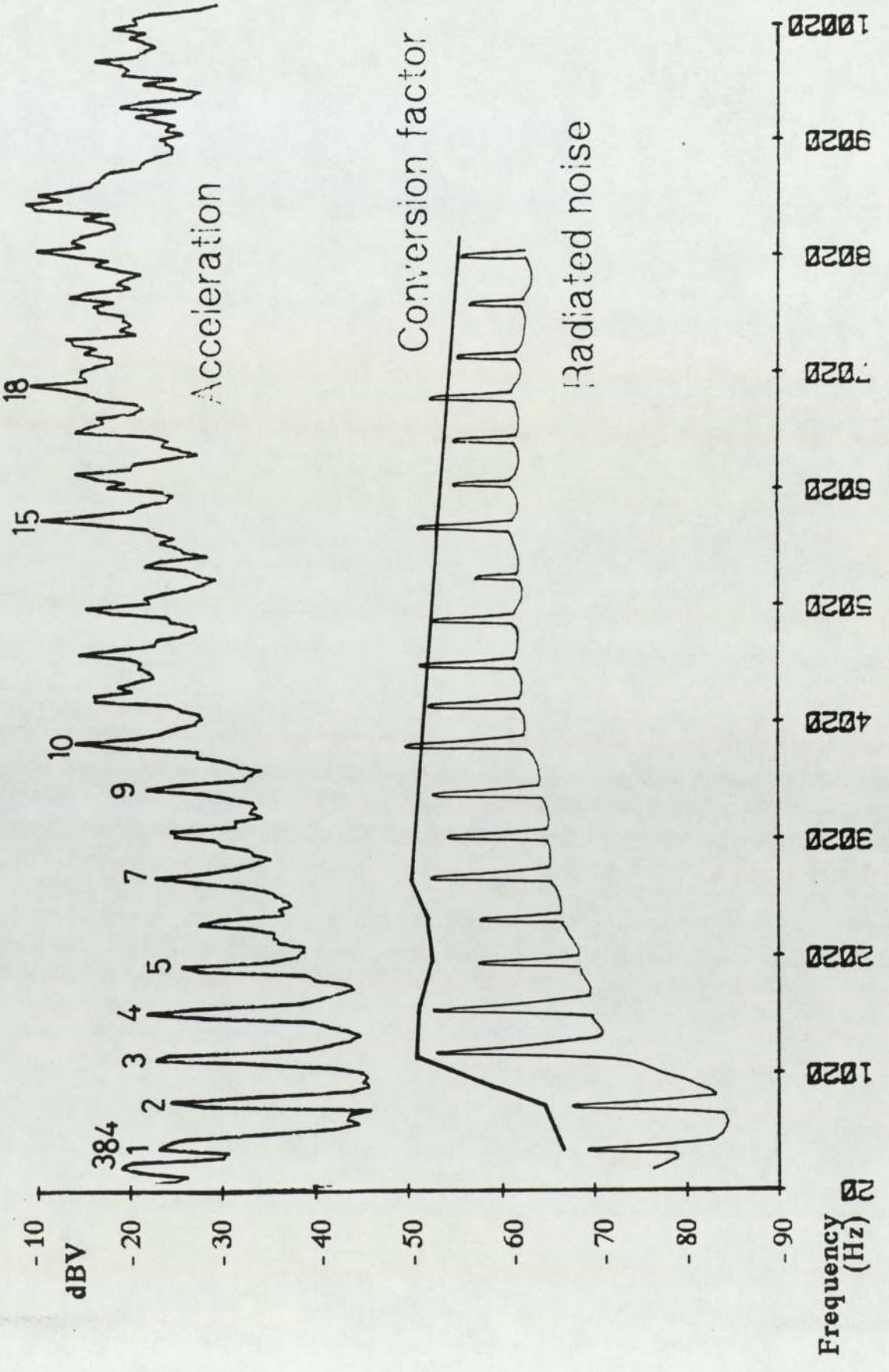

Figure 3.50 Manual conversion from acceleration to radiated noise

Figure 3.51 Manual conversion from acceleration to radiated noise

3.4 Review of the initial noise and vibration survey

The main conclusions drawn from this initial work are as follows: With respect to reducing noise in all Hydrovane compressors the main problem occurs at rotor vane passage frequency and its harmonics. The experimental work has shown that these harmonics predominate the radiated noise spectra which are very similar in frequency content to the casing vibration spectra. The investigation into compressor noise has also shown that noise radiated from the air-end due to casing vibration is a major source. It was therefore necessary to gain a greater understanding of the source of casing vibration.

Cooling fan noise was also seen as a particular problem with the two pole compressor; it was identified as the noisiest of the three components (75.0 dB(A) compared with a maximum of 72.2 dB(A) for the air-end and 73.1 dB(A) for the motor) and is responsible for much of the broadband noise which has been shown to be a problem below 2 kHz. The peak corresponding to fan blade passage frequency was also predominant at locations either side of the compressor.

It is at this point that some explanation must be made as to the sequence of further contents of this thesis. Three distinct aspects require further investigation and at this stage the path branches into three routes. A theoretical investigation, utilising modal analysis was used to determine whether there were any resonance type problems within the compressor structure and is explained in Chapter 4. The investigation into the source of casing vibration was considered most important since the fundamental sliding vane operation relates to all compressors and this is dealt with in Chapters 5, 6 & 7 which all follow directly on from each other. Finally, Chapter 8 deals with the cooling fan noise problem that is particular to the high operating speed of the series 15 compressor.

Table 3.3 Summary of important peaks

Two pole frequency	Probable cause	Four pole frequency
100	Magnetostriction	100
200	2nd harmonic of magnetostriction	200
384	Vane passage frequency	192
480	Cooling fan frequency	---
672	Motor fan frequency	336
768	2nd harmonic of vane passage	---
864	?	---
960	2nd harmonic of cooling fan + interference of blades and fixed supports	---
1152	3rd harmonic of vane passage	576
---	Harmonic of rotation	672
1536	4th harmonic of vane passage	768
---	?	864
1920	5th harmonic of vane passage	960
2304 2692	Higher harmonics	1536 1728 1920

Figure 3.2 Noise spectrum at 10.5 bar, location 4, 2 pole

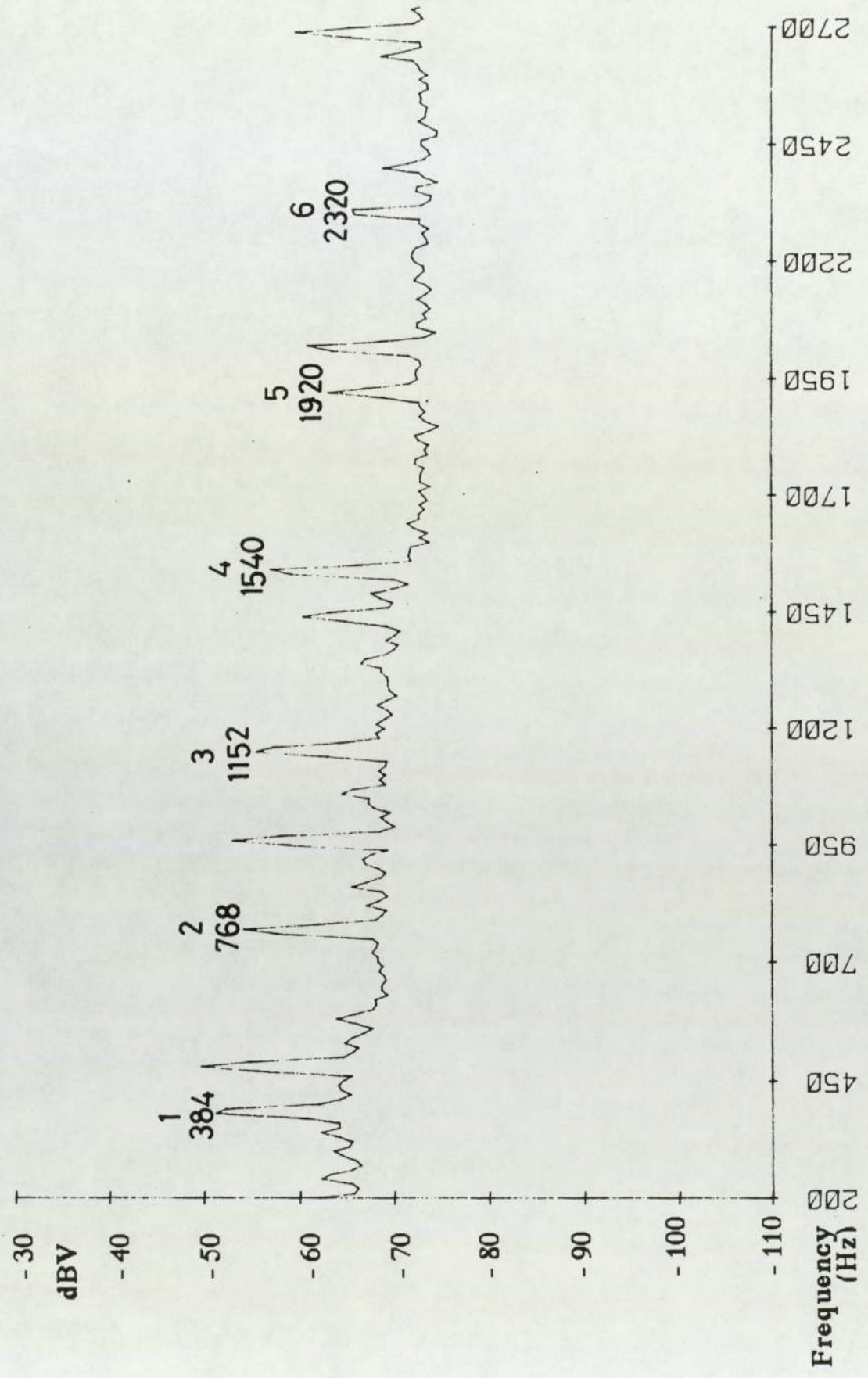

Figure 3.3 Noise spectrum at 10.5 bar, location 5, 2 pole

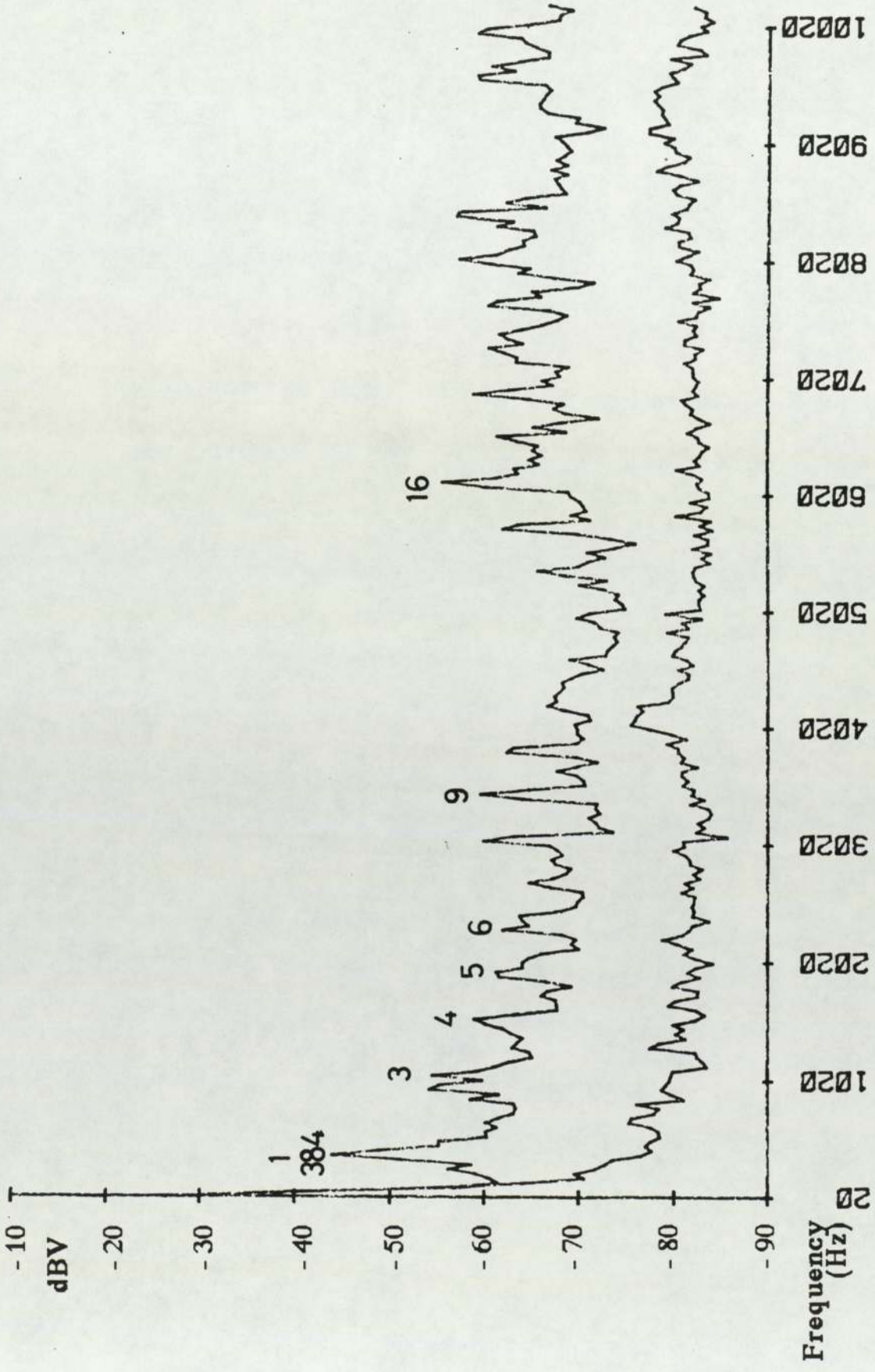

Figure 3.4 Noise spectrum at 10.5 bar against background for 2 pole motor

Figure 3.5 Noise spectrum at 6.5 bar, location 4, 2 pole

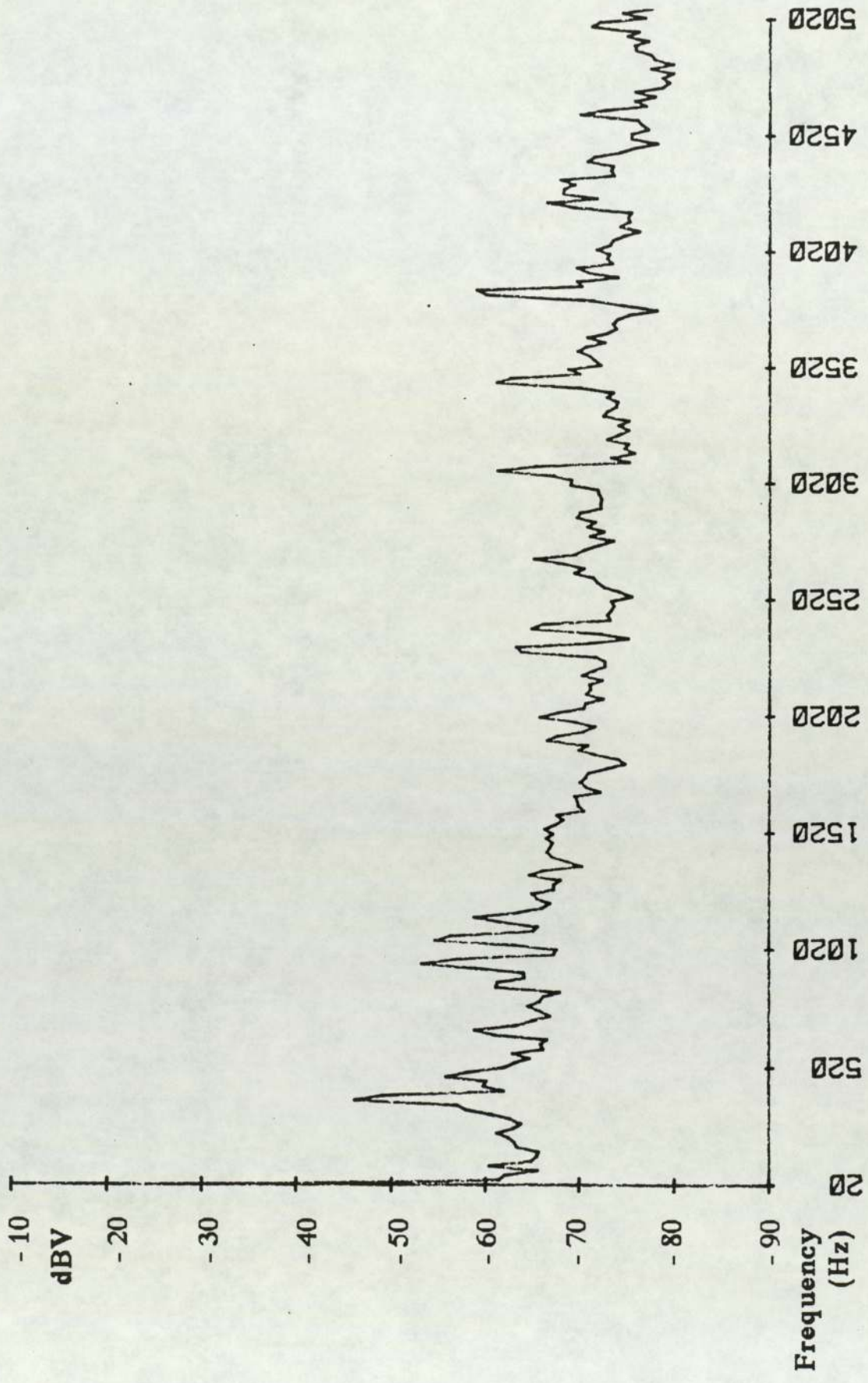

Figure 3.6 Noise spectrum at 10.5 bar, location 4, 2 pole

Figure 3.7 Noise spectrum recirculating, location 4, 2 pole

Figure 3.8 Noise spectrum at 6.5 bar, location 5, 2 pole

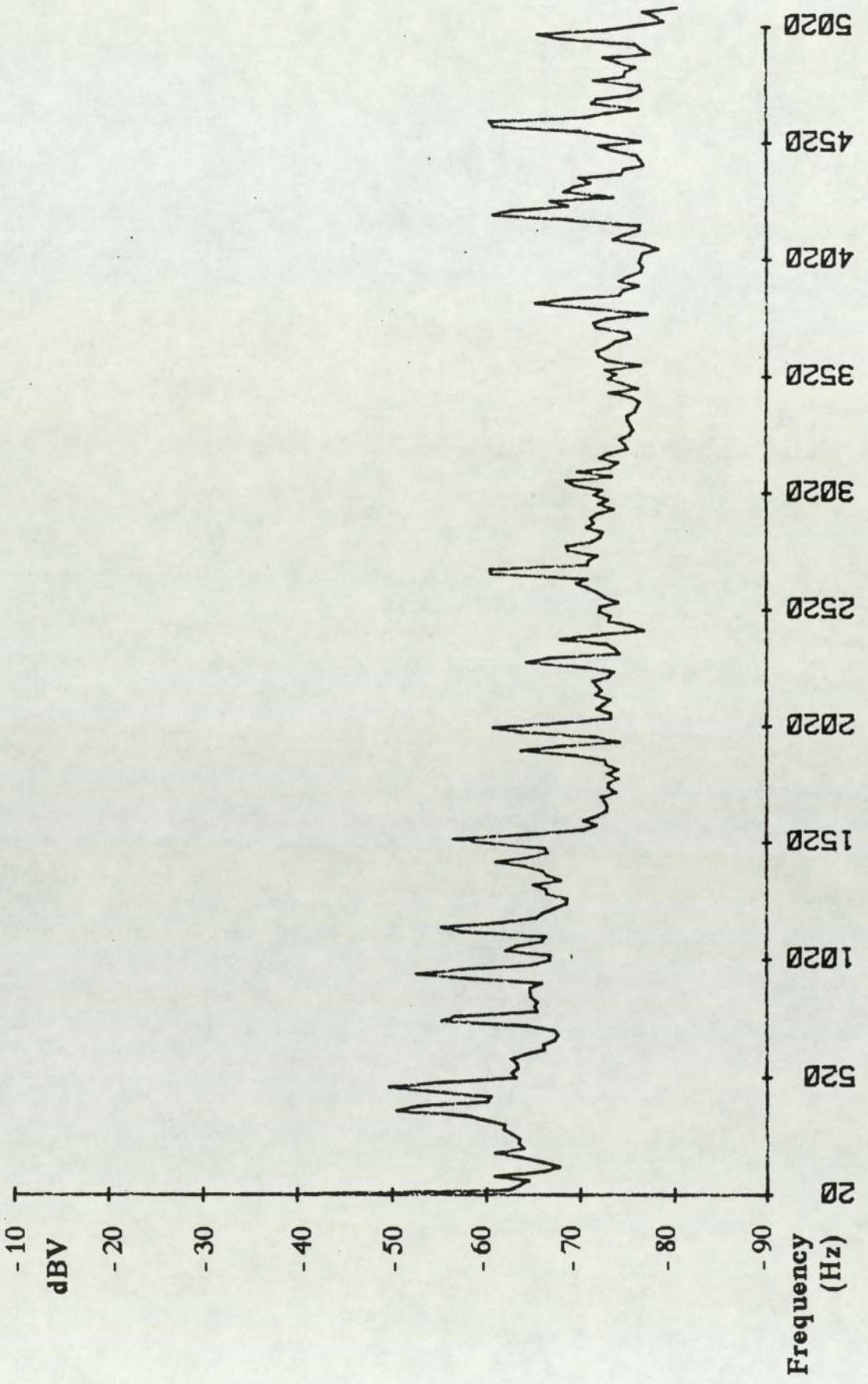

Figure 3.9 Noise spectrum at 10.5 bar, location 5, 2 pole

Figure 3.10 Noise spectrum recirculating, location 5, 2 pole

Figure 3.11 Noise spectrum at 6.5 bar, location 6, 2 pole

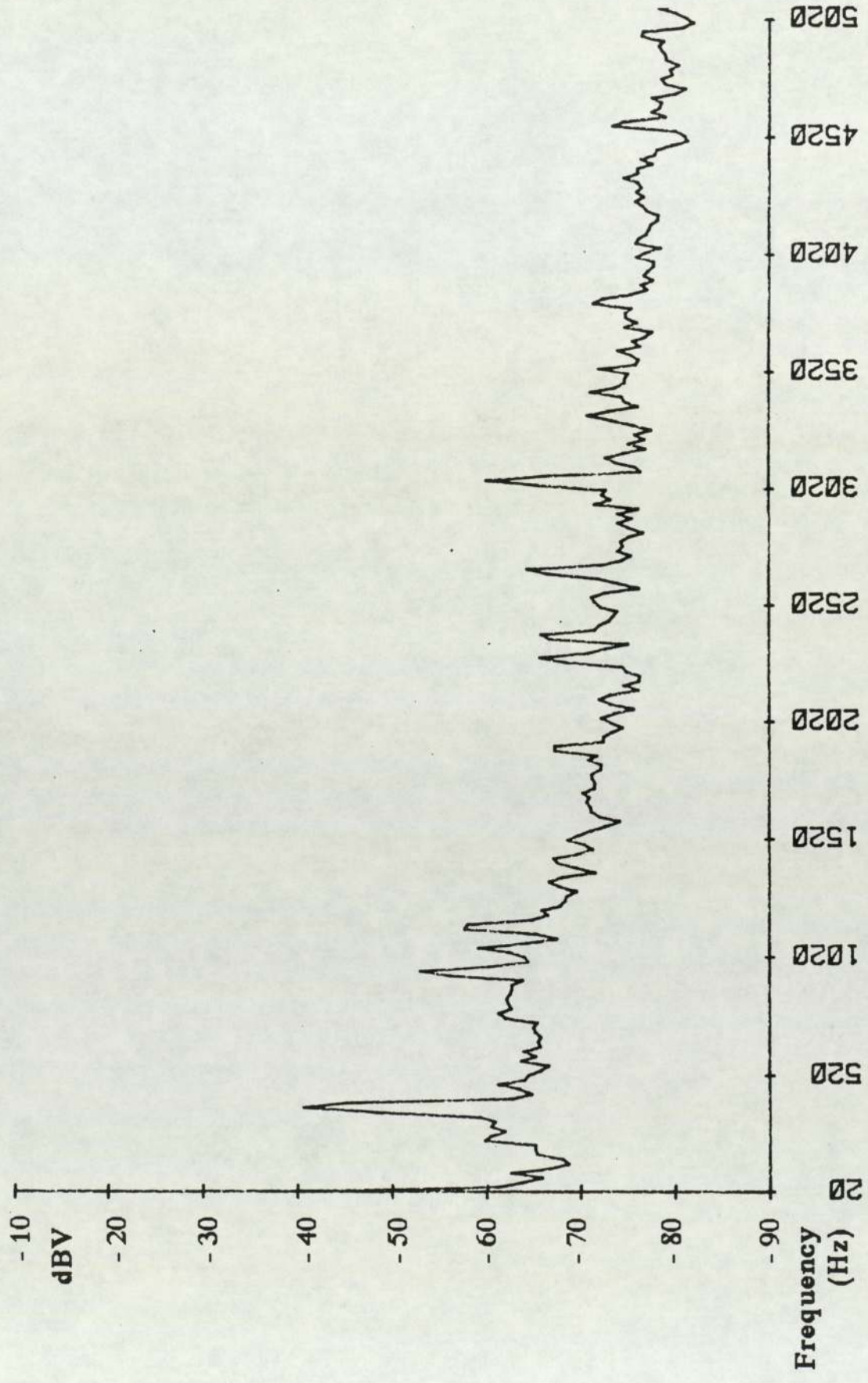

Figure 3.12 Noise spectrum at 10.5 bar, location 6, 2 pole

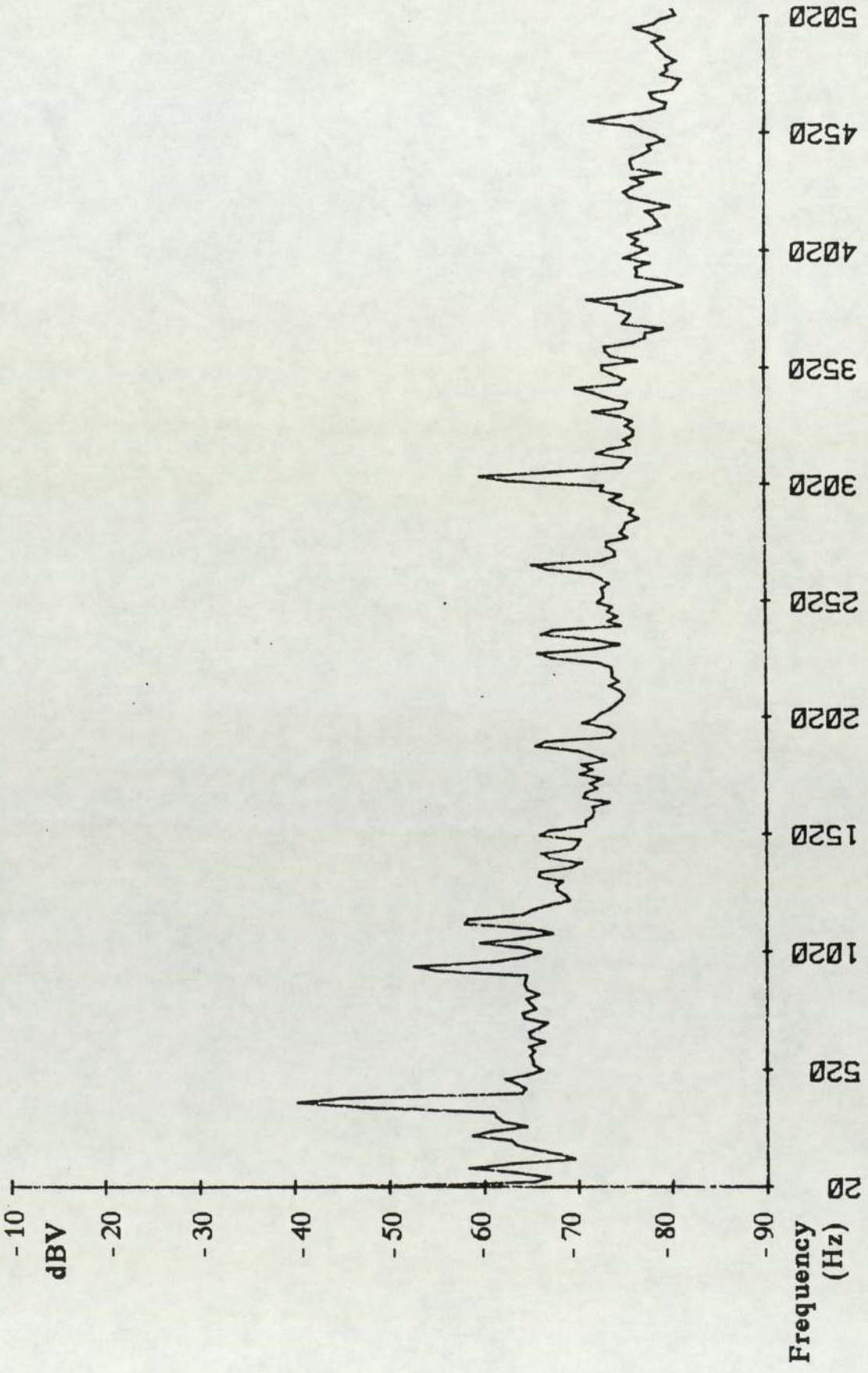

Figure 3.13 Noise spectrum recirculating, location 6, 2 pole

Figure 3.14 Noise spectrum at 6.5 bar, location 8, 2 pole

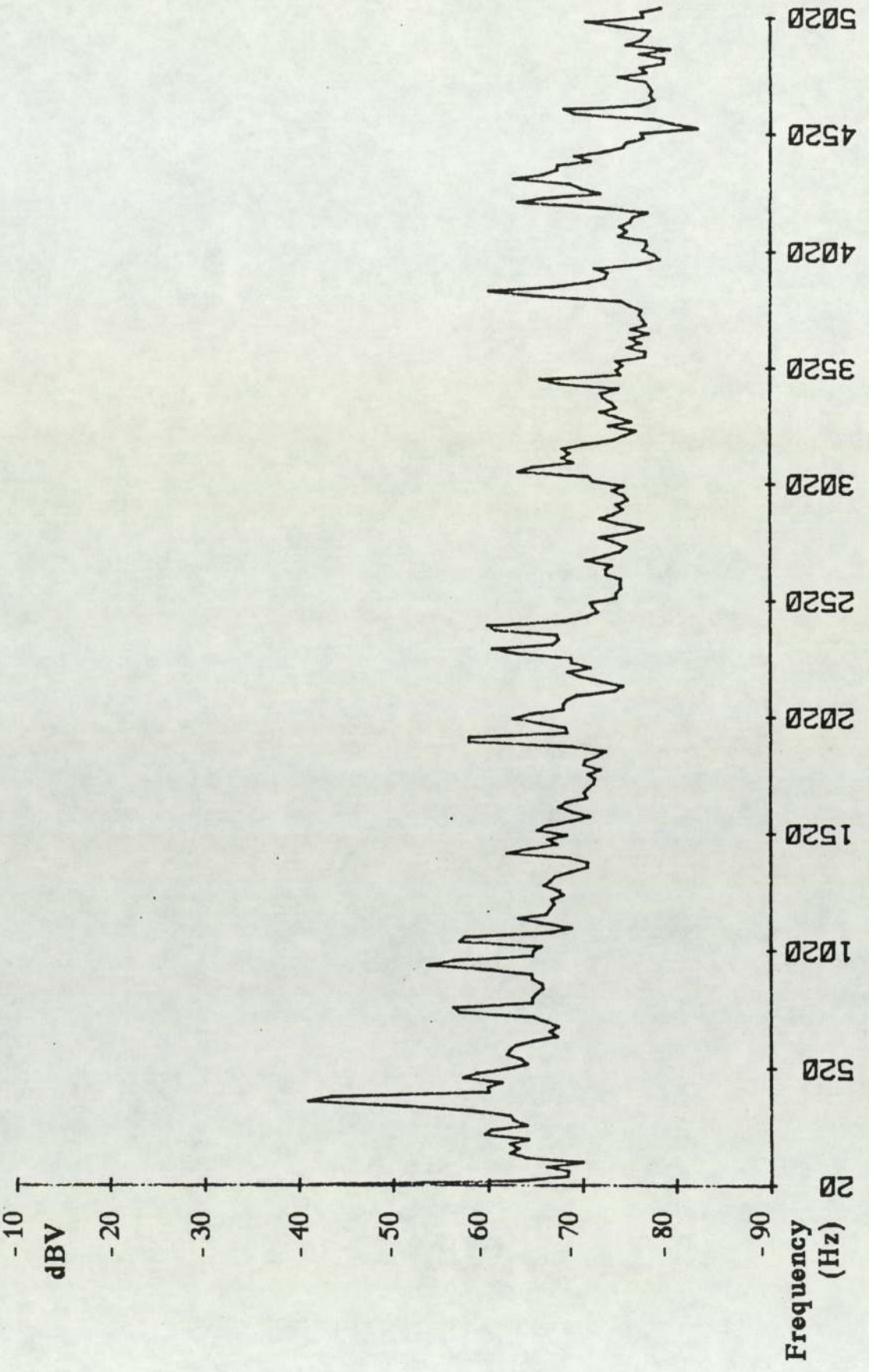

Figure 3.15 Noise spectrum at 10.5 bar, location 8, 2 pole

Figure 3.16 Noise spectrum recirculating, location 8, 2 pole

Figure 3.17 Background noise spectrum (5 kHz)

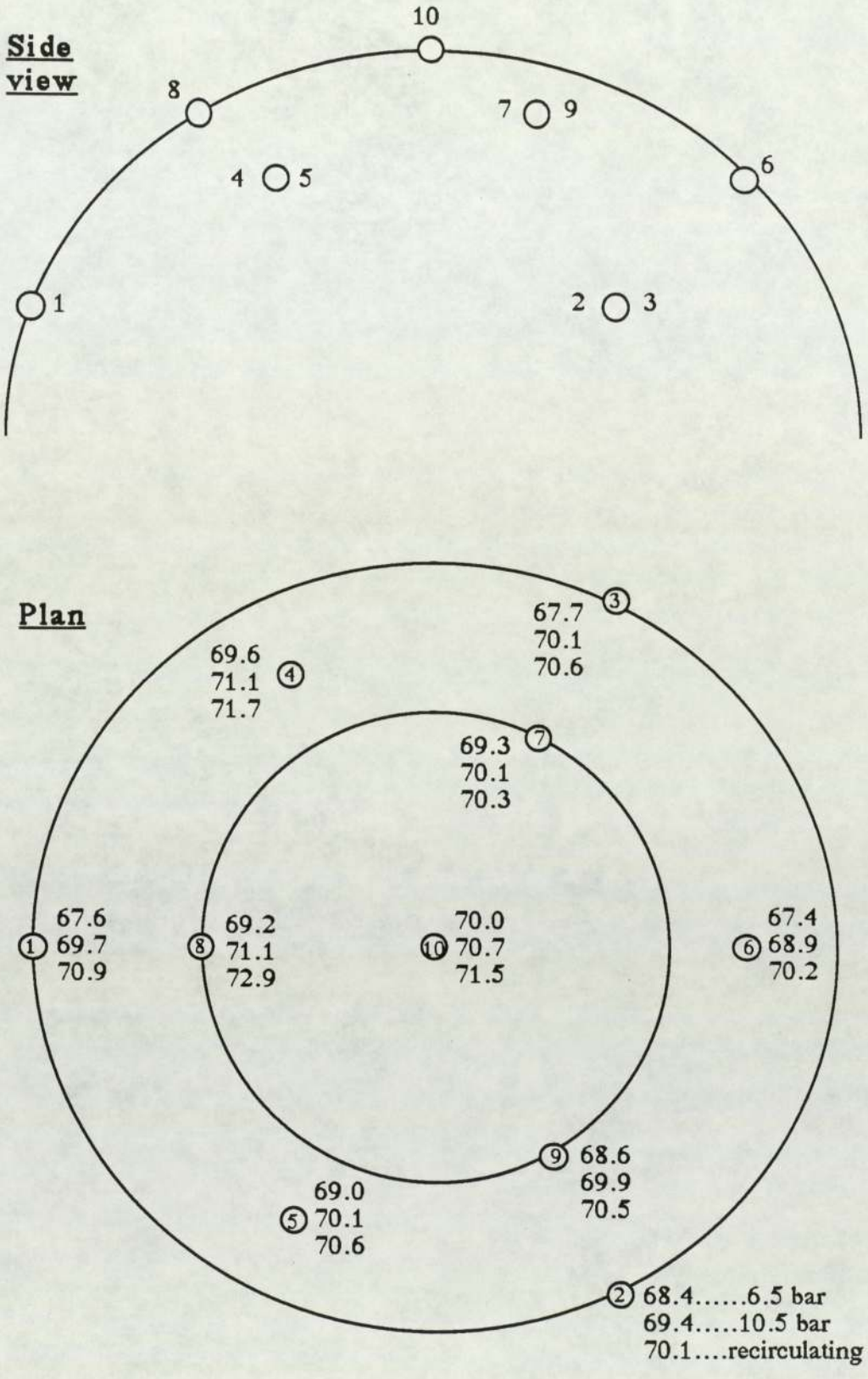

Figure 3.18 Measurement locations and SPL results on hemisphere surrounding compressor

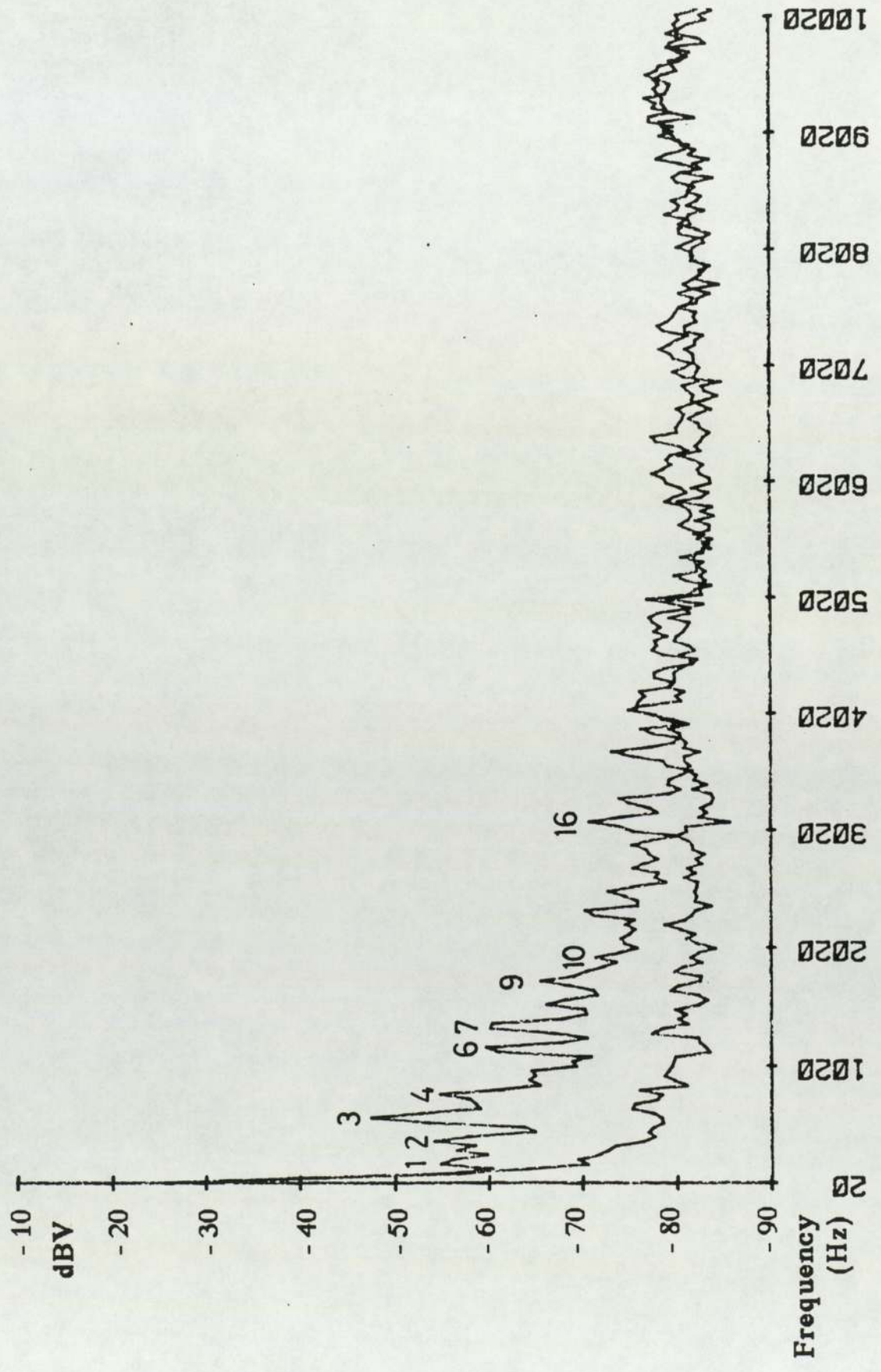

Figure 3.19 Noise spectrum at 10.5 bar against background, Four pole motor

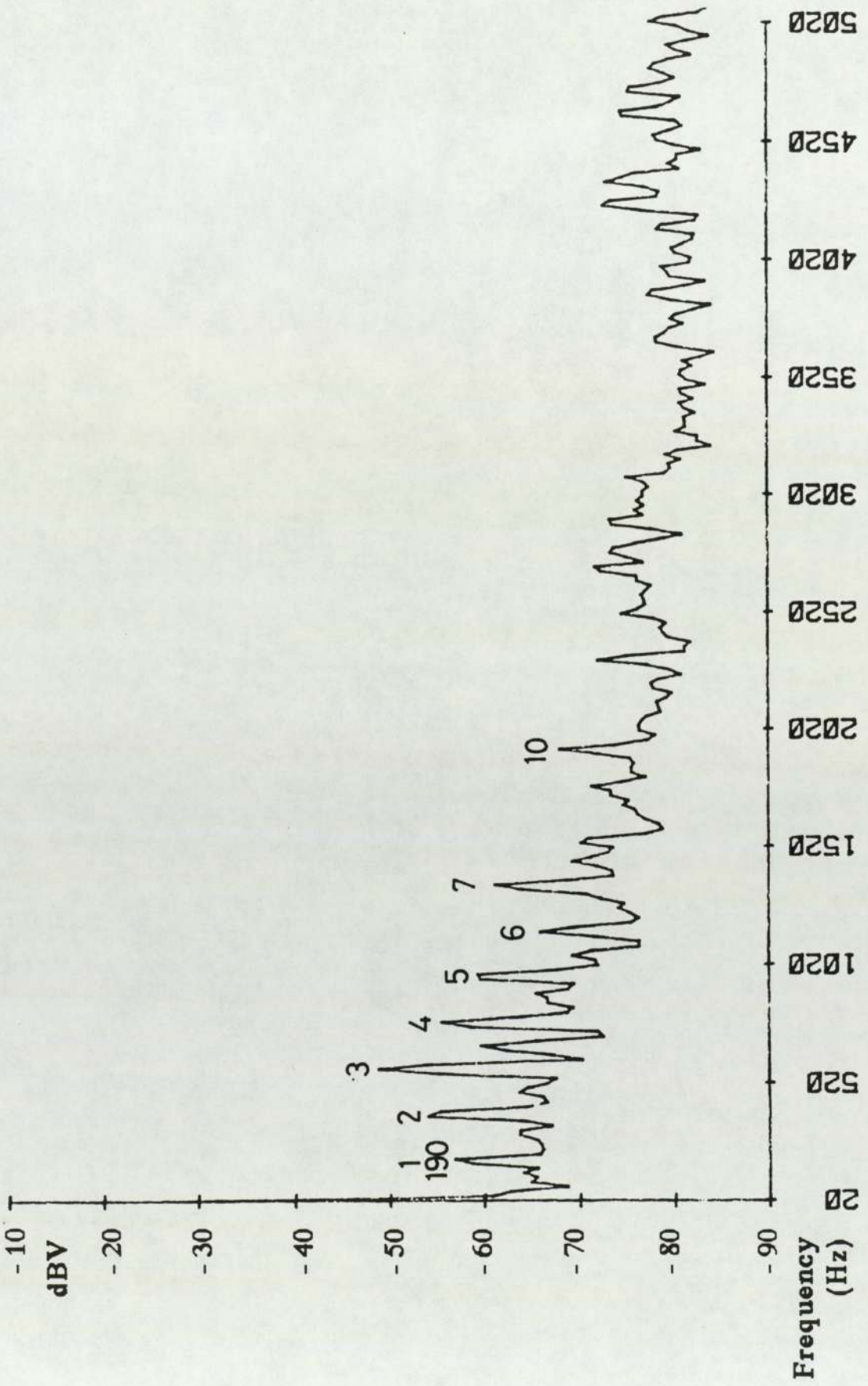

Figure 3.20 Noise spectrum at 10.5 bar, (5 kHz), 4 pole

Figure 3.21 Noise spectrum at 6.5 bar, location 4, 4 pole

Figure 3.22 Noise spectrum at 10.5 bar, location 4, 4 pole

Figure 3.23 Noise spectrum recirculating, location 4, 4 pole

Figure 3.24 Noise spectrum at 6.5 bar, location 5, 4 pole

Figure 3.25 Noise spectrum at 10.5 bar, location 5, 4 pole

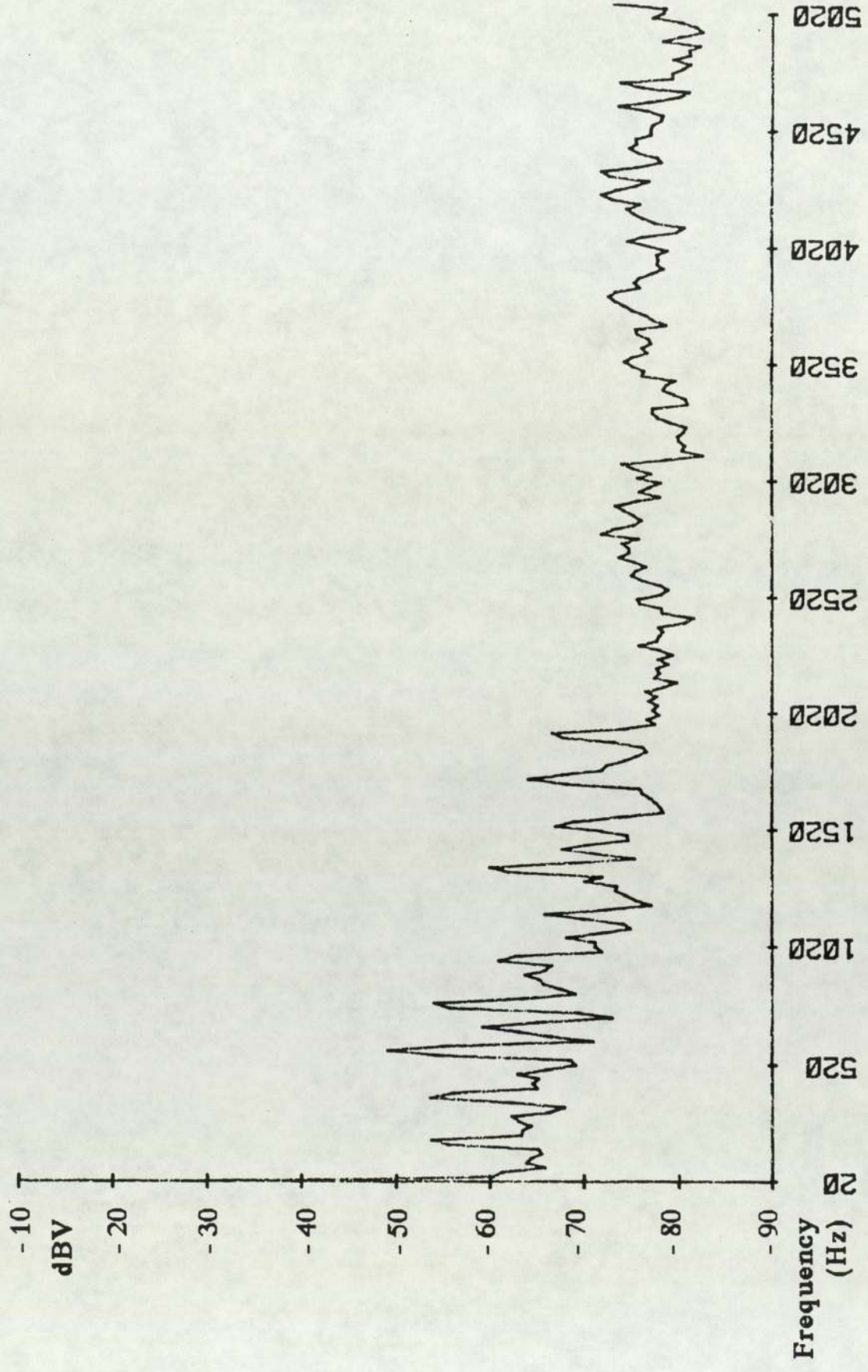

Figure 3.26 Noise spectrum recirculating, location 5, 4 pole

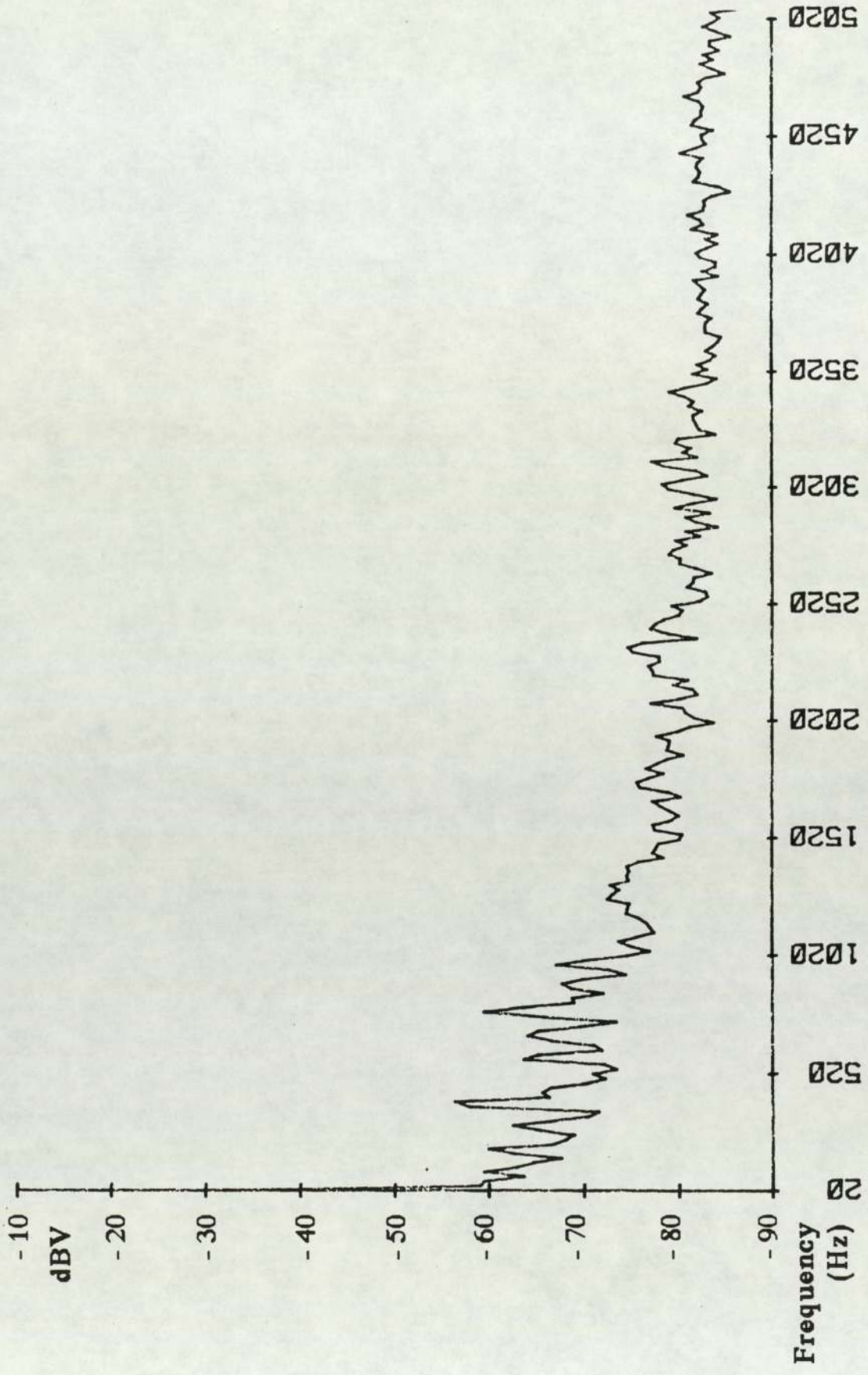

Figure 3.27 Noise spectrum at 6.5 bar, location 6, 4 pole

Figure 3.28 Noise spectrum at 10.5 bar, location 6, 4 pole

Figure 3.29 Noise spectrum recirculating, location 6, 4 pole

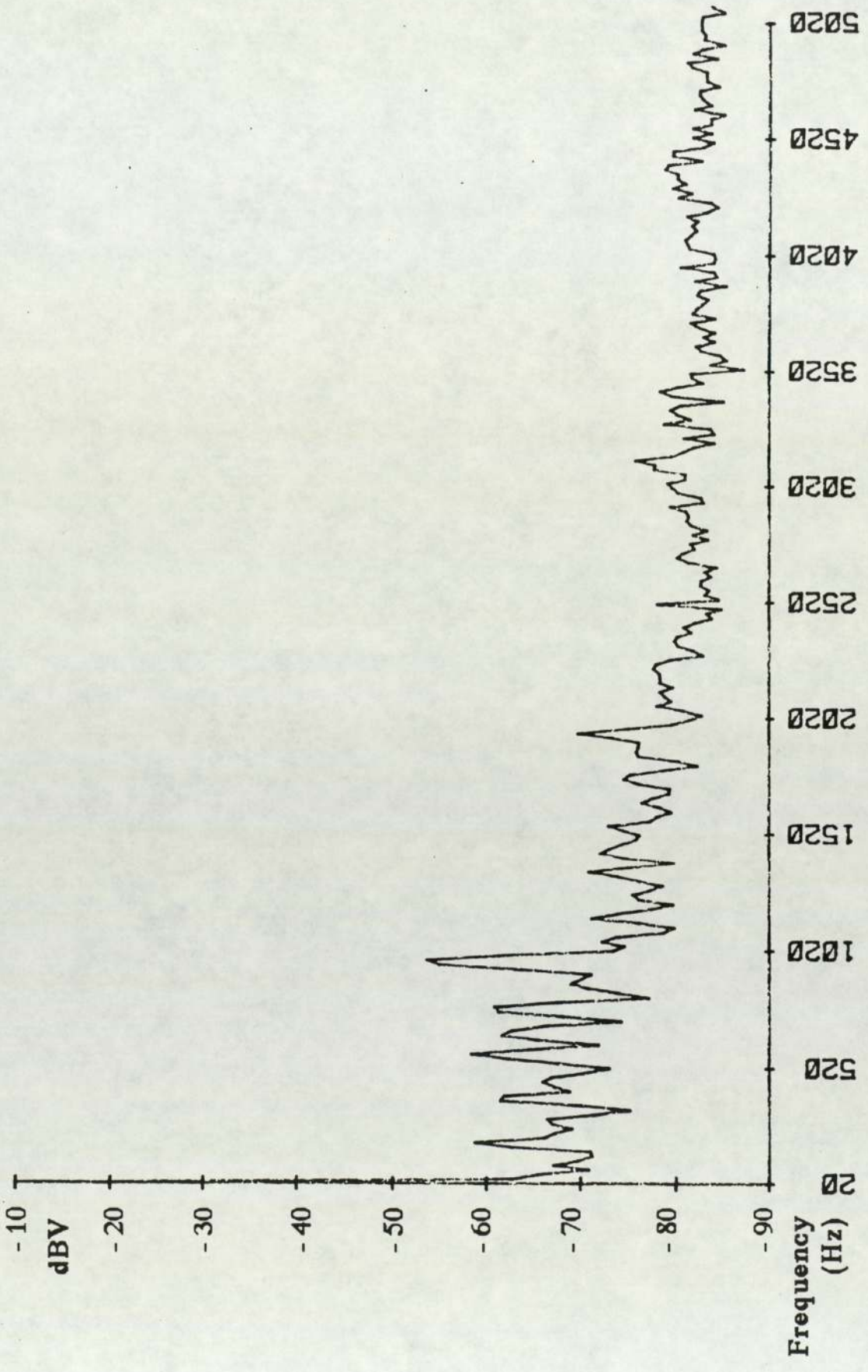

Figure 3.30 Noise spectrum at 6.5 bar, location 8, 4 pole

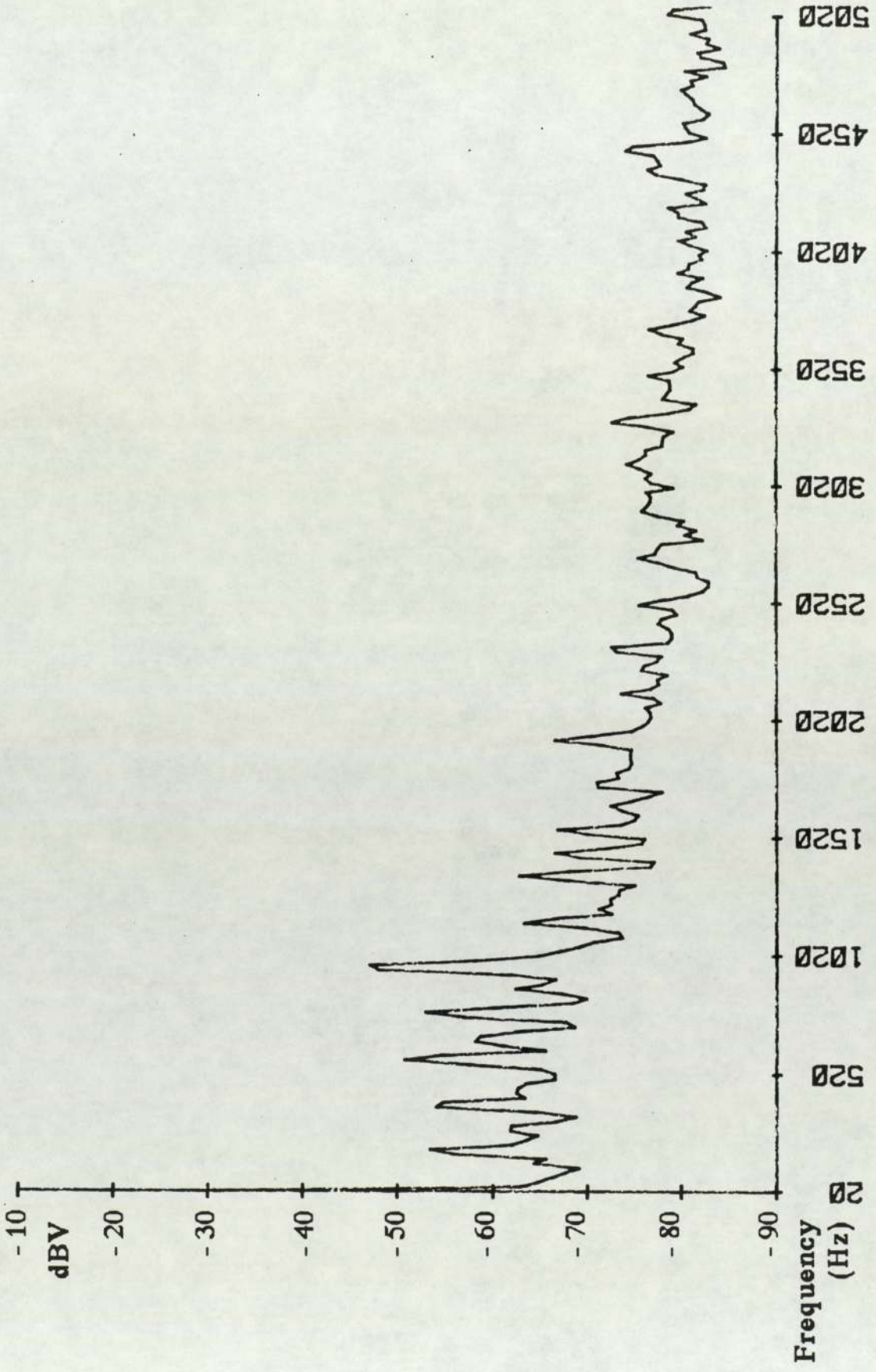

Figure 3.31 Noise spectrum at 10.5 bar, location 8, 4 pole

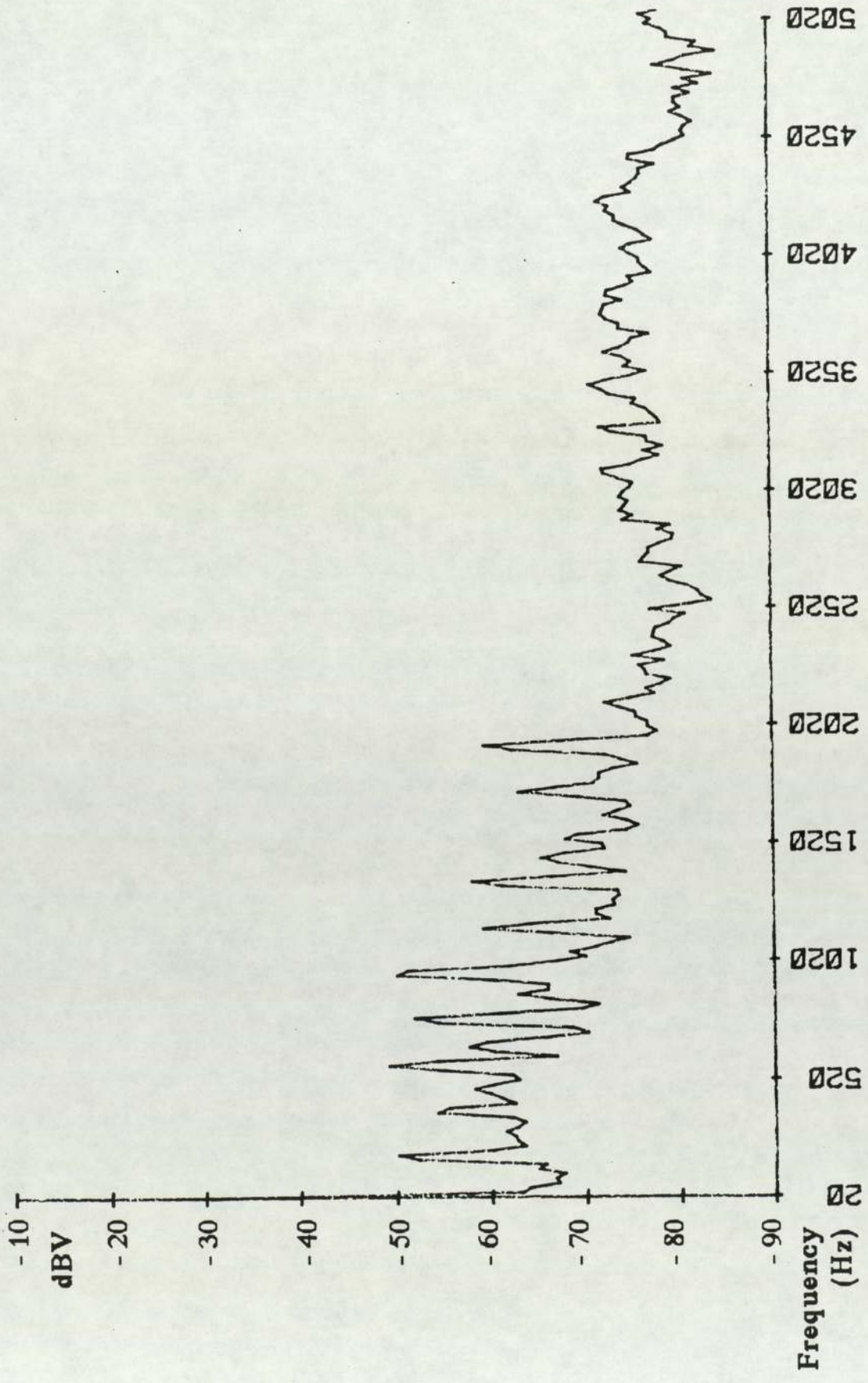

Figure 3.32 Noise spectrum recirculating, location 8, 4 pole

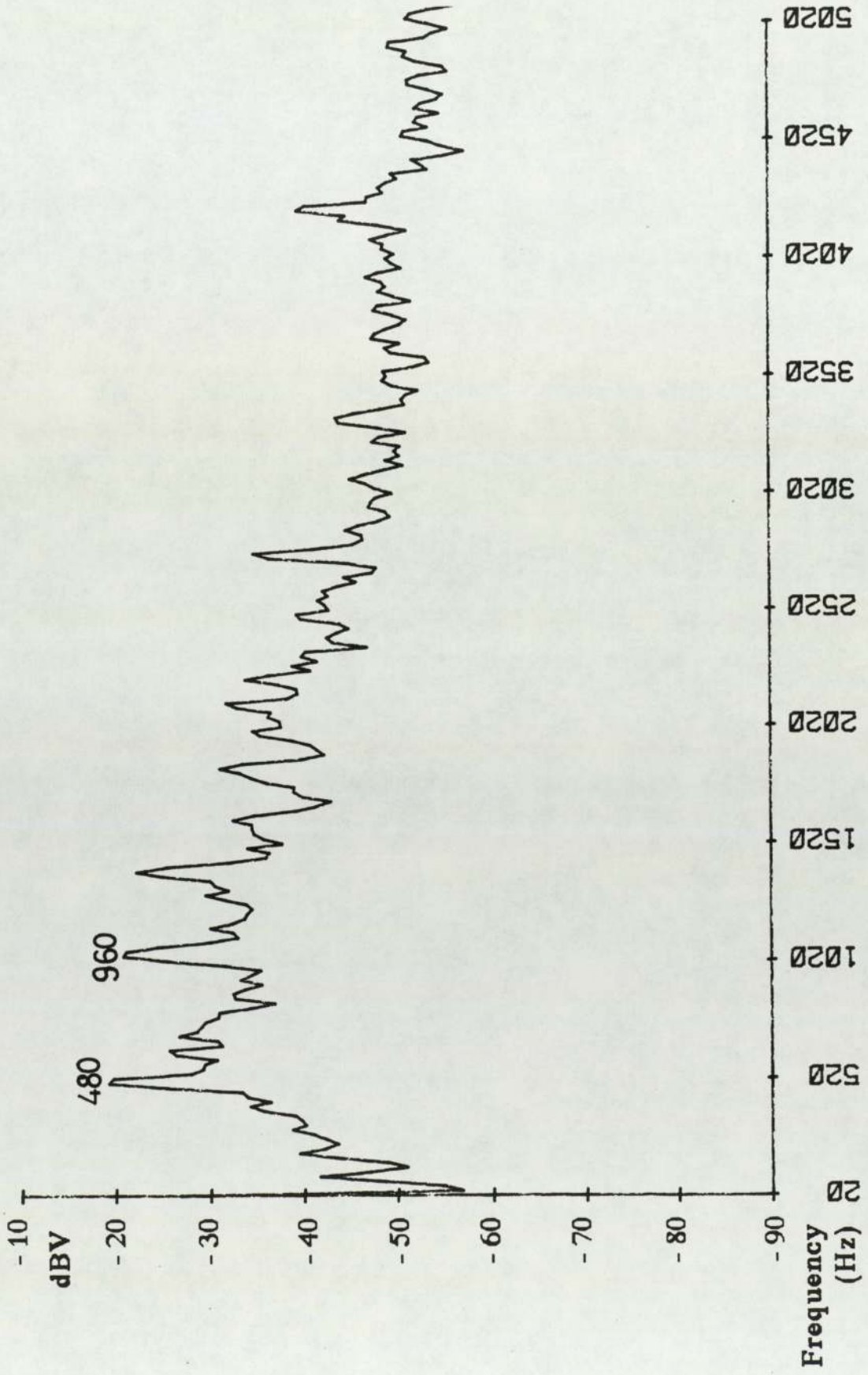

Figure 3.36 Noise spectrum from motor and cooling fan

Figure 3.38 Casing vibration spectrum at 6.5 bar at location 2, 2 pole

Figure 3.39 Casing vibration spectrum at 10.5 bar at location 2, 2 pole

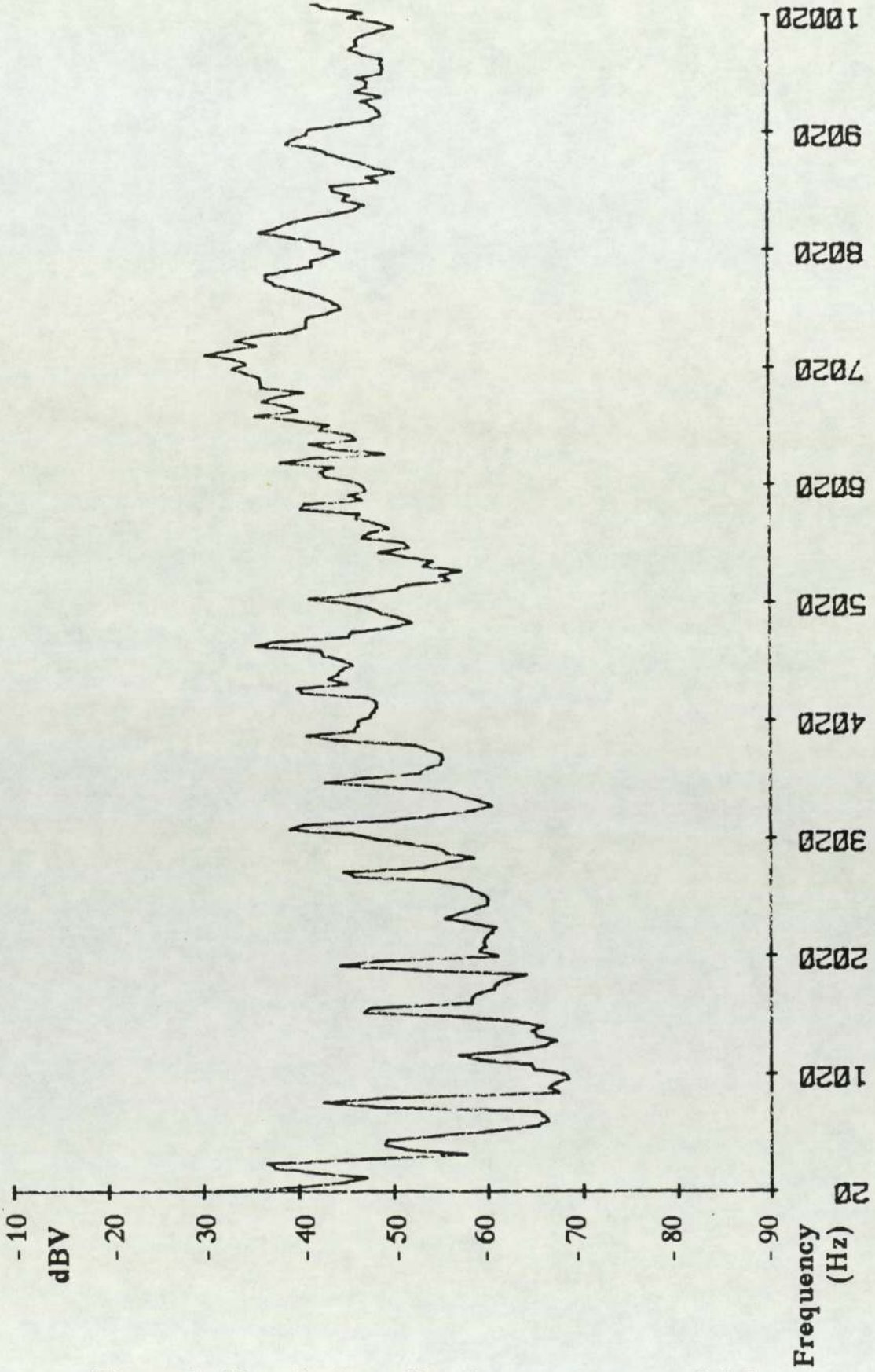

Figure 3.40 Casing vibration spectrum at 6.5 bar at location 4, 2 pole

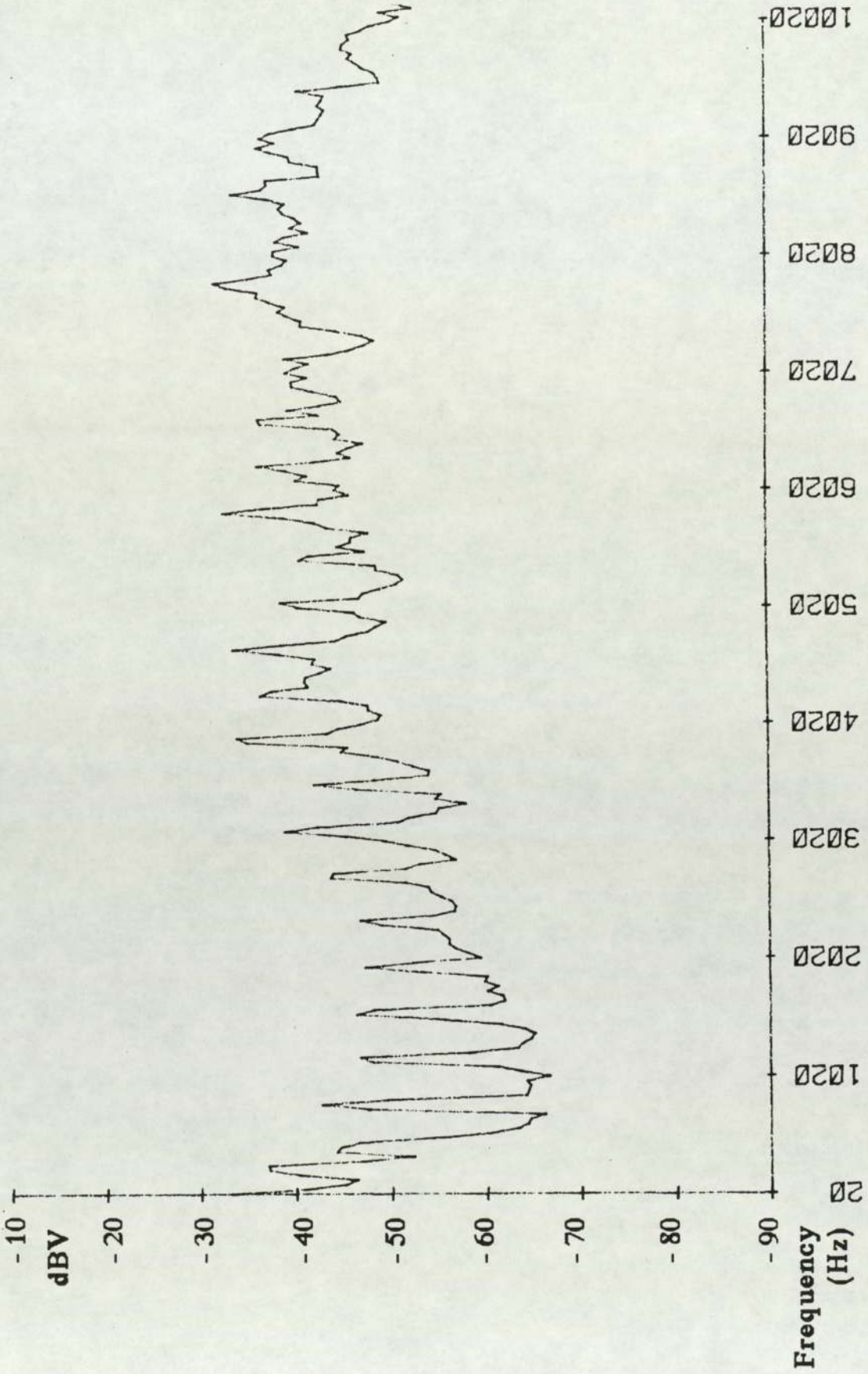

Figure 3.41 Casing vibration spectrum at 10.5 bar at location 4, 2 pole

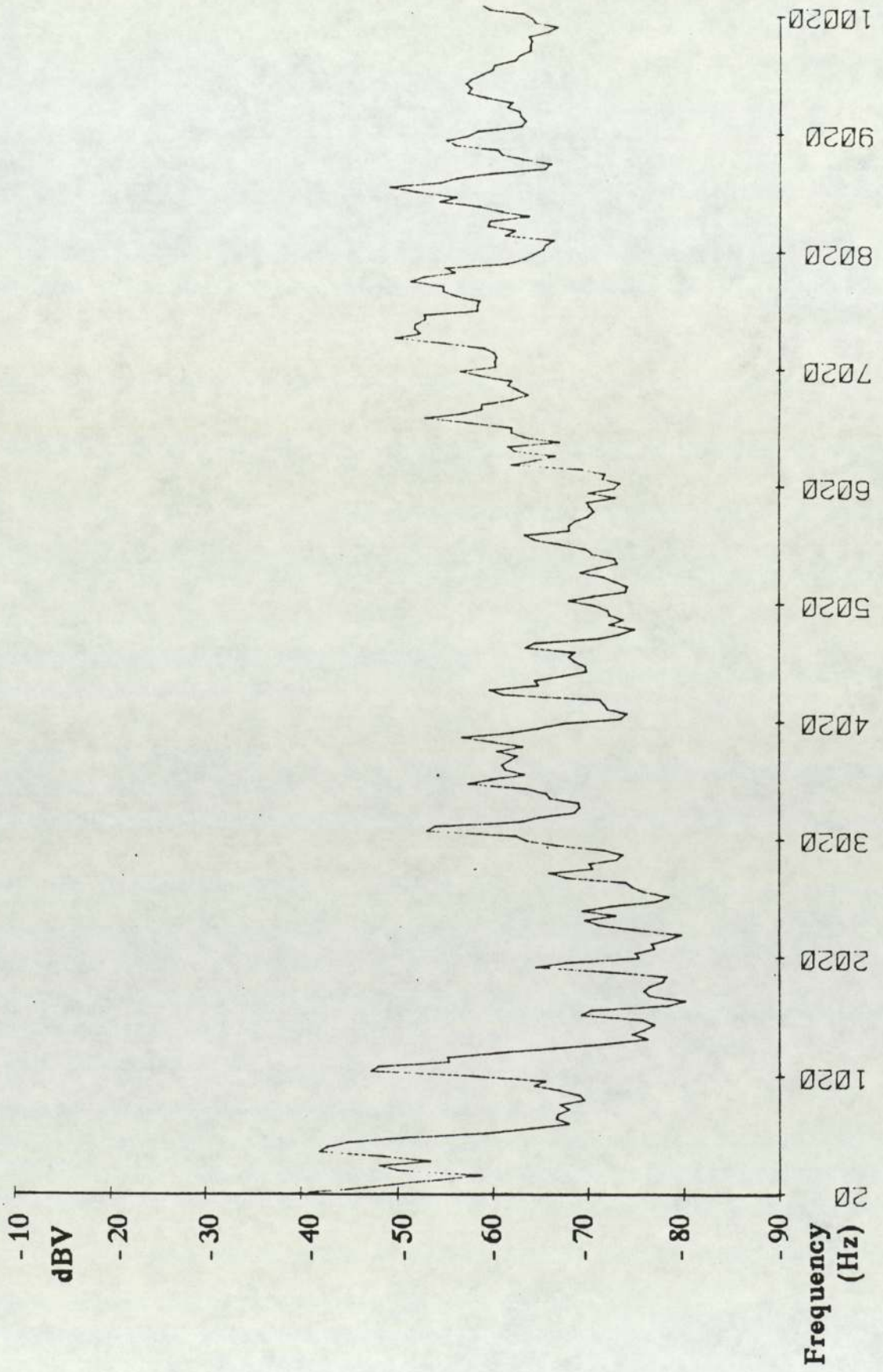

Figure 3.42 Motor flange vibration spectrum at 6.5 bar, location 2, 2 pole

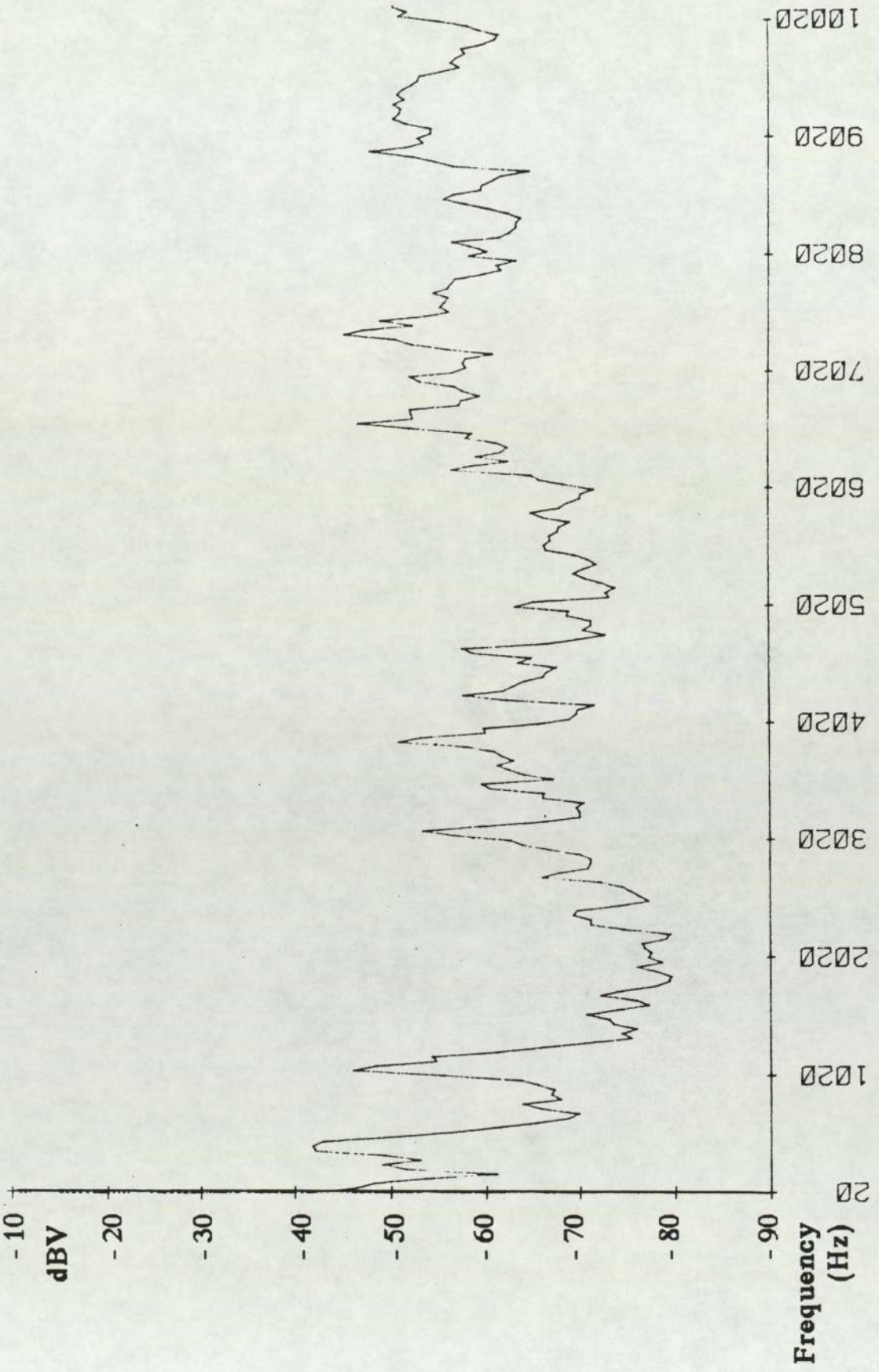

Figure 3.43 Motor flange vibration spectrum at 10.5 bar, location 2, 2 pole

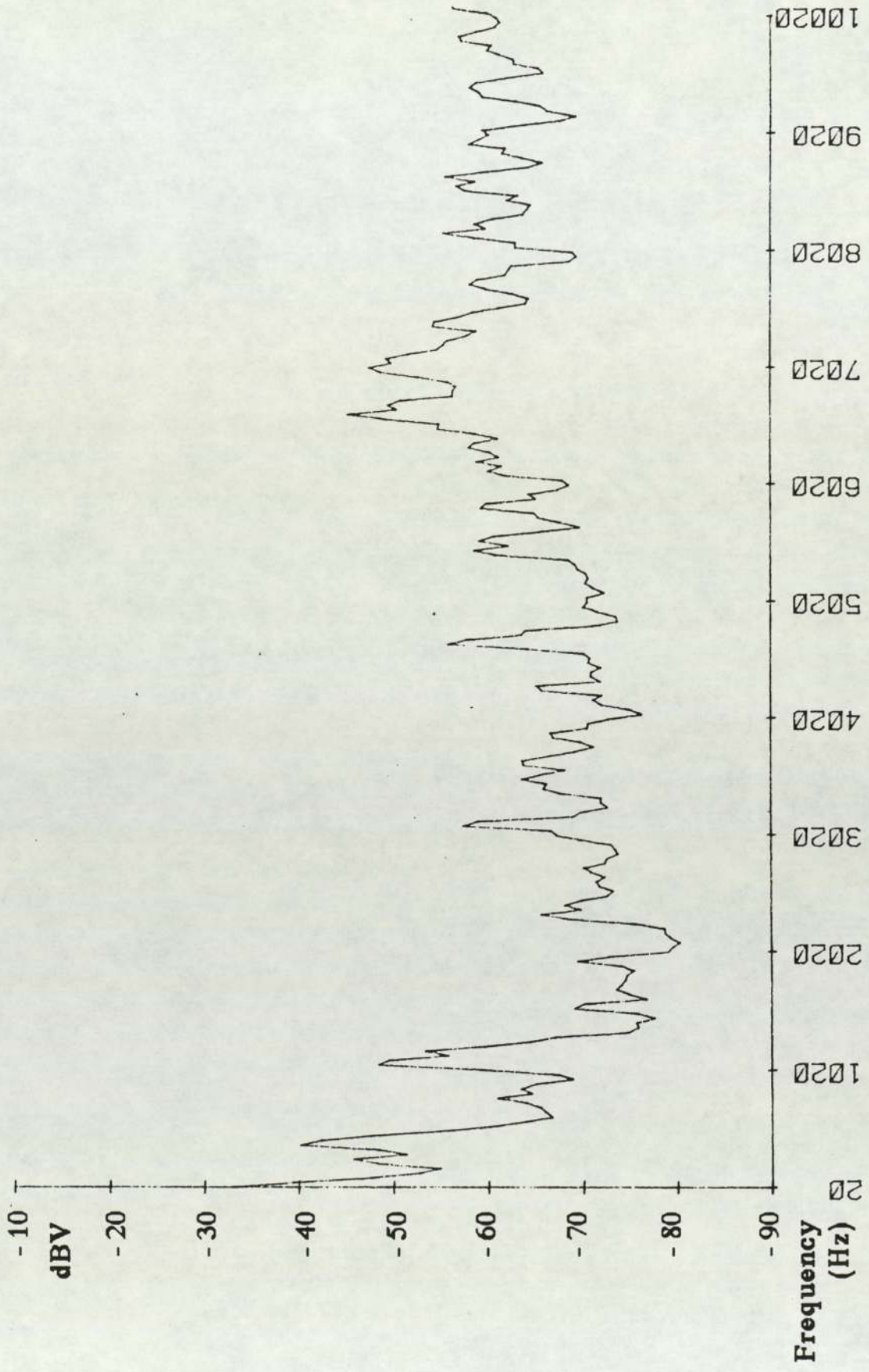

Figure 3.44 Motor flange vibration spectrum at 6.5 bar, location 5, 2 pole

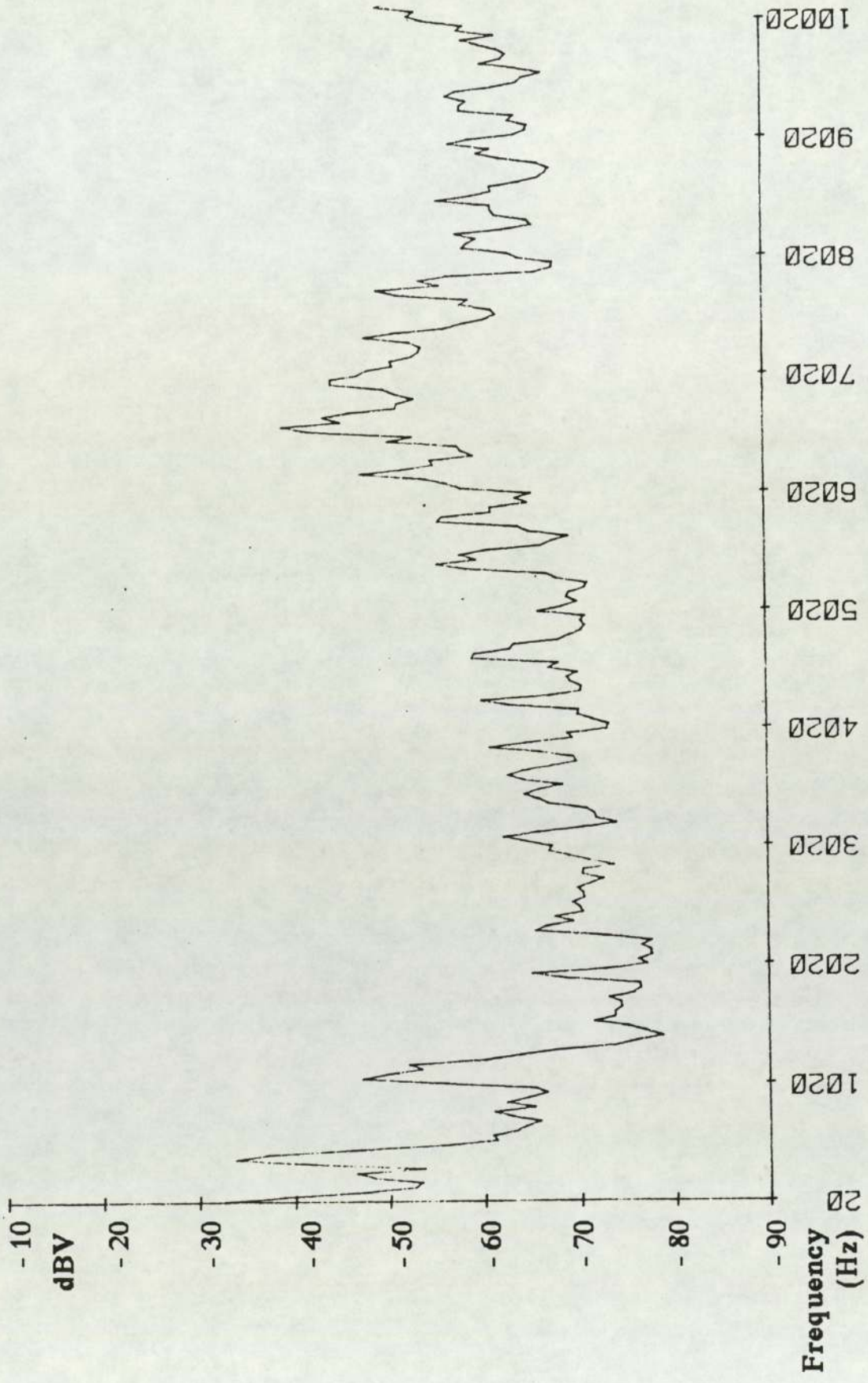

Figure 3.45 Motor flange vibration spectrum at 10.5 bar, location 5, 2 pole

Figure 3.46 Motor flange vibration spectrum at 6.5 bar, location 2, 4 pole

Figure 3.47 Motor flange vibration spectrum at 10.5 bar, location 2, 4 pole

Figure 3.48 Motor flange vibration spectrum at 6.5 bar, location 4, 4 pole

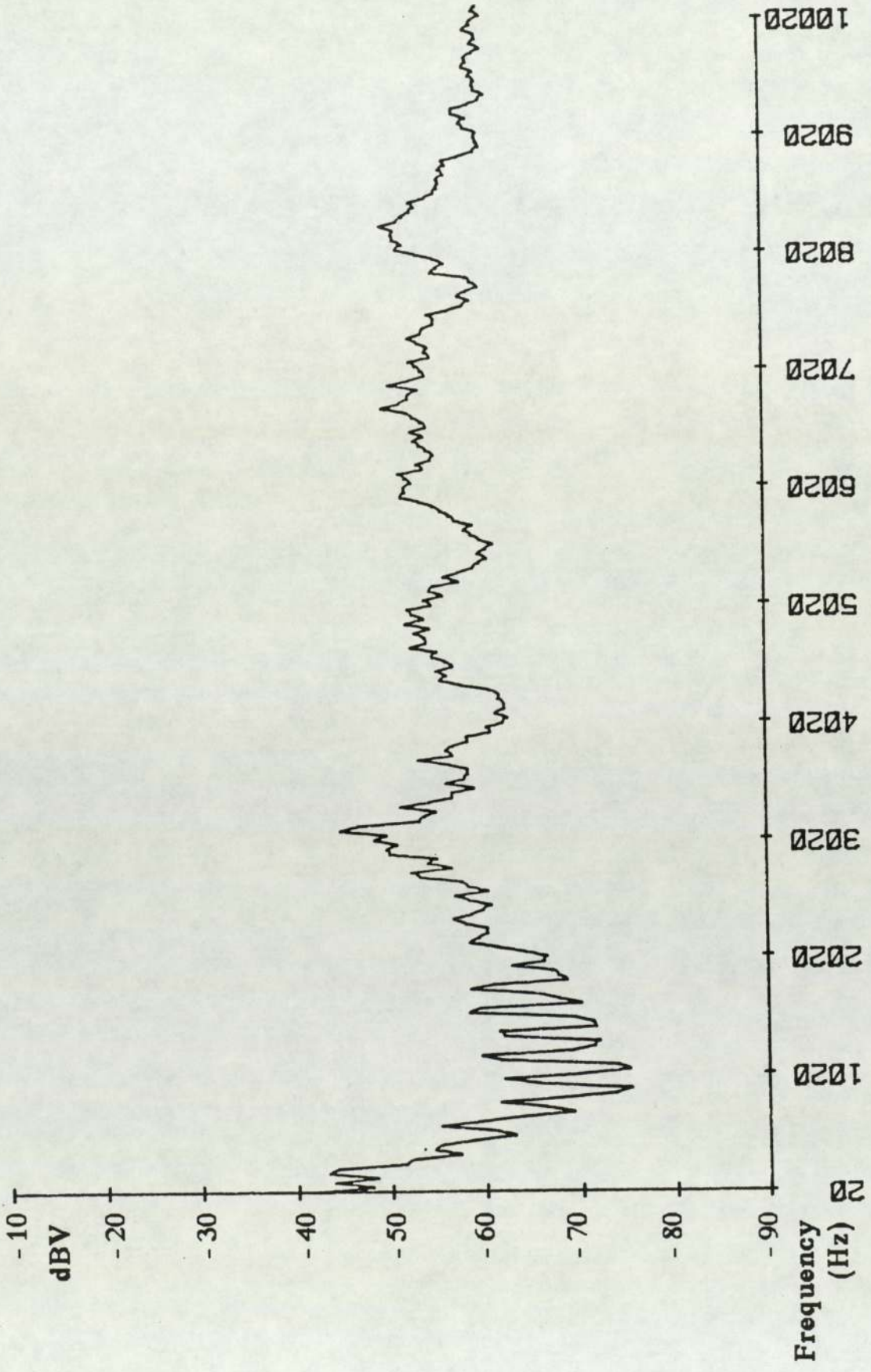

Figure 3.49 Motor flange vibration spectrum at 10.5 bar, location 4, 4 pole

4.0 Modal testing of stator and casing

Chapter 3 dealt with the initial noise and vibration survey of the Hydrovane compressor and established the need to examine the natural vibrational characteristics in greater detail: the analysis, whether theoretical or practical, is commonly termed Modal Testing. This chapter deals with the modal testing of the major components which transmit vibration and radiate noise.

The stator is exposed to all the forces that exist within the compressor. As the stator is rigidly connected to the casing, vibration will be transmitted readily to the large surface area of casing from which the air-end noise is radiated. If either the stator or casing has a resonant frequency which is identical to or close to harmonics of the rotor vane passage frequency or other forcing signal then this will amplify vibration levels within the compressor structure which in turn will increase the noise radiated from the compressor.

Existing software (Pafec Pigs finite element analysis package) was used to predict the natural frequencies and mode shapes of the stator and casing under free and fixed conditions. The fixed boundary conditions simulated the restraints that exist in an assembled compressor. This theoretical work was complemented with experimental modal testing to determine the free response of the stator and the free and fixed response of the casing to hammer impulses.

4.1 Literature review

Since the advent of the digital computer the time required and the accuracy achieved by utilising modal testing has enabled the experimental analysis of structures to be minimised, particularly if they are comprised of regular shapes, ie. flat rectangular or circular plates.

The vibrational behaviour of cylindrical shells is most relevant to the present investigation. Leissa (1988) has summarised the majority of work completed on shells. His assumtions are as follows: the shell has constant thickness; the shell walls are thin (< 10% of shell radius); the shell walls are composed of a linear, elastic, homogeneous isotropic material; there are no loads applied to the shell; the deformations of the shell are small in comparison with the shell radius; rotary inertia and shear deformation are neglected.

The circumferential and axial modes of vibrational behaviour of a cylindrical shell are regarded as independant and are considered separately. The nodal patterns for a thin cylindrical shell are shown in Fig.4.1, however, neither the stator or casing fall precisely into this category: the stator does not have constant thickness and the walls are not thin; the casing has a complete and integral base, has axial stiffeners and includes abrupt changes in section to accomodate the filler plug and drain plug.

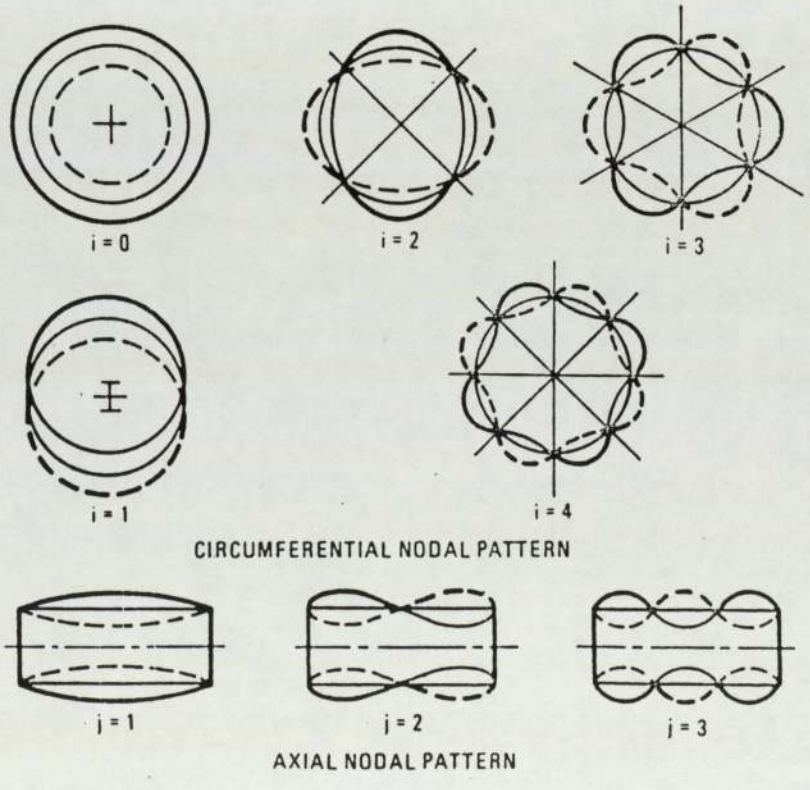

Figure 4.1 Nodal patterns of thin cylindrical shell

There has been no relevant analysis of the stator or casing within the compressor industry. However, there has been research concerned with the stator vibrations of electric motors and the findings have some relevance to the present problem. In both cases basic shells are subject to internal forces due to a rotor. A recent paper by Verma Singal and Williams (1987) showed excellent correlation for a pure cylinder between theoretical predictions (utilising energy methods) and experimental results. The study has not yet been extended to measure the effect of windings and ribs. However, this has encouraged the use of a theoretical analysis to complement the experimental work.

The aircraft industry has been involved extensively in understanding and reducing the effect that engine noise and vibration has on passenger comfort. A paper by McGary (1987) compared the effects that direct noise from the engine and vibration transmitted through the structure had on a plate representing a section of fuselage. This depends greatly on the fuselage structure which is basically a thin cylindrical shell. The effect of both radial and axial stiffeners is considerable and was investigated in two papers by Mead and Bardell (1986 & 1987). These papers highlighted the effect of stiffeners and indicated that their properties must be included in a theoretical analysis if it is to be accurate.

Modal testing is comprehensively covered by Ewins (1984) which introduces the need for such testing, details the theoretical and practical methods to obtain modal information and discusses interpretation of the data. The principles are described by the following assumption:

Response = f (Vibration Properties x Input Force).

Modal testing measures both the response and input for a structure, from which its vibrational characteristics can be determined. Mobility measurement is the response of a structure to a single point

excitation. The excitation or input force can be either continuous (from a mechanical vibrator) or transient (from a hammer impulse): the magnitude of input force is measured by a force transducer. The response is normally an acceleration measured by an accelerometer at the point of interest. Since input force levels can be small it is of particular importance that the accelerometer does not have a significant effect on the response of the structure.

The hammer impulse technique was used throughout the modal testing since it is more convenient to apply than continuous mechanical excitation. The experimental details are described in Chapter 2

When input and response signals are fed simultaneously to a spectrum analyser the transfer function can be calculated. The transfer function is the ratio of response to input and includes phase information.

A paper by Bovey (1982) used the transfer function technique to measure the effect on the surrounding environment of noise caused by railway vibrations. The advantage of the transfer function technique in that study was that it enabled the dynamic parameters of any structural path to be determined independently of a moving train. An impulse method was used as this was the only suitable method of providing a large enough force over the distances (30m) for which response measurements were required. The particular transfer function measured was the "inertance", which is defined as the ratio of the response acceleration to the input force. The study was undertaken to obtain quantitive data for different structural paths ie. different track form, sleeper arrangement and soil types. From this information a better understanding of the vibration transmission mechanism was possible.

4.2 Theoretical analysis of the stator and casing

An Apollo 550 engineering work station operating at 1.8 mips and running a Pafec Pigs finite element package was used to predict the natural frequencies and non-rigid body mode shapes of non uniform shells. The most important software features are Automatic Front Ordering that introduces and discards nodes and elements automaticly so the system does not become overloaded with too many degrees of freedom (DoF) at any time, and Automatic Selection of Master DoF which uses the Guyan reduction technique based on the minimum strain energy. The main assumption of the software is that the material from which the simulated structure is constructed is linear and homogeneus.

The component to be analysed is modelled from a number of elements bounded by nodes which are all fixed in space. The Topology describes the manner in which the nodes are joined to form elements, the order and additional properties are crucial for a correct description. For example: a rectangular element will be bounded by nodes at its four corners and requires the thickness to complete its geometric description; a beam is bounded by a node at each end and requires the 2nd Moment of Area to complete its geometric description. Material properties are required for all elements and these include Youngs modulus, Poissons ratio and density.

In most cases the greater the number of elements the greater the accuracy with respect to frequency. However the time required to create the model and calculate the result increases disproportionally. The aim of the theoretical prediction was to give an indication of possible resonance phenomena occurring in the compressor during normal operation: the models were therefore relatively simple.

4.2.1 Stator : Model

The General Arrangement of an actual stator is shown in Fig.4.2 and the configuration used for the model is shown in Fig.4.3. The stator was modelled as a cylinder comprised of 8 sections of equal arc length but varying thickness. It was assumed that the 8 sections lay on a circle constructed by the neutral axis of each element. The diameter of this circle was taken as the outside diameter of the stator minus the half the sum of the maximum and minimum thicknesses and was calculated as 83.4 mm. The thickness of each circumferential element was taken as the average of the thickness at each end. The axial length of the stator is 55 mm and was split into five elements each 11 mm in length.

To determine the natural response, or free vibrational behaviour, of the stator no constraints were applied to the end nodes. To simulate the vibrational characteristics of the stator in-situ the nodes at each end were pinned in position. This condition restrained the nodes in an axial direction but allowed rotation.

4.2.2 Stator : Results

Under free vibration the computer prediction generates six rigid body modes of vibration which correspond to three translational and three rotational. The first non-rigid body mode of vibration otherwise described as the first resonance was predicted to occur at a frequency of 2.76 kHz. The deformation pattern is shown in Fig.4.4 and it can be seen that this is similar to the ovalling mode. Further modes then occur at 5.34 kHz, 7.95 kHz and 11.48 kHz: the deformation patterns or mode shapes are shown in Figs.4.5 - 4.7.

Under pinned conditions the first mode occurred at 10.86 kHz. In the real situation the actual frequency of this first resonance depends on

how rigidly the stator is supported and the stiffness of the supporting components. If the end connections are stiffer than the pinned joint used in the model, ie. rotation is restricted as in a built-in joint, then the first resonant frequency will be higher. However the supporting components are not completely rigid and will have some axial and rotational flexibility which will tend to reduce the resonant frequency.

The model showed that the ratio of first resonant frequencies for the stator under pinned and free conditions will be approximately 3:1. If the measured natural frequencies are similar to the predicted natural frequencies then this ratio can be used to gain some idea of the expected first resonant frequency when the stator is installed within the compressor.

4.2.3 Casing : Model

The casing is quite a complicated casting and a simplified geometric model was used in the computer prediction. The dimensions of the actual casing and modelled casing are shown in Figs.4.8 & 4.9 respectively. The two main assumptions made were that the integral base behaved as a relatively stiff disc of uniform thickness and the recess for the filler plug was ignored. These were both acceptable for the accuracy required since the vibrational behaviour would be dominated by the large thin cylindrical section, which was therefore modelled in greater detail.

The cylindrical section comprised 12 trapezoidal circumferential plate elements each 4 mm thick and subtending 30° but increasing with radius at greater axial distances from the base. The total axial length of 140 mm was split into five 24.4 mm sections plus one 18 mm section. A circumferential ring of beams 4 mm square were attached to the nodes between the end two elements and six 4 mm square beams ran the full

axial length at alternate nodes (60° intervals) to represent the axial stiffening ribs. The base comprised two main sections: a central disk and a concentric annulus. Both were split into 12 elements each subtending 30°.

No restraints were applied under free conditions, but to simulate the behaviour of the rubber O ring, which is the only contact between the casing and endcover, springs were fixed radially between each of the 12 end nodes and ground. The undeformed model with the O ring restraint is shown in Fig.4.10. The stiffness of each spring was calculated as the radial stiffness of a section of rubber 4 mm square and 52.4 mm in length (one twelfth of circumference) using the following formula

$$E = \frac{F\,l}{e\,A} \quad \text{therefore stiffness} \quad \frac{F}{e} = \frac{E\,A}{l} = 78600 \ {}^{N}\!/_{m^2}$$

where E is the Youngs Modulus for rubber (1.5×10^6 N/m^2), A is the radial cross section (.004m x .0524m) and l is the radial length (.004m).

4.2.4 Casing : Results

Under free conditions the first resonance was predicted to occur at a frequency of 446 Hz, others then follow at 950 Hz, 1.67 kHz, 2.60 kHz, 3.76 kHz and 4.05 kHz to give some idea of the modal density the 10th mode occurs at approximately 5.0 kHz, the 20th at 7.2 kHz and the 30th at 8.8 kHz. The deformation patterns for the first three modes of vibration are shown in Figs.4.11 - 4.13.

There is very little difference between the free and restrained conditions. the first resonance increased to 480 Hz and others followed at 962 Hz,1.68 kHz, 2.61 kHz, 3.76 kHz and 4.05 kHz. These results

indicate that it is possible for some of the harmonics of rotor vane passing frequency to coincide with a natural resonant frequency of the casing.

4.3 Practical analysis of the stator and casing

This investigation was split into three sections, an analysis of the free vibration of the stator, the casing and also the complete compressor.

4.3.1 Free vibration of the stator.

The stator was suspended from a retort stand by a thin length of cord tied round the discharge port. An accelerometer was positioned at an arbritary location on the stator which was then excited with an impulse from the Bruel & Kjaer hammer discussed in Chapter 2.

4.3.2 Stator vibration : Results

A clear ringing tone could be heard when the stator was struck and this was identified by both the accelerometer and a sound level meter. The frequency spectrum produced from the accelerometer signal is shown in Fig 4.14 over a 5 kHz range: The first non rigid body mode of vibration occurs at a frequency of 3.46 kHz. Fig 4.15 shows further modes of vibration at approximately 5.2 kHz, 7.1 kHz and 10.4 kHz. These results compare reasonably well with the model, which predicted values of 2.8 kHz, 5.3 kHz, 7.9 kHz and 11.5 kHz respectively. The experimental results confirm that a ratio of at least 3:1 exists between the first natural frequencies for restrained and free conditions and indicates that there are not likely to be any resonance problems arising from the stator.

4.3.3 Free vibration of the open ended casing

The open ended casing was attached to the motor in a normal fashion and two accelerometers were attached at arbritary locations. The casing was excited with an impulse using the hammer.

4.3.4 Open ended casing vibration : Results

The frequency spectra obtained from the individual accelerometers are shown in Figs 4.16 & 4.17. The peaks which correspond to natural modes of vibration occur at approximately 540 Hz, 1.4 kHz, 2.5 kHz, 3.6 kHz, 4.4 kHz and 5.0 kHz. Considering that the additional stiffness provided by the filler plug recess was not built into the computer model the order of magnitude and modal density agree reasonably well with the theoretical predictions calculated as 450 Hz, 950 Hz, 1.7 kHz, 2.6 kHz, 3.8 kHz and 4.1 kHz respectively.

4.3.5 Free vibration of complete casing

Since the casing is the surface from which noise is finally radiated in the working compressor this section of the experimental work was undertaken in greater detail. Accelerometers were located on the casing in the five positions used in the earlier vibration measurement discussed in Chapter 3 (Fig.3.37).

For each of the five accelerometer positions the average frequency response was measured for four impulses provided at each of the other four locations. In a linear system reciprocity applies between two points ie. there should be no difference between providing an impulse at either location and measuring at the other. However for many structures it is prudent to complete both tests. For each combination the

experiment was repeated until the coherence was satisfactory over the whole frequency range. The coherence is a measure of the difference between the individual frequency response and the average response.

The initial experiments were completed using a compressor that had remained inoperative for many hours. In order to determine the casing response to a hammer impulse under normal operating conditions the experiments were repeated with the impulses applied immediately after the compressor had been switched off. This ensured the casing was at 80°C and contained compressed air at approximately 10 bar. The pressure gradually decreased with time after the compressor was stopped but four impulses could be provided before the pressure dropped below 9 bar.

4.3.6 Complete casing vibration : Results

Typical transfer function plots for the "cold" casing are shown in Figs 4.18, 4.19 & 4.20 and for the normal casing at the same locations in Figs 4.21, 4.22 & 4.23 respectively. A comparison shows that there is little difference in response, particularly below 5 kHz. Maximum receptance values occur at approximately 4.5 kHz

These results do not show a series of strong natural frequencies but some peaks are common to most spectra and occur at 420 Hz 1.9 kHz, 2.8 kHz, 3.4 kHz and 4.4 kHz. The frequencies predicted by the model for this condition were 480 Hz, 962 Hz, 1.68 kHz, 2.61 kHz, 3.76 kHz and 4.05 kHz. Considering the modelling difficulties, particularly the behaviour of a rubber 'O' ring seal and the induced stresses due to both the fixing bolts and internal pressure the modal density the theoretical and experimental results compare well.

Coincidence of the natural frequencies for the complete casing and the harmonic frequencies of any forcing functions could lead to unnecessarily high levels of radiated noise. Analysis of both the theoretical and practical results show that there are five resonance frequencies within the most prominent and sensitive region of the noise spectrum and it is likely that at least one could coincide. In fact the experimental results discussed above indicate that this could occur at the 5th harmonic (1920 Hz) and the 9th harmonic (3456 Hz) assuming only small changes in running speed.

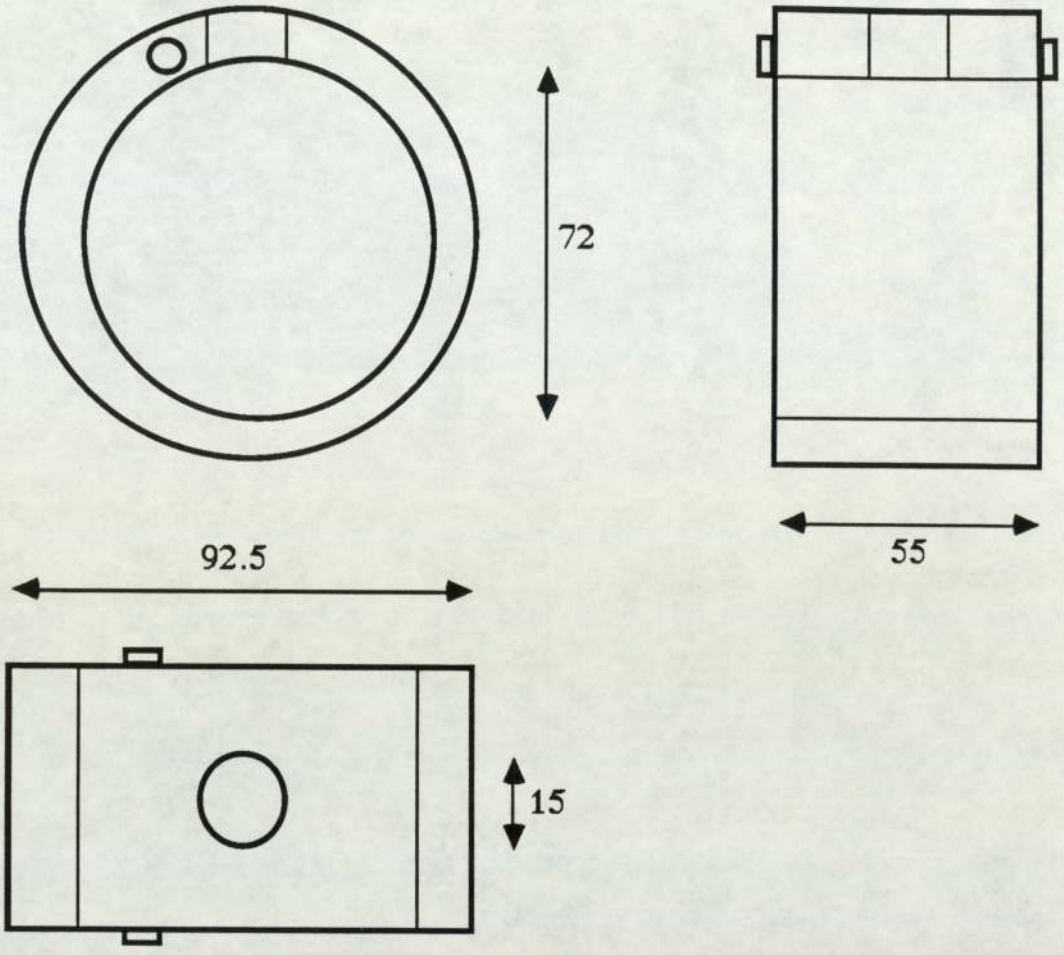

All dimensions (mm)

Figure 4.2 General arrangement of stator

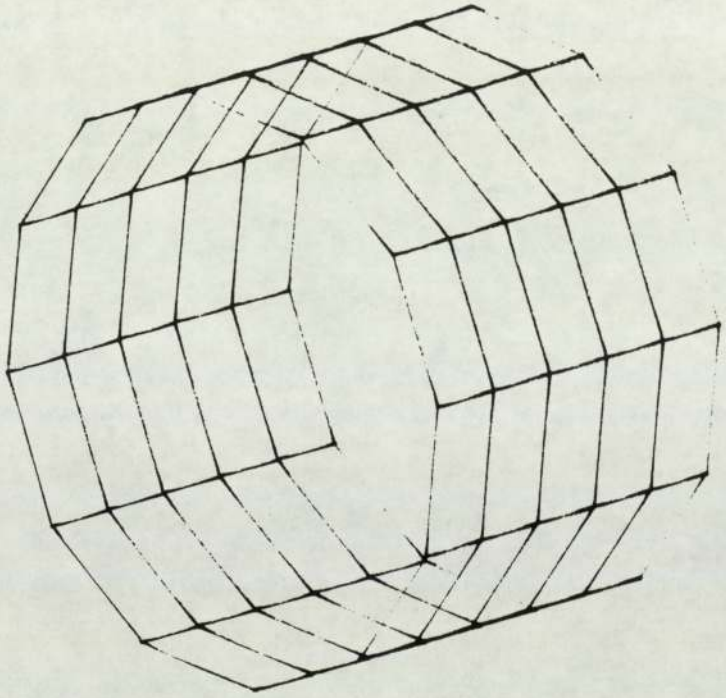

Figure 4.3 Undeformed model of stator

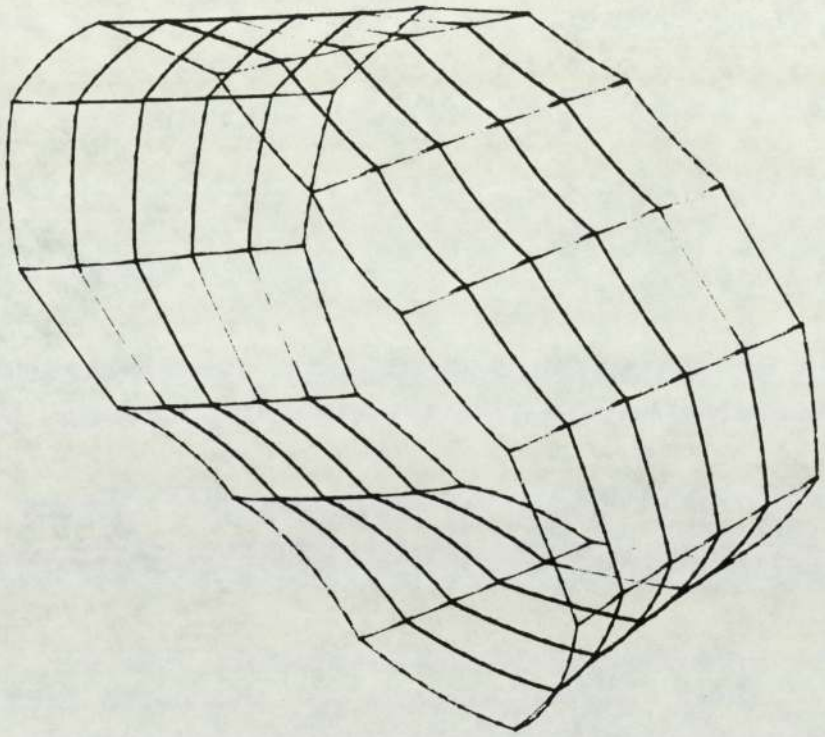

Figure 4.4 Stator deformation pattern, first mode

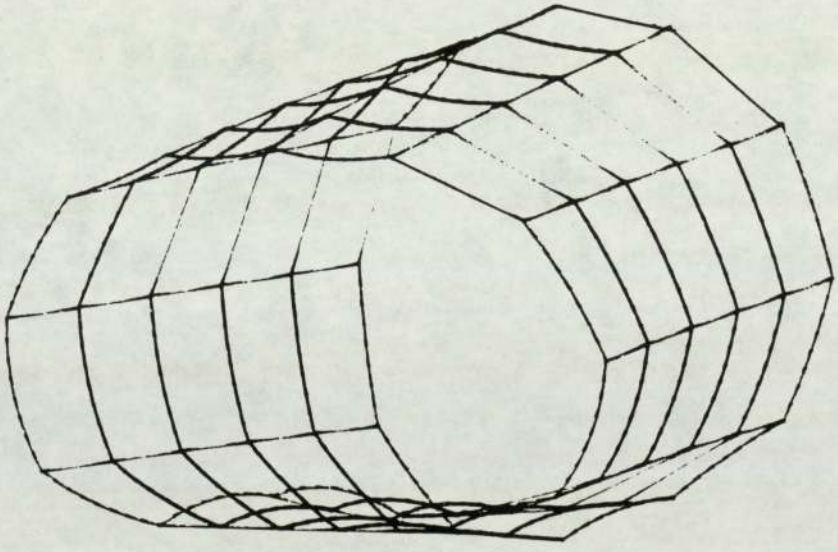

Figure 4.5 Stator deformation pattern, second mode

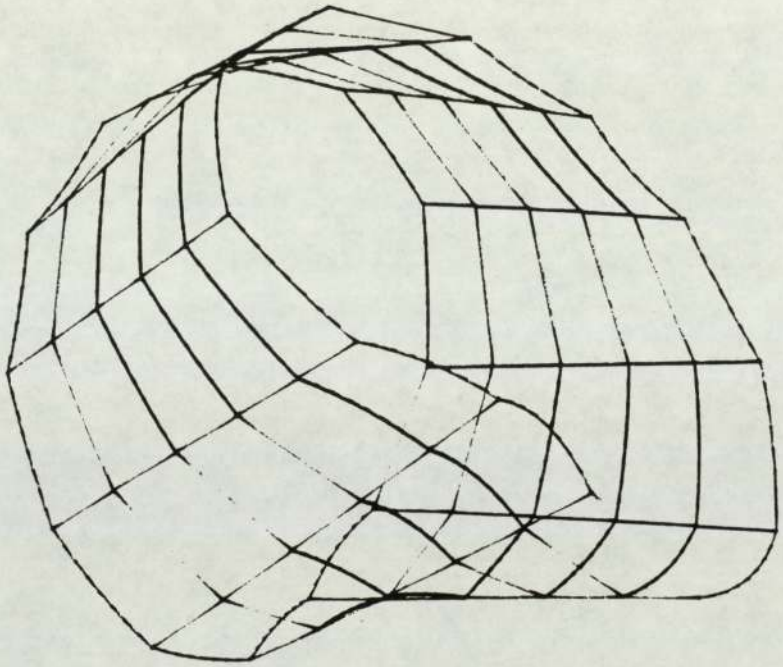

Figure 4.6 Stator deformation pattern, third mode

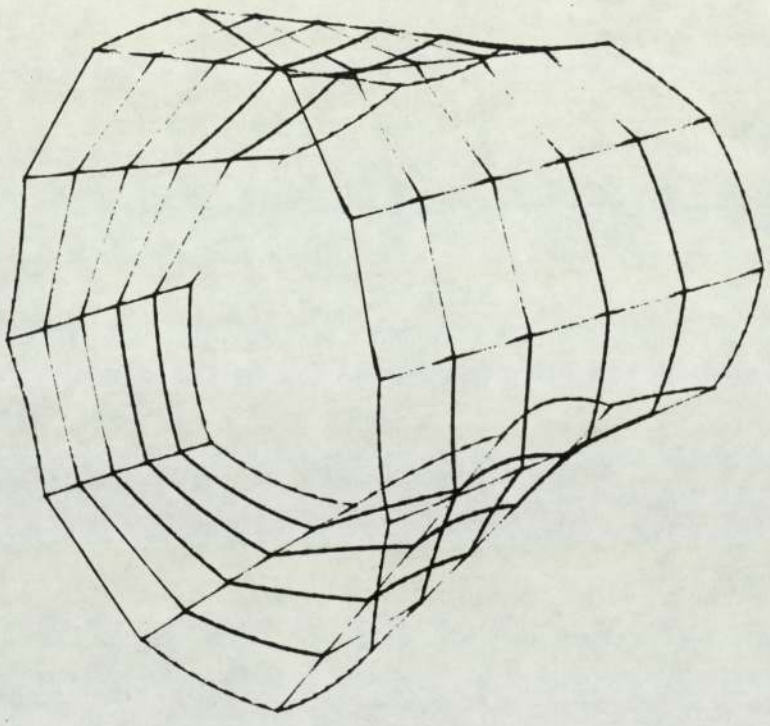

Figure 4.7 Stator deformation pattern, fourth mode

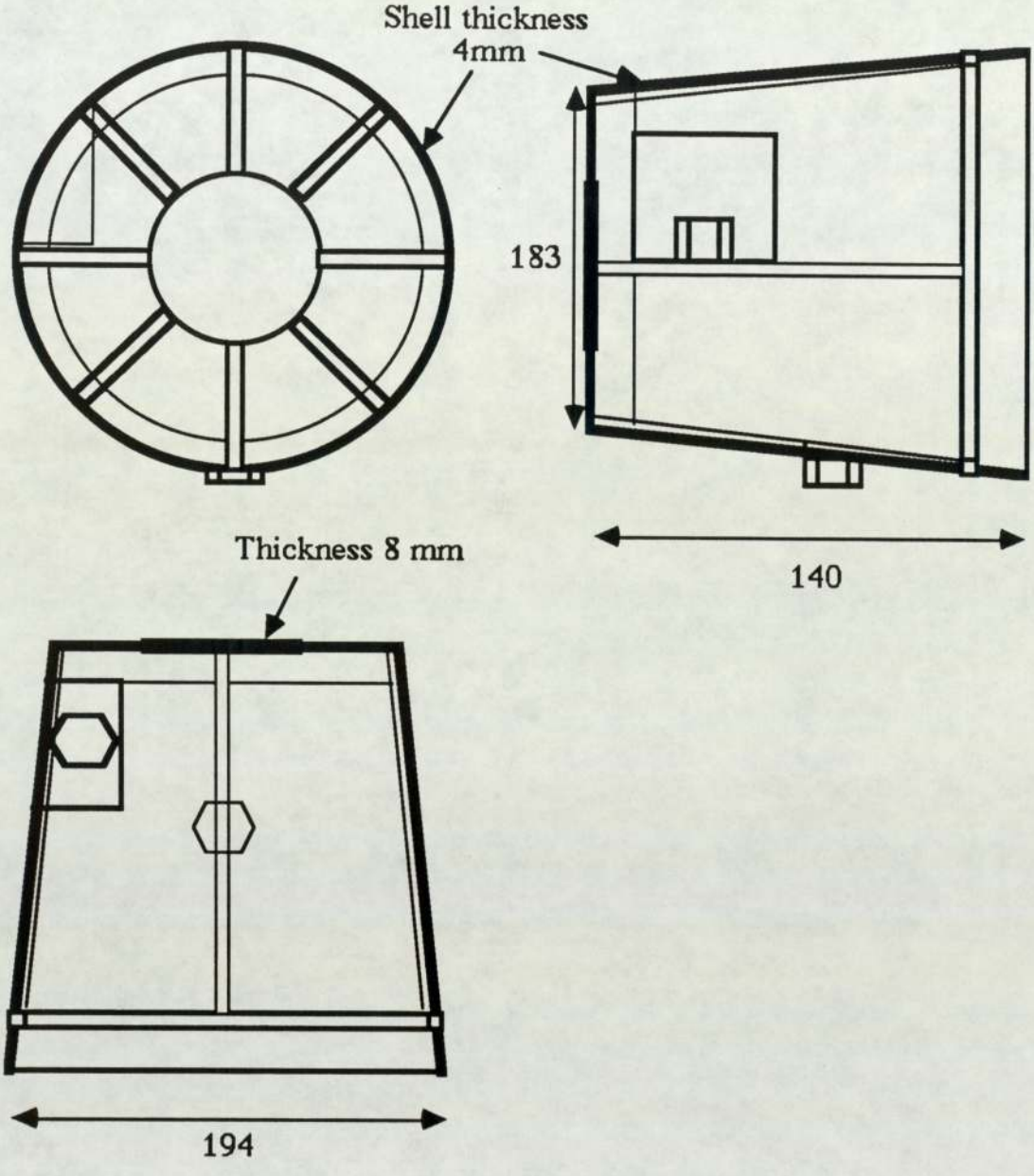

All dimensions (mm)

Figure 4.8 General arrangement of casing

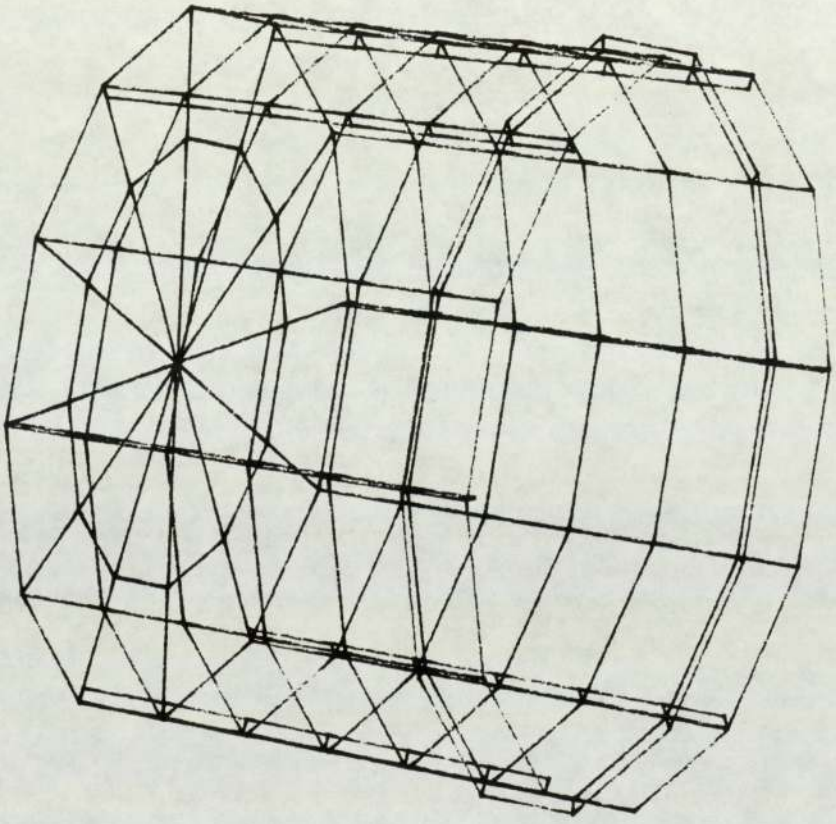

Figure 4.9 Undeformed model of open ended casing

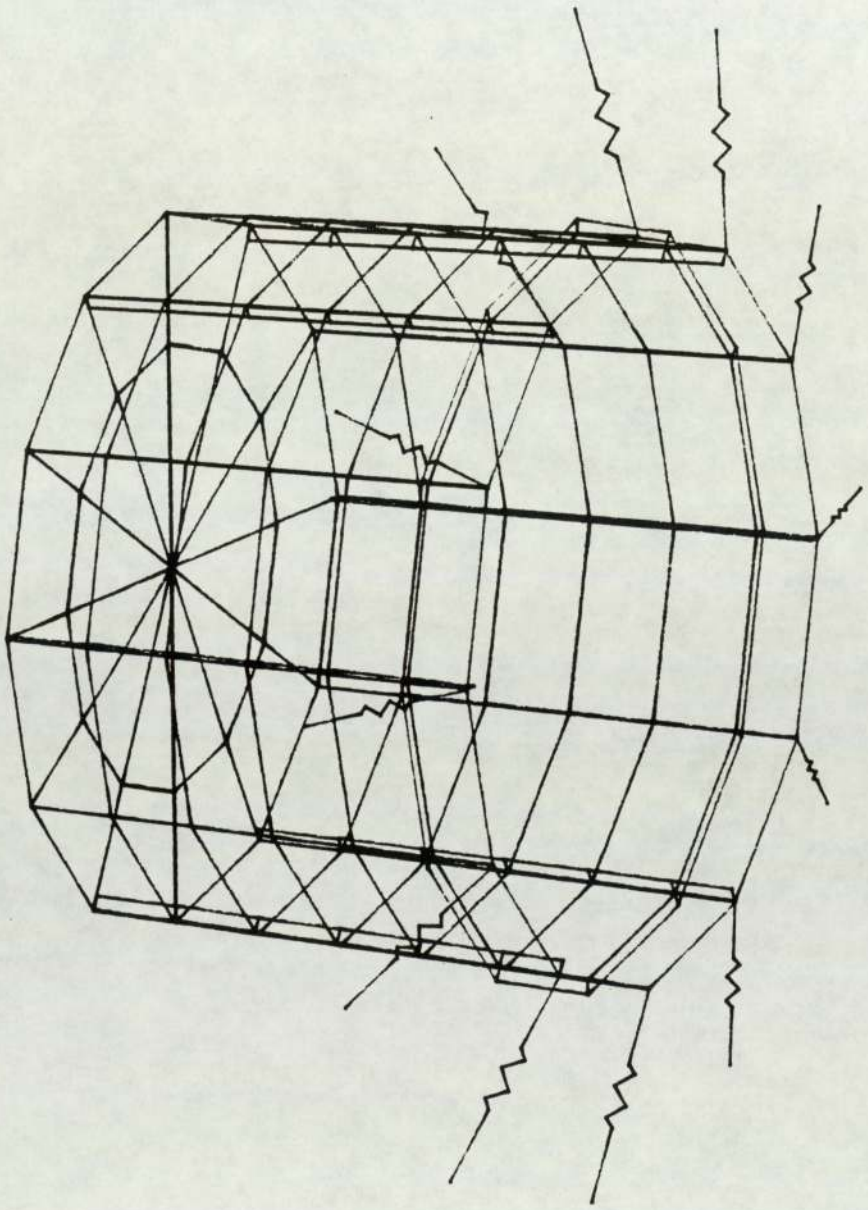

Figure 4.10 Undeformed model of complete casing with O ring

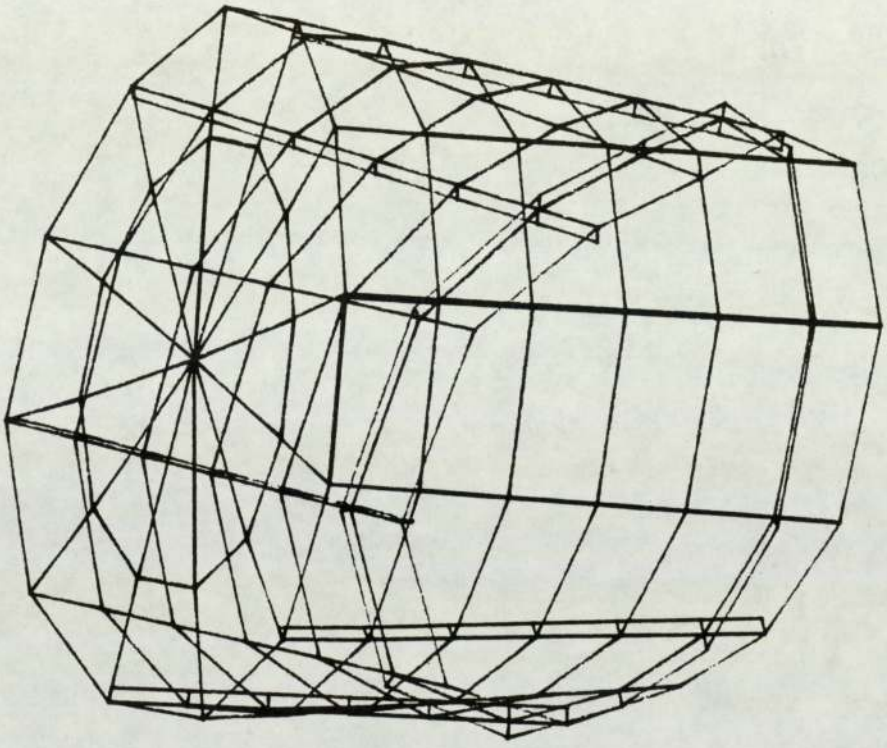

Figure 4.11 Open ended casing deformation pattern, first mode

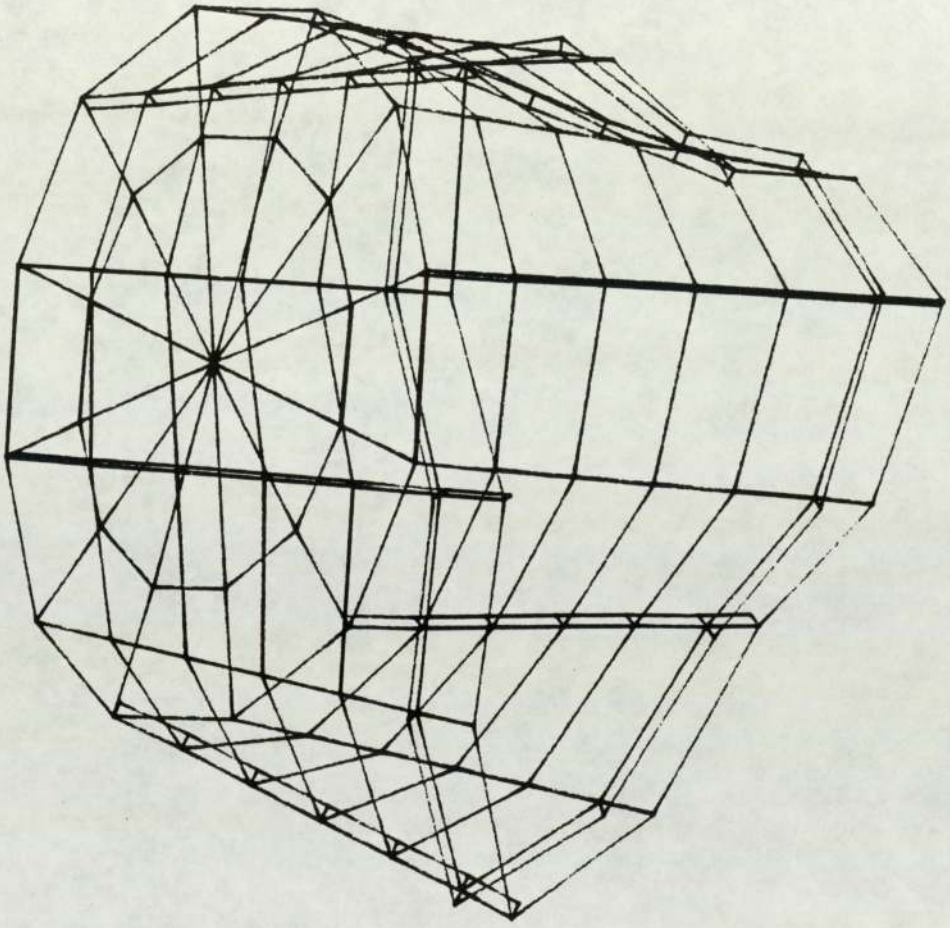

Figure 4.12 Open ended casing deformation pattern, second mode

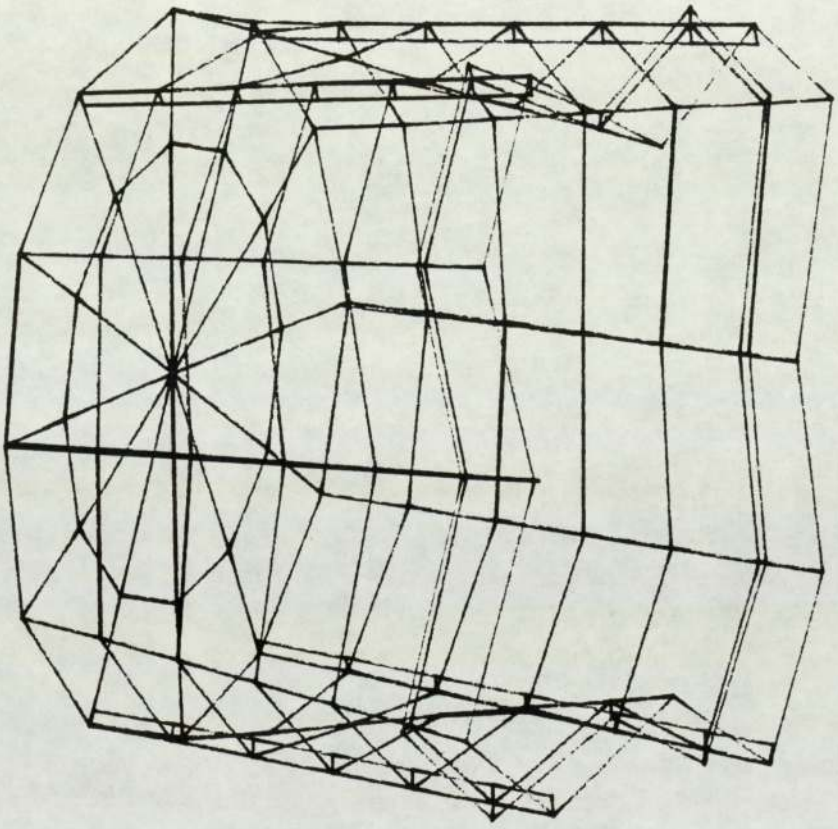

Figure 4.13 Open ended casing deformation pattern, third mode

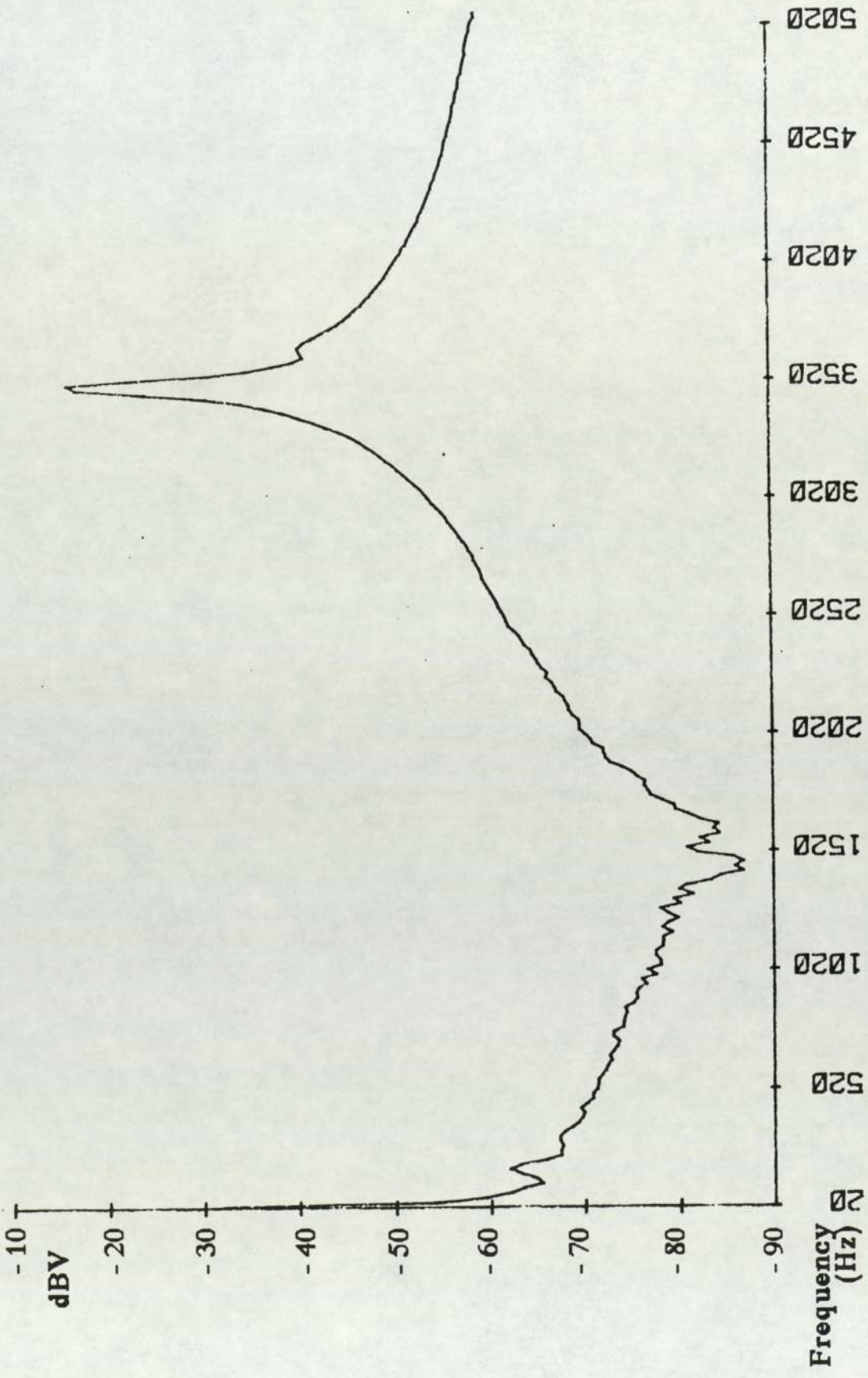

Figure 4.14 Vibration spectrum from stator excited with a hammer impulse

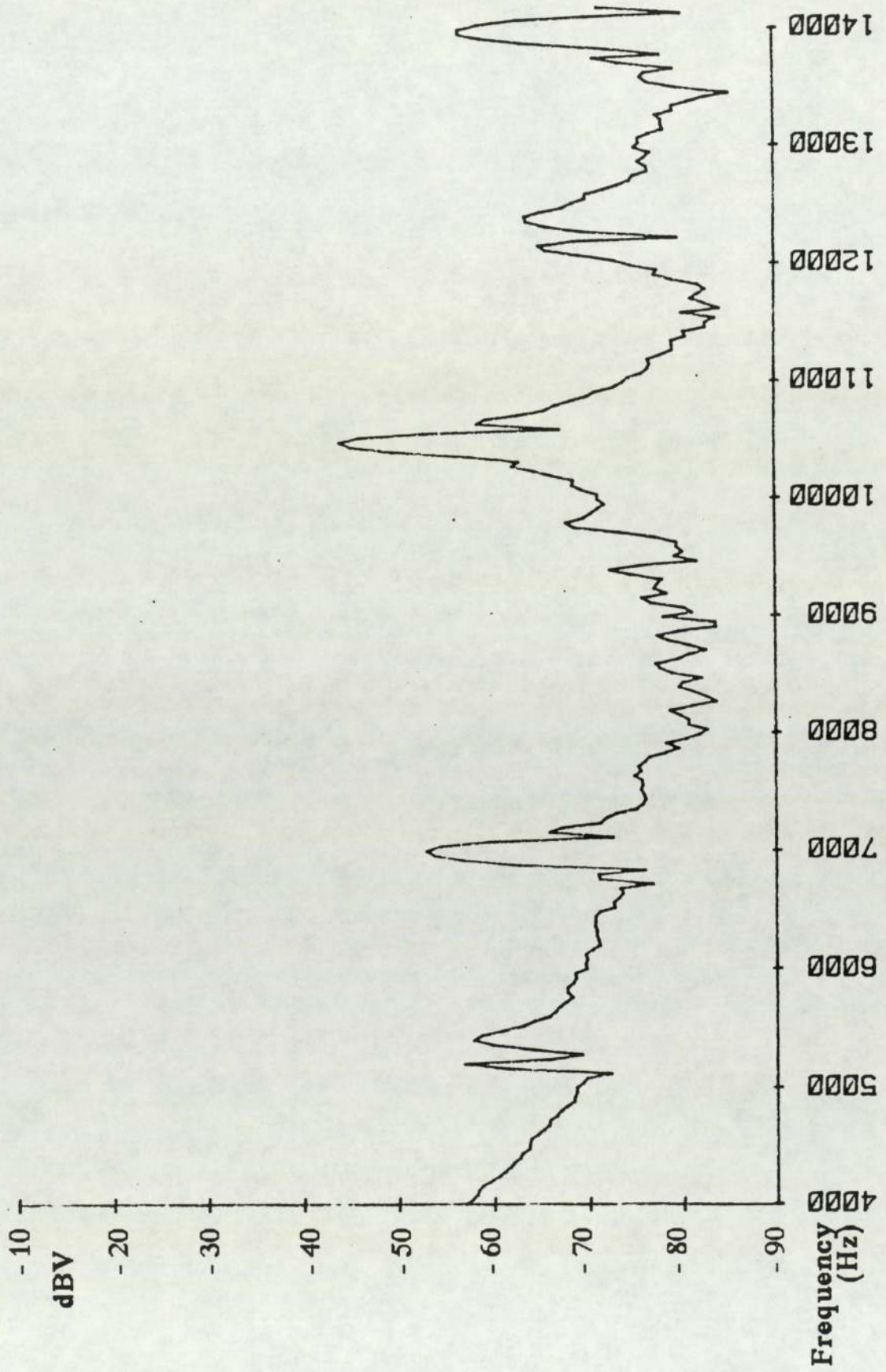

Figure 4.15 Vibration spectrum from stator excited with a hammer impulse

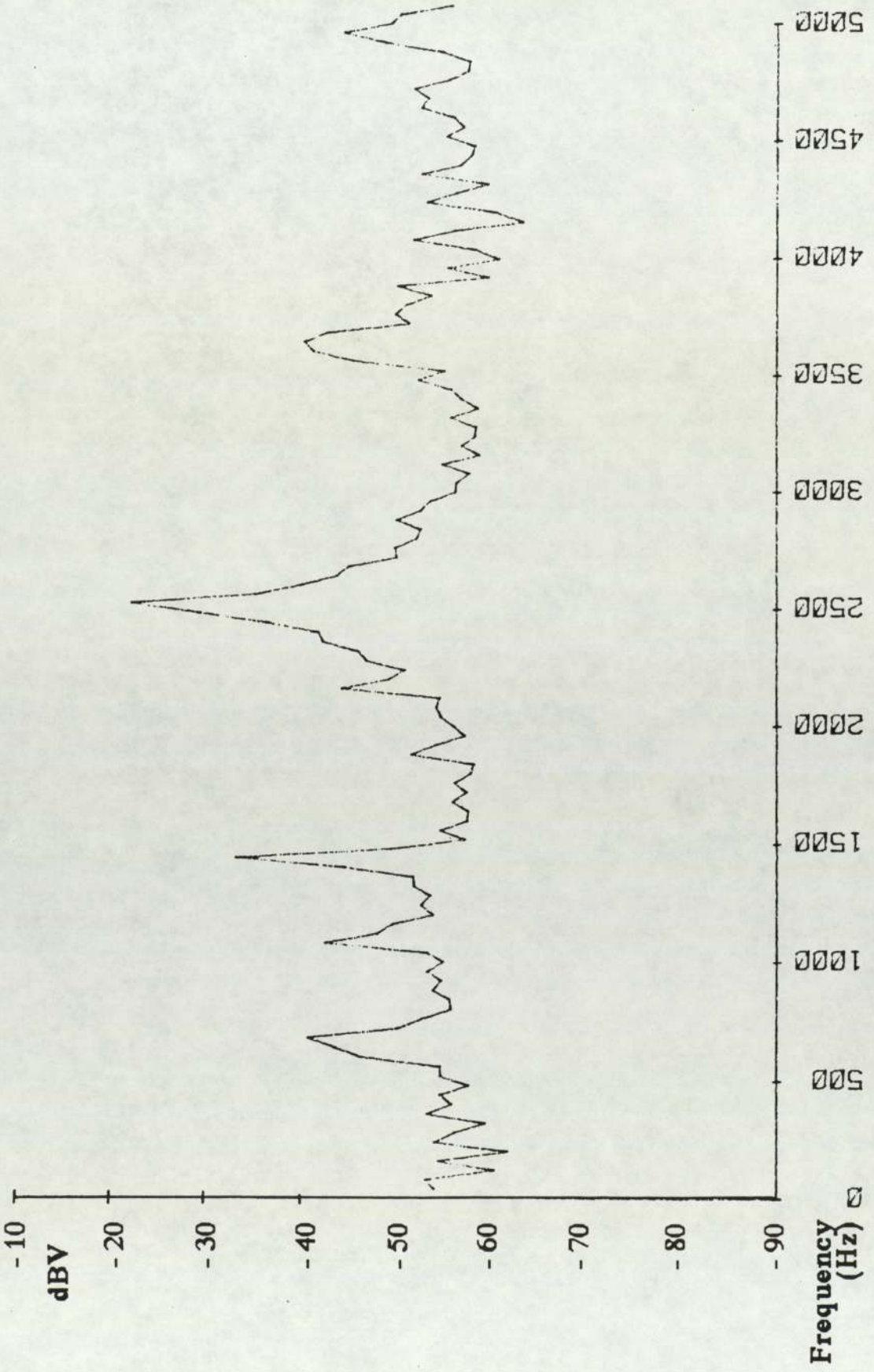

Figure 4.16 Vibration spectrum from open ended casing when excited with a hammer impulse

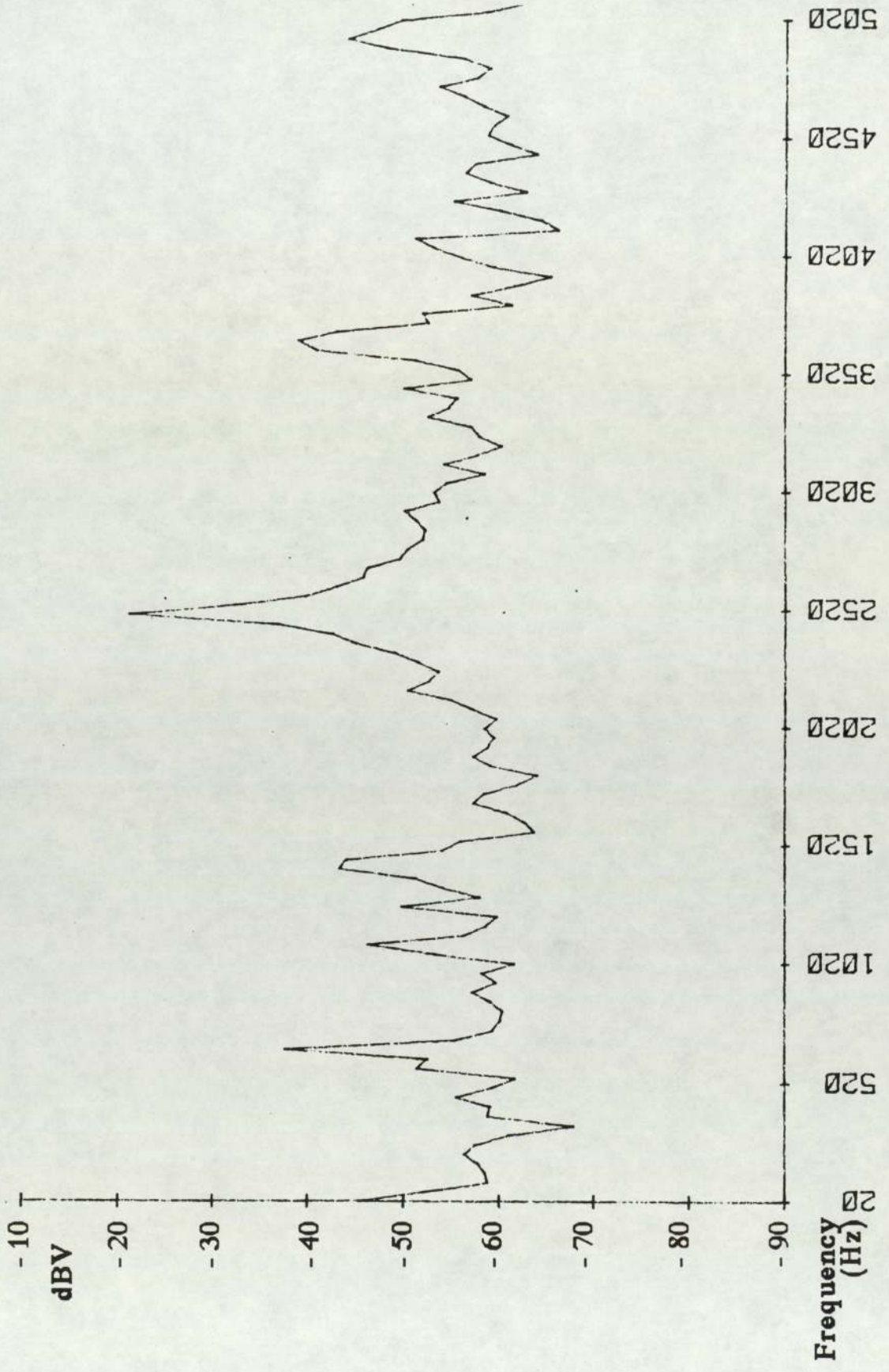

Figure 4.17 Vibration spectrum from open ended casing when excited with a hammer impulse

Figure 4.18 Receptance spectrum for casing (cold)

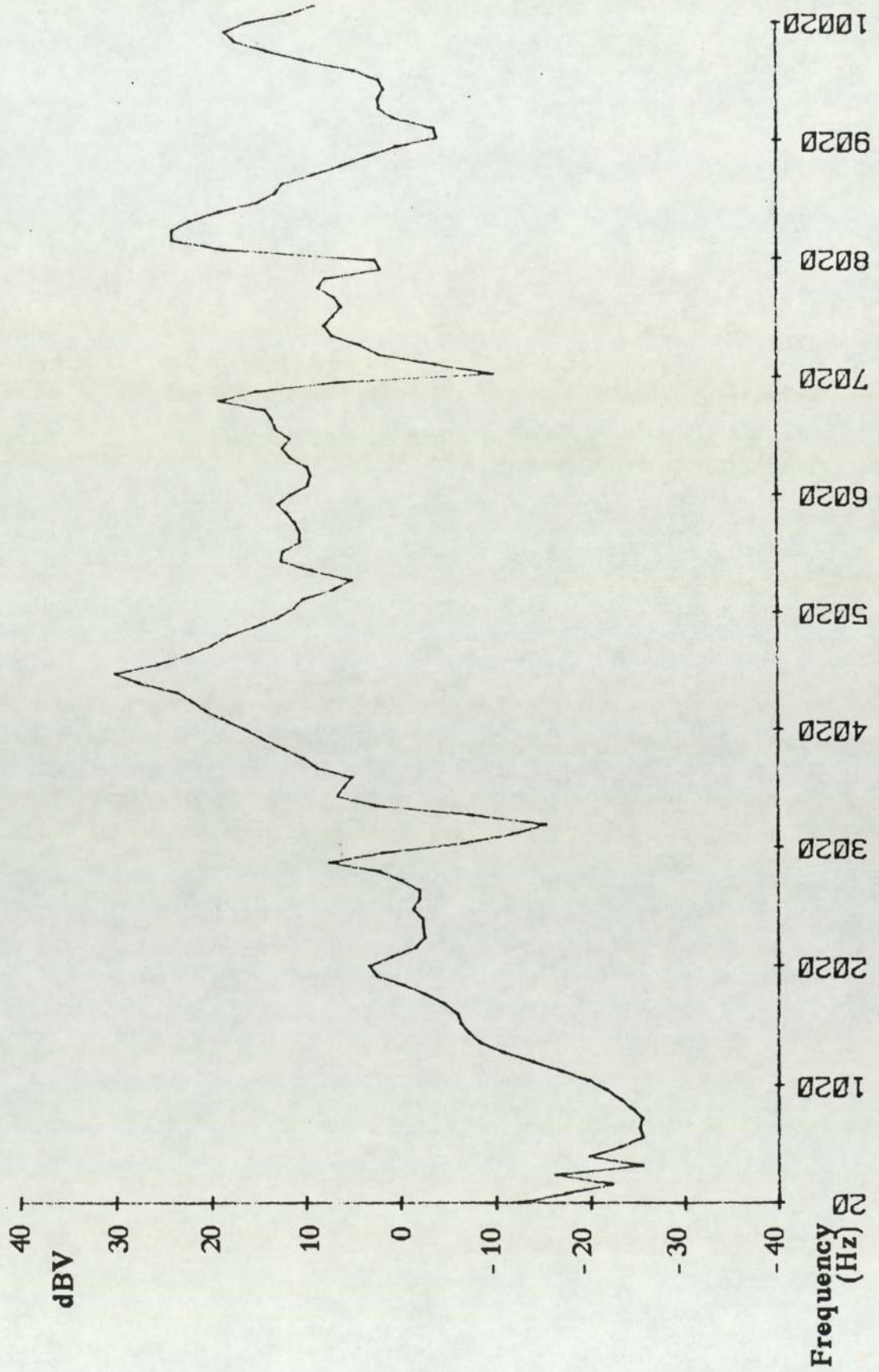

Figure 4.19 Receptance spectrum for casing (cold)

Figure 4.20 Receptance spectrum for casing (cold)

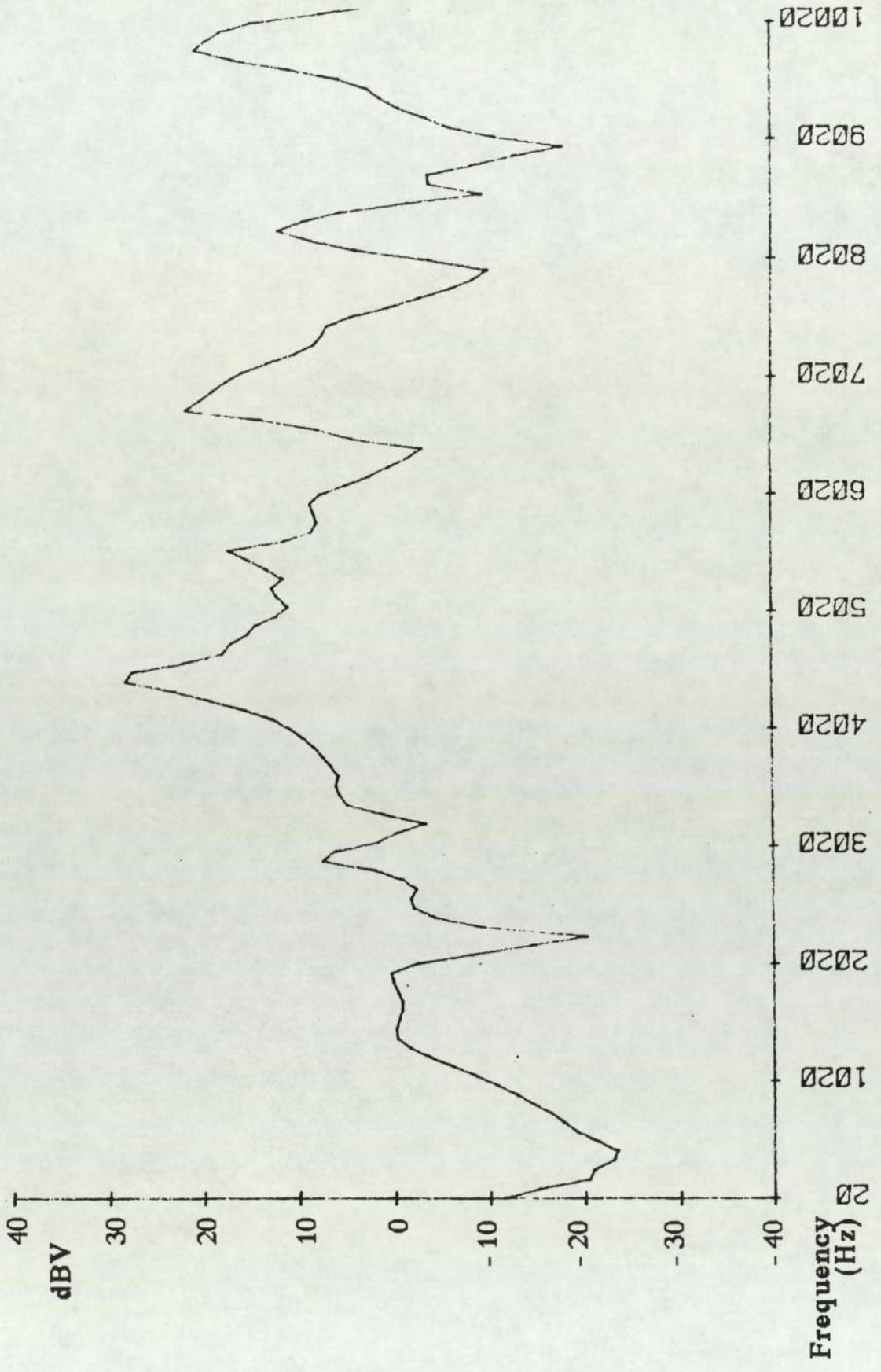

Figure 4.21 Receptance spectrum for casing (hot)

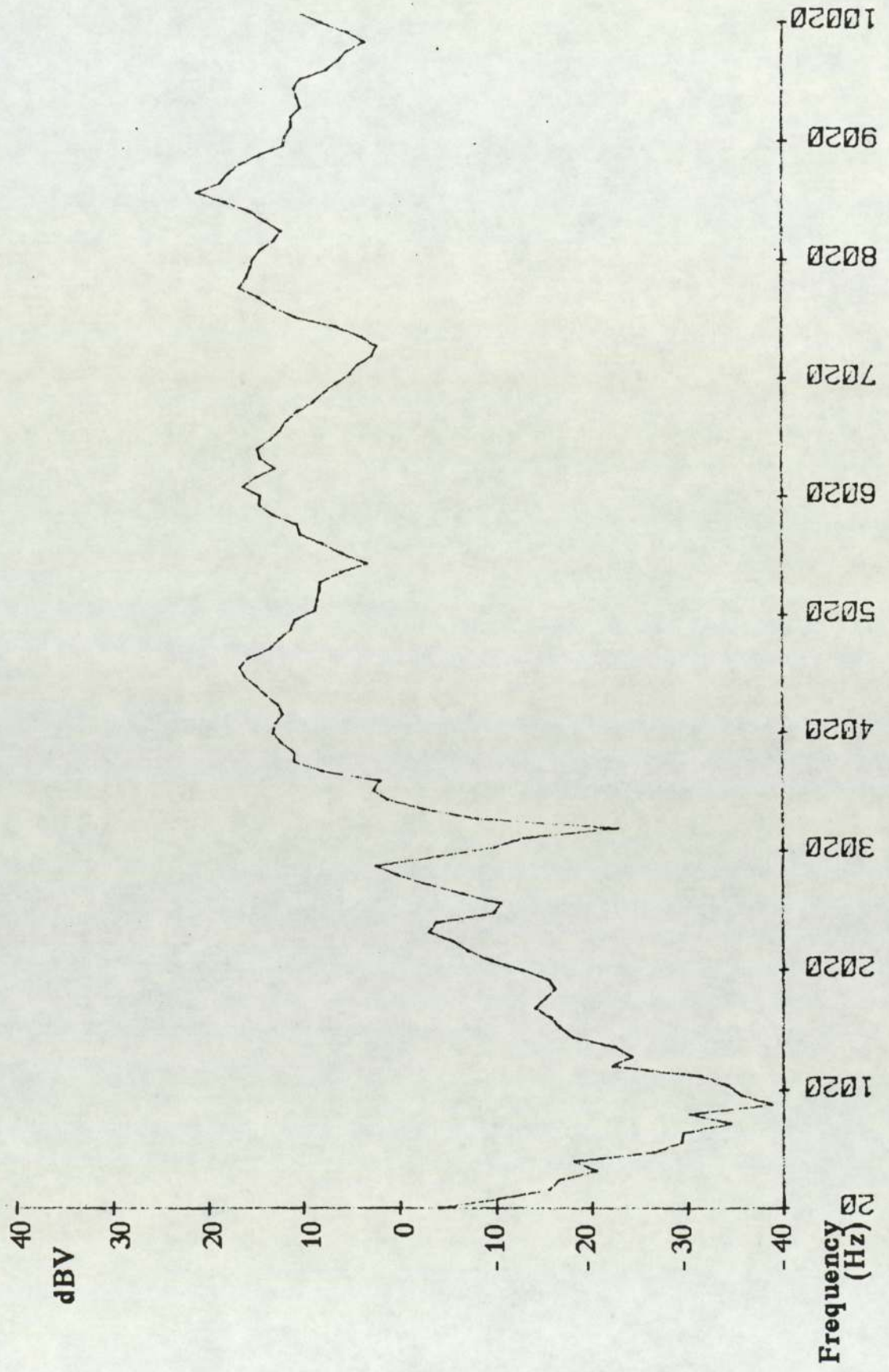

Figure 4.22 Receptance spectrum for casing (hot)

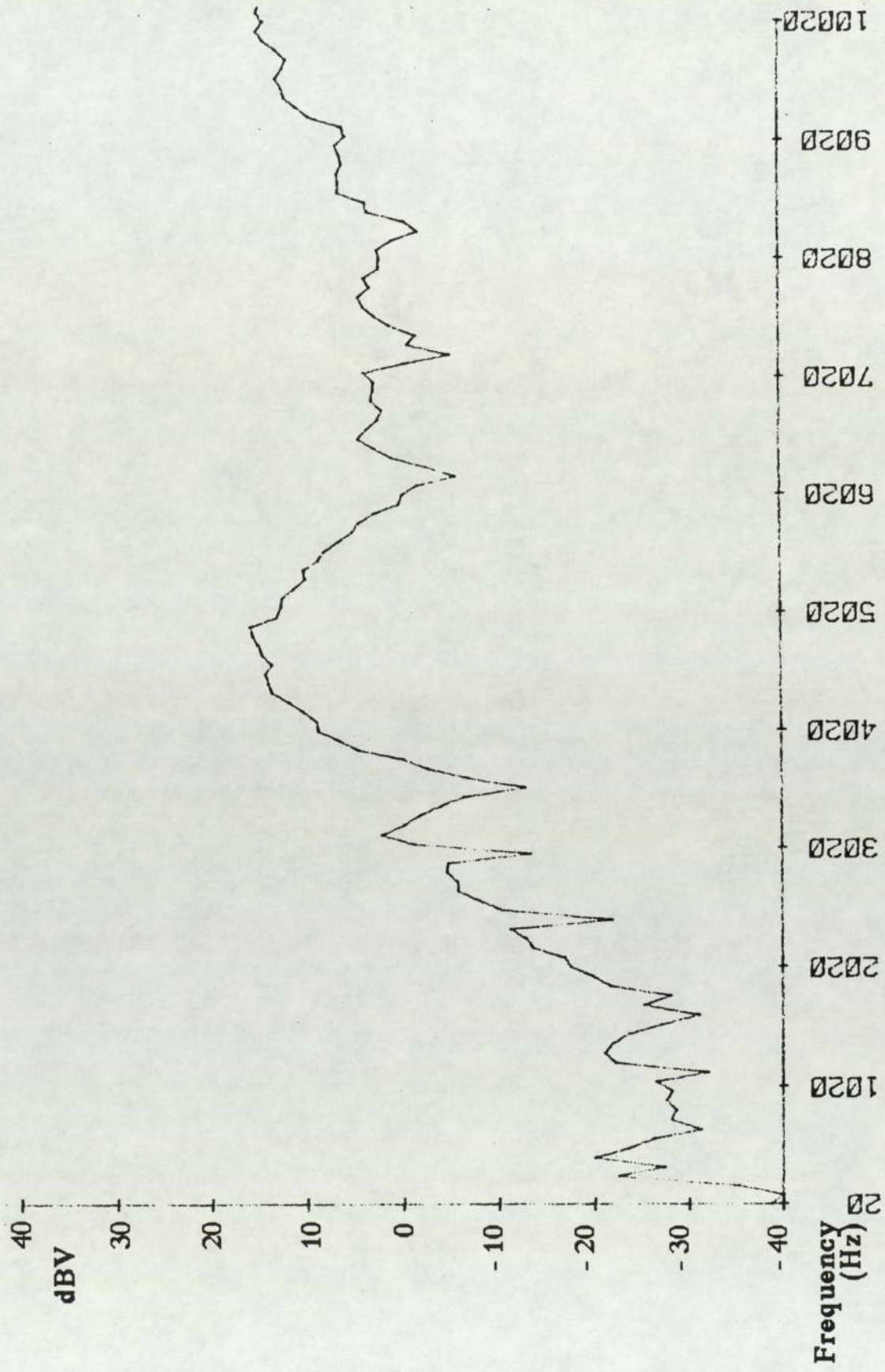

Figure 4.23 Receptance spectrum for casing (hot)

5.0 Air-end noise

Turning now to the experimental investigation of the source of air-end noise, which has been shown to radiate from the cylindrical casing. Only two causes of casing vibration exist; firstly a mechanical source which consists of vibration transmitted via a solid path from the rotor / stator unit to the casing ie. structure-borne noise and secondly an aerodynamic source which may be noise generated at the discharge port and radiated to the casing via the air / oil medium or pressure fluctuations within the casing that directly excite the casing or a combination of both.

Casing vibration measurements on a standard 2 pole compressor (Chapter 3), have shown a very strong harmonic content, particularly over the first 5 kHz of the frequency spectrum. Forces exerted within the rotor / stator unit will generate vibration on both the rotor and stator. Vibration transmission from the stator rather than the rotor is considered the main source of casing vibration since it is directly connected (Fig.5.1a). The transmission path from rotor to casing is through the journal bearings, which will provide some resilience.

To further the understanding of the vibration source, stator vibration levels (during normal operation) and the transfer function between stator and casing were measured in order to predict casing vibration levels due to stator vibration alone. Comparison between the predicted casing vibration levels and measured levels for the standard casing during normal operation allowed the relative importance of stator vibration to be determined. Casing vibration levels due to aerodynamic excitation alone were also measured to support this experimental work.

The transfer function determines the relationship between the vibration levels at two locations as a function of frequency. If, during

normal operation, it is impractical to measure vibration levels at one particular location then knowledge of the transfer function will enable the vibration levels at that location to be predicted from the measurement of vibration levels at the other.

Sisson and Simpson (1984) successfully used a transfer function technique to determine the correlation between the vibration levels of the internal compressor mechanism and those of the external casing and also between the sound levels measured internally and externally. Their results indicated that there was poor isolation between the internal components and the shell which allowed a high transmission of vibrational energy. Their sound measurements, on the other hand, indicated that there was no significant transmission of energy from the internal cavity to the outside. Further experimental work showed that modification of the suspension system reduced the transmission problem. The equipment used by Sisson and Simpson enabled them to make measurements on the internal compressor components during normal operation. Such measurements were not possible on the Hydrovane compressor, therefore the transfer function technique had to be used in conjunction with other experimental results.

5.1 Transfer function measurement between stator and casing

This section of research was designed to determine the relationship between stator vibration and casing vibration for a pseudo-random input force applied to the stator of a normally assembled air-end.

5.1.1 Transfer function : Experimental procedure

The method employed is illustrated diagramatically in Fig.5.1b.

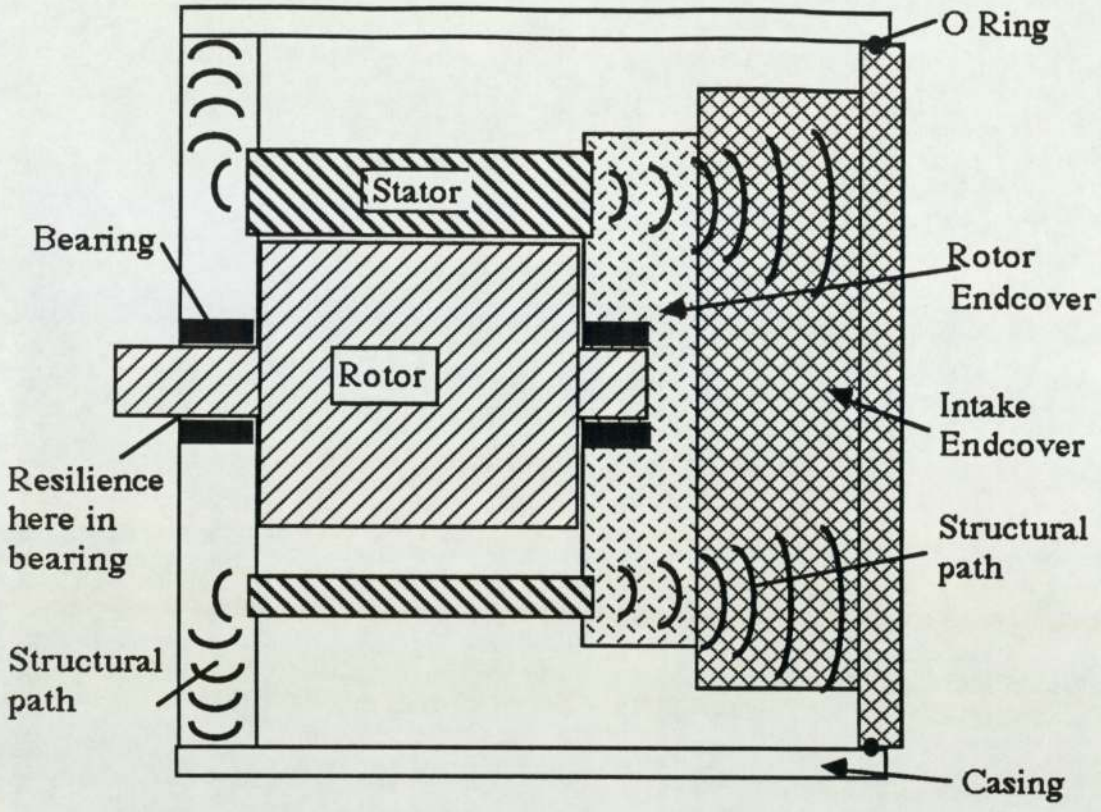

Figure 5.1a Vibration transmission paths to casing

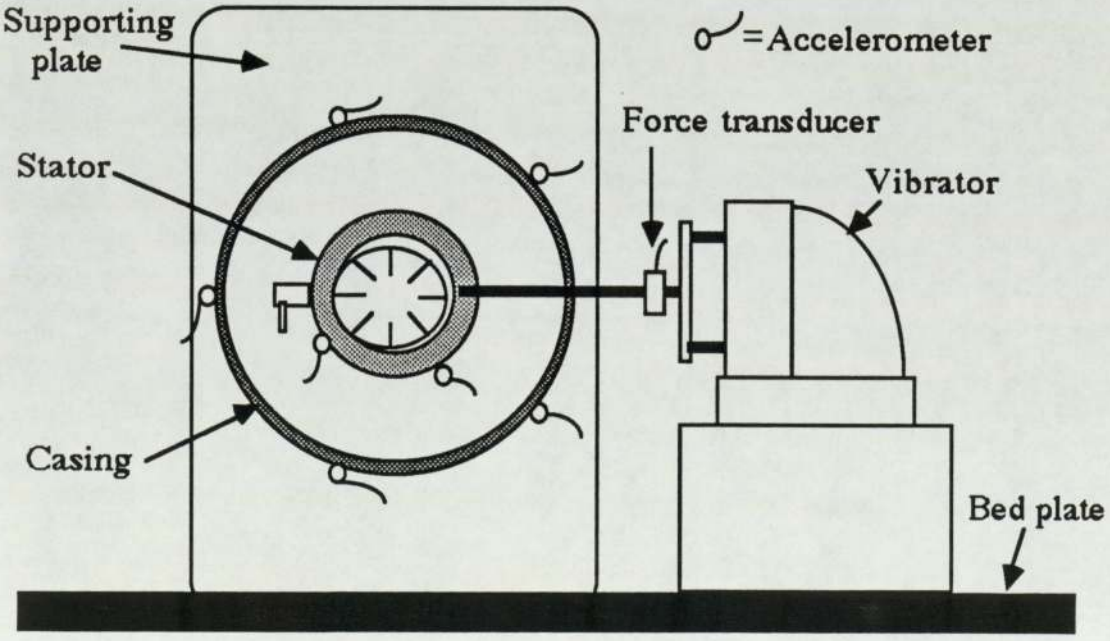

Figure 5.1b Rig employed to determine relationship between stator and casing vibration levels

The casing and rotor / stator unit were rotated through 90° and the stator, which had been drilled and tapped, was attached to an electrically driven vibrator by passing a length of threaded rod through the oil drain hole. This ensured sufficient transmission of the exciting force from the vibrator. The air-end was then reassembled and filled with the specified quantity of oil. The vibrator was controlled by the "noise source" from the spectrum analyser which generates a broadband periodic pseudo random signal whose period is automatically adjusted, depending on the frequency range, to ensure that periodicity does not affect the spectral analysis.

Accelerometers were positioned at two locations on the stator as shown in Fig.5.1. The locations were chosen as follows:

1 22° from TDC This is as close as possible to the centre of the "sealing arc" (plane about which the stator is symmetrical).The true central position is obstructed by a supporting bolt.

2 90° from the first accelerometer ie.112° from TDC

Accelerometers were positioned on the casing at four of the five equispaced locations used previously, refer to Fig.3.37.

Vibration levels were recorded at two different values of input force, the higher force produced r.m.s acceleration levels on the casing similar in magnitude to the levels measured during normal operation. This experiment was performed to determine whether the vibration transmission between stator and casing remained constant with frequency over the range of forces.

5.1.2 Transfer Function : Experimental results

Fig.5.2 shows the two vibration spectra measured at one stator location for the two different force levels. The difference was measured as 17 dB and is seen to be constant over the whole frequency range. Fig.5.3 shows the frequency spectra obtained for one casing location at the two force levels. The difference in levels was also measured as 17 dB. This indicates that the vibration transmission between the stator and casing does indeed remain constant over this range of forces.

The modal shape of the casing at a particular frequency determines the vibration levels over the complete surface. Fig.5.4 shows eight transfer function plots of the ratio of casing vibration to stator vibration at the higher force level. The eight plots are generated by the various permutations of four casing and two stator accelerometer locations. The vibration levels at each accelerometer location will be different: If an accelerometer is close to a node it will exhibit little vibration at that frequency, whereas at an antinode maximum vibration will occur. Comparing a node to an antinode will produce a large negative transfer function value whereas comparing an antinode to a node will produce a large positive transfer function value. For arbritary accelerometer locations, the transfer function values could lie anywhere in this range. This consideration not only accounts for the sudden peaks and troughs but also the differences between each graph.

If the visual average of the eight transfer function values at different frequencies is taken over the first 6 kHz then it is found that, at both input force levels the ratio of stator vibration to casing vibration is approximately 1:1 (the 0 dB line). Above this frequency the transfer function gradually increases indicating that casing vibration is marginally greater than stator vibration.

This result shows that there is no significant amplification or

attenuation of vibration between stator and casing and consequently stator vibration levels would be very similar to casing vibration levels below 5 kHz, provided stator vibration is the main source of casing vibration.

5.2 Exposed stator vibration

Stator vibration must be measured during normal compressor operation to provide the necessary information to predict the casing vibration levels due to stator vibration. However, the casing acts as a pressurised oil chamber into which hot air and oil are discharged and it was not possible to use the available equipment to measure stator vibration in this harsh environment. It was therefore necessary to remove the casing and expose the stator to enable vibration measurements to be made. This assumes there is negligible energy feedback from the casing to the stator.

5.2.1 Exposed stator vibration : Experimental procedure

The rig used for this experimental work is shown in Fig.5.5. A separate oil chamber was provided into which the discharge air and oil was piped directly from the stator. Return lines were fed from the base of the oil chamber to the stator so as to provide the necessary oil for lubrication and cooling. This closed system allowed the compressor to operate as normal but with the stator exposed. The back pressure in the system was maintained at 10.5 bar with a valve which controlled the discharge of clean air from the separate oil chamber.

Accelerometers were positioned on the exposed stator at the two locations used previously, 22° from TDC and 112° from TDC. Accelerometers were also positioned on the motor flange at two of the

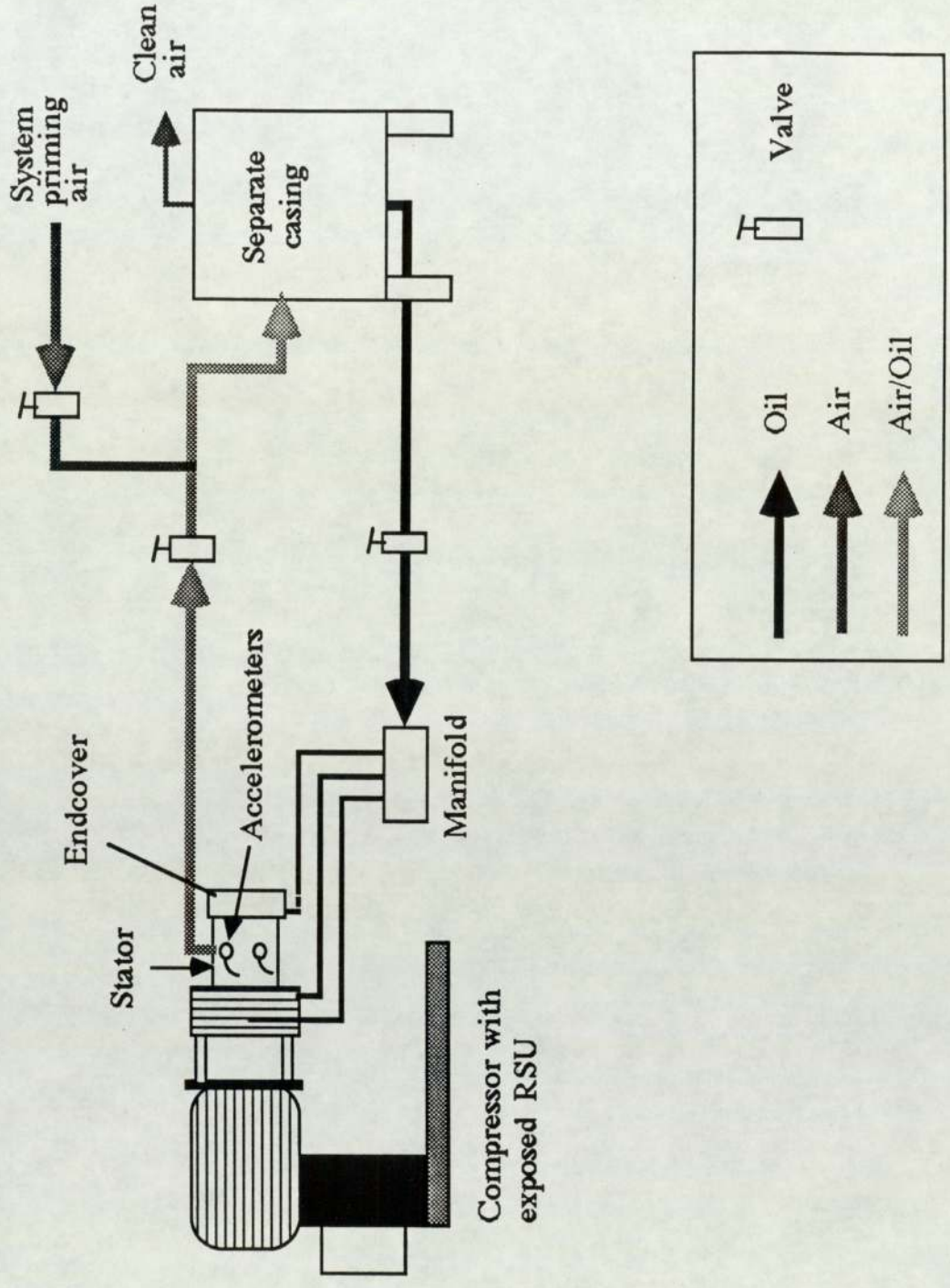

Figure 5.5 Exposed stator vibration rig

five locations used earlier (described in Chapter 3). This enabled a direct comparison of motor flange vibration levels to be made for the two experiments.

5.2.2 Exposed stator vibration : Experimental Results

Figs.5.6 & 5.7 show vibration spectra for the exposed stator at the two locations. In both spectra peaks exist at all the harmonics of the vane passage frequency. The harmonic content of these spectra is similar to the harmonic content of the vibration spectra obtained earlier from the casing of a standard compressor.

The vibration spectra for the motor flange are shown in Figs. 5.8 & 5.9. These were recorded with the input attenuator of the tape recorder set at 0.2. The vibration levels recorded on the motor flange in the earlier experiments (described in Chapter 3) were recorded with the input attenuator set at 1. For two identical signals this difference in attenuator settings would produce a 14 dB difference in the spectra levels since the spectrum analyser was set to the same scale. Taking this adjustment into consideration a comparison of the motor flange vibration levels from the two separate experiments shows that the frequency and magnitude content of both spectra at each location were very similar. Since the transmission path from the rotor / stator unit to the motor flange is identical in both experiments this result confirms that the forcing function within the rotor / stator unit has not been altered by the removal of the outer casing. Therefore the measured vibration levels on the exposed stator are an accurate reflection of the stator vibration levels that exist in a normal compressor.

A comparison was also made between the vibration levels on the exposed stator and the vibration levels on the casing of the standard compressor (Fig. 5.10). On the exposed stator the vibration levels were

recorded with the input attenuator set at 0.5. The peaks below 2.5 kHz all have a magnitude in the range of 0.01g to 0.04g. Between 2.5 kHz and 5 kHz the peaks have a magnitude in the range 0.03g to 0.07g. Above 5 kHz the magnitudes of the peaks increase to approximately 0.1g at about 7 kHz. For the standard compressor casing at frequencies below 2.5 kHz the peaks are in the range 0.02g to 0.06g. Between 2.5 kHz and 5 kHz the peaks are in the range 0.07g to 0.15g. Above 5 kHz they increase to approximately 0.5g at 7 kHz.

It is apparent that for peaks below 2.5 kHz the vibration levels are similar to those on the stator. However, above this frequency range the vibration levels on the casing are higher. Between 2.5 kHz and 5 kHz the peaks on the casing are approximately twice as high (this is measured as a 6 dBV difference on the frequency spectrrum by the relationship defined in Chapter 2). Above 5 kHz there is a general increase that varies from 6 dBV at 5 kHz to 15 dBV at 7 kHz.

The results from this experiment combined with the transfer function information, which showed a 1:1 ratio, have indicated that stator vibration is responsible for the casing vibration below 2.5 kHz. Above 5 kHz the increase in casing vibration levels is due to the natural response of the compressor casing.

5.3 Casing vibration : Effect of discharging air

The results from the two tests described above indicate that stator vibration is responsible for the casing vibration below 2.5 kHz. This implies that the aerodynamic source was responsible for casing vibration between 2.5 kHz and 5 kHz. It was therefore desirable to simulate the aerodynamic excitation within the casing and measure casing vibration levels without interference from stator vibration.

This was achieved by piping air and oil from the discharge port of the exposed stator to the oil filler plug hole of a separate stationary compressor casing. The experimental rig is shown in Fig.5.11. It was accepted that the noise and pressure fluctuations transmitted through the pipe would be affected by the pipe geometry and stiffness and would not produce effects identical to those effects that occur in the standard compressor casing. To minimise any adverse effects it was important to maintain the same internal diameter of tube and keep the length as short as possible. This conflicted with the interests of minimising vibration transmission between the two compressors. To reduce vibration transmission a combination of steel tube (0.4 m) and nylon hose (0.2m) was used. To prevent any external acoustic excitation from the operating compressor acoustic separation was achieved by passing the tube through a solid brick wall, the gaps being filled with a sound absorbent material.

Noise and vibration measurements were made on the stationary compressor casing at three of the five locations used previously to determine the effect on the casing of pressure pulses and aerodynamic noise only.

5.3.1 Casing vibration : Experimental results

Casing vibration spectra due to aerodynamic excitation are shown in Figs. 5.12 & 5.13. These were recorded with the input attenuator set at 0.5. Peaks at harmonics of the vane passage frequency are predominant throughout the first 6 kHz of the spectrum. The results show that below 2.5 kHz the magnitude of the peaks are in the 0.005g to 0.02g range and above 5 kHz the peaks are in the 0.02g to 0.05g range. In both these ranges the casing vibration levels are lower than both the exposed stator vibration levels and the standard compressor casing

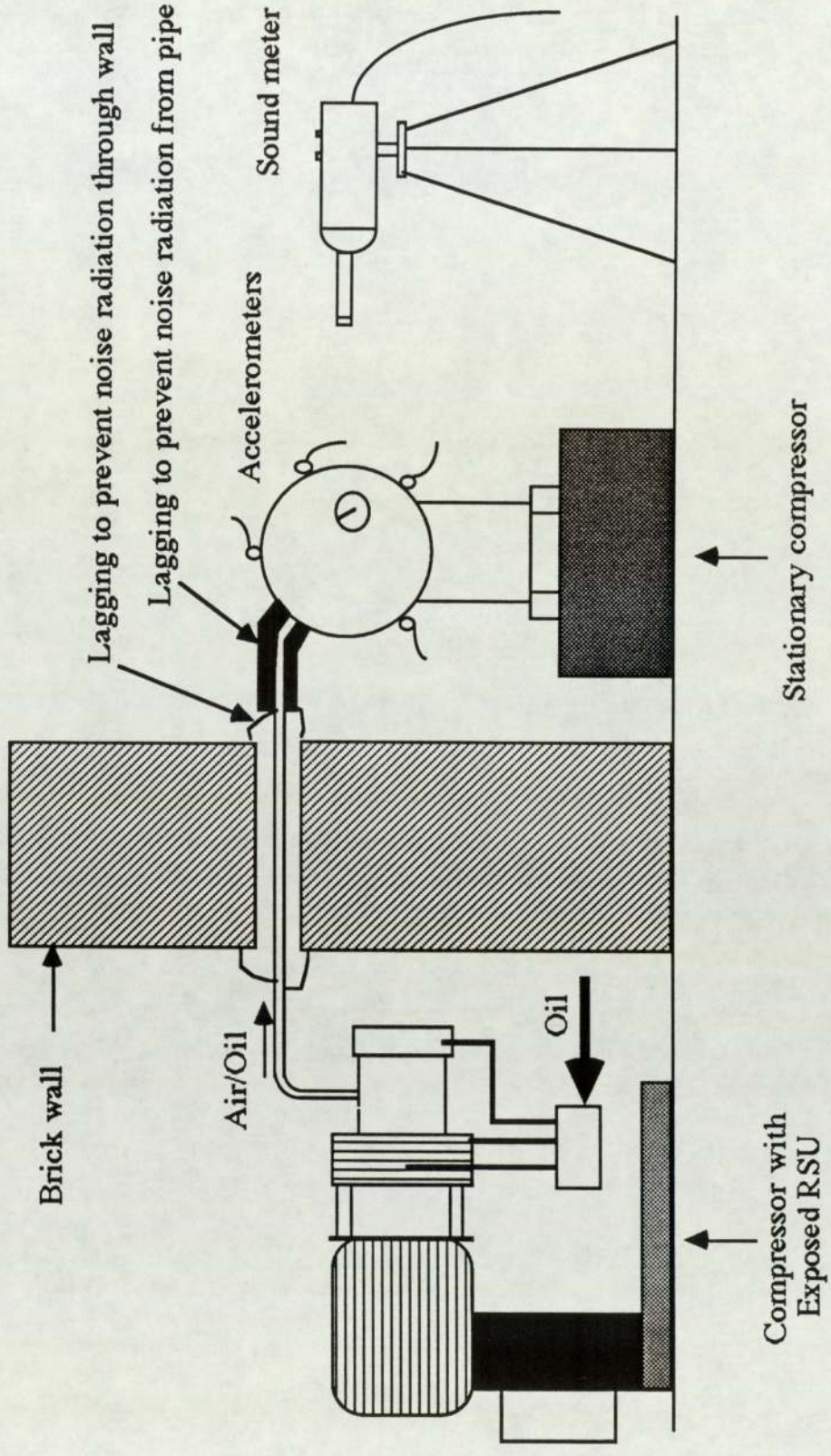

Figure 5.11 Aerodynamic noise rig

vibration levels. Between 2.5 kHz and 5 kHz the magnitude of the peaks is in the 0.05g to 0.2g range. In this range the casing vibration levels due to aerodynamic excitation are of a similar level to those on the standard casing. This result agrees well with the earlier findings and suggests that the aerodynamic source is responsible for the casing vibration in the 2.5 kHz to 5 kHz region.

5.4 Air-end noise : Conclusions

It has been shown that the casing vibration problem is two fold. At low frequencies (below 2.5 kHz) the transmission of mechanical vibration from the stator is the major source of casing vibration and at the higher frequencies (2.5 kHz - 5 kHz) aerodynamic noise generated at the discharge port is the major cause of casing vibration. Above 5 kHz the natural response of the casing amplifies the stator vibration levels transmitted to the casing but it has already been shown that noise is not a problem in this higher frequency range.

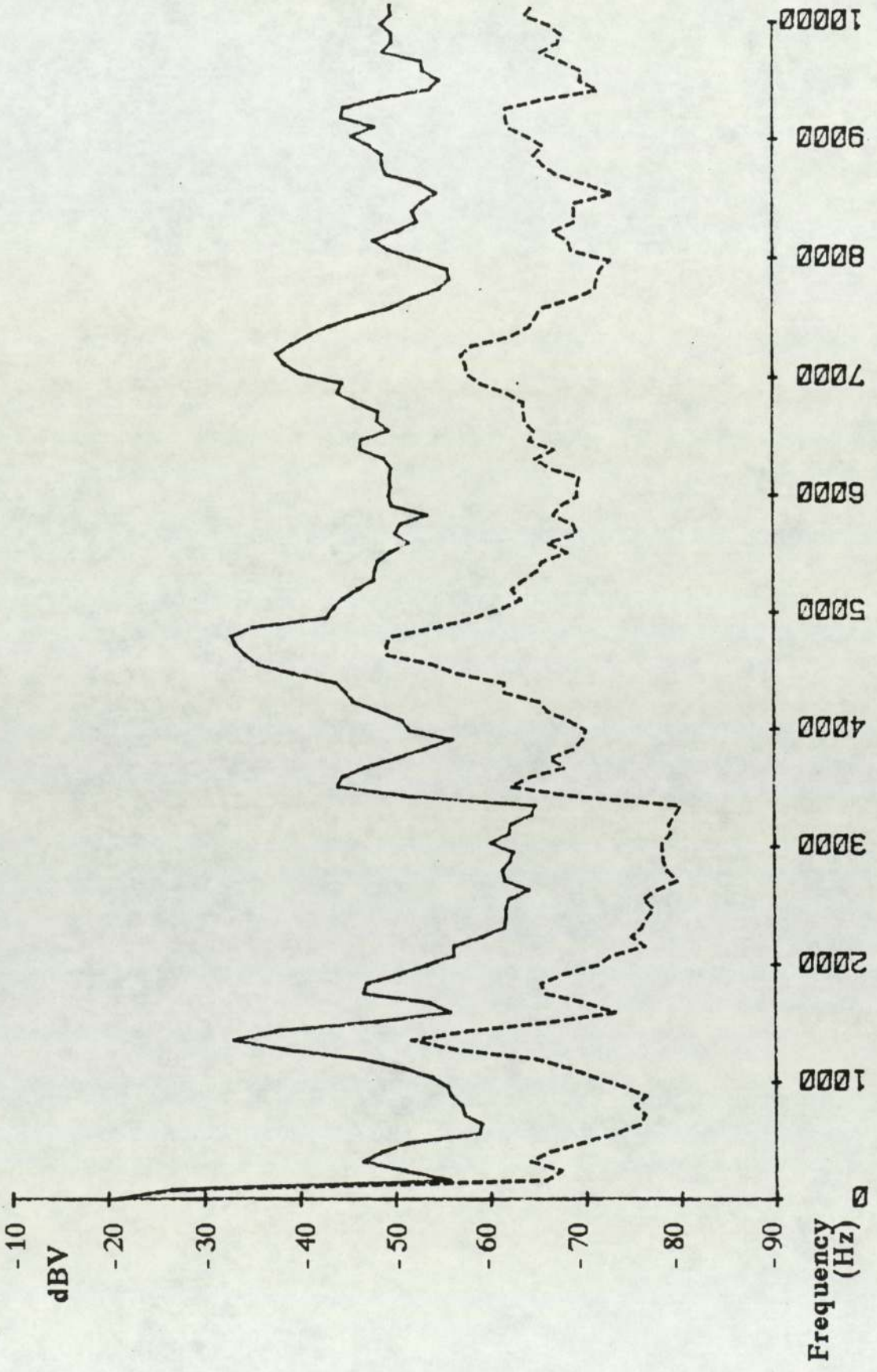

Figure 5.2 Stator vibration spectrum at two force levels

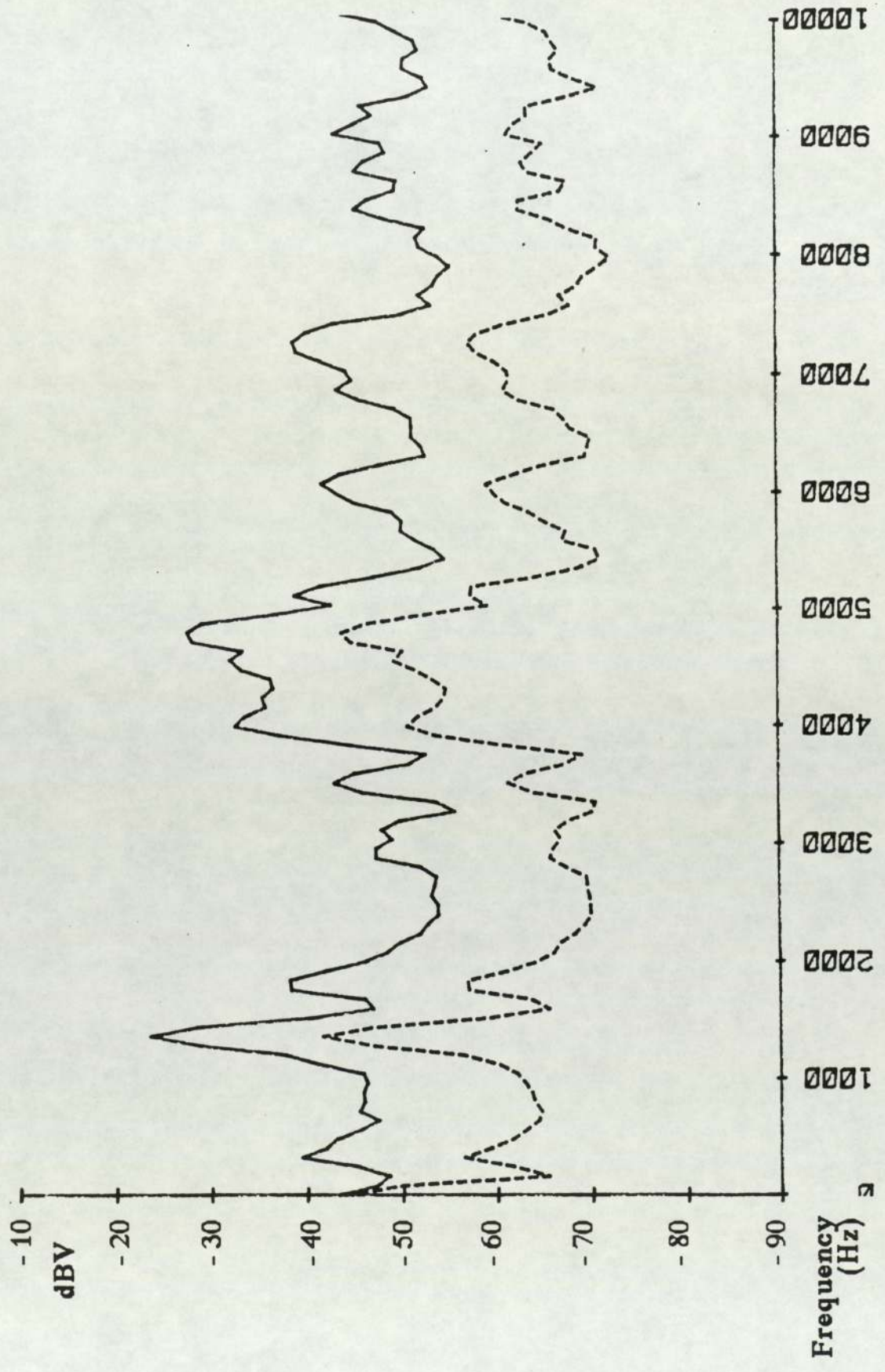

Figure 5.3 Casing vibration spectrum at two force levels

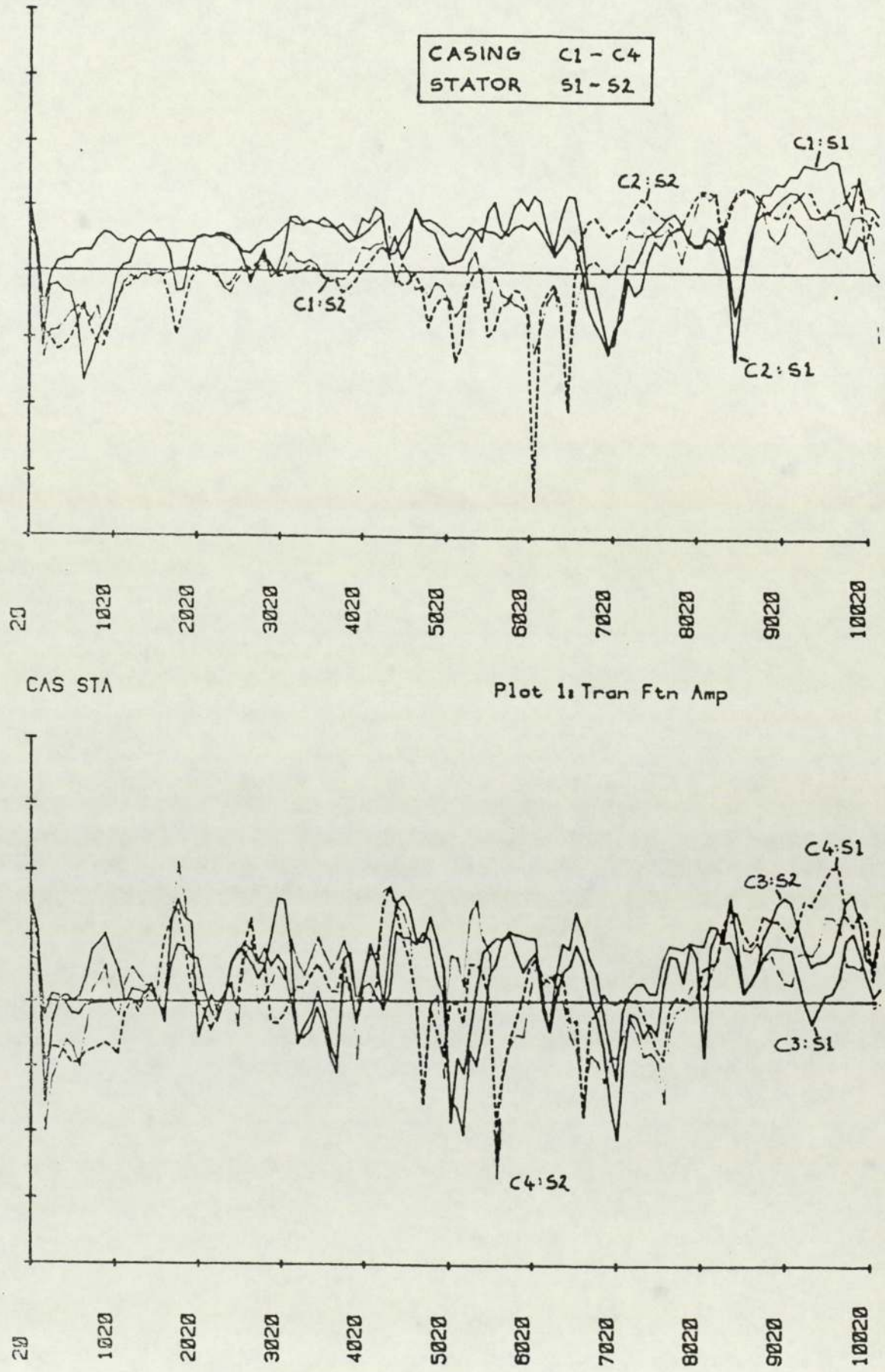

Figure 5.4 Transfer function spectra between stator and casing

Figure 5.6 Vibration spectrum on exposed stator (sealing arc)

Figure 5.7 Vibration spectrum on exposed stator (90° to SA)

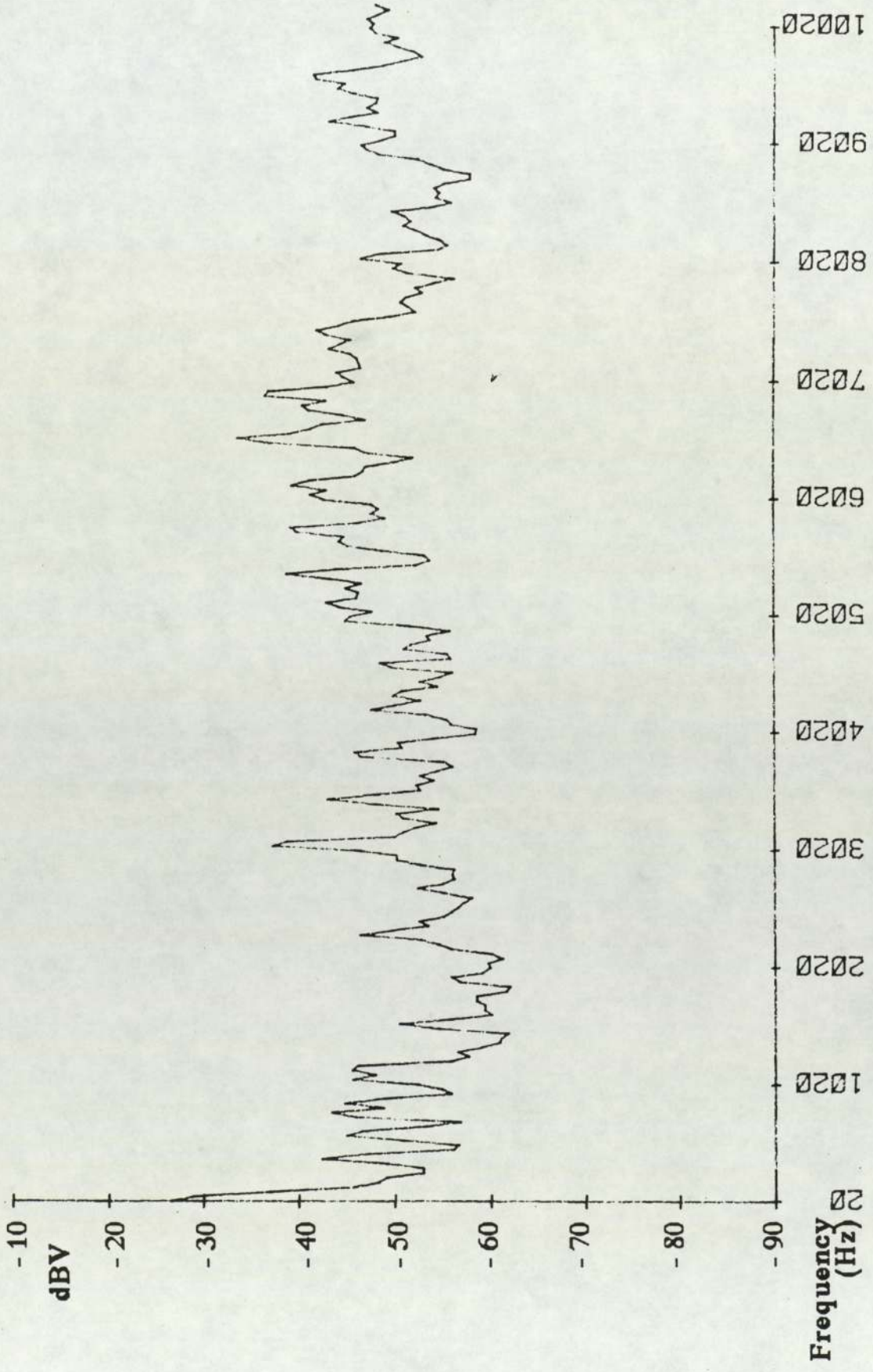

Figure 5.8 Vibration spectrum on motor flange (location 2)

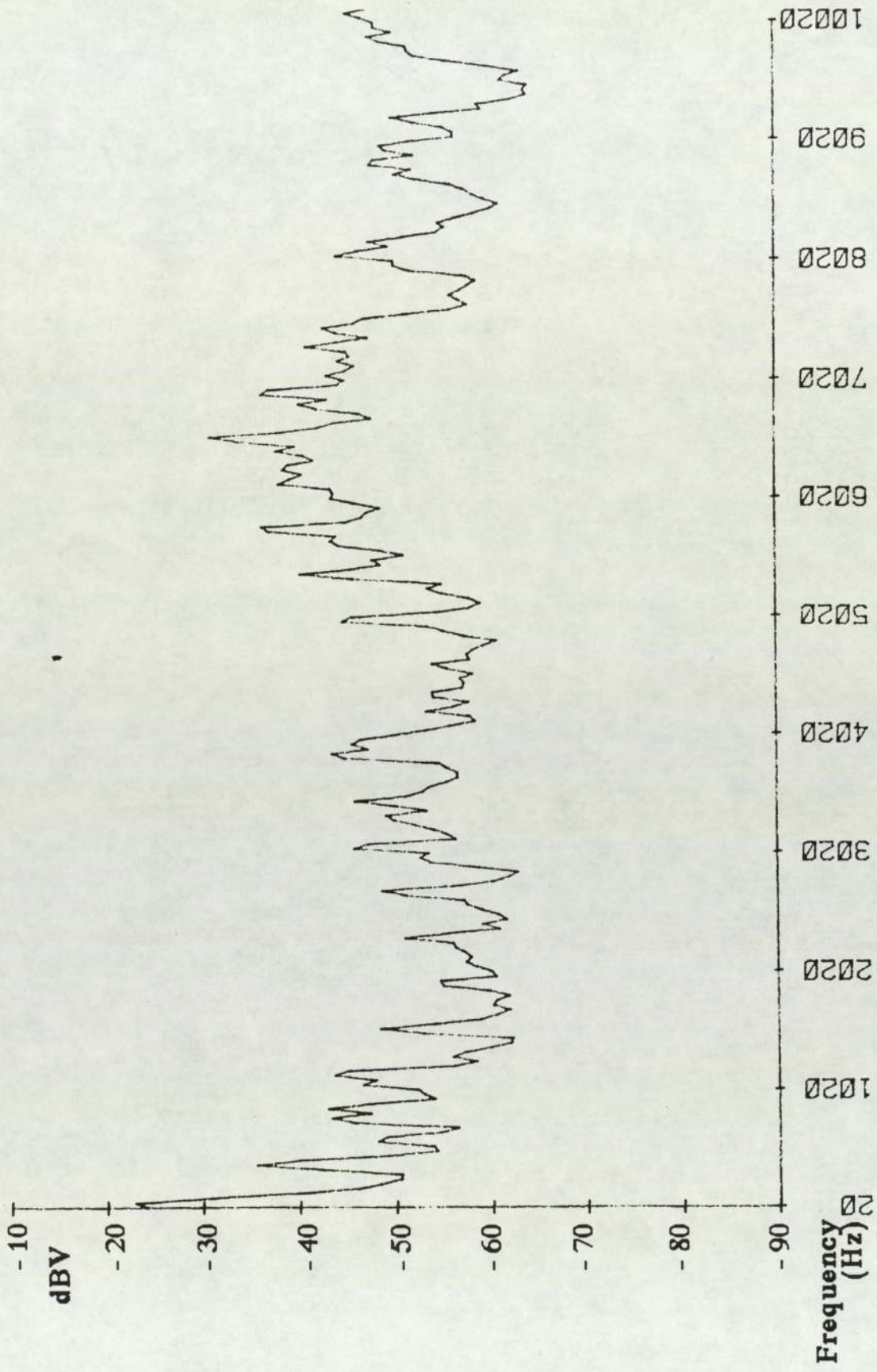

Figure 5.9 Vibration spectrum on motor flange (location 4)

Figure 5.10 Vibration spectrum from standard casing

Figure 5.12 Casing vibration spectrum aerodynamic noise only

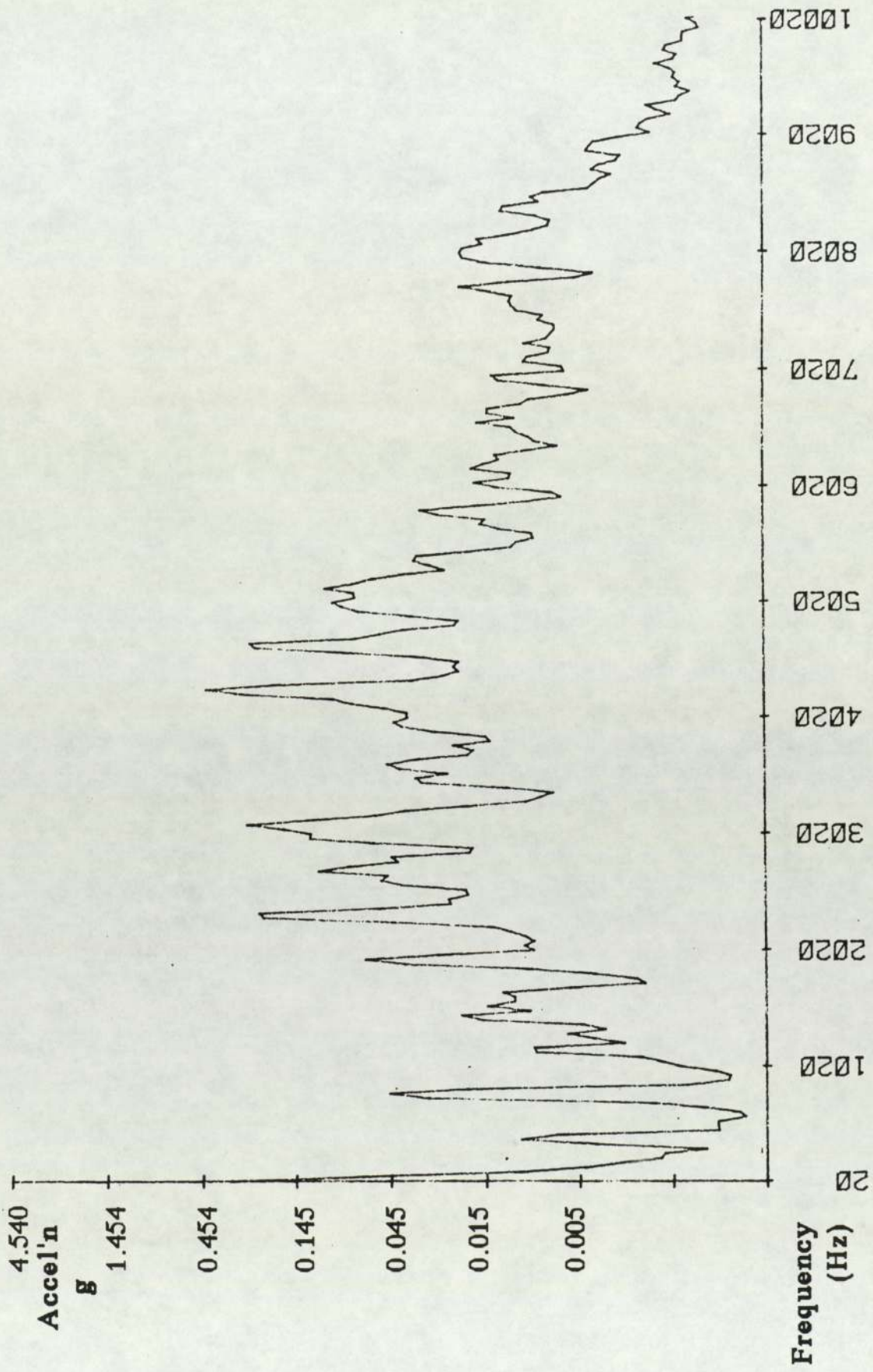

Figure 5.13 Casing vibration spectrum aerodynamic noise only

6.0 Theoretical and experimental investigation of casing vibration and its sources

The casing vibration problem has been shown to be two fold being generated both by vibration transmission from the stator and direct aerodynamic excitation. It is therefore necessary to reduce both these components if a significant overall reduction in noise is to be achieved.

Consideration of the forces arising within the rotor / stator unit during operation show that stator vibration might be generated by three distinct sources. The different rates of change of cell pressure during compression, which occur more rapidly just before discharge than during the remainder of the cycle, will induce an inbalance of force within the rotor / stator unit. Then there are the vane forces, which alter suddenly due to the large changes in acceleration as the vanes enter and leave the sealing arc from the eccentric bore of the stator and finally the possibility of hydraulic locking which could occur as the wedge of oil, known to exist at the vane tip (Fig.6.1), becomes squeezed on approaching the sealing arc.

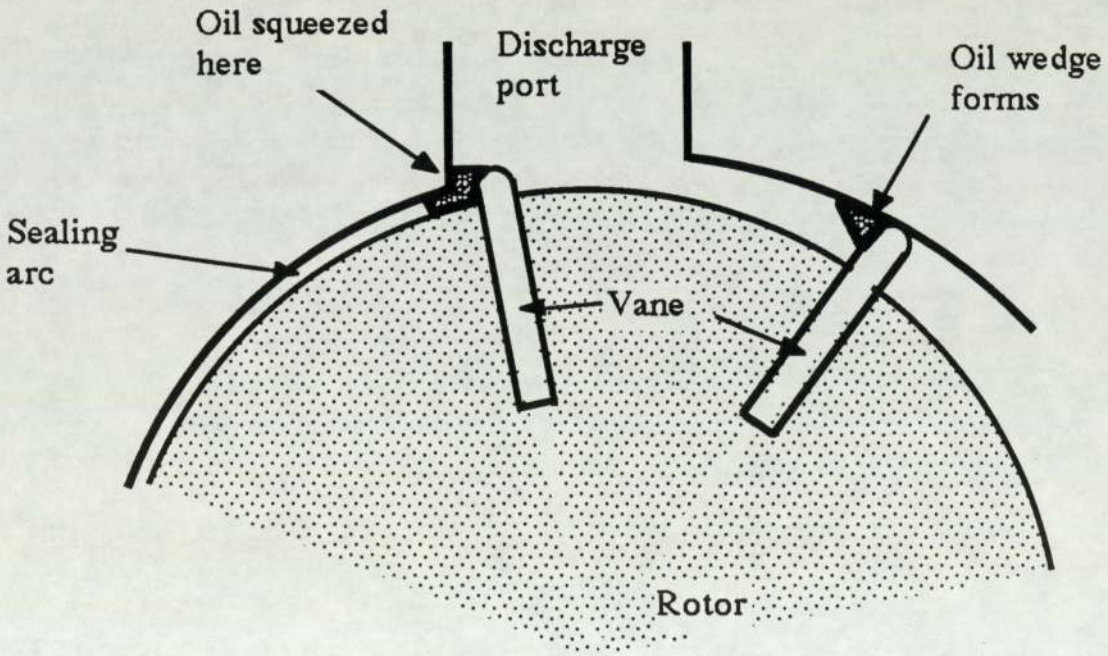

Figure 6.1 Schematic showing oil wedge

The only sources of aerodynamic excitation considered were internal pressure fluctuations caused by the intermittent delivery of air, which effectively "pump" the casing and noise generated at the discharge port due to sudden pressure changes between the cell and casing and also the interference of passing vanes in this region.

To reduce noise generation through improved design, it is essential to gain a greater understanding of the possible sources of noise and vibration. If the use of a mathematical model can simulate accurately the processes of noise generation which exist in a standard compressor then the effect of any alterations can be predicted very efficiently without the need for extensive experimental work. The time required to generate and validate a model must be weighed against the possible saving in experimental time.

To simplify the development of a prototype model the noise generation within the compressor was only considered to be related to the magnitude of pressure fluctuations generated at the discharge port and the magnitude of forces exerted within the rotor / stator unit due to internal pressure changes and vane dynamics. At this stage no account was made for the effect of oil on internal forces or the generation of noise at the discharge port.

The principal requirement of a model would be to show the relative effects of varying significant geometric parameters. It was hoped that a model could be developed to an extent whereby the change in pressure fluctuations could be predicted for different discharge port flow areas; also the effect on internal force levels if, for example, the compressor was operated with no internal pressure or no sealing arc.

Absolute accuracy of prediction was not considered essential and this permited the use of justifiable assumptions and simplifications which avoided the excessive development time required by a model

which attempted to link both thermodynamic and tribological phenomena.

To validate the model the behaviour of a series of compressor configurations was monitored during normal operation: modifications were made to the stator which in practice would affect only one of the possible sources: Pressure fluctuations were compared for various port configurations. Stator vibration levels were measured for firstly a relieved stator which had no internal pressure and secondly a circular stator which had no sealing arc. The equivalent theoretical modifications were also applied to the model and new pressure fluctuations and force levels calculated. Finally, as part of the experimental investigation only, stator vibration levels were compared for different oil injection rates.

6.1 Mathematical model

Chang (1983) generated a mathematical model as part of a theoretical and practical study to improve the thermodynamic design of oil flooded sliding vane compressors. This required the development and validation of a model before an optimisation algorithm could be used to improve the various aspects of compressor performance. The study aimed to predict the optimisation of specific air output with respect to three geometric parameters; rotor diameter, stator diameter and rotor / stator offset. Chang comments that this is only one set of many possible parameters that can be used with an optimisation procedure.

Chang's study considered the following aspects; compressor geometry, thermodynamic properties within the cell, mass flow through ports, leakage flows between cells and also the dynamic behaviour of the vane in the slot. The model included the thermodynamic and frictional effects of oil where appropriate. Chang did not model the discharge

process in the detail required by the present investigation but his predictions for the compression process and their comparison with test results were used to validate the adequacy of the present model.

The compressor which Chang used for his experimental work was basically similar to the Series 15 machine with respect to suction, compression and oil injection. The major difference was in the relative geometric details of the discharge arrangement: the discharge port of Chang's machine was of square cross section giving a very abrupt port opening and linear increase in port area with angular rotation and the flow path from discharge port to casing was via a "gallery" of sufficient area to present minimal restriction to flow. In the compressor presently under investigation the discharge port is circular and connected to the casing via a tube of relatively small cross section.

The flow of air from the discharge port to the compressor casing is important in terms of efficiency as well as noise. The smaller the pressure fluctuations the smoother the flow: this theoretically increases efficiency and should reduce noise and vibration. There is no delivery valve in the rotary compressor: valve action is provided by the increase in discharge port area with time. If the variation of increase in flow area with time is too fast then reverse flow will occur and if the increase in area is too slow then over-compression will occur, which can lead to harmfull pressure fluctuations in the discharge region and higher impulsive forces on the stator. Any further restrictions in flow area can also produce fluctuations. Ideally, after the start of discharge there should be no reduction in flow area.

Chang's experimental work showed that the maximum pressure always occurred as the discharge port opened, dropping rapidly to the nominal discharge pressure and finally falling steadily as the cell continued to discharge and pass through the sealing arc. Chang's theoretical predictions showed discrepancies in this region, indicating

that cell pressure would remain at the nominal discharge pressure during discharge then fall uniformly through the sealing arc. These discrepancies were larger at higher nominal discharge pressures.

It was known that reverse flow does occur in the compressor under investigation at high delivery pressures only (Williams 1987) and generates further pressure increases after the discharge port has opened. The discharge process must therefore be modelled with sufficient accuracy to determine the magnitude of pressure fluctuations.

6.1.1 Mathematical model: Structure and assumptions

The computer model is split into three major sections. The first section uses fixed compressor geometry to determine cell volumes at 1° intervals. It is assumed that the vane tip centre is in contact with the stator surface at all locations and the changing inclination of the vane, caused by eccentricity of the stator, is neglected. As the suction port closes, the trapped air is assumed to be at atmospheric pressure and 30°C, its temperature having been raised due to heating effects in the intake ports.

As the cell volume reduces between suction and discharge the changes in pressure and temperature are calculated in accordance with the first law of thermodynamics. No account is taken of the effect on the compression process of oil injection into the compressor or leakage between cells. These effects are compensated for by two methods: firstly altering the value of heat transfer coefficients before and after oil injection and secondly including a leakage factor that is simply a function of discharge pressure and cell position. The various factors are adjusted so that the theoretical results generated when the dimensions of Chang's compressor are input into the model are compatible with Chang's experimental results. The same values of heat transfer

coefficient and leakage factor were then used to calculate the cell pressures and temperatures for the different dimensions of the Series 15 compressor.

The second section of the model simulates the discharge process from cell to manifold to determine the magnitude of pressure fluctuations in both chambers. The flow path from cell to manifold is relatively complex and may be regarded as a series of two separate orifices. The discharge process is modelled as quasi-steady flow through a single nozzle whose effective area is calculated from the actual areas of the two orifices. The flows from the manifold to the casing and casing to atmosphere are each considered as quasi-steady flow through a single orifice. The pressure difference across an orifice determines the mass flow through the orifice while the change in air mass, for a fixed chamber volume, enables the calculation of a new set of pressures and temperatures. The cycle is then repeated for all the chambers. The only known parameter change for each new degree of rotation is the volume reduction of the discharging cell.

The third section of the model uses vane dynamics and the internal pressure information to determine all the internal forces acting on the rotor, stator and vanes. The forcing function acting on the stator as vanes and cells pass is then determined as a function of stator angle.

It is important to emphasise that this model was generated to give guidelines as to the effect of altering various parameters. In this respect the actual values may not be close to measured values but indicate the relative magnitude of changes likely to arise. The details of the calculations are given in Appendix B. The trends are summarised in the following section.

6.1.2 Mathematical model : Discussion of theoretical results

The theoretical modifications applied to the model were based on altering the algorithm which determined the port area and consequently the equivelant discharge flow area. Five different configurations were modelled as shown in Fig.6.2 and pressure fluctuations calculated for three nominal discharge pressures, 6.5 bar, 8.5 bar and 10.5 bar. The five port configurations are referred to as standard, 3 slots, 9 x 6mm holes, 9 x 6mm reversed and triangular. The rate of increase of port area with angular position for the different configurations tested is shown in Figs.6.3a & 6.3b. Graph (a) shows the area for the complete discharge and graph (b) shows the initial opening in greater detail.

Before reaching the port the discharging air must pass through the narrow slot between rotor and stator (Fig.6.1). The physical dimensions of this slot are 55mm x 1.5mm and the geometry of the machine is such that after the first few degrees of discharge the flow rate is dominated by this slot since the port area has increased to be greater than the slot area. In addition both the slot and port may become partially blocked with oil which will significantly reduce the effective flow area. The peak to peak pressure fluctuations predicted in the manifold located immediately downstream of the discharge port are summarised below in Table 6.1.

Table 6.1 Predicted discharge port pressure fluctuations

	Nominal Discharge Pressure (bar)		
Port Shape	6.5	8.5	10.5
Standard	0.33	0.27	0.26
3 Slots	0.38	0.33	0.28
9 x 6mm	0.38	0.30	0.29
9 x 6mm rev	0.33	0.28	0.27
Triangular	0.39	0.31	0.28

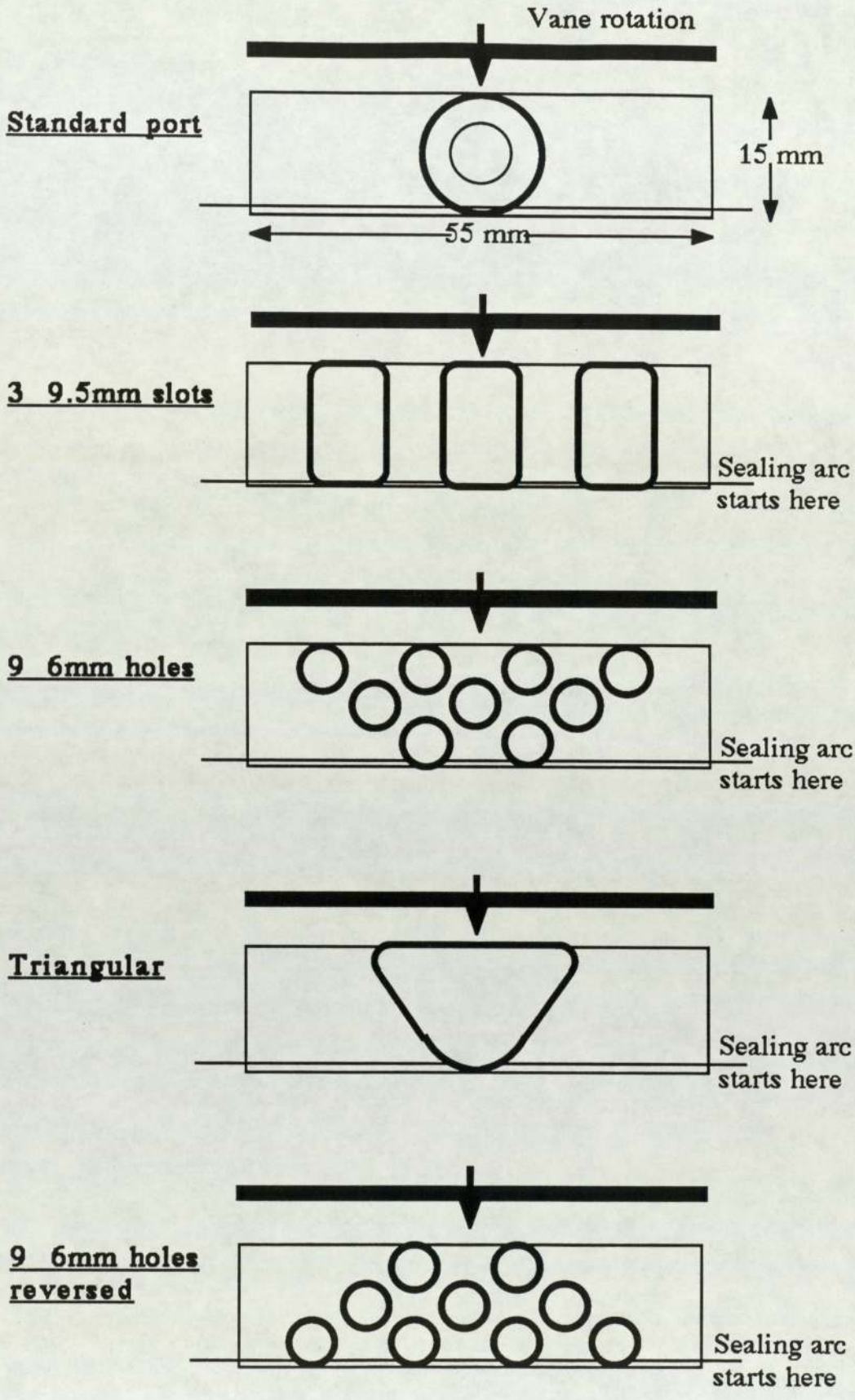

Figure 6.2 Schematic showing various port configurations

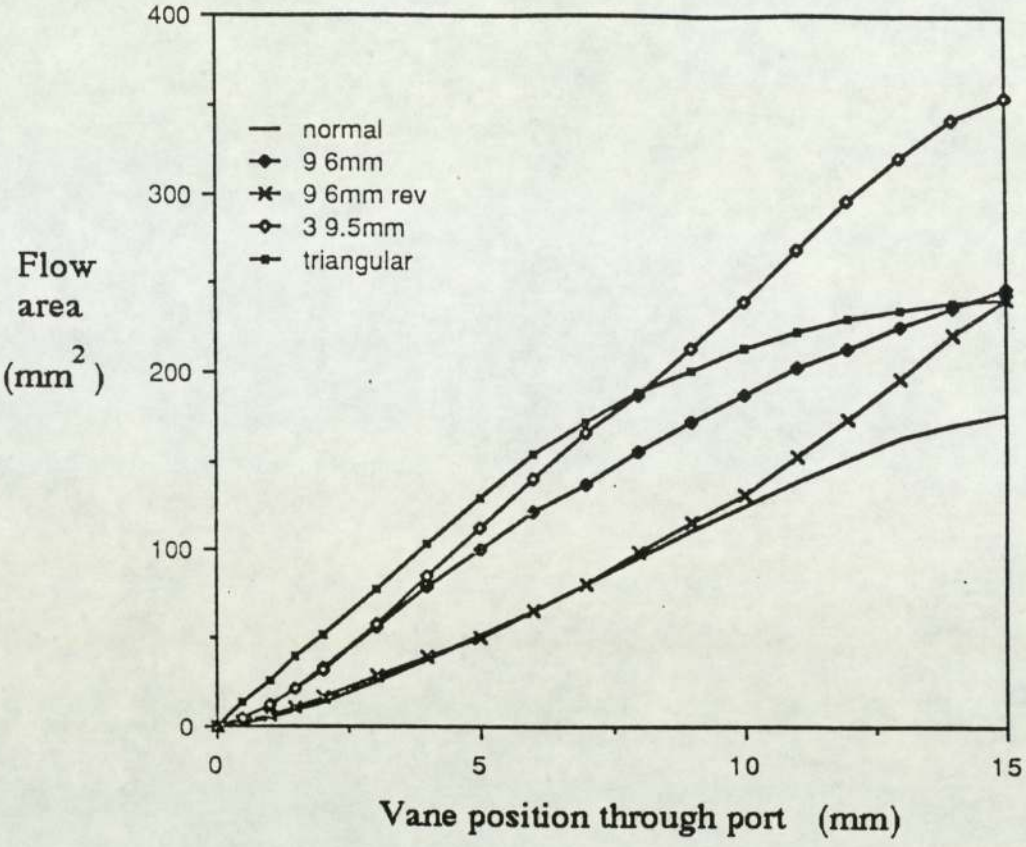

Figure 6.3a Rate of increase of port area with vane position

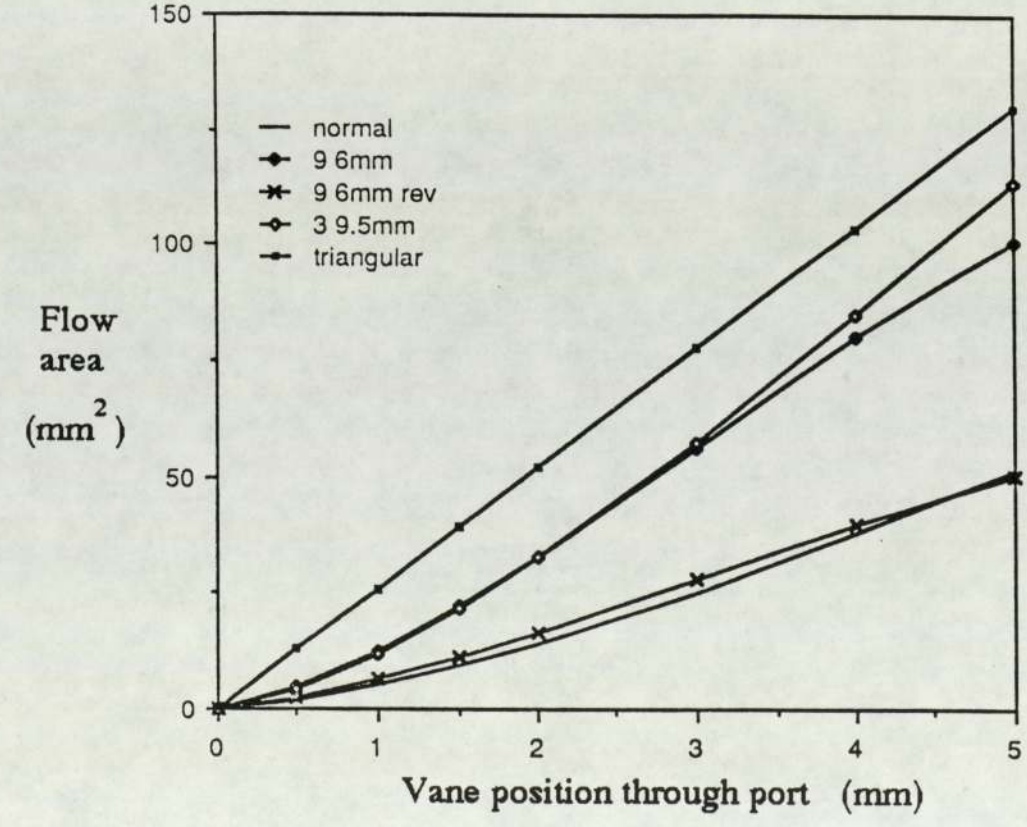

Figure 6.3b Rate of increase of port area with vane position

In all port arrangements the fluctuations were highest at a discharge pressure of 6.5 bar due to the larger difference between cell and casing pressure. At 8.5 bar and 10.5 bar the fluctuations were of similar magnitude.

After much development time the initial data produced for the standard compressor configuration appeared reasonable, however introduction of different configurations revealed that the calculations were based on an inadequate model which was dominated by a discharge process in which flow areas and volumes became too small, the effects of "oil clogging" remained unknown and therefore it could not be modelled in sufficient detail considering the two phase unsteady flow. After a few fruitless changes it was at this stage that it was considered that excessive time required to improve the model would not be justified by the quality of results. It is hoped that the information discussed in this chapter and details provided in Appendix B may provide a useful base from which a more accurate model can be developed at a later date.

6.2 Casing vibration : Experimental investigation

The experimental work in this chapter was all completed on the basic rig described in Chapter 5. However, modifications were made to enable pressure fluctuations to be measured immediately downstream of the discharge port and repeatability was improved through better control of oil flow rates and temperatures.

A manifold was manufactured to accommodate discharge port configurations which differed from the tapped hole used in the standard compressor (Fig.6.4). A temperature compensated pressure transducer, installed in the manifold, measured the pressure fluctuations produced by different port shapes.

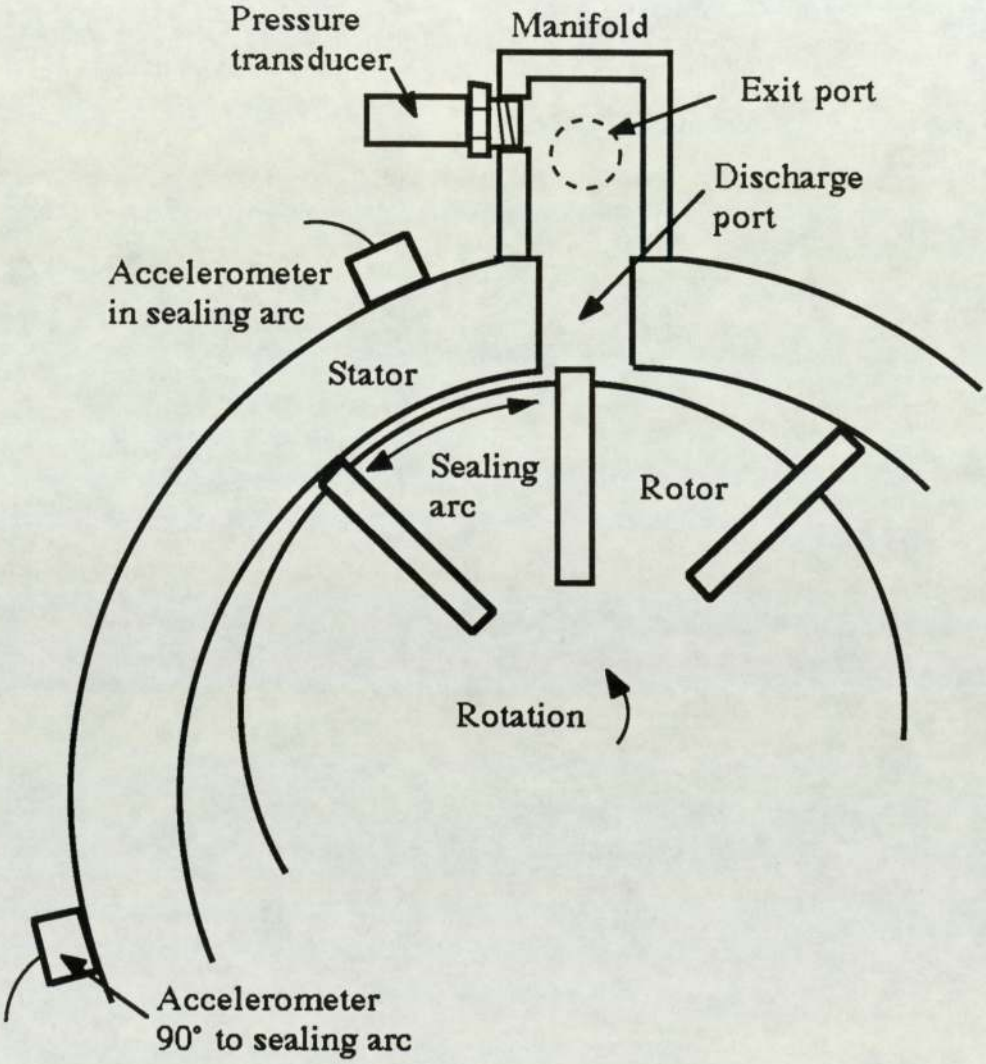

Figure 6.4 Schematic showing manifold arangement

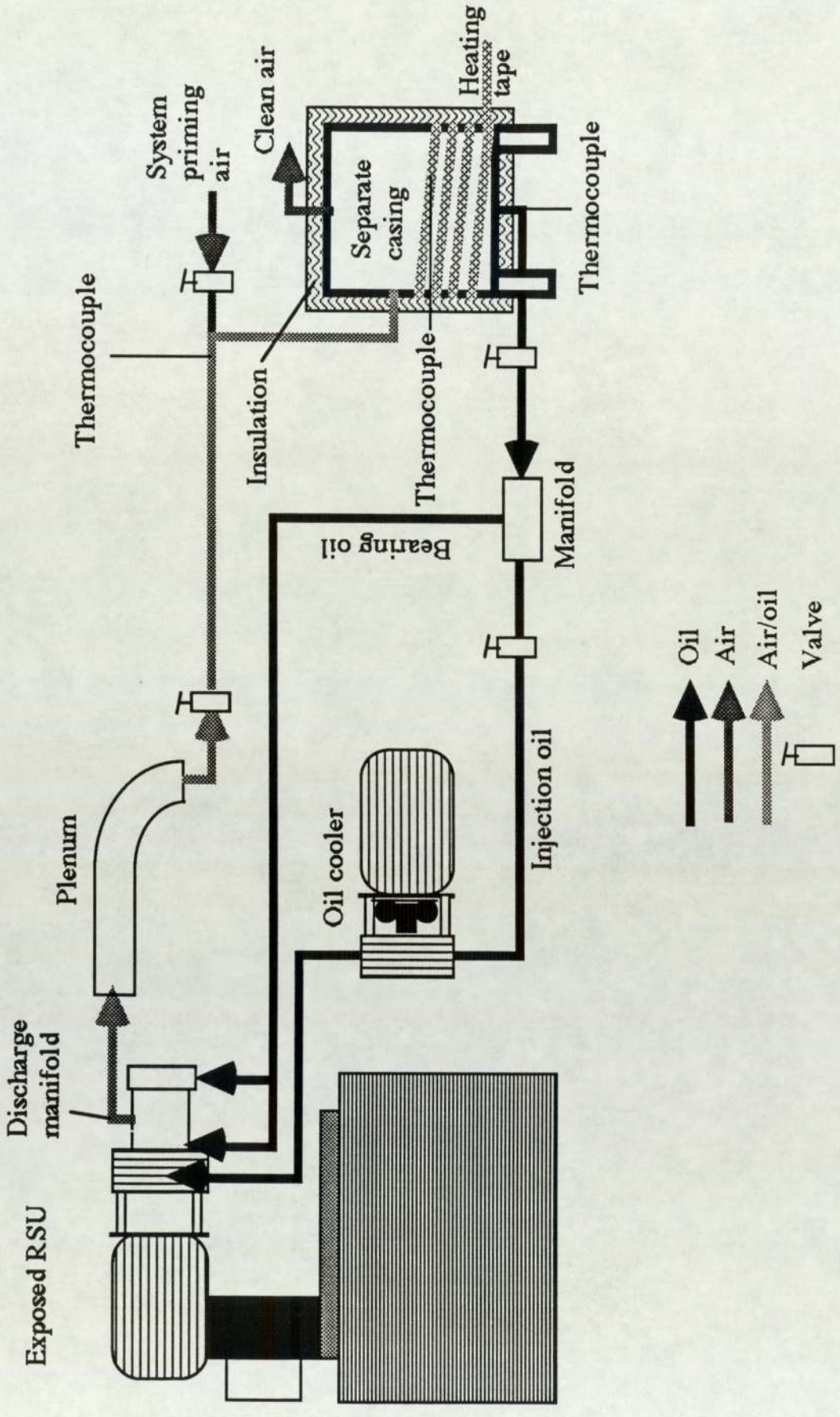

Figure 6.5 Modified exposed rotor / stator unit rig

The improved rig is shown above in Fig.6.5. To simulate the operating conditions in the normal compressor, air and oil from the manifold were piped along the shortest possible length of flexible hose to an expansion chamber whose volume was similar to the volume of the standard compressor casing. The air and oil were then piped to a large reservoir in which they were separated and where the back pressure in the system was controlled. Pipe lengths were kept to a practical minimum and the flow areas of all pipes were sufficiently large to ensure no adverse effects due to restrictions in flow downstream of the discharge port.

The large reservoir was heated to keep the the bulk oil at a similar temperature to the standard compressor temperature of 80°C. The oil was then piped either directly to the shaft bearings or via a standard oil cooler to the injection orifice. The rig operated as a closed loop and it was found that the air / oil temperature downstream of discharge settled at 90°C after a warm up period of 15 minutes. This modification ensured identical operating conditions for all experiments.

Vibration measurements were made at the two stator locations used previously (shown in Fig.6.4). Incorporation of an optical timing signal triggered by a cooling fan blade identified the vane positions relative to vibration and pressure signals.

6.3 Pressure fluctuations for various port configurations

The cell pressure at the start of the discharge cycle is controlled by rotor / stator geometry, the degree of internal leakage and port position, therefore any pressure fluctuations are theoretically only a function of port shape and downstream back pressure. Pressure fluctuations were measured at three different operating back pressures (6.5 bar, 8.5 bar and 10.5 bar) and for the five port configurations

discussed previously (Fig 6.2). The angular position at which discharge commenced was identical for each configuration.

6.3.1 Pressure fluctuations : Discussion of results

The pressure fluctuations measured in the manifold for each port configuration and back pressure are shown in Figs 6.6 - 6.10. A summary of the peak to peak pressure fluctuations for each arrangement is tabulated below in Table 6.2. Using the trigger information it was possible to relate the pressure fluctuations to the discharge cycle which lasts 20.8 msecs.

Table 6.2 Measured discharge port pressure fluctuations

	Nominal Discharge Pressure (bar)		
Port Shape	6.5	8.5	10.5
Standard	0.45	0.50	0.40
3 Slots	0.55	0.50	0.20
9 x 6mm	0.30	0.20	0.10
9 x 6mm rev	0.40	0.30	0.20
Triangular	0.40	0.35	0.40

When discharging to a back pressure of 10.5 bar manifold pressure is higher than cell pressure at the start of the discharge cycle which allows the possibility of reverse flow. For the standard port arrangement (with respect to the interaction between the discharging cell and the 15mm tapped port) the fluctuations were measured as 0.45 bar. For the first 7 msecs there is a drop in manifold pressure of 0.2 bar that indicates reverse flow from the manifold to the cell as expected. Over the next 6 msecs there is a rapid increase in manifold pressure of

0.45 bar due to over compression in the cell and a fully open port. There is a steady decline in manifold pressure over the next 5 msecs of 0.25 bar as air passes into the casing and the final 3 msecs of the discharge cycle shows a steady level.

For the three slot arrangement the overall fluctuation was slightly higher at 0.55 bar and the behaviour was similar with respect to timing. The initial drop in pressure of 0.3 bar is sharper and occurs in 7 msecs and the subsequent rise of 0.55 bar over 10 msecs is shallower. These slight variations are logical as the initial flow area is larger than the standard port allowing greater reverse flow.

For the 9 x 6mm reversed arrangement the pressure fluctuations were measured as 0.45 bar. Initially there was a drop in pressure of 0.25 bar in 6 msecs followed by a sharp increase of 0.45 bar in 6.5 msecs. This behaviour is similar to the standard port arrangement except there is a slight increase in pressure at the end of the discharge cycle. The general behaviour was expected since their flow areas are almost identical during discharge.

For the triangular port the fluctuations were measured as 0.45 bar. The first 9 msecs shows a drop of 0.25 bar follwed by a rise of 0.45 bar in 6 msecs. The flow area is largest for this port however no significant increase in fluctuation was measured.

For the 9 x 6mm hole arrangement the fluctuations were measured as 0.3 bar. There is a small increase in pressure a steady drop and then rise. This pattern is completely different to the other port arrangement and offers no logical explanation.

When discharging to a back pressure of 8.5 bar the cell pressure and manifold pressure are similar at the start of discharge. For the standard port arrangement the fluctuations were measured as 0.5 bar

and are generally smoother with more equal rises and drops in pressure. For the first 7 msecs there is a drop of 0.3 bar followed by a rise of 0.5 bar in 9 msecs. This behaviour indicates that either the port discharge area is too small or the manifold discharge area is too large, which allows more air to flow from the manifold than can enter from the cell despite the rapid rise of cell pressure.

For the three slot arrangement the pressure fluctuations were also measured as 0.5 bar. The first half of the cycle shows a steady drop in pressure, the second half a steady rise in pressure. If the port shape does dominate the size of fluctuation then this behaviour would not be expected since the flow area is larger than the standard port and this should reduce the time for which a pressure drop occurs.

For the 9 x 6mm reversed arrangement the pressure fluctuations were measured as 0.3 bar and the timing was similar to that at 10.5 bar. The reduced pressure fluctuations are logical in comparison to the behaviour of the same port at 10.5 bar, but not in comparison to the behaviour of the standard port at 8.5 bar. One explanation is the fact that the nine holes are all separate and not connected in the same fashion as the standard port even though total flow areas are identical: this may allow flow in opposite directions in the different holes when the pressure differences between the cell and manifold are relatively small.

For the triangular arrangement the fluctuations were measured as 0.35 bar: there is a slight drop in pressure of 0.05 bar over the first 4 msecs followed by a steady increase of 0.35 bar in 9 msecs followed by a steady decline of 0.3 bar in 8 msecs. The smaller pressure difference has reduced the magnitude of fluctuation and the larger flow area has reduced the time before the pressure increases.

For the 9 x 6mm port arrangement the pressure fluctuations were measured as 0.2 bar. Again the magnitude of fluctuations were smaller,

as expected, but the timing was the same as occurred at 10.5 bar which did not follow a logical pattern.

When discharging to a pressure of 6.5 bar the manifold is at a lower pressure than the cell before discharge starts therefore flow should always be positive ie. from the cell. Careful design of both port flow area and manifold discharge flow area should enable pressure fluctuations to be minimised. For the standard port arrangement the pressure fluctuations were measured as 0.4 bar, as expected the first half of the cycle shows a steady increase in pressure and the second half a steady decline in pressure.

For the three slots arrangement the pressure fluctuations were measured as 0.2 bar however the timing showed an initial fall in pressure before a final rise. This behaviour was completely opposite to that which was expected and identical to both the nine hole reversed arrangement, the nine hole arrangement and the triangular port arrangement where the pressure fluctuations were measured as 0.2 bar, 0.1 bar and 0.4 bar respectively.

It is sufficient at this stage to conclude that this experimental work has shown that the different discharge port arrangements and nominal back pressures do affect the pressure fluctuations in the manifold even though the magnitude of pressure fluctuation is not simply a function of back pressure and port flow area. The different port shapes and pressures produced levels of pressure fluctuations in the range 0.1 bar to 0.55 bar (peak to peak). The fluctuations generated by the nine hole hole arrangement were the lowest measured at each of the three back pressures, hence it was decided to compare noise levels radiated from a complete compressor when a stator with the standard port was replaced with the stator with the nine hole port.

6.3.2 Pressure fluctuations : Effect on radiated noise

To determine the effect that a reduction in pressure fluctuations had on radiated noise levels the modified nine hole port stator and standard stator in turn were assembled in a normal compressor and allowed to discharge directly into the casing without any cover or discharge pipe. Despite a reduction in the magnitude of manifold pressure fluctuations during delivery the results for the modified stator showed an 8 dB(A) increase in SPL at 1m from the casing. This is probably due to three factors: firstly the vane passes nine separate ports and tonal noise will be generated in a siren fashion at each one; secondly tonal noise will also be generated by vortex shedding at the greater number of sharp edges and finally broadband noise will be generated due to turbulence. This significant increase in radiated noise indicates that it is discharge port noise rather than fluctuations in internal pressure which is responsible for harmonic excitation of the casing. In fact the measured pressure fluctuations show a generally smooth sinusoidal pattern which indicates that casing excitation will occur mainly at vane passage frequency with little harmonic excitation and this behaviour has not been exhibited by previous spectra.

This has proved that noise generated at the discharge port and transmitted to the casing via the air / oil mixture is the major aerodynamic source of casing vibration, rather than internal pressure fluctuations.

6.4 Stator vibration : Contributing factors

Three possible sources of stator vibration were considered. Forces due to internal pressure, centripetal vane forces which alter significantly due to the large accelerations as the vanes enter and leave the sealing arc and oil squeeze which occurs when the wedge of oil at the

vane tip has no escape in the sealing arc. Experiments were devised to remove each source individually and measure the effects on stator vibration levels at the two locations used previously.

1 The effect of sudden changes in vane acceleration in the sealing arc was eliminated by the use of a circular stator with no secondary sealing bore.

2 The effect of internal pressure was removed by relieving the stator endcover to atmosphere during compression.

3 The effect of oil on the hydraulic locking process within the sealing arc was measured by varying the oil flow rate to the compressor.

6.4.1 Stator vibration : Influence of the sealing arc

The dynamic predictions from the computer model showed sudden changes in acceleration as the vanes rotate through the sealing arc, indicating that vibration will be produced (These results are shown in Appendix B). This had been confirmed by analysing the acceleration signals against time from an earlier experiment (Chapter 5.2.2) in which vibration was measured on an exposed stator. A typical time trace (Fig.6.11) shows 20 msecs of the 20.83 msecs required for one complete rotor reveloution and this clearly shows a vibration pattern repeated eight times a revolution. Incorporation of the trigger signal information which is shown in Fig.6.12 indicates that a sudden increase in acceleration occurs as each vane enters the sealing arc. Further proof was gained when stator vibration levels were measured on an exposed stator fitted with a rotor from which alternate vanes had been removed. This four-vane rotor maintains dynamic balance and the time trace in Fig.6.13 reveals quite clearly that vibration is generated as the vane

rotates through the sealing arc but no vibration is caused by passage of the empty slot.

Stator vibration levels were measured using a non-standard stator with a purely circular bore (no sealing arc) and compared with levels for a standard stator. The sealing arc was removed by increasing the diameter of the bore as shown in Fig.6.14, however this led to two minor problems. Firstly the geometric change would have an adverse effect on the compression ratio due to the increase in final cell volume at the normal discharge position. To compensate for this and maintain the original compression ratio the discharge port was positioned 3 degrees later. The second adverse effect would be the continued compression as the cell volume reduced between the end of the discharge port and the point of closest contact between the rotor and stator (Fig.6.15). To prevent further compression the stator was relieved in this region to allow air and oil to escape back into the discharge port.

6.4.1.1 Influence of sealing arc : Discussion of results

The graphs in Fig.6.16 & 6.17 show the vibration signals against time for the standard stator at both accelerometer locations. These results were recorded at a different sensitivity from that used in the earlier tests but show quite clearly that the stator receives an impulse eight times per revolution. The timing signal indicates that this impulse occurs as one vane has just entered the sealing arc and another vane is approaching the discharge port, where cell pressure is changing rapidly. The remaining six vanes are all at locations where there is no possible process by which an impulse could be generated.

Fig.6.18 shows the vibration signal for the circular stator. A comparison to the standard stator (Fig.6.16) shows a slightly higher

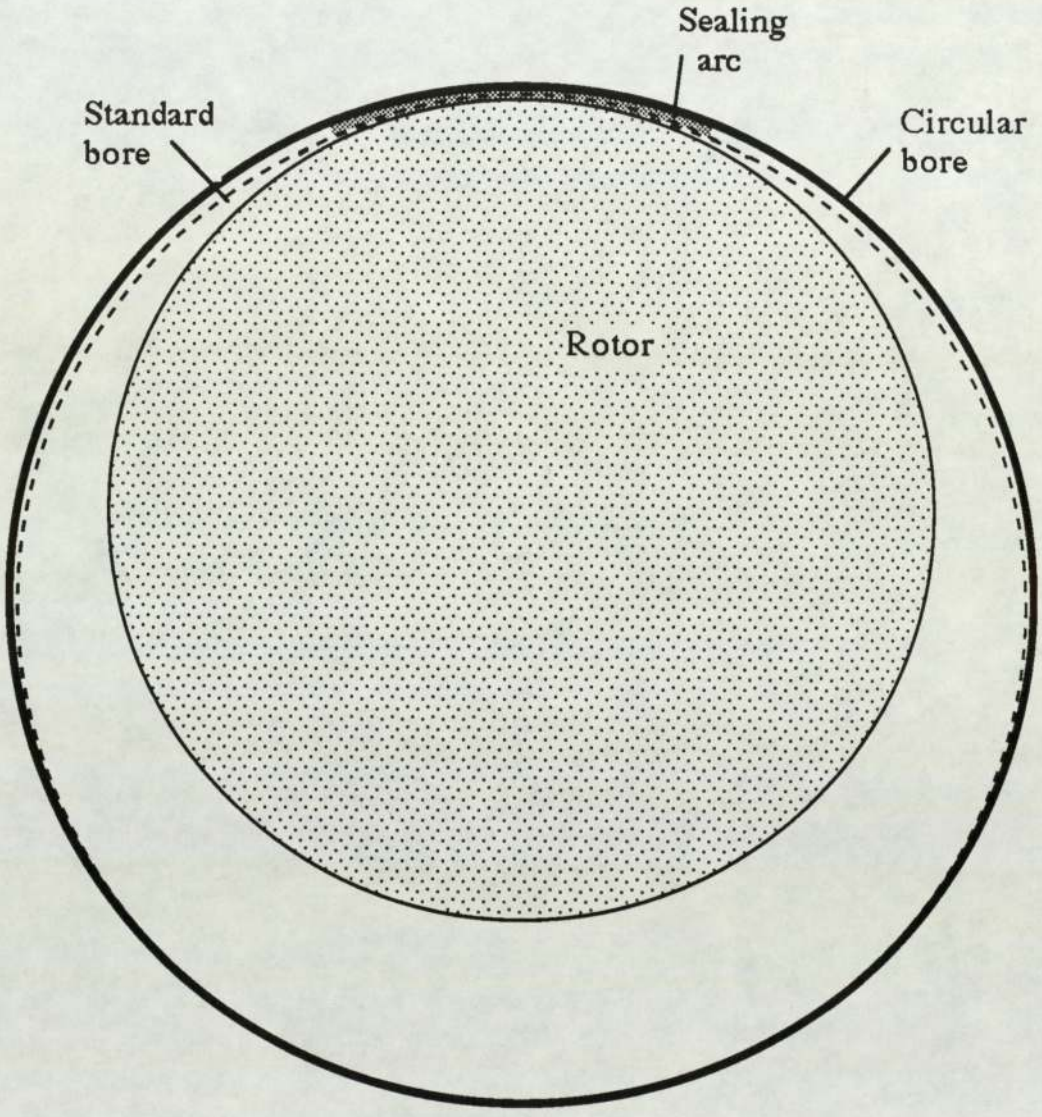

Figure 6.14 Schematic of stator with circular bore

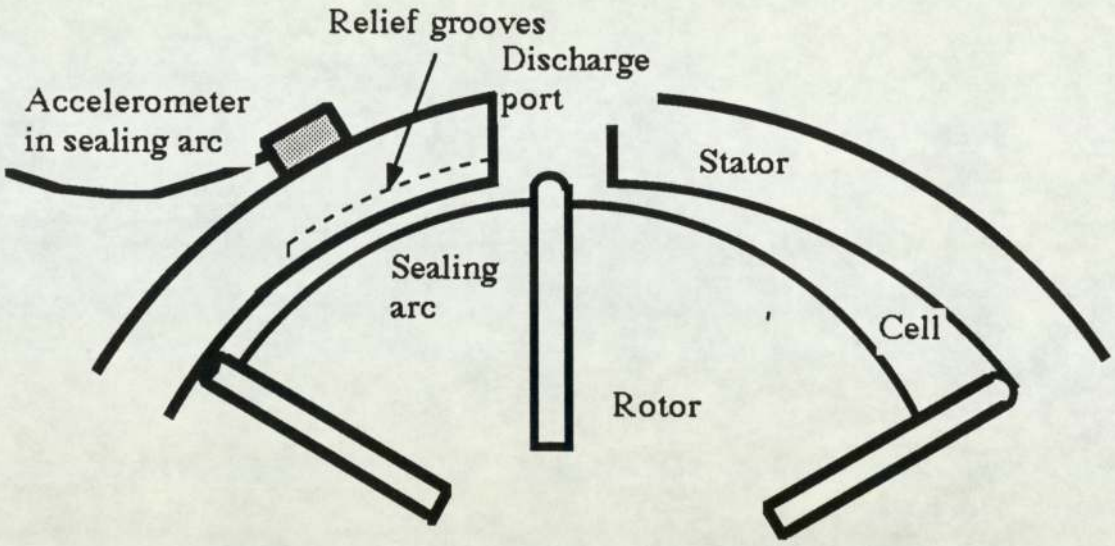

Figure 6.15a Sectional view of stator showing relief grooves

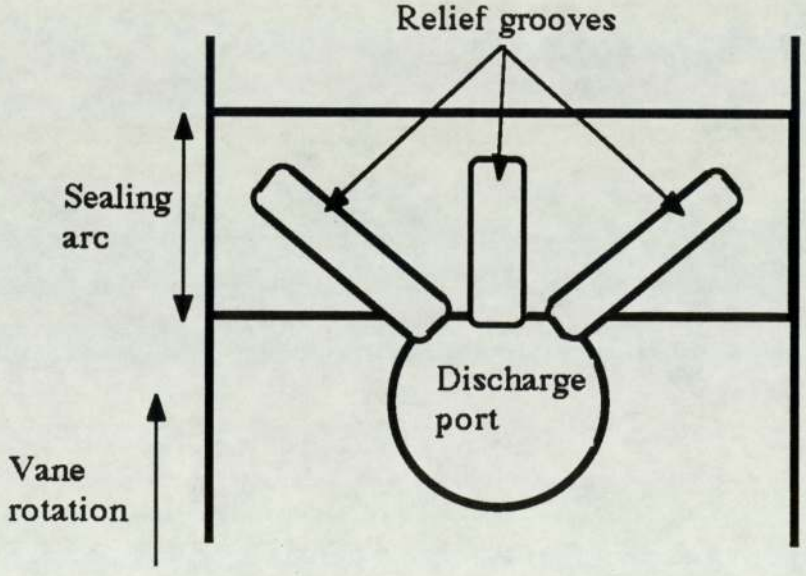

Figure 6.15b Plan view of stator showing relief grooves

general vibration level but there is not such a strong impulse. From the timing pulse it is apparent that each vane produces a similar vibration pattern, rising slightly as the vane approaches the line of closest contact and decreasing afterwards.

Fig.6.19 shows a vibration spectrum for the standard stator and Fig.6.20 shows a vibration spectrum for the circular stator. The vibration levels for the circular stator at the following harmonic frequencies (760 Hz, 1140 Hz, 1540 Hz, 1920 Hz and 2720 Hz) were between 8 dB and 20 dB lower, they were similar at 380 Hz and higher at 2340 Hz, there is no consistent comparison above 3 kHz. These results agree well with those above which showed a reduction in the impulsive character of the vibration.

Obviously the nature of the forcing function has changed, resulting in a significant overall reduction in the vibration levels at the harmonic peaks which dominate the radiated noise spectrum. The sealing arc is therefore a major cause of stator vibration.

6.4.2 Stator vibration : Influence of internal pressure

The forces on the stator due to internal pressure vary considerably during compression. The change in pressure is very gradual throughout most of the compression process. However, just before discharge and during the early stages of discharge the pressure rises sharply due to the large percentage reduction in cell volume and the relatively small discharge port flow area. This large but smooth rise in pressure during comprerssion will generate fluctuating forces at the vane passage frequency but it is the smaller, sharper changes in pressure during discharge which could provide repeated impulses to the structure at the vane passage frequency and so generate the strong harmonic content shown in previous experimental results.

To determine the effect which internal pressure has on stator vibration it was necessary to relieve the exposed stator of pressure during compression. This was achieved by replacing the standard endcover with an endcover which had a slot milled in its face over the area between the stator and rotor (Fig.6.21). Two circumferential slots were also milled in the stator body just before the discharge port to ensure complete relief.

Since there was no significant pressure generated oil could not be recirculated in the normal way and the system could not operate in the closed loop fashion as described in the introduction to this chapter. Instead, there being no cooling requirements, oil was supplied for lubrication purposes only by keeping the external reservoir at 70°C with a heating tape and at 4 bar using an auxillary source of compressed air. This provided normal oil flow rates to the compressor.

6.4.2.1 Internal pressure : Discussion of results

The graph in Fig.6.22 shows the stator vibration signal for the relieved rotor / stator unit. A comparison with the standard stator (Fig.6.16) shows the impulses are of a similar magnitude and occur at the same vane positions.

Fig.6.23 shows the spectrum for the relieved rotor / stator unit: comparing this to a spectrum for the standard unit (Fig.6.19) shows that the harmonics of the vane passage frequency are very similar for both stators. However, for the relieved rotor / stator unit the peaks can be seen more clearly and the base vibration levels are generally 2-3 dB higher. This unexpected increase in vibration is probably due to the instability of the rotor in the shaft bearings since there is no longer pressure acting over half the rotor circumference to maintain the rotor's position in the bearings.

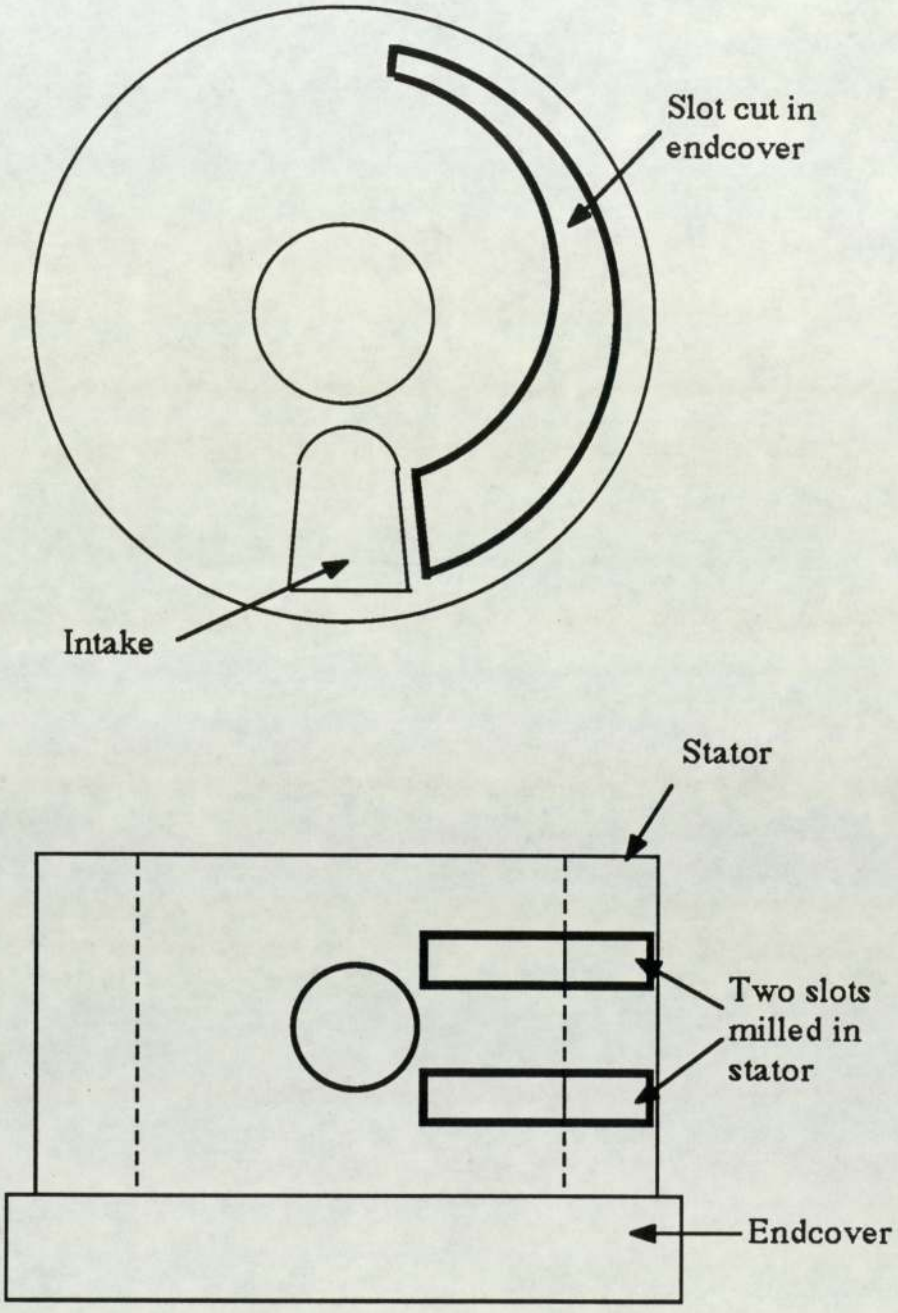

Figure 6.21 Schematic showing relief slots milled in stator and endcover

The circular stator was also tested with the relieved endcover to provide further information on the behaviour with and without compression. The vibration signal for the relieved circular stator is shown in Fig.6.24 and for the non-relieved circular stator in Fig.6.18. The corresponding vibration spectra are shown in Figs.6.25 & 6.20 respectively. The results were identical to those discussed above for the standard stator; the harmonics of vane passage frequency are of similar magnitude for both normal and relieved circular stator and the harmonics of the rotational frequency were more dominant in the case of the relieved rotor / stator unit.

No significant difference was indicated by providing relief for either the standard or circular stator and internal forces due to pressure acting internally on the rotor / stator unit must be eliminated as a major source of vibration.

6.4.3 Stator vibration : Influence of oil flow

The oil was considered as another possible source of vibration. This was thought to be due to the wedge of oil likely to be generated at the tip of the rotating vane which imparts a large impulsive force on the system as it has no means of escape in the sealing arc region. Photographic evidence (Saunders 1986) of this wedge was produced for Hydrovane on a compressor which incorporated a transparent endcover. Vibration analysis utilising the optical timing signal has already shown that an impulse occurs just after the vane has entered the sealing arc. A reduction of oil flow rates into the rotor / stator unit should therefore prevent the formation of a large oil wedge and reduce the possibility of hydraulic locking. This in turn will minimise the generation of impulsive forces.

The oil flow rate was varied using the control valve in the supply line between the oil cooler and compressor. Vibration measurements were made at three flow conditions; normal, reduced and temporarily stopped, using both the standard and circular stators. The actual flow rate was not measured for the reduced setting but the valve position, supply pressure and oil temperature were identical each time this condition was used.

6.4.3.1 Influence of oil flow : Discussion of results

The vibration signal for the standard stator with reduced oil flow rate is shown in Fig.6.26. A comparison to the standard stator with normal oil flow (Fig.6.16) has shown that the reduction has produced no significant change in the vibration pattern: an impulse still occurs just after the vane has entered the sealing arc. The vibration spectrum is shown in Fig.6.27. A comparison with the standard spectrum (Fig.6.19) shows that the peaks are similar at the first two harmonics, 5 dB higher at the third and then generally lower at other harmonics.

The effect of temporarily stopping the oil supply to the compressor can be seen in Fig.6.28. This spectrum, when compared with the spectrum for reduced oil flow (Fig.6.26), shows a 10 dB reduction in the peak at vane passage frequency and smaller reductions at 1140 Hz, 2340 Hz and 2720 Hz but shows an increase at peaks above 3 kHz.

Very similar results were obtained from the circular stator. Comparison of a spectrum for reduced oil flow (Fig.6.29) with that for standard oil flow (Fig.6.20) shows a slight reduction at the first harmonic, a slight increase at the third harmonic and similar levels at higher harmonics. Temporarily stopping the oil (Fig.6.30) further reduced peaks at 2340 Hz and 2720 Hz but significantly increased peaks

above 3 kHz: the effect on vibration was greater than for the standard stator. The most likely reason for this is that removal of oil leads to a breakdown of sealing along the line of closest contact between the rotor and circular stator. This allows significant leakage from the high pressure to low pressure regions which increases noise and vibration levels.

For the circular stator operating without compression, ie. relieved endcover, comparison between the spectrum for reduced oil flow (Fig.6.31) with that for normal oil flow (Fig.6.25) shows a 10 dB drop in vibration level at vane passage frequency (380 Hz): the other harmonics are all similar. This and the earlier results indicate that the oil wedge does affect stator vibration, probably in the manner suggested, but is not the main cause. As oil flow rates are reduced vibration levels are reduced. Starving the compressor of oil for too long dramatically increases noise and vibration due to both leakage and bearing rumble. Unfortunately, oil is an essential part of the compressor operation and future work must find the optimum balance between the various functions performed by the oil.

Fig.6.31 actually represents the circular stator vibration spectrum with no internal pressure, no sealing arc and reduced oil flow i.e. with the three expected sources of vibration removed. The harmonics of vane passage frequency still appear, particularly above 3 kHz. The only possible cause of the remaining peaks is the forces exerted by the vanes sliding in and out as the rotor rotates.

6.5 Casing vibration : Review of results

Stator vibration was considered as the dominant source of casing vibration via a structural transmission path. The experimental work detailed in this chapter has shown that the main source of stator

vibration is the forces exerted due to the sudden changes in acceleration of each vane as they enter and leave the sealing arc. Eliminating the sealing arc with a circular stator reduced vibration levels at the harmonics of vane passage frequency below 2.5 kHz by as much as 20 dB. This reduction in stator vibration levels would lead to a similar reduction in casing vibration levels and the associated radiated noise.

Removing the internal pressure by relieving the stator during compression showed slight reductions at some harmonics and increases at others but no overall improvement was achieved. This indicated that during normal compressor operation the fluctuation in internal forces due to changes of internal pressure were not of an impulsive nature and do not contribute significantly to stator vibration.

A reduction in the oil flow rate was shown to reduce the magnitude of the fundamental harmonic peak by 10 dB with smaller reductions at some higher harmonics. There was a slight increase in general vibration levels above 3 kHz. This has indicated that hydraulic forces on the stator due to oil entrapment in the sealing arc region does influence vibration levels and therefore an optimum flow rate must exist between vibration, thermodynamic and lubrication requirements. Time restrictions in relation to comprehensive monitoring of thermodynamic performance and particularly long term wear due to inadequate lubrication have prevented further analysis into this aspect of compressor vibration.

The principal source of aerodynamic excitation of the casing was shown to be tonal noise generated at the discharge port. Further investigation into this source of noise is discussed in Chapter 7.

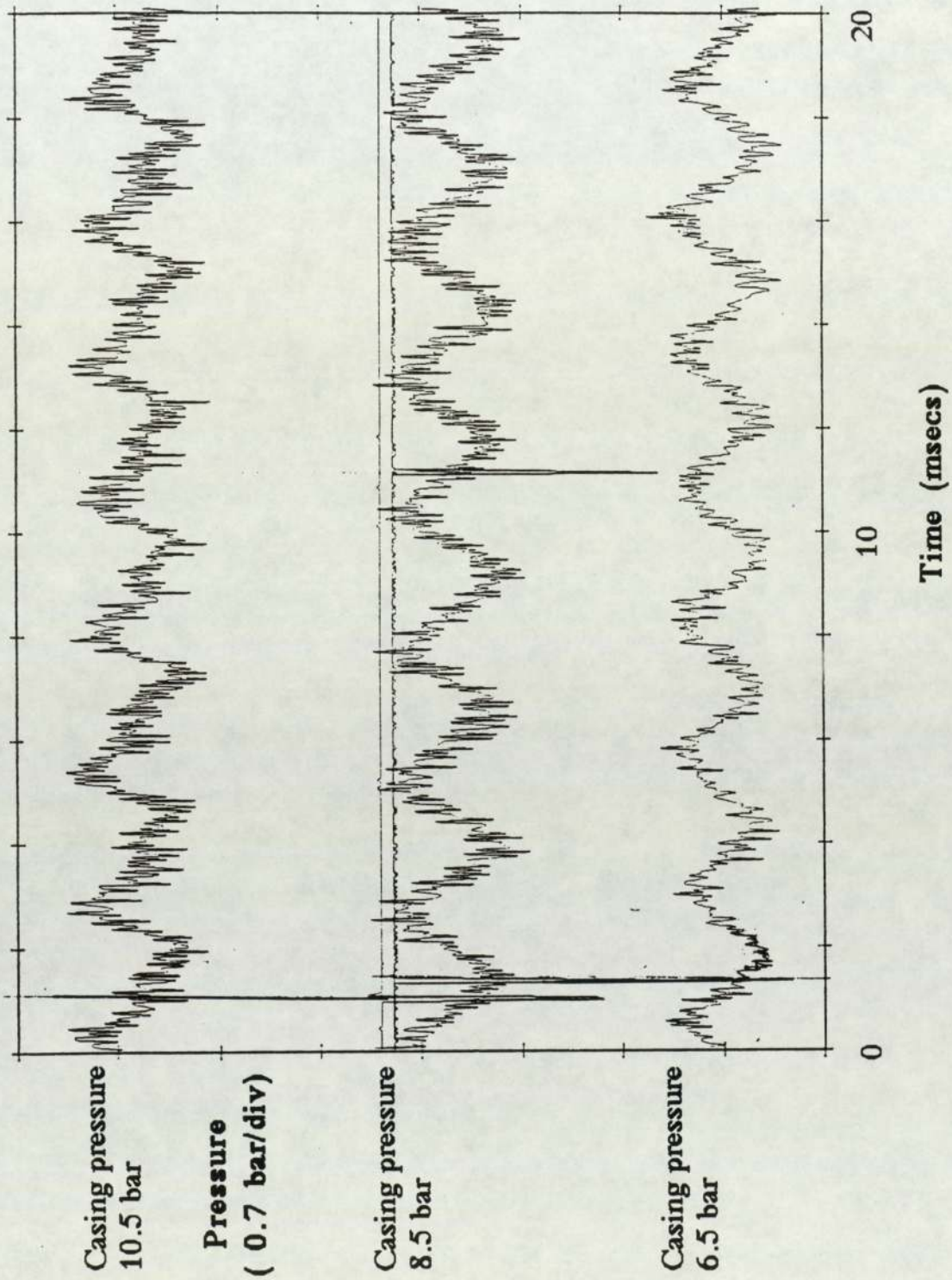

Figure 6.6 Pressure fluctuations standard port

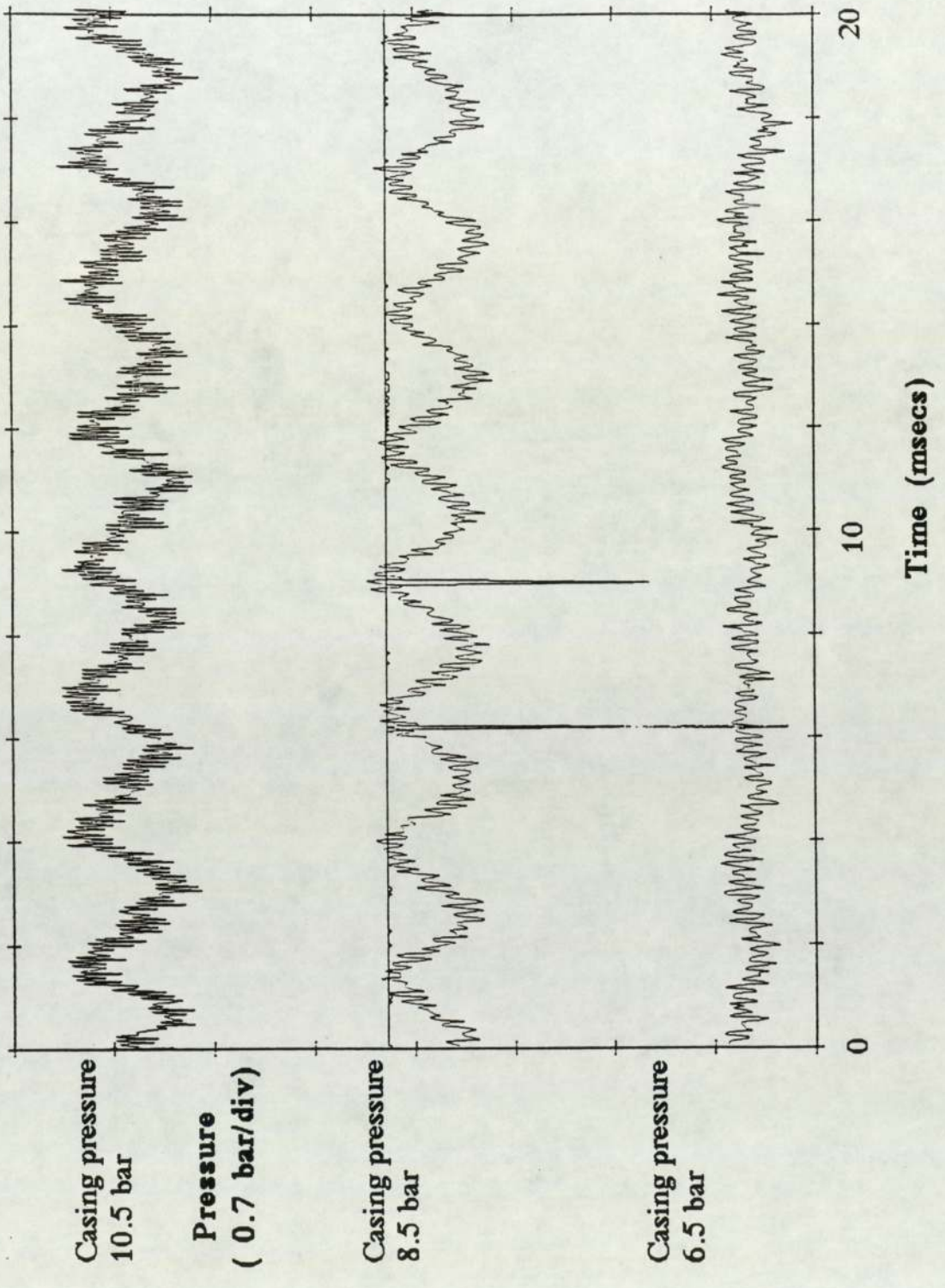

Figure 6.7 Pressure fluctuations three 9.5 mm slots

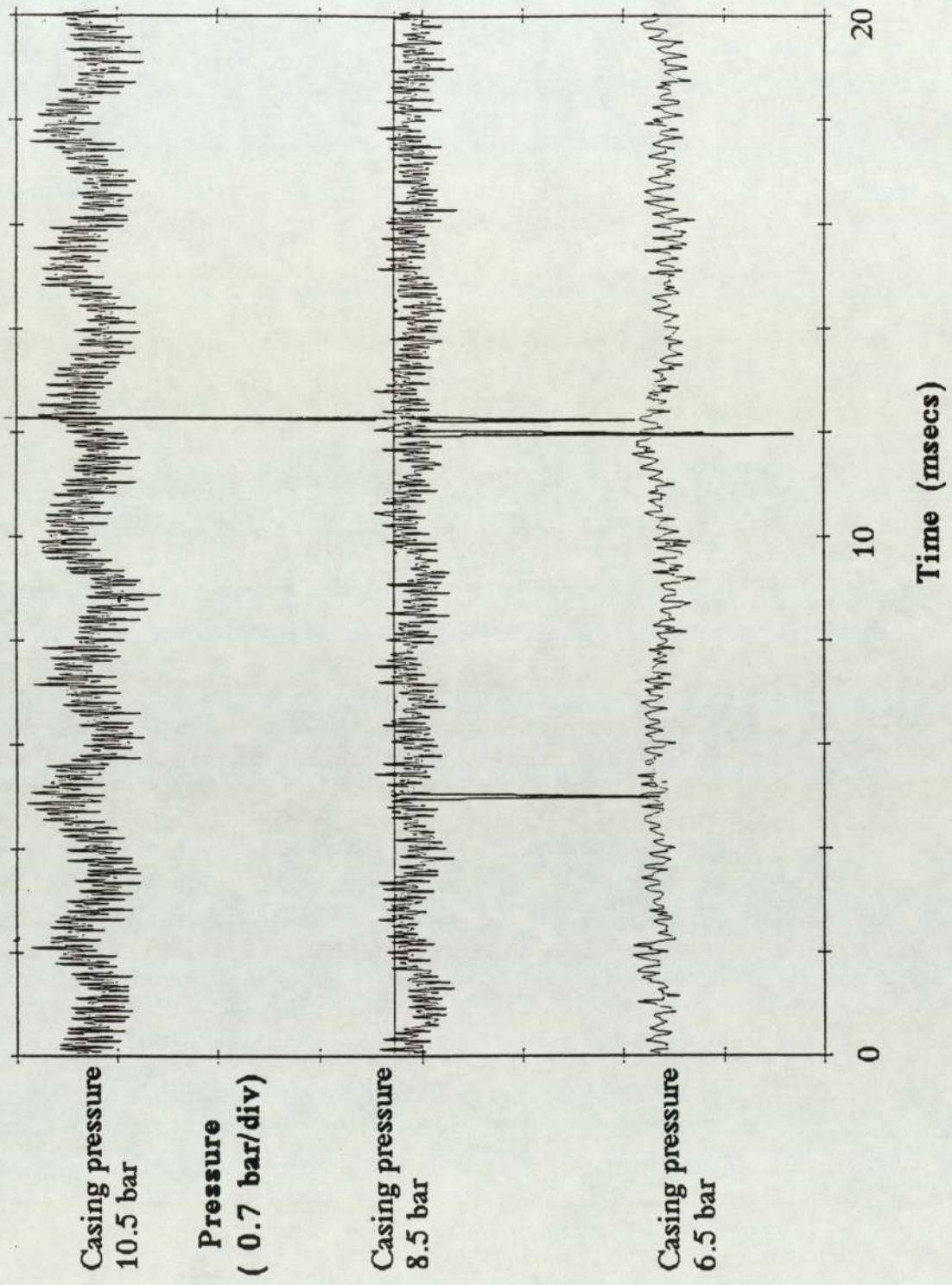

Figure 6.8 Pressure fluctuations nine 6 mm holes

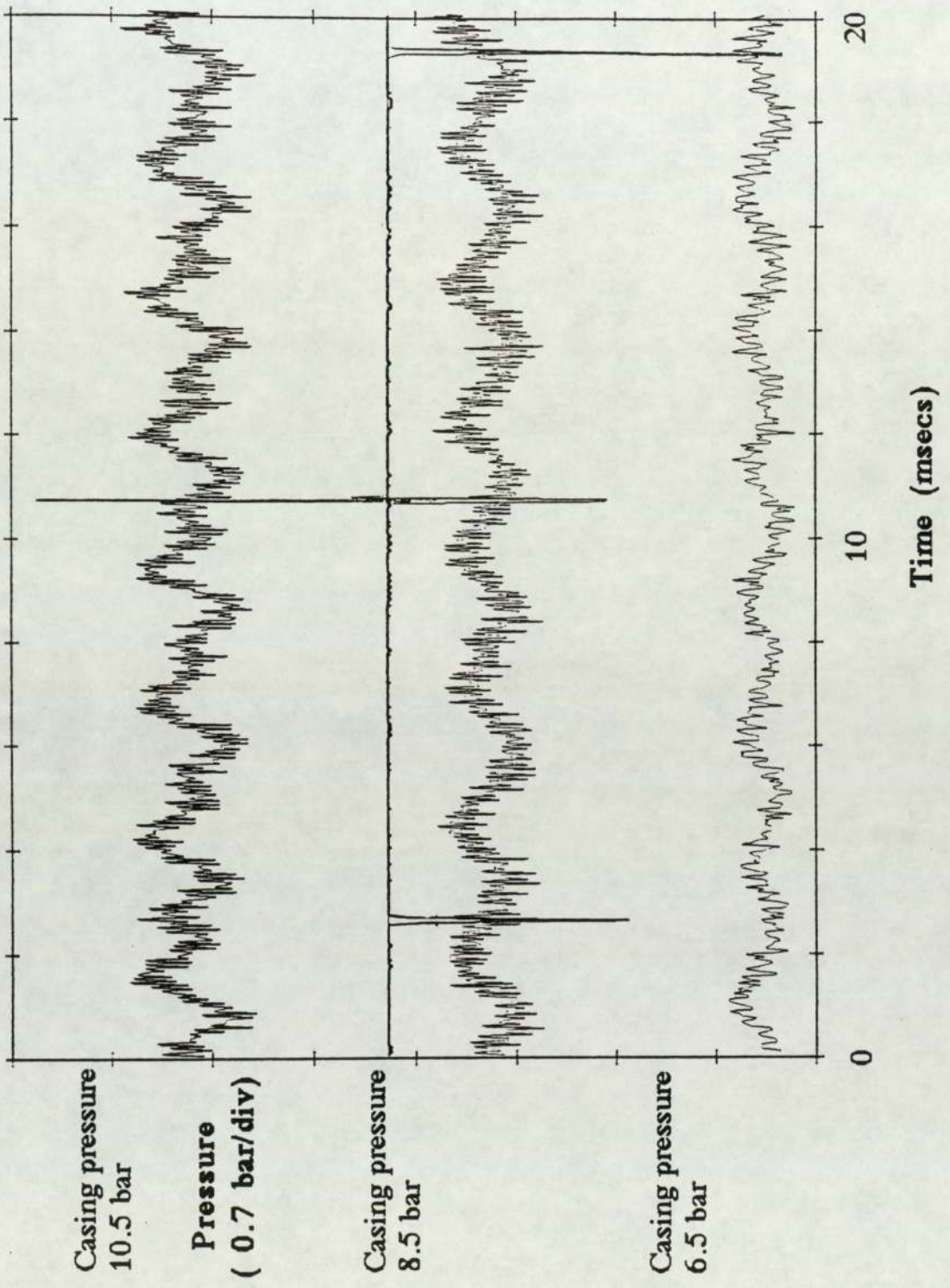

Figure 6.9 Pressure fluctuations nine 6 mm holes reversed

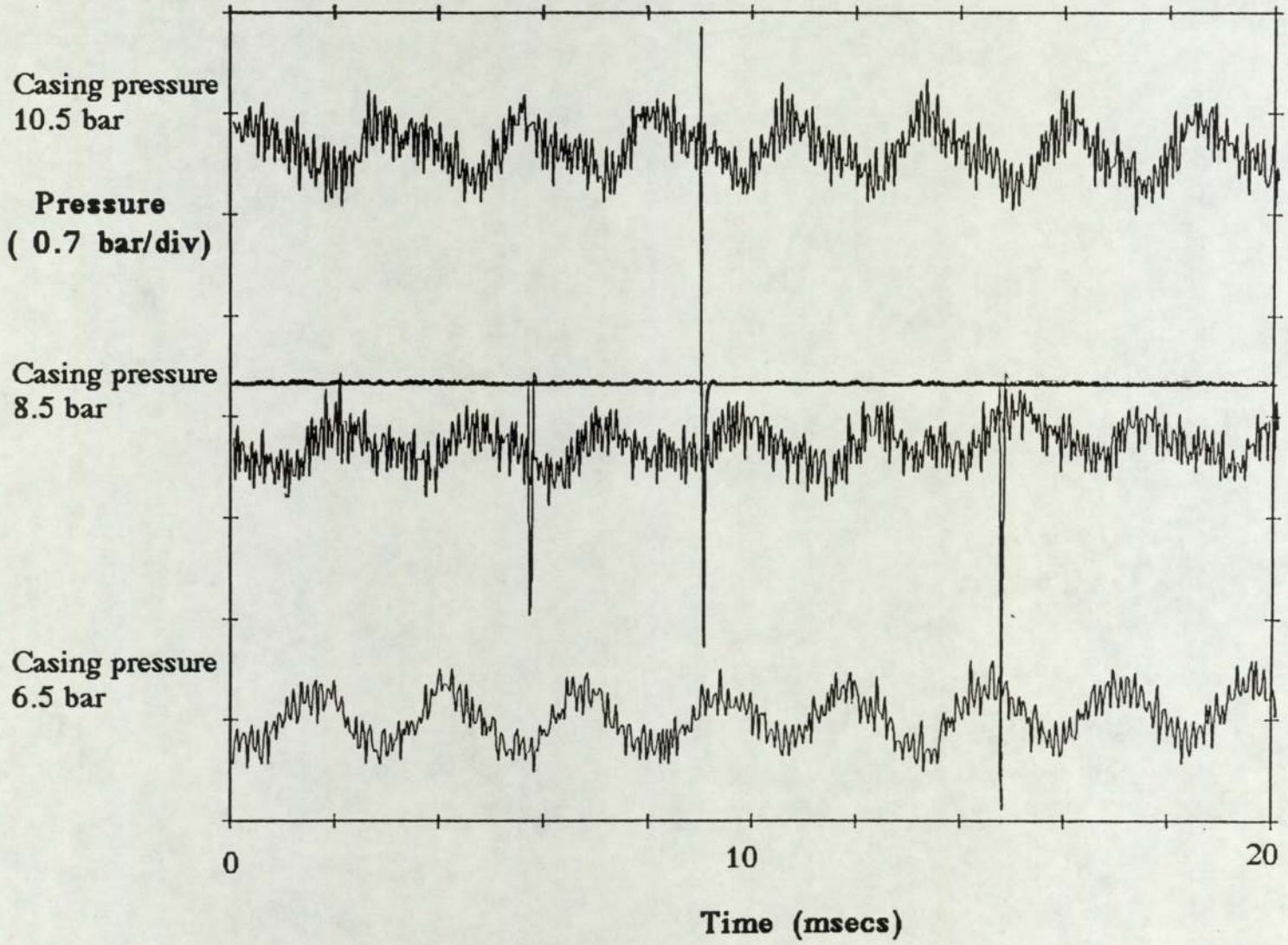

Figure 6.10 Pressure fluctuations triangular

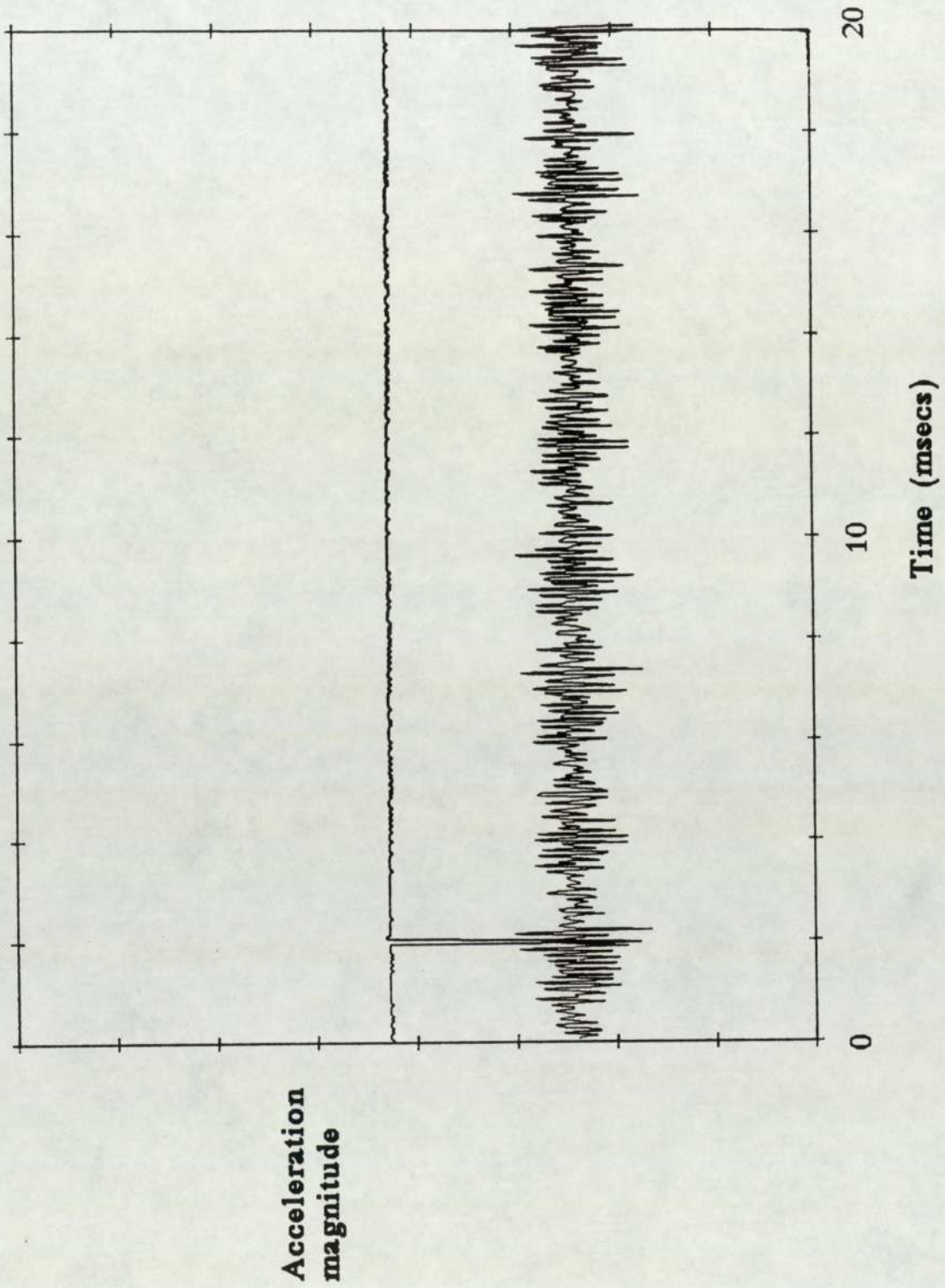

Figure 6.11 Typical stator vibration signal for standard port

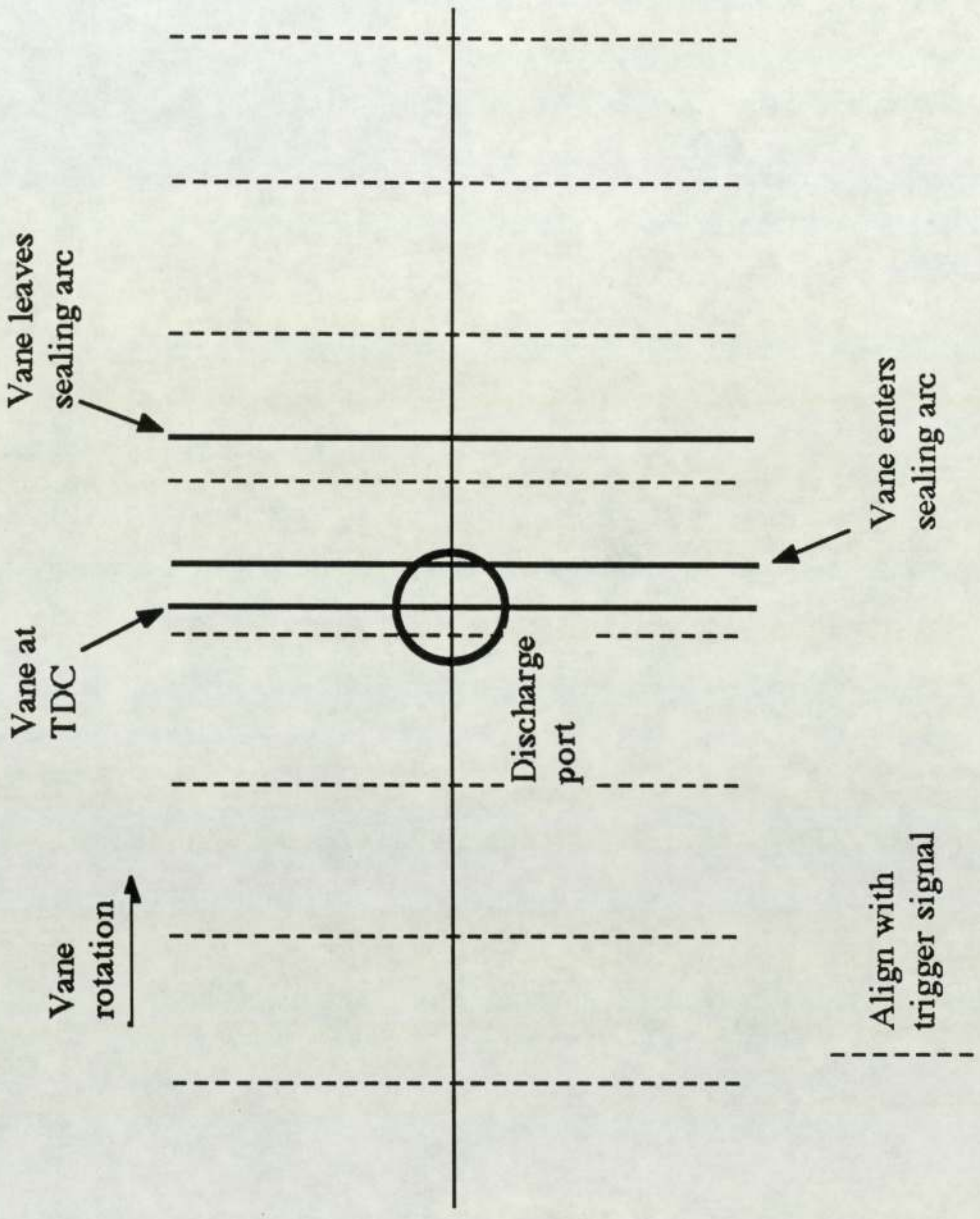

Figure 6.12 Relationship between trigger signal and vane position within stator

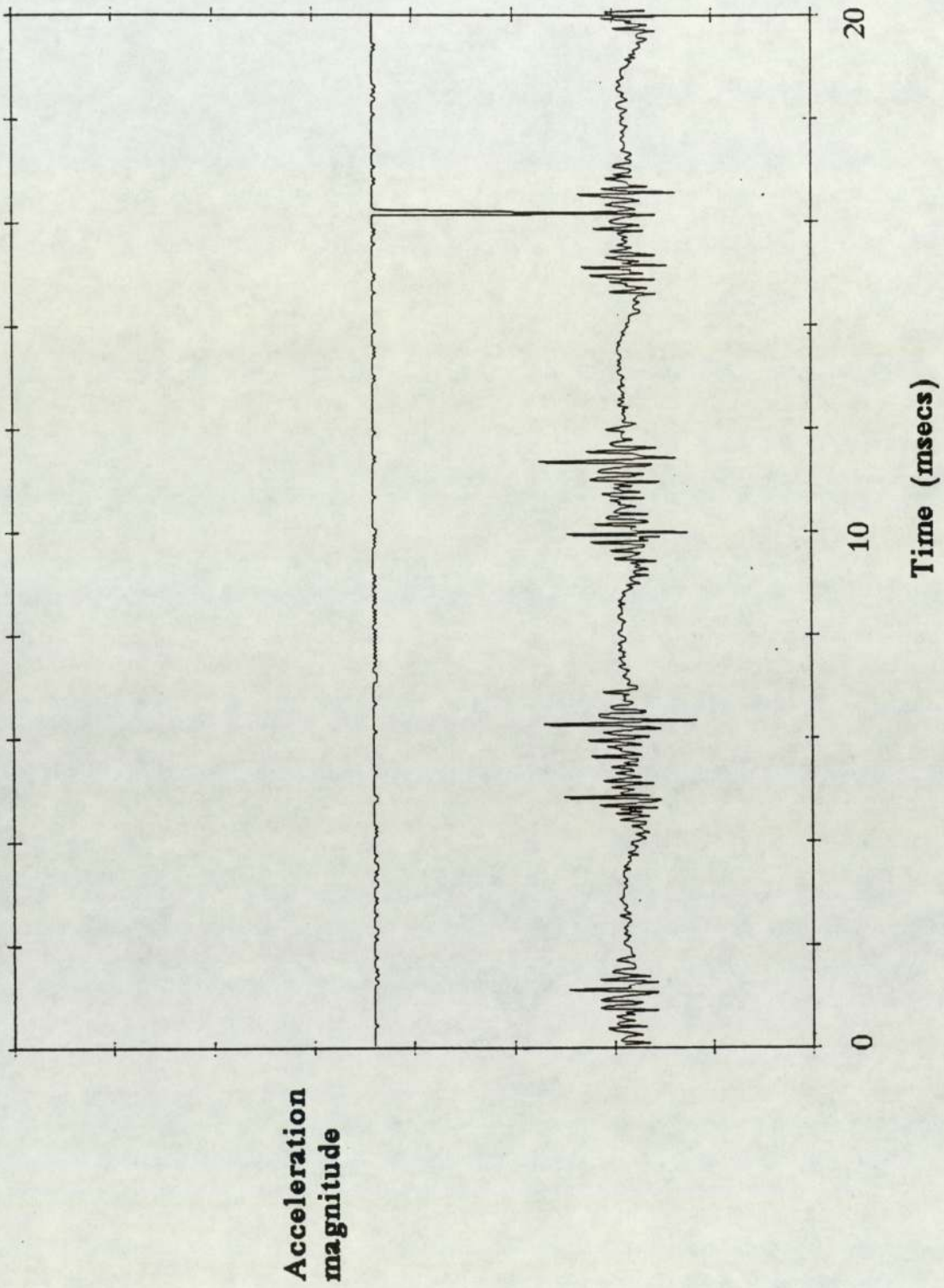

Figure 6.13 Vibration signal with four alternate vanes removed

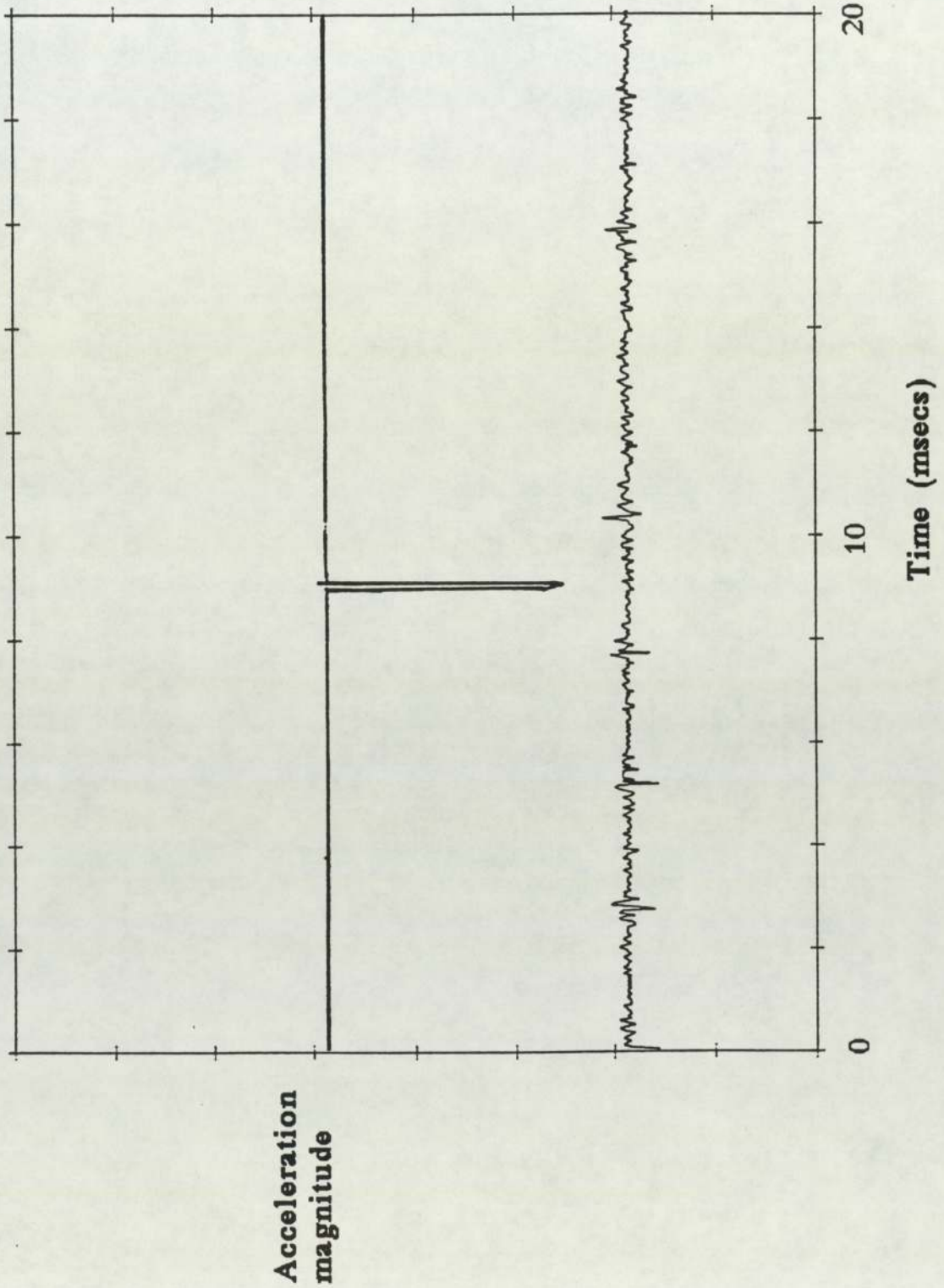

Figure 6.16 Vibration signal standard stator (sealing arc)

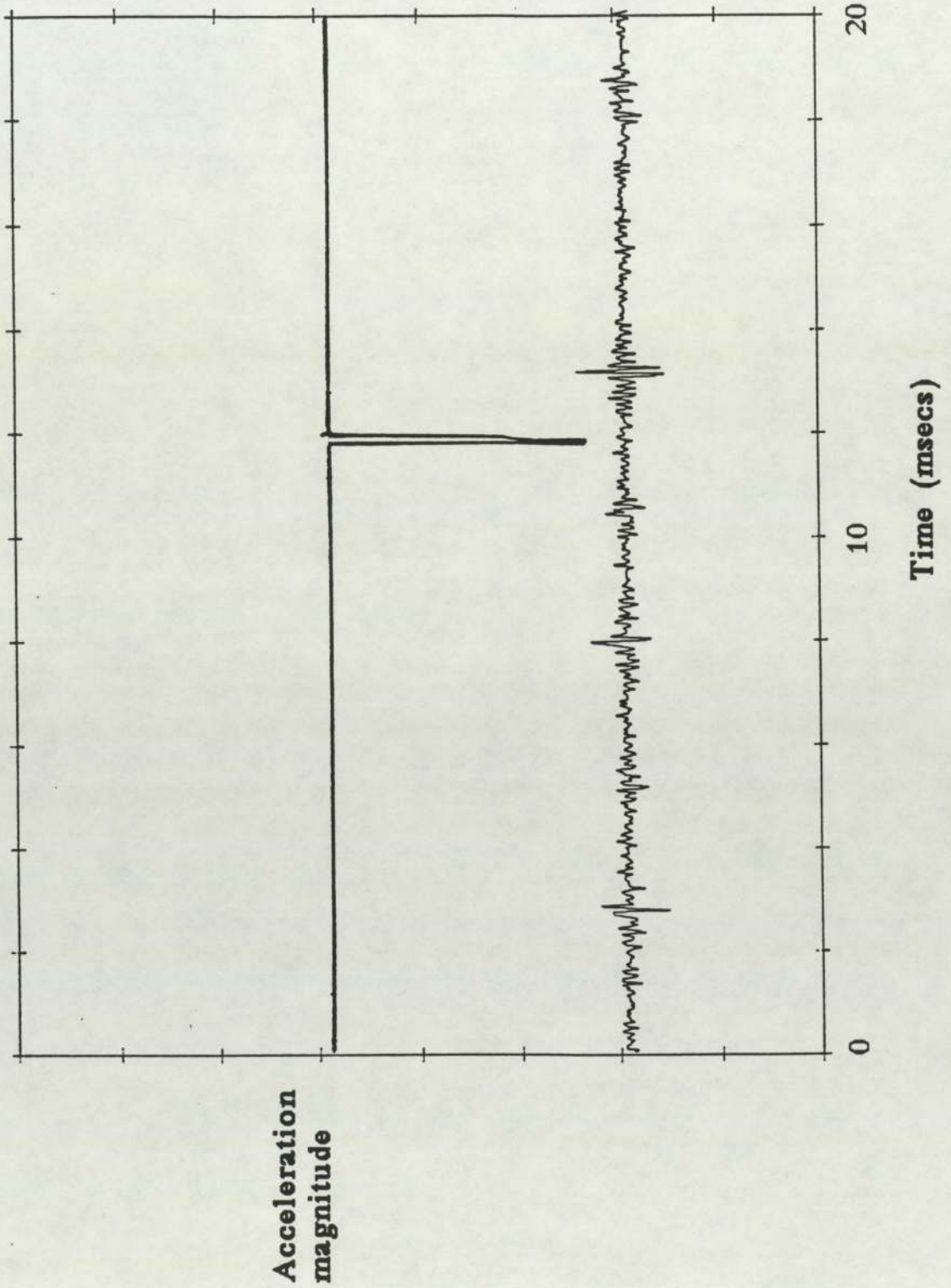

Figure 6.17 Vibration signal standard stator (90° to SA)

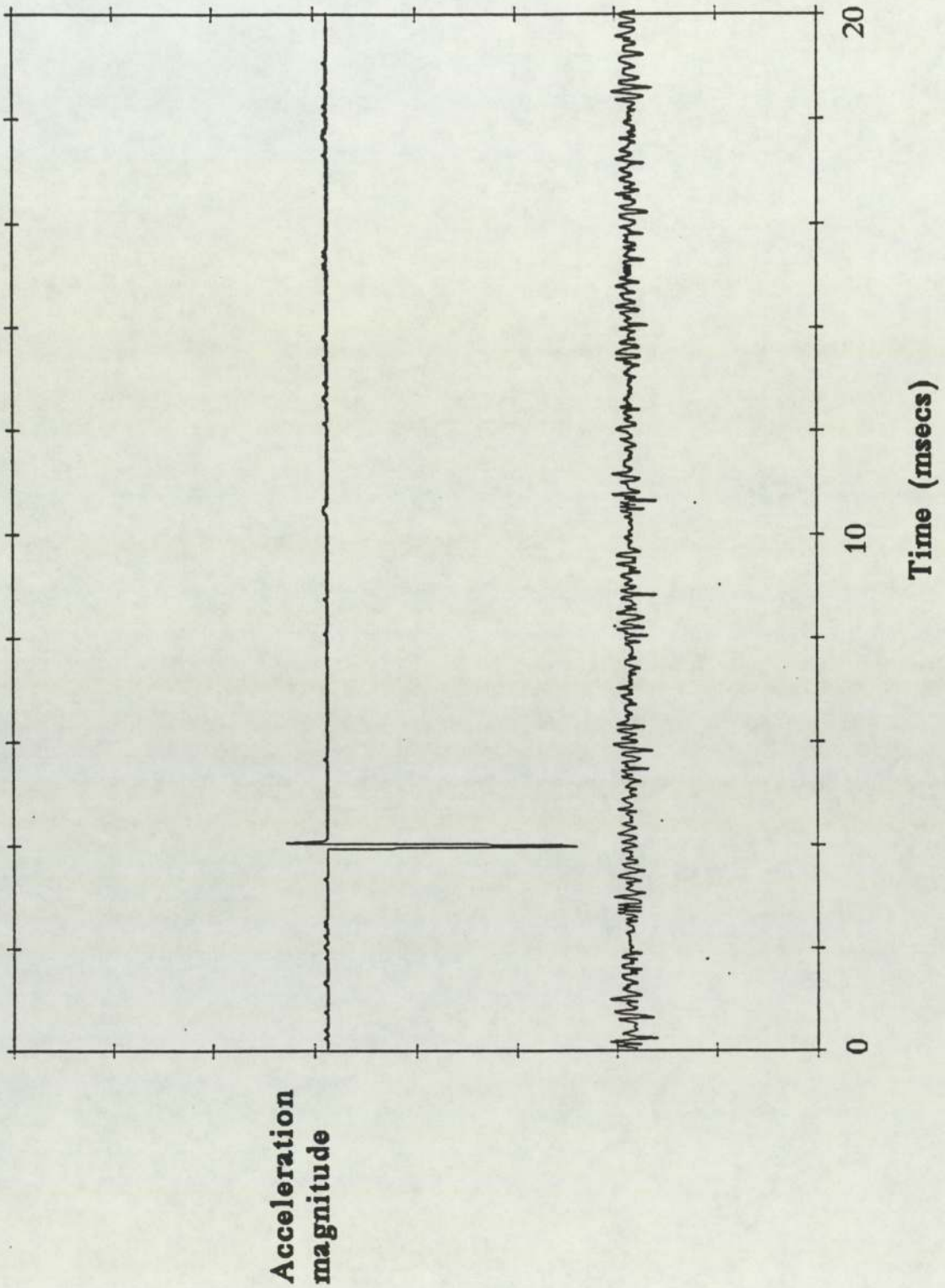

Figure 6.18 Vibration signal circular stator

Figure 6.19 Vibration spectrum standard stator

Figure 6.20 Vibration spectrum circular stator

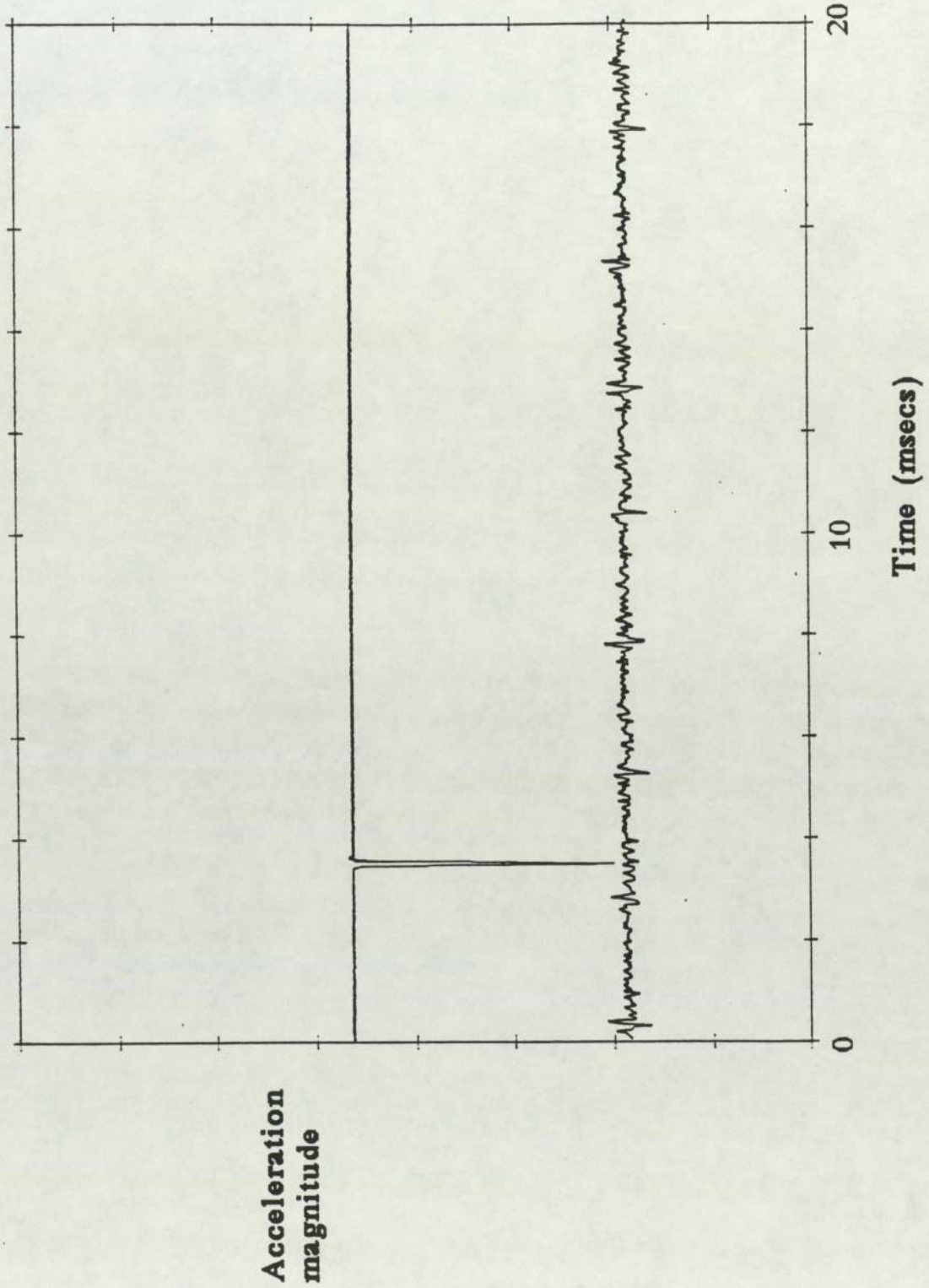

Figure 6.22 Vibration signal relieved stator

Figure 6.23 Vibration spectrum relieved stator

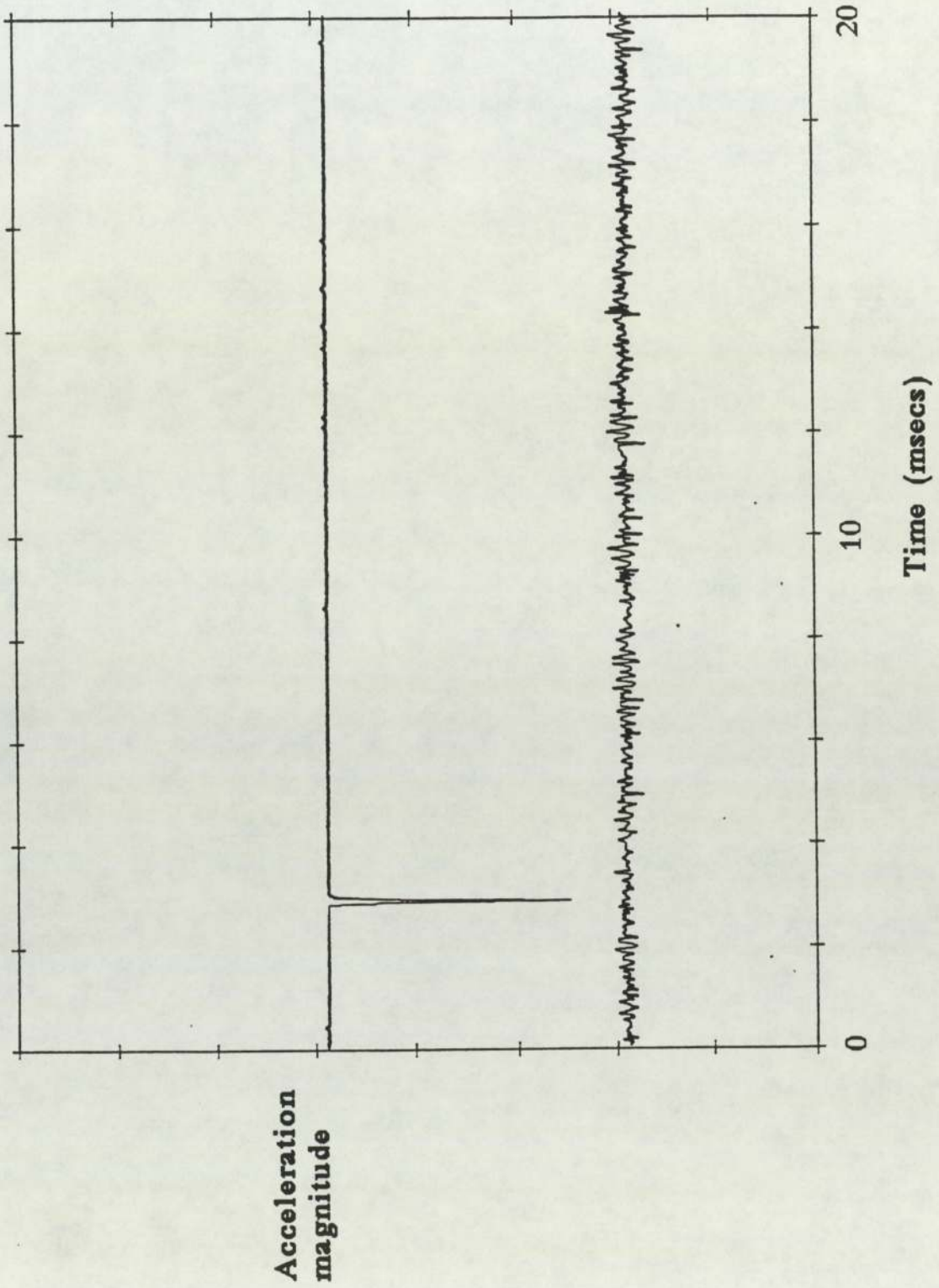

Figure 6.24 Vibration signal circular and relieved stator

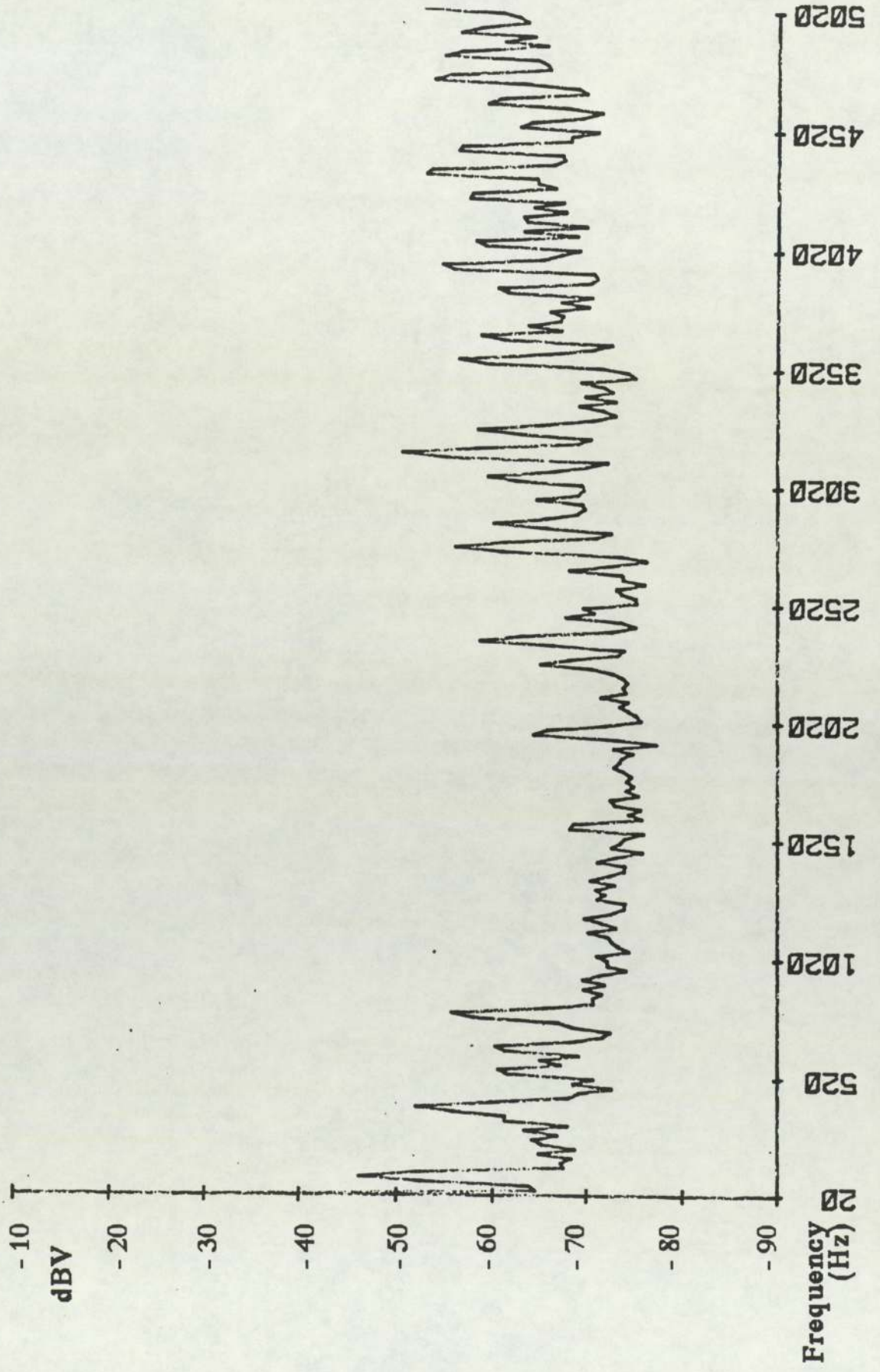

Figure 6.25 Vibration spectrum circular and relieved stator

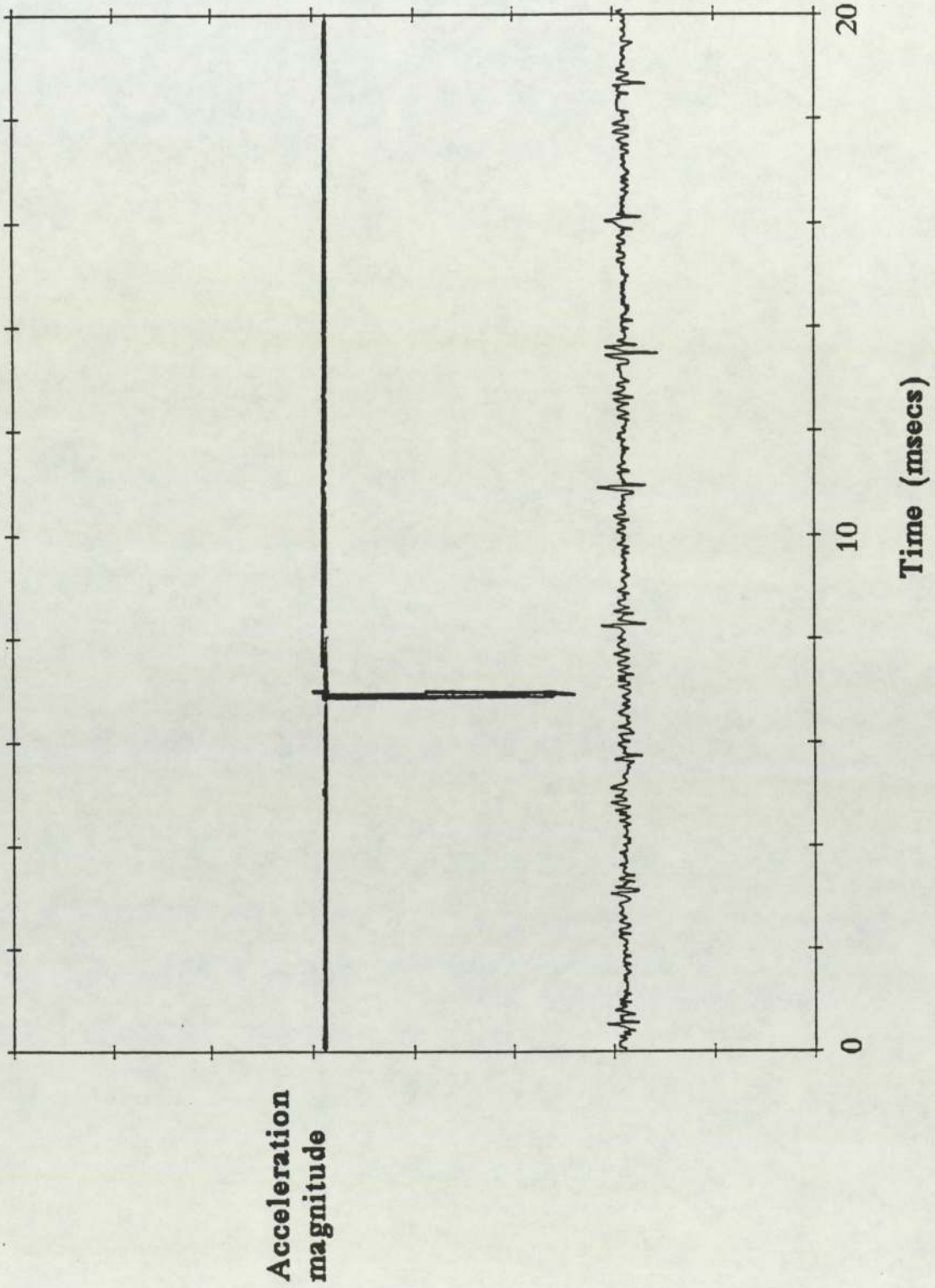

Figure 6.26 Vibration signal reduced oil flow

Figure 6.27 Vibration spectrum reduced oil flow

Figure 6.28 Vibration spectrum oil flow stopped

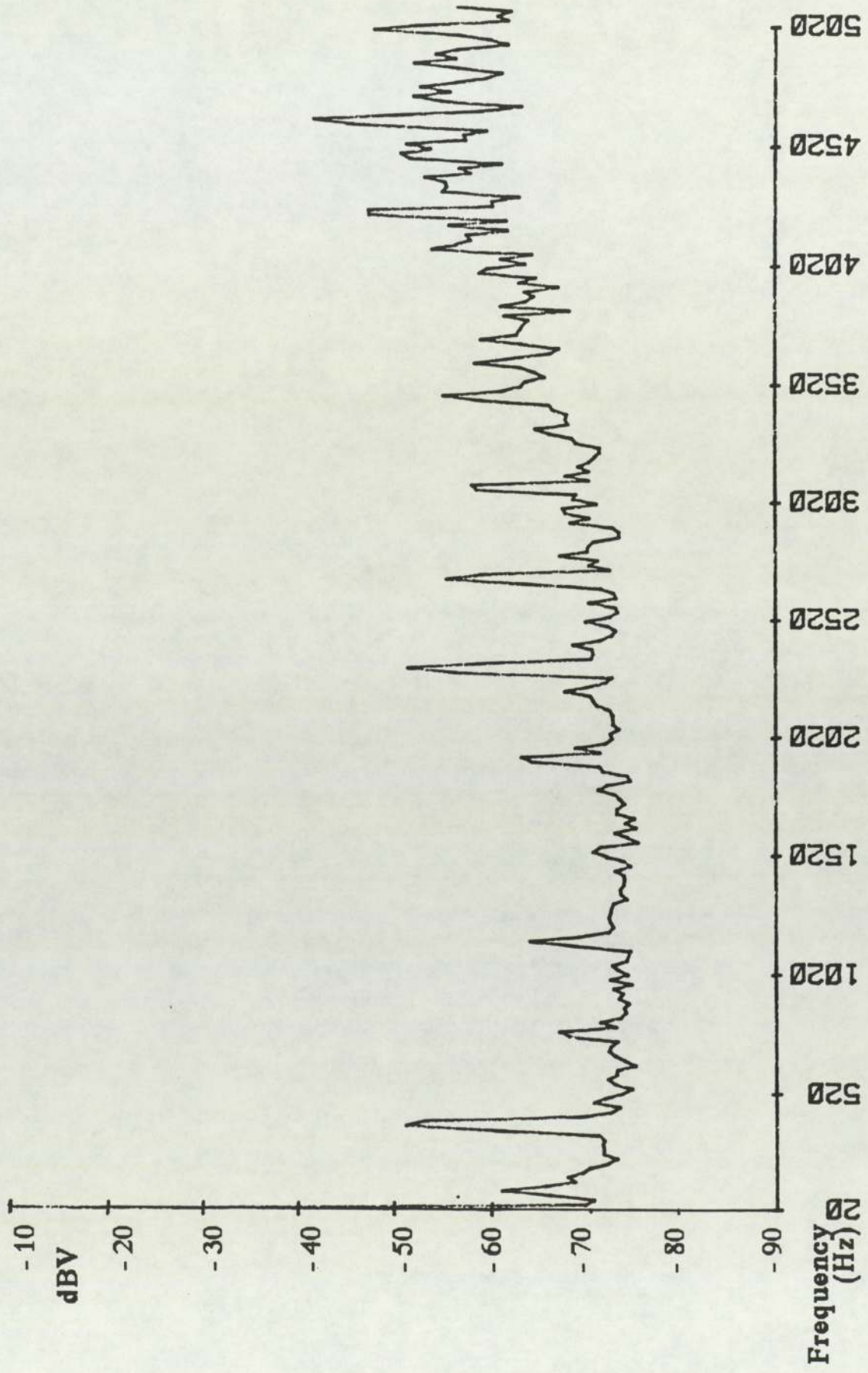

Figure 6.29 Vibration spectrum circular stator reduced oil flow

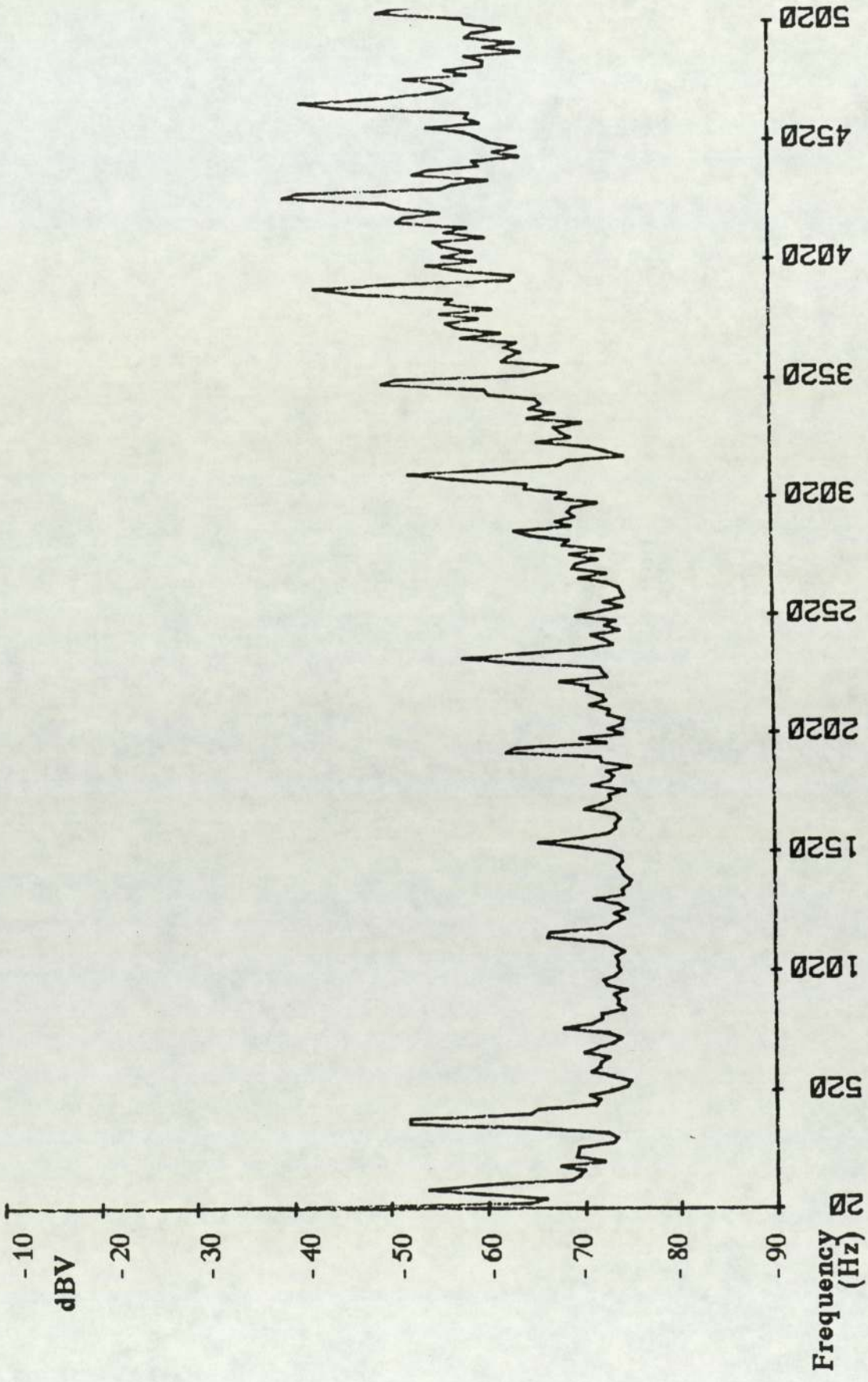

Figure 6.30 Vibration spectrum circular stator oil flow stopped

Figure 6.31 Vibration spectrum circular and relieved stator oil flow stopped

7.0 Aerodynamic noise within the compressor

It has been shown in Chapter 6 that aerodynamic noise, generated by a series of pulses at the discharge port, excites the casing at harmonics of the vane passage frequency. Since the noise has a strong tonal content then the use of a well designed reactive type silencer would be effective in reducing, to different degrees, all of these harmonic peaks.

A reactive silencer reflects noise back towards its source: the degree of reflection is a function of both silencer length and the wavelength of sound, which is frequency dependant. Therefore, to design a silencer of optimum length the wavelengths must be determined at the dominant frequencies, which requires knowledge of the speed of sound in the compressed air and oil medium just after discharge. The speed of sound in a homogeneous air / oil mixture is theoretically a function of the ratio of oil and air densities and their volume fractions. Since the mixture discharged from the stator is not constrained to be homogeneous it was necessary to determine the speed of sound by experiment.

This chapter details the theoretical and experimental procedure to determine the speed of sound and describes the design and testing of an internal silencer. Cavity resonance is also discussed as the conditions within the compressor casing lend themselves to this phenomenon in which the excitation of the gases at certain frequencies within a cavity can be amplified due to the geometric properties of the cavity alone.

7.1 Literature review

Most noise control books (Beranek 1971, White and Walker 1982, Harris 1979) contain a chapter on silencers or mufflers. Beranek states "A silencer is a device which reduces the transmission of sound without

a significant detrimental effect to the flow process in which the sound is travelling". Two types of silencer exist; absorbtive and reactive. An absorbtive silencer reduces broadband noise by dissipating the acoustic energy as heat in the flow resistive material within the silencer. A reactive silencer provides an impedance mismatch for the acoustic energy due to the different geometric shapes of its chambers. The geometric shape can therefore be altered to cope with specific frequencies.

Since the compressor has shown strong tonal content a reactive silencer is the more suitable for use in the discharge system and is therefore the only type of silencer discussed further. Beranek summarises the design criteria at the operating condition as; acoustic, aerodynamic, geometric, mechanical and economical. The acoustic criterion considers the minimum noise reduction as a function of frequency; the aerodynamic criterion specifies the maximum allowable pressure drop and resistance to flow; the geometric criterion determines the maximum volume and restrictions on shape; the mechanical criterion considers materials, temperature and corrosion while the economic considerations are the initial capital cost plus operating costs.

The simplest reactive silencer is an abrupt expansion chamber, as shown in Fig.7.1. The three important geometrical properties are the silencer length (l) the silencer cross section (As) and the pipe cross section (Ap). The acoustic performance of the silencer or the transmission loss (L_{TL}) can then be determined from the parameters m (the ratio of cross sections = As/Ap) and kl (a function which is proportional to the ratio of silencer length to the wavelength of sound in the medium). It is calculated using the equation shown below.

$$L_{TL} = 10 \log_{10}\left[1 + \frac{1}{4}\left(m - \frac{1}{m}\right)^2 \sin^2 kl \right]$$

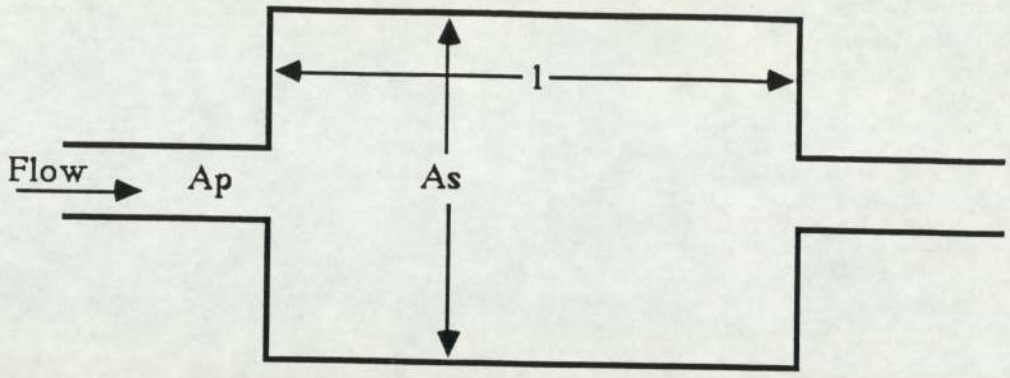

$$m = \frac{As}{Ap}$$

Figure 7.1 Simple reactive silencer

In fact this equation describes a series of transmission loss curves as shown in Figs.7.2a & 7.2b which show the transmission loss in dB against (kl). It can be seen that this function is a maximum when l= $\lambda/4$, $3\lambda/4$, $5\lambda/4$..., and a minimum when l= $\lambda/2$, λ, $3\lambda/2$.... These curves only apply to silencers for which the largest transverse dimension is less than 0.8 λ and the steady flow is less than 35 m/s. Outside these ranges there is no standard data so predictions are less accurate and should be based on experimental results. The transmission loss is actually defined as ten times the logarithm, to base ten, of the ratio of sound power incident on the silencer to the sound power transmitted by the silencer.

As mentioned in the introduction to this chapter the speed of sound in the discharge region was required in order to determine the wavelengths at various frequencies. No information could be found in the literature that predicted the speed of sound in an air / oil mixture equivelant to the conditions just after discharge. Some information (Moody 1973) was discovered relating to the speed of sound in homogeneous air / petrol mixtures. This work is summarised by the

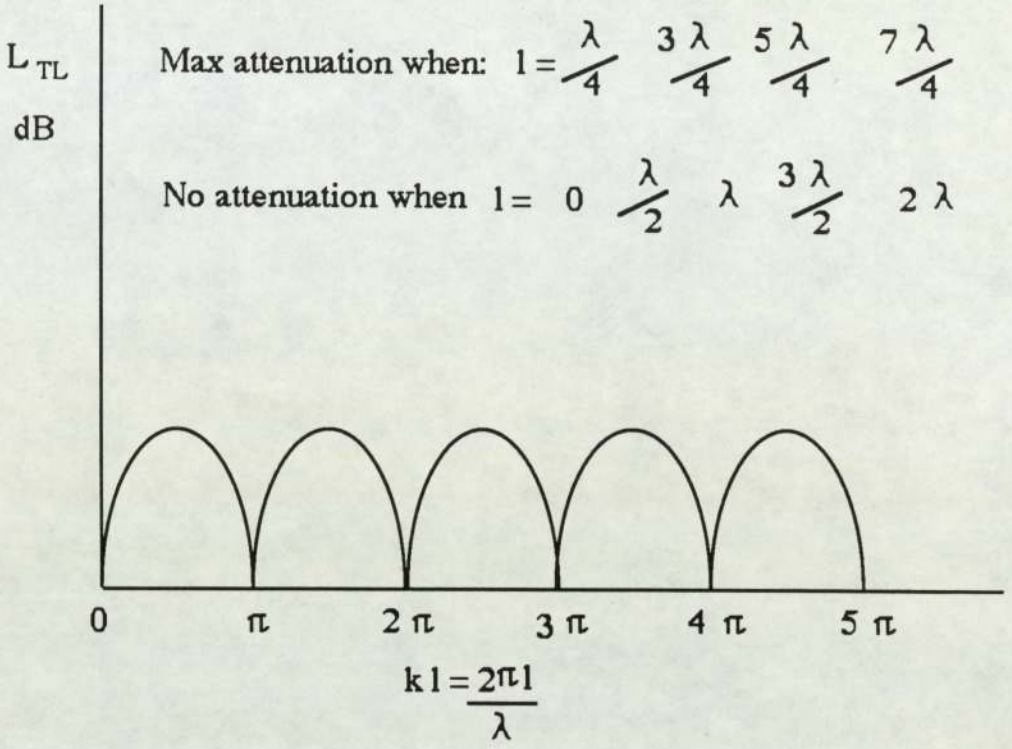

Figure 7.2a Transmission loss curve

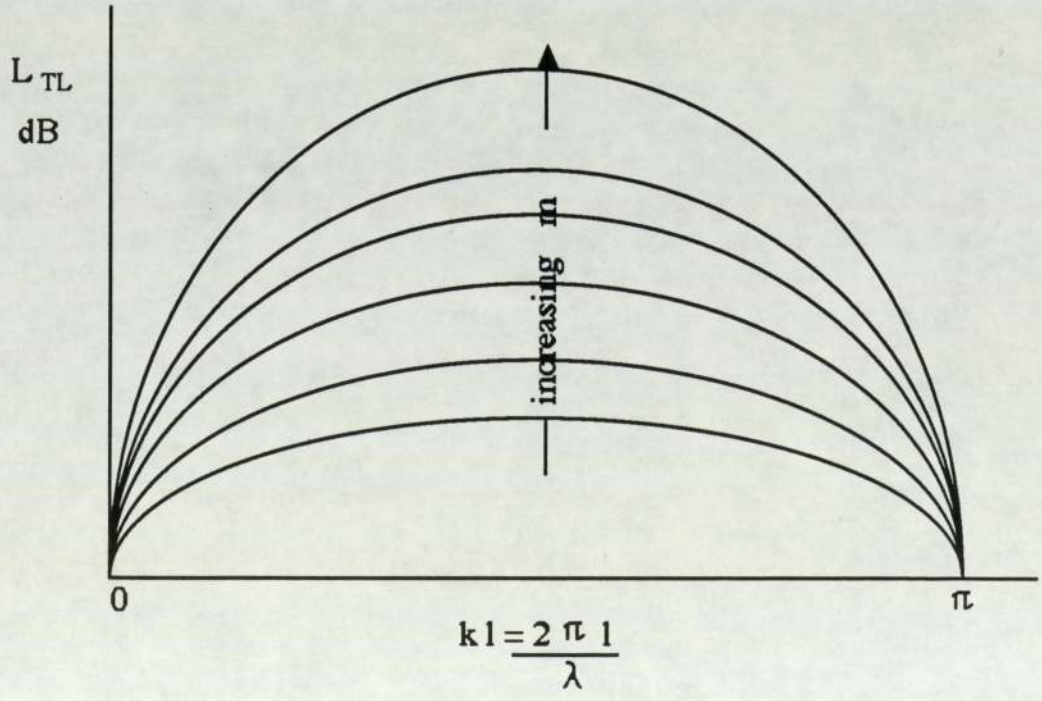

Figure 7.2b Transmission loss curves for increasing m

equation shown below which relates the speed of sound in the mixture to the density (ρ) and liquid volume fraction (a) of its constituents.

$$C = \frac{C_g}{a}\sqrt{\frac{1}{1+\frac{1-a}{a}\left(\frac{\rho_l}{\rho_g}\right)}}$$

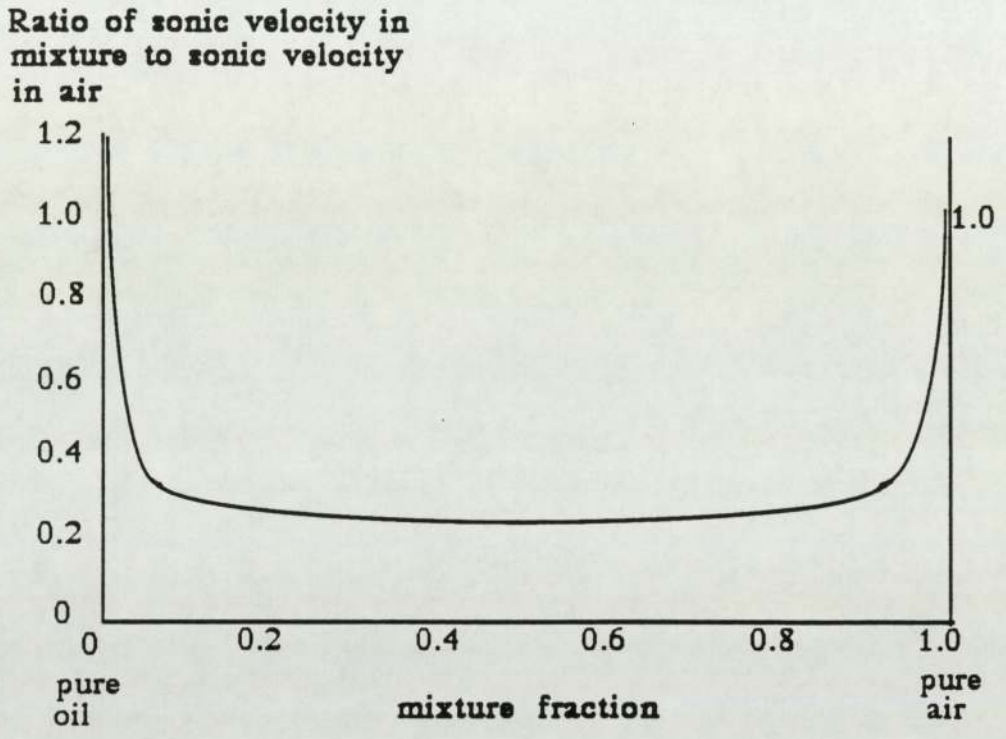

Figure 7.3 Graph of sonic velocity in air / oil mixture

Fig.7.3 shows a graph of the speed of sound against air / oil volume fraction and it can be seen that at volume fractions other than those very close to pure air or pure oil the speed of sound is approximately 20% of the speed of sound in pure air.

Under normal compressor operating conditions the volume fraction at discharge is approximately 93% air, 7% oil and after separation approximately 99% air, 1% oil (based on manufacturers flow specifications). Assuming the above relationship for the air / oil mixture

the speed of sound is predicted as 149 m/s before initial separation and 285 m/s after separation. If this assumption is accurate then the figure for the speed of sound of 149 m/s when combined with the available frequency information would enable a silencer to be designed which could be installed immediately after the discharge port.

One interesting phenomenon discovered in the literature (Yildiz 1988) is the attenuation of sound waves due to scattering from bubbles or liquid drops. Visual inspection of the flow conditions at discharge has shown that it consists of oil droplets of various sizes. It is possible therefore that some attenuation of discharge noise is achieved by this process.

Cavity resonance is another phenomenon that could be responsible for excitation of the compressor casing. Any excitation of the gas within a cavity could be significantly amplified if a resonant frequency of the cavity (determined by its geometric shape and internal conditions) is coincident with the frequency of excitation. Johnson and Hamilton (1972b) showed that this was a particular problem in their rotary compressor whereby the fourth harmonic of the gas pumping frequency (460 Hz) was significantly amplified. They discovered this through alteration of the gas temperature. The degree of amplification at the fourth harmonic varied considerably with temperature. At 177.5°F the sound pressure level at 460 Hz was 30 dB; this increased to 47 dB at 192°F and dropped to 38 dB at 197°F.

An interesting paper by Noguchi et al (1983) identified a similar problem in a 3/4 hp rolling piston type rotary compressor. By simulating the sound source with a loudspeaker mounted at the discharge port and measuring the transfer function at three locations in the cavity they showed that cavity resonance existed and its effects could be reduced by incorporating a discharge muffler. The location of the muffler outlet was also critical to the degree of attenuation.

7.2 Experimental procedure to determine the speed of sound

Since silencer length is critical in relation to acoustic performance it was decided to check the predicted value for the speed of sound against an experimentally determined value. The basic procedure was as follows: the transmission loss at certain frequencies was measured for a silencer of known length, the transmission loss curves were used to determine the various values of (kl) at which that level of transmission loss exists. The corresponding wavelengths were then predicted and since the frequencies of excitation are known the speed of sound was calculated.

As mentioned above the transmission loss is a function of the ratio of sound power incident on the silencer to the sound power transmitted by the silencer. In practice the transmission loss is difficult to measure and a more common measure of silencer performance is the difference in SPL's at the same point in space with and without the silencer in situ: this is defined as the insertion loss of the silencer. However sound pressure measurement was not possible for a silencer attached to the discharge system of the compressor, as it operates at a high temperature and pressure.

The best measure of silencer performance was therefore the difference in casing vibration levels with and without a silencer. It was assumed that the whole system behaved linearly and any percentage change in SWL would produce an identical percentage change in casing vibration level. The experimental rig used for these tests was basically that described earlier in Chapter 5 and shown in Fig.7.4 in which noise from the discharge port of the exposed stator was piped to the casing of a separate stationary compressor. However, two modifications were made as shown in Fig.7.5; the elbow was replaced with the standard discharge fitting and a flexible rubber hose was used rather than a combination of steel tube and nylon pipe.

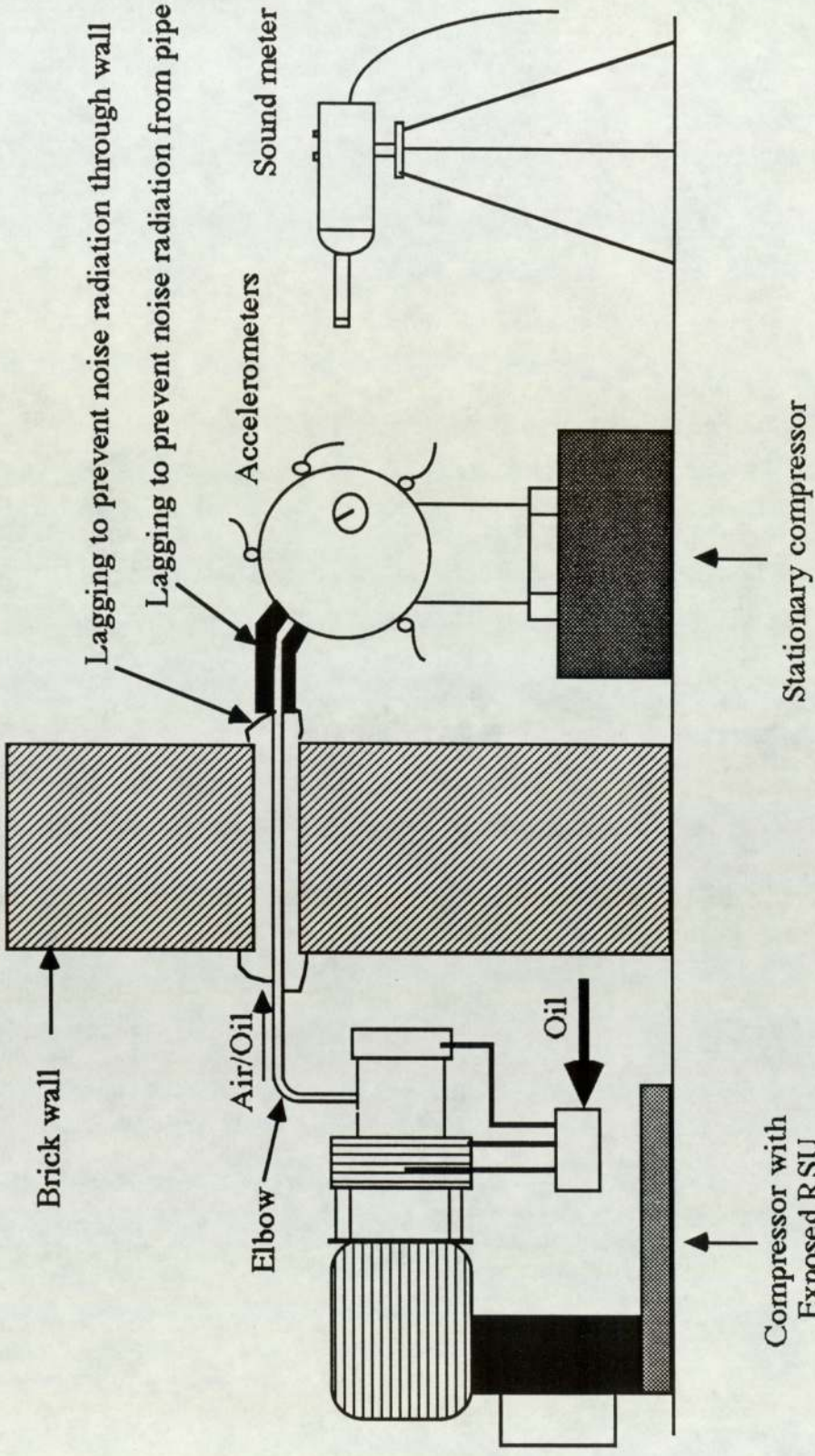

Figure 7.4 Aerodynamic noise rig

Figure 7.5 Modified aerodynamic noise rig

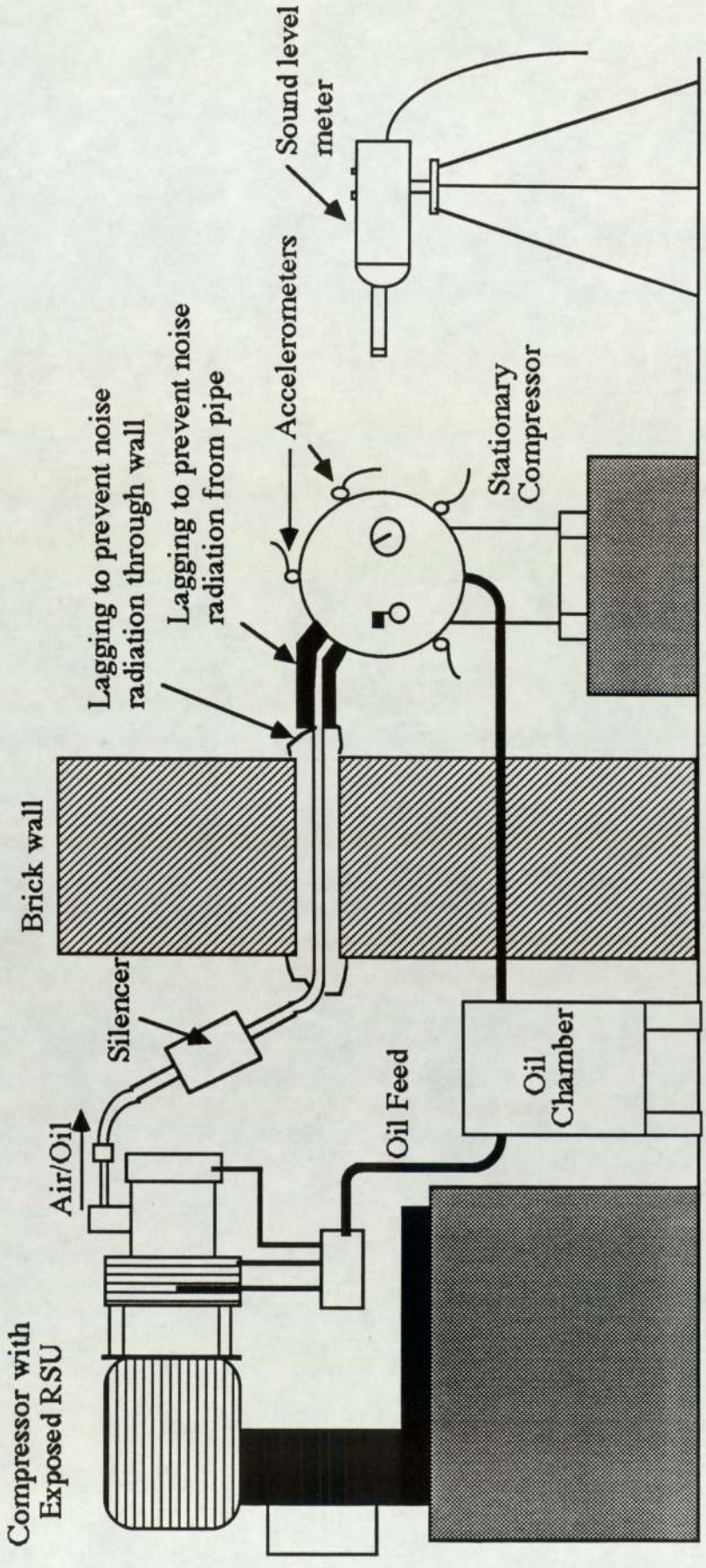

Figure 7.6 Modified aerodynamic noise rig with silencer

Table 7.1 Measured vibration levels for reactive silencers

Frequency (Hz)	380	780	1160	1540	1920	2320	2700
NO SILENCER							
Location							
1	49	61	72	52	52	65	65
2	53	60	69	63	57	66	52
3	44	52	65	60	59	55	50
SILENCER (.059 m)							
Location							
1	56	68	75	59	66	67	70
Difference	7	7	3	7	14	2	5
2	64	69	74	69	67	69	61
Difference	11	9	5	6	10	3	9
3	57	63	72	68	69	58	62
Difference	13	11	7	8	10	3	12
SILENCER (.074 m)							
Location							
1	62	70	76	60	67	67	66
Difference	13	9	4	8	15	2	1
2	68	70	75	68	67	70	57
Difference	15	10	6	5	10	4	5
3	61	65	73	69	68	60	58
Difference	17	13	8	9	9	5	8

For a continuous length of hose between stator and casing and a back pressure of 10.5 bar, datum vibration levels were recorded at three locations on the casing. A silencer of known length (l = 59 mm) and cross sectional ratio (m = 10.6) was then inserted into the pipeline (Fig.7.6) and the new casing vibration levels recorded. The silencer was mounted at an angle to prevent any build up of oil. Finally another silencer of identical cross sectional ratio but different length (l = 74 mm) was also tested. Five separate recordings were completed for each of the three experiments.

7.2.1 Speed of sound : Results and calculations

From the generated spectra the vibration levels were recorded at the peaks corresponding to the first seven harmonics of vane passage frequency. Typical spectra for the unsilenced and both silenced arrangements are shown in Figs.7.7 - 7.9. From all recorded spectra an average level was calculated to give a "transmission loss" value for each frequency. A summary of all the results is shown in Table 7.1 above.

At most frequencies the repeatability was excellent, with the variation in vibration level no greater than 3 dB. However at some frequencies the repeatability was poor and variations were as large as 7 dB. The assumption that the system behaved linearly was not completely valid as the same decibel reduction had not been recorded at all three locations. For only those frequencies at which repeatability was good was the average value used to determine the transmission loss. Interpolation of the transmission loss curves enabled different ratios of l/λ and therefore different values of λ to be obtained. By comparing the values of λ produced for the two different silencer lengths the value at which they were identical would, when multiplied by the frequency, give the speed of sound in the air / oil mixture. The details of this calculation are shown below.

The frequency at which results were most consistent was 2320 Hz where the "transmission losses" for the 59 mm and 74 mm were taken as 3 dB and 4.5 dB respectively. The wavelengths associated with these values were calculated as 2180 mm, 120 mm, 110 mm, 62 mm, 57 mm for the 59 mm silencer and 1940 mm, 160 mm, 140 mm, 76 mm, 70 mm and 50 mm for the 79 mm silencer. Below these wavelengths and at this frequency the speed of sound is less than 100 m/s. Since the speed of sound in air at a temperature of 470K (the assumed temperature immediately after discharge) is 430 m/s, based on the 25% figure mentioned earlier the range in which coincidence of wavelength was expected is 100 m/s to 300 m/s. The minimal percentage difference in wavelength between the two silencer lengths was 62 mm and 70 mm; based on the average of these figures the speed of sound was calculated as 153 m/s. This value is similar to the theoretical value which was predicted as 149 m/s. Using the 153 m/s value to confirm experimental results at other frequencies the expected "transmission losses" are shown below in Table 7.2.

Table 7.2 Predicted transmission losses for silencers

	Frequency (Hz)						
Silencer Length	380	780	1160	1540	1920	2320	2700
59 mm	11	13	4	10	14	3	8
74 mm	12	10	8	14	4	4	10

Comparison to measured results in Table 7.1 shows that for both silencer lengths at most frequencies the predicted value is encompassed in the range of measured values. The speed of sound was taken as 153 m/s for future design.

7.2.2 Speed of sound : Discussion of results

A slightly different aspect of these experiments with the modified rig is worthy of discussion. The results for this rig with the two apparently minor changes were significantly different to those obtained with the original rig. To discover the reasons for these changes further experiments were completed which measured casing vibration levels for the various combinations of discharge attachment and interconnecting pipework. A direct comparison was made between the relatively smooth 90° bend and the standard discharge fitting and also the steel / nylon combination of pipe with the rubber hose. These experiments revealed that the different discharge attachments and the pipe material all affected the noise transmission and consequently casing vibration.

The smooth 90° bend allowed high transmission of noise to the casing, whereas the standard fitting which has a very sharp 90° elbow reflects a large amount of the noise back towards the port. Figs.7.10 & 7.11 show the casing vibration spectra for the standard fitting and smooth bend respectively which highlight the significant increase in vibration, particularly above 2 kHz, for the smooth bend.

The transmission of noise was reduced when the steel / nylon combination was replaced with the rubber hose. Figs.7.12 & 7.13 show the different spectra for the two types of pipe. Since the hose is more flexible there will be greater absorption of both the sound and vibration travelling within the hose, resulting in reduced excitation of the casing.

These experiments have shown clearly that noise is generated at the discharge port and does excite the casing. Consequently an internal reactive type silencer was designed as it was considered the most suitable method by which to reduce the effect that this particular noise source has on the casing.

7.3 Internal silencer : Design

The use of a reactive silencer on the exposed rig had achieved reductions in vibration level by as much as 15 dB. It was therefore necessary to design a reactive silencer system that could be incorporated within the casing of a standard compressor without a significant detrimental effect on compressor performance. The main difficulties were the limited space available and the possibility of a detrimental affect on oil separation. To prevent the collection of oil in the bottom of a horizontally mounted expansion chamber (which would impair silencer performance) it was essential to mount the expansion chamber vertically to ensure complete drainage.

These concerns led to the system shown in Fig.7.14 whereby two interconnected expansion chambers were looped around the stator and then discharged onto the oil separation baffle in a manner identical to the standard compressor arrangement. Analysis of the earlier results revealed that a silencer length of 59 mm gave high attenuation at the dominant frequencies. The lengths of the expansion chambers were set at 59 mm and at 51 mm to achieve the maximum reductions over the widest possible frequency range. The ratio of silencer cross section to pipe cross section was 7.6.

7.3.1 Internal silencer : Testing and conclusions

SPL's were recorded at two locations in the near field 250 mm from the compressor and vibration measurements were made at two locations on the casing. Casing vibration spectra for the standard compressor and "silenced" compressor are shown in Figs.7.15 & 7.16 respectively and noise spectra are shown in Figs.7.17 & 7.18. The silenced compressor showed a 1 dB(A) overall SPL improvement and, as can be seen from the casing vibration spectra, there is a reduction of vibration levels at certain

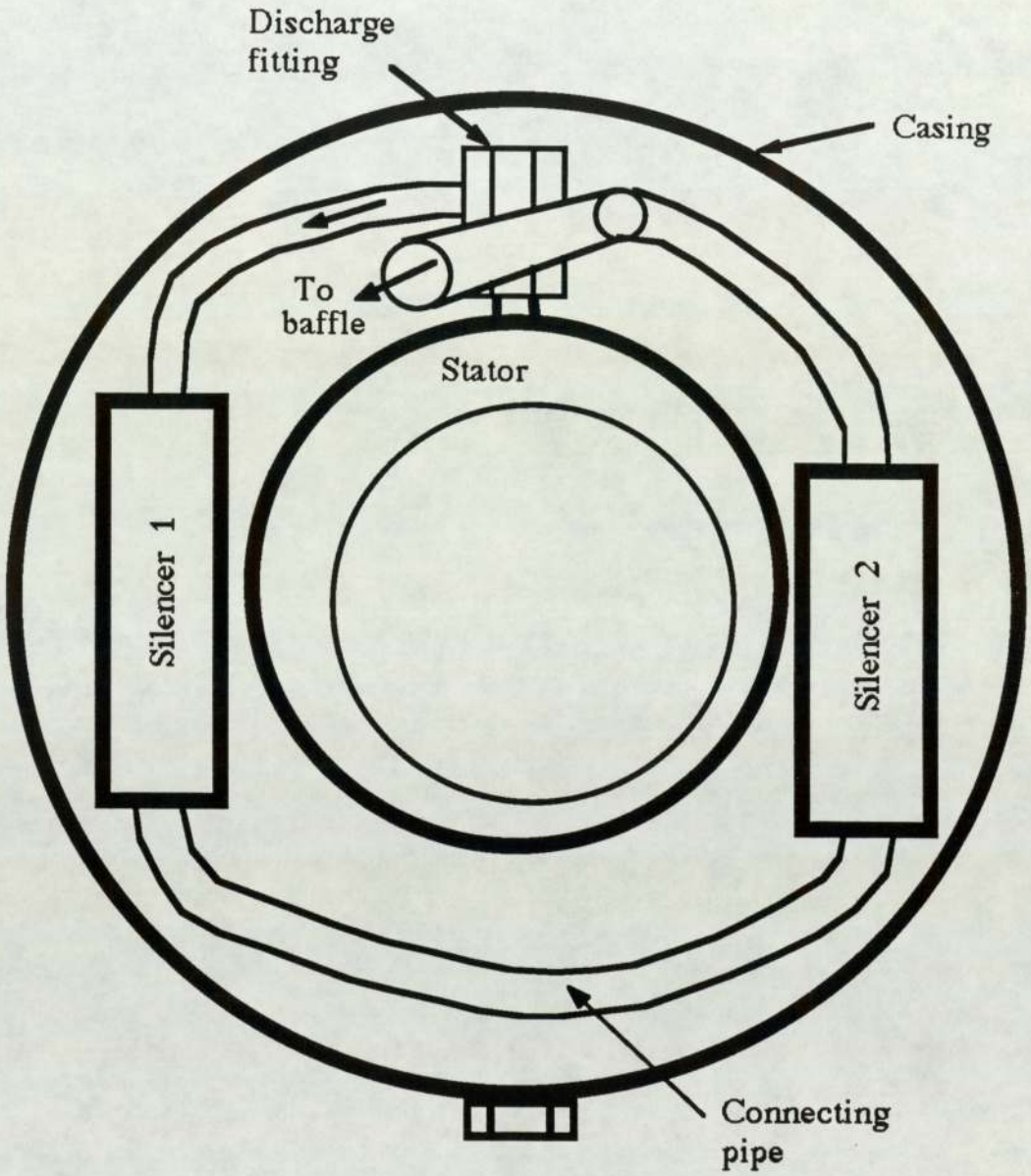

Figure 7.14 Schematic showing location of internal silencers

harmonic peaks and consequently a similar reduction is shown in the noise spectra, particularly the first few harmonics.

It must be emphasised that the SPL measurements included noise generated by the cooling fan and motor. Previous results have shown the contribution from the cooling fan, air-end and motor to be 75.0 dB(A), 72.2 dB(A) and 70.1 dB(A) respectively and that these components together generate an overall SPL of 77.7 dB(A). Since a 1 dB(A) overall reduction to 76.7 dB(A) was measured as the result of improvement to the air-end alone, this in fact indicates that the noise level of the air-end must have been reduced by 5.2 dB(A) from 72.2 dB(A) to 67.0 dB(A), which is a significant improvement.

The 5 dB(A) improvement to the air-end by the use of an internal silencer would be equivelant to a noticeable reduction in radiated noise if it were the sole noise source. However the 1 dB(A) reduction that was measured was not noticeable and this highlights further the predominant contribution of the cooling fan to the total SWL. One further consideration that was not accounted for with this experimental work is any detrimental effect to the thermodynamic efficiency or the separation process (which could lead to increased oil carry-over).

7.4 Cavity resonance

Johnson and Hamilton's papers have shown the effects that cavity resonance can have on the overall noise level. Since an annular type cavity exists between the stator and casing, into which pulses of air and oil are discharged, then it is possible that cavity resonance exists in the Hydrovane compressor.

For two concentric cylinders the frequency at which transverse resonance will occur in the cavity can be derived from the following frequency equation (Johnson and Hamilton 1972).

$$\left[{}^{m}/_{a}\ J_m(Ka) - K\ J_{m+1}(Ka) \right] x \left[{}^{m}/_{b}\ Y_m(Kb) - K\ Y_{m+1}(Kb) \right] -$$

$$\left[{}^{m}/_{b}\ J_m(Kb) - K\ J_{m+1}(Kb) \right] x \left[{}^{m}/_{a}\ Y_m(Ka) - K\ Y_{m+1}(Ka) \right] = 0$$

where

m = mode of vibration

J_m = Bessel function of first kind of order m

Y_m = Bessel function of second kind of order m (Neumann function)

a = radius of outer cylinder

b = radius of inner cylinder

K = wave number

For the compressor the outer cylinder is taken as the casing and the inner cylinder as the stator, the dimensions of which are fixed. Utilising a recurrance relationship to determine higher order Bessel functions from tabulated lower order Bessel functions the equation can be solved for m=1 (lowest mode of transverse vibration). Substituting a value for K of 14.3 satisfied the equation. Now $\mathbf{K = 2\pi f/c}$ and the speed of sound in the air / oil medium that exists in the compressor casing was calculated earlier as 285 m/s (based on a temperature of 380K and a 99% air, 1% oil mixture) therefore the first cavity resonant frequency (f) is calculated as 649 Hz. Repeating for m = 2 gives a value for K of 26.6 and the second cavity resonant frequency as 1206 Hz.

As neither stator nor casing are true cylinders, the casing is approximately a third full with oil and the speed of sound is a predicted value it is possible that the calculations could include a high percentage error. In this case the first cavity resonance could coincide with a pumping frequency harmonic at 768 Hz and the second cavity resonance with a pumping frequency harmonic at 1152 Hz when the compressor is operating at both two and four pole speeds.

7.4.1 Cavity resonance : Experimental investigation

To confirm the theoretical calculations an interesting experiment was completed to measure the pressure fluctuations within the casing. This was achieved by drilling and tapping the filler plug to allow a strain gauge pressure transducer to be attached.

For the four pole, 1420 rpm, compressor the pressure fluctuations were very small (approx 0.02 bar) which tends to indicate that they would not be a major source of casing vibration. However when the compressor was operating at 6.5 bar the spectral analysis (Fig.7.19) shows an expected pressure fluctuation at the pumping frequency (192 Hz), but also a fluctuation at five times the pumping frequency (980 Hz) which was predicted. This peak gradually diminished as the casing pressure was increased (Fig.7.20).

For the two pole, 2880 rpm, compressor the pressure fluctuations were again very small (0.05 bar) and they diminished as the casing pressure was increased. The spectral analysis at 6.5 bar (Fig.7.21a) indicates peaks at the pumping frequency (384 Hz) and the third harmonic (1152 Hz) which also coincides with the prediction.

One point of concern was the effect the oil had on the pressure fluctuations. To determine this the compressor was first run with a third of the recommended oil and then completely drained. In the first case the pressure fluctuations doubled with a corresponding increase in the peak at 1152 Hz (Fig.7.21b). With no oil the pressure fluctuations increased by a factor of 15 however the spectral analysis (Fig.7.21c) revealed a peak at the second harmonic (768 Hz) only.

7.4.2 Cavity resonance : Conclusions

Cavity resonance will occur if the resonant frequency of the cavity is close to a harmonic of the pumping frequency, the pressure fluctuations at the resonant frequency being significantly amplified and resulting in increased vibration and noise. The theoretical and experimental results indicate that this phenomenon did occur within the casing. The oil obviously has a considerable effect on the cavity properties and cavity resonance is more prominent when the casing is drained of oil. However as the compressor is approximately a third full of oil during normal operation the annular cavity is obstructed and cavity resonance is not seen as a significant problem.

Obviously, from Hydrovanes viewpoint, investigations should be undertaken on other compressor models which have cavities subject to similar excitation to determine whether cavity resonance is a problem despite the different dimensions of other machines.

Figure 7.7 Casing vibration spectrum no silencer

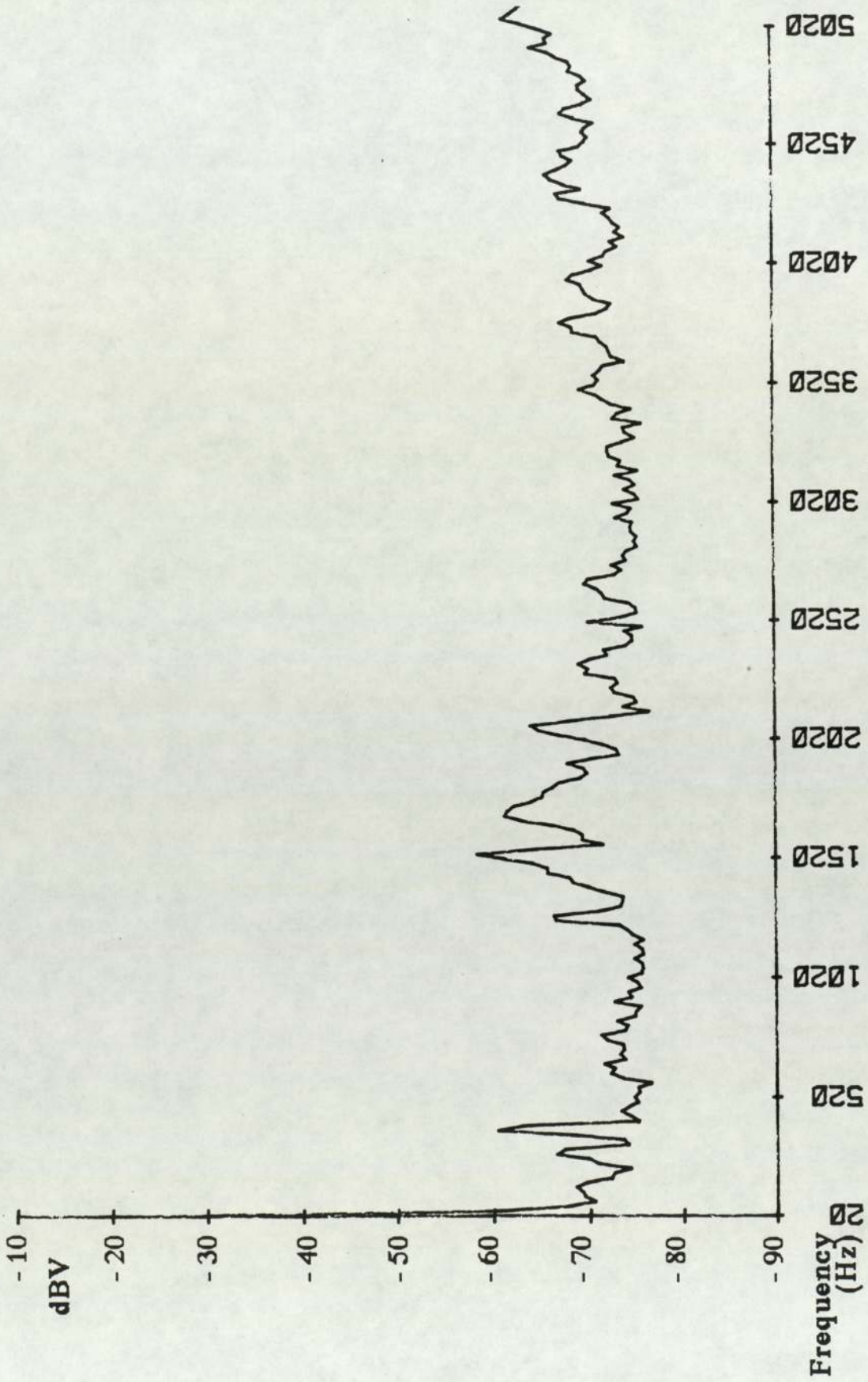

Figure 7.8 Casing vibration spectrum 59 mm silencer

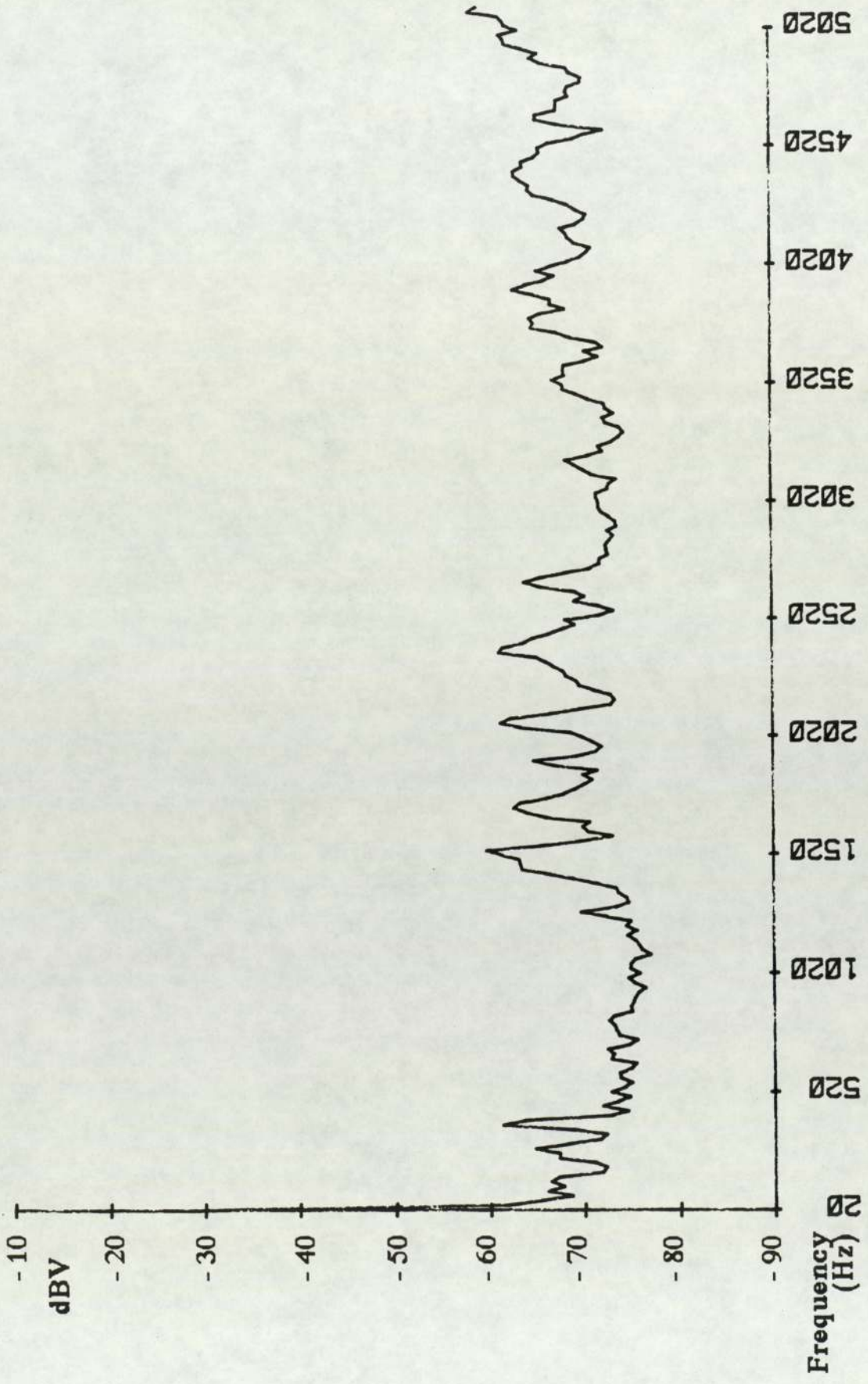

Figure 7.9 Casing vibration spectrum 74 mm silencer

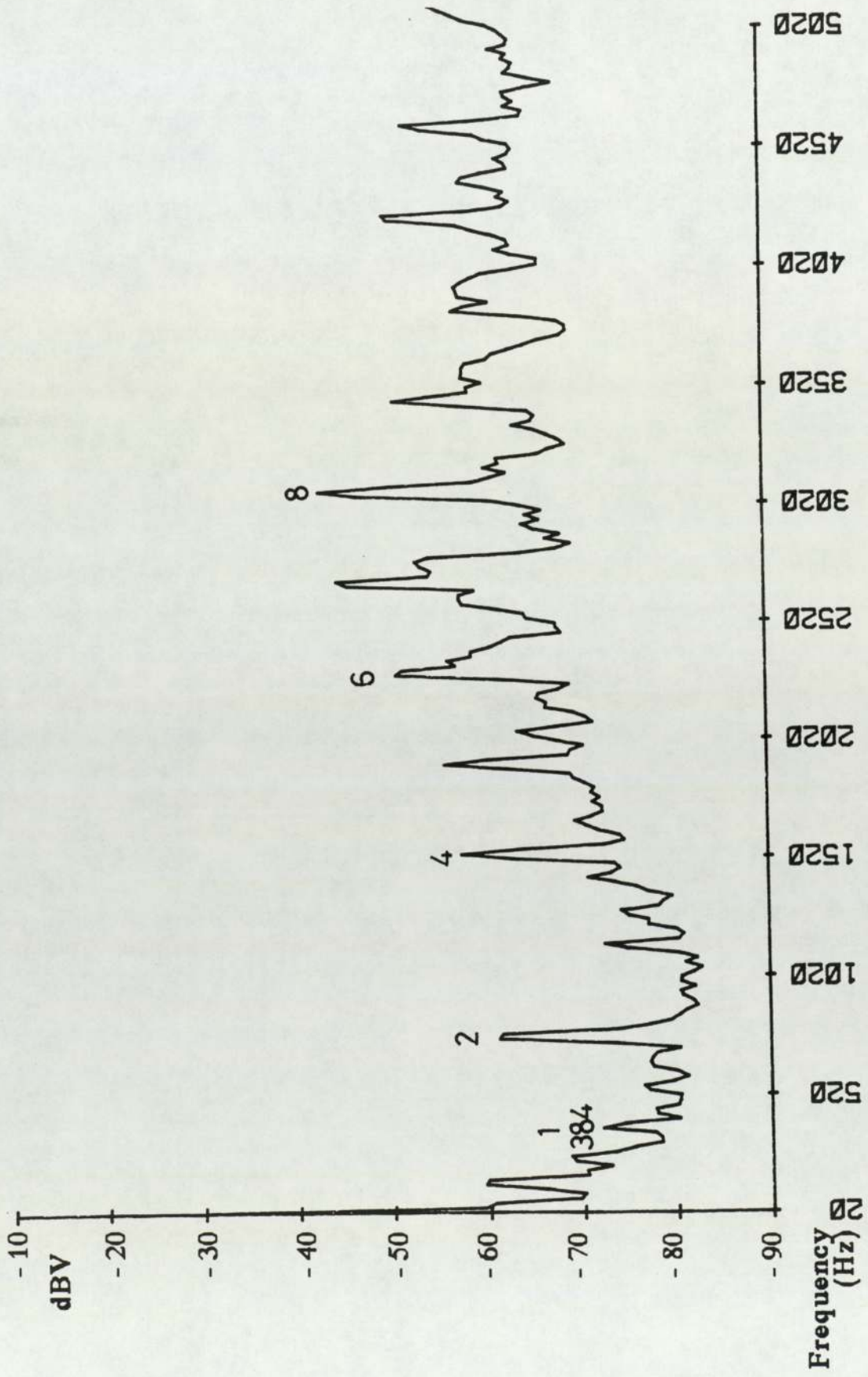

Figure 7.10 Casing vibration spectrum with fitting

Figure 7.11 Casing vibration spectrum with smooth bend

Figure 7.12 Casing vibration spectrum with steel/nylon tube

Figure 7.13 Casing vibration spectrum with rubber hose

Figure 7.15 Casing vibration spectrum standard compressor

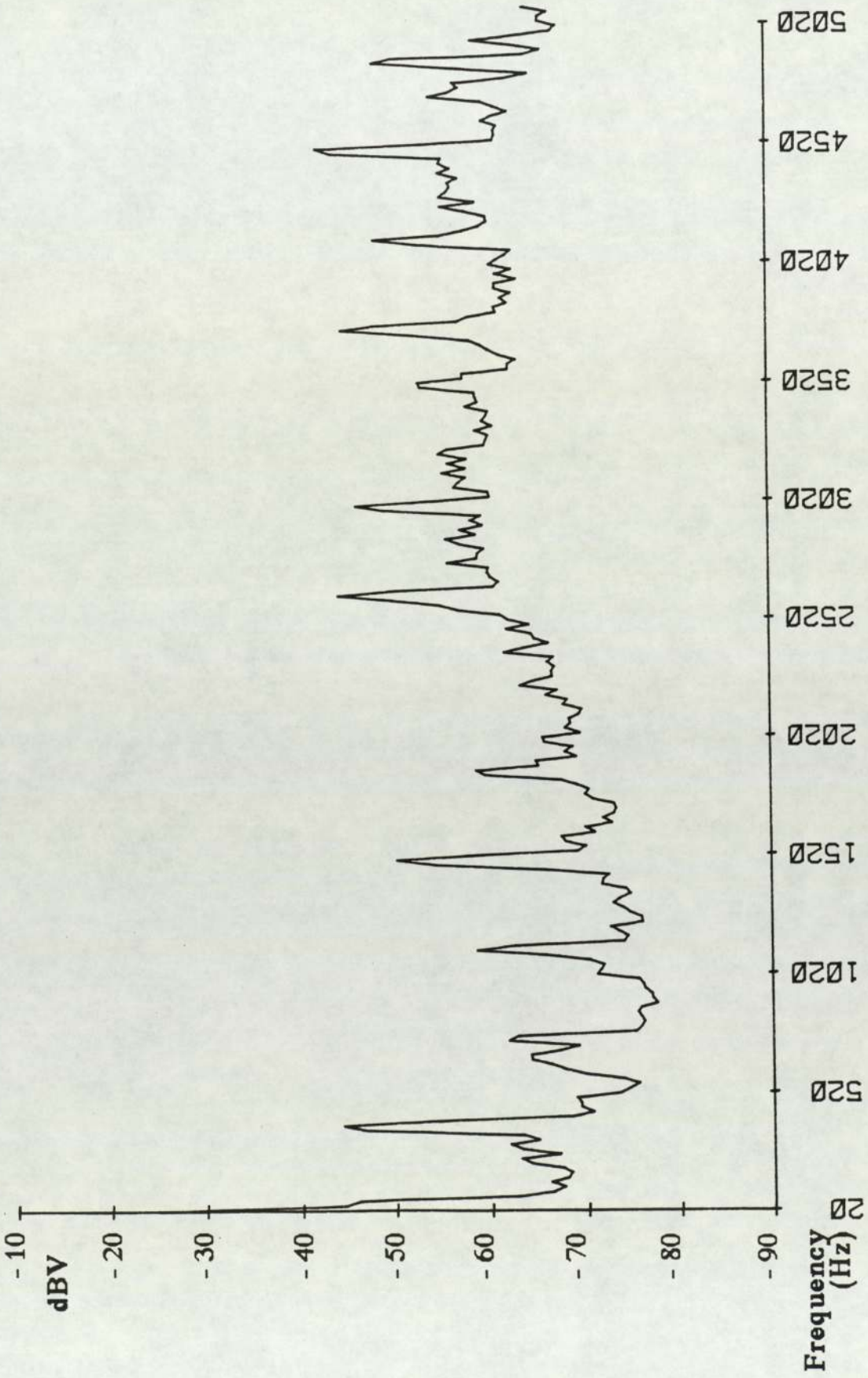

Figure 7.16 Casing vibration spectrum silenced compressor

Figure 7.17 Noise spectrum standard compressor

Figure 7.18 Noise spectrum silenced compressor

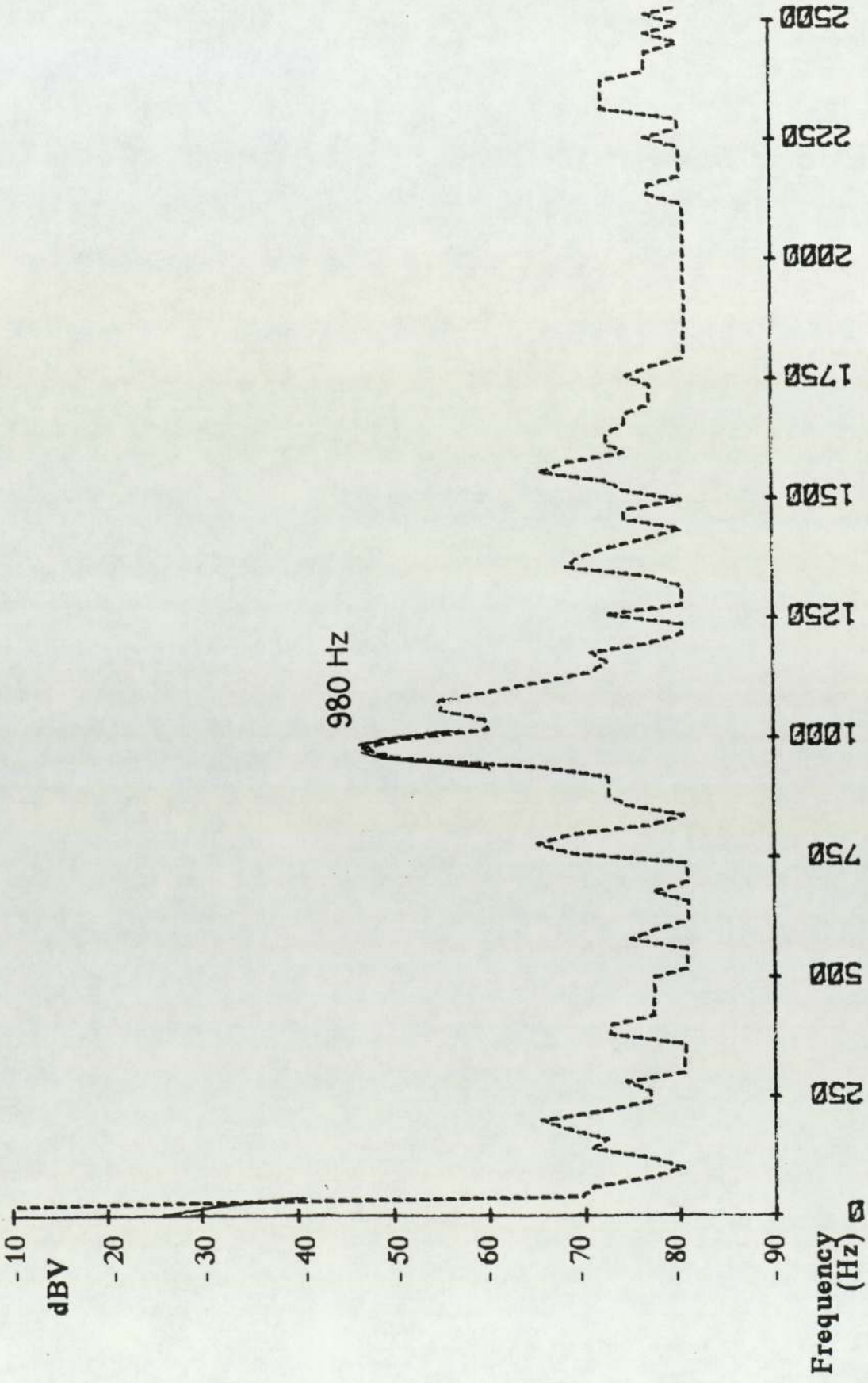

Figure 7.19 Pressure fluctuation spectrum, 6.5 bar, 4 pole

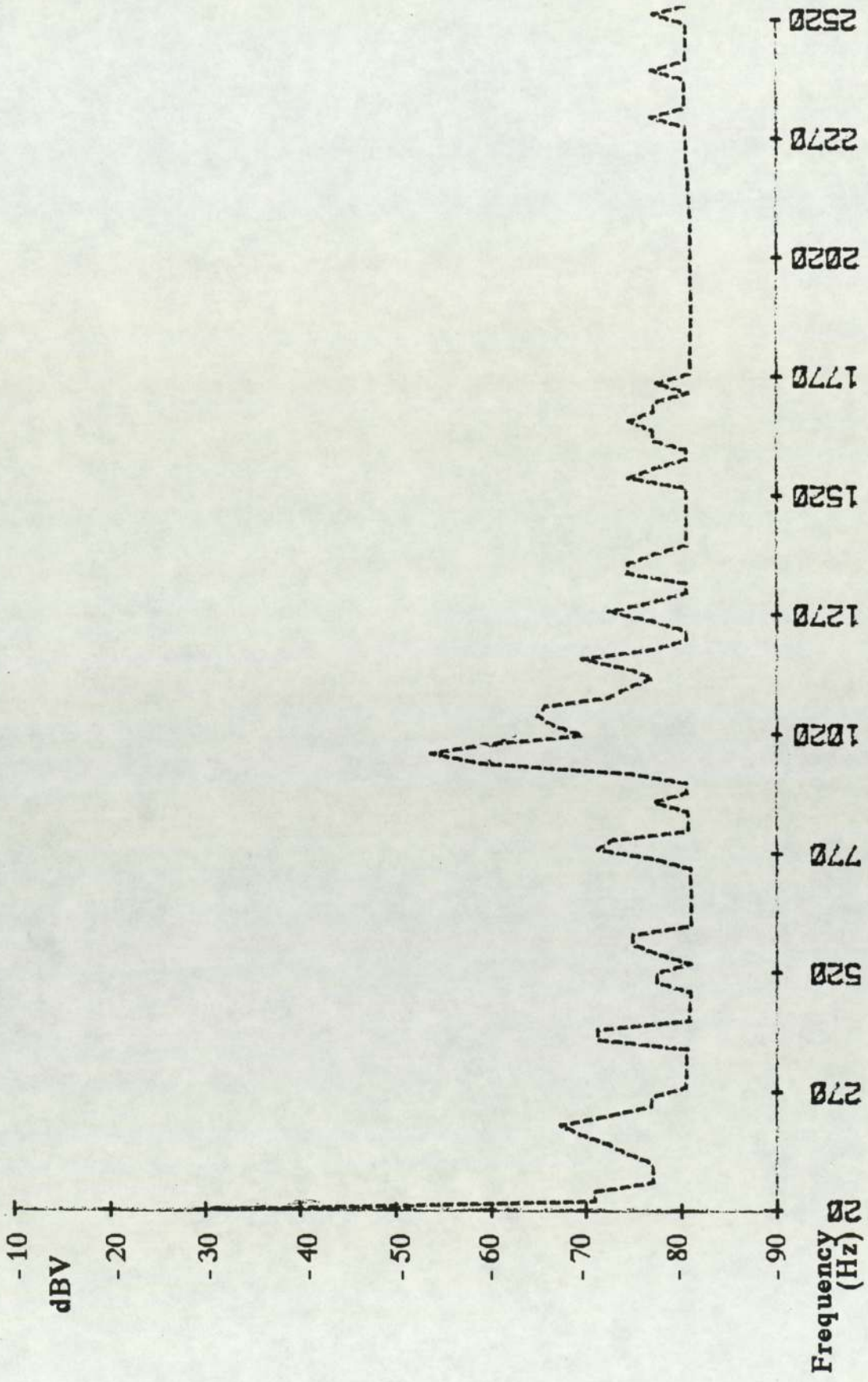

Figure 7.20 Pressure fluctuation spectrum, 10.5 bar, 4 pole

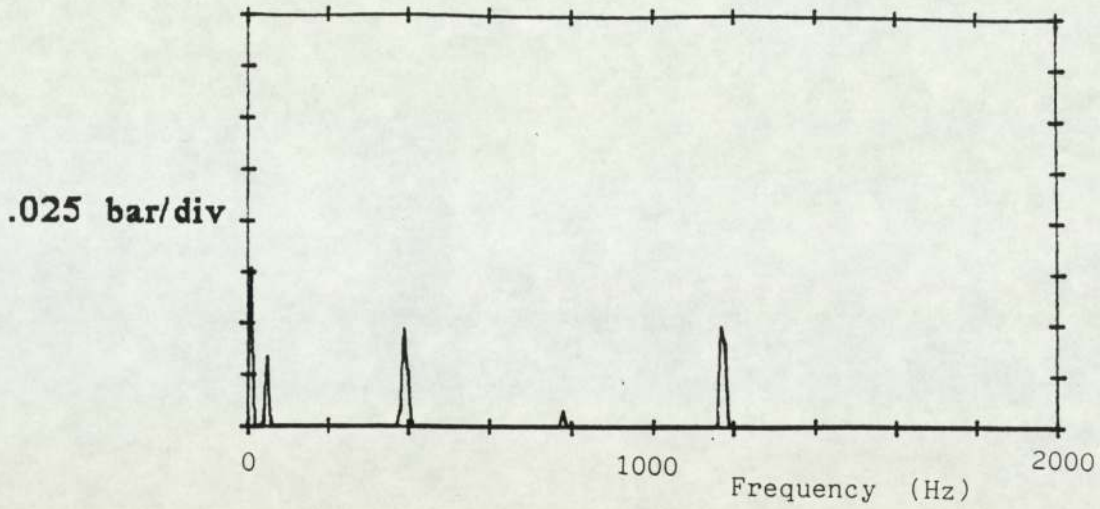

Figure 7.21a Pressure fluctuation spectrum, max oil

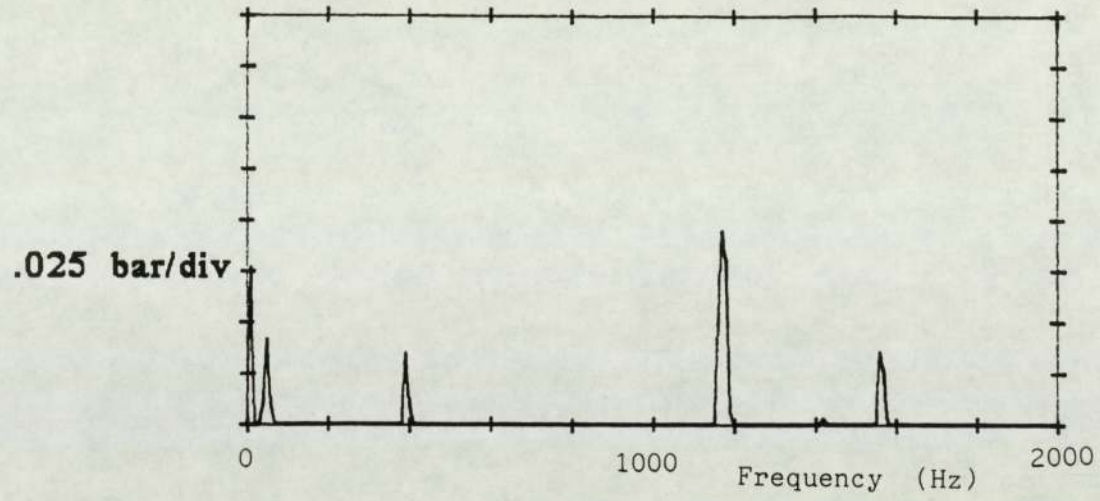

Figure 7.21b Pressure fluctuation spectrum, 1/3 oil

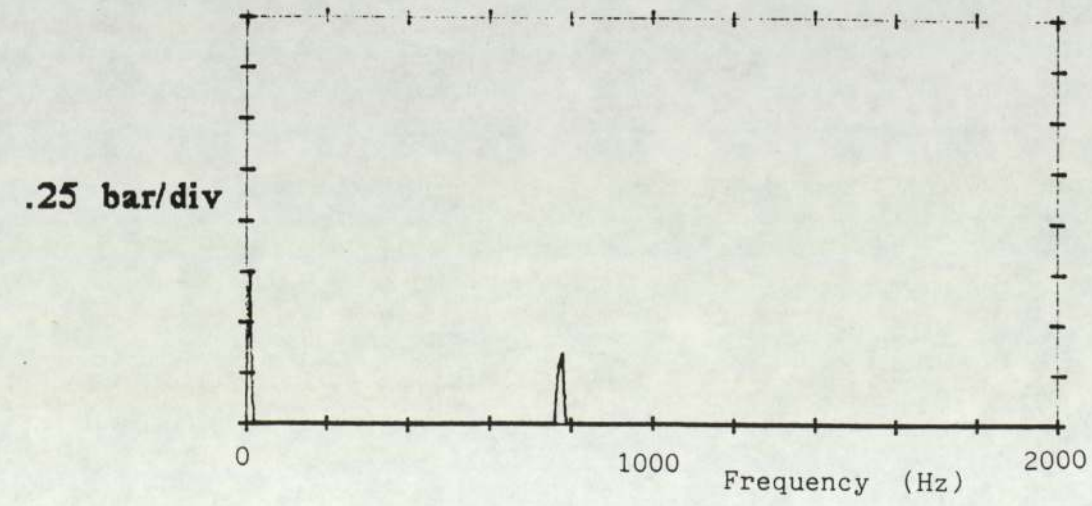

Figure 7.21c Pressure fluctuation spectrum, no oil

8.0 Cooling fan noise

The experimental results discussed in Chapter 3 showed that the cooling fan contributes significantly to the overall compressor noise. In particular, the fan was shown to be the dominant noise source when the compressor is driven by the two pole motor (2880 rpm).

The noise generated by all types of fan has been the subject of much attention in the literature on machine noise. There are two major types of fan: centrifugal flow and axial flow. Each type can be sub-divided further depending on construction, flow behaviour and blade configuration ie. forward curving or backward curving blades for radial flow machines, axial or oblique inlet or outlet flow for axial flow machines. The cooling fan in the Hydrovane compressor (Fig.8.1) is a centrifugal flow type with radial blades.

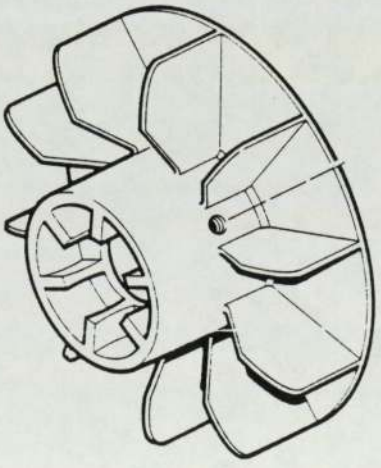

Figure 8.1 Schematic of cooling fan

Eck (1975) provides a comprehensive text book on fans and presents both theoretical and practical aspects of fan design. In Ecks chapter on fan noise which deals with noise generated by air-flow only ie. noise created by flow processes along the blade, wake formation as blades "cut" the air, vortex shedding and turbulence, the most important factor that determines overall fan noise levels is the peripheral velocity at the blade tips; which depends on rotational speed and fan diameter. When designing the most efficient fan it is essential to reduce peripheral velocities and a large diameter slow speed fan is preferable to a small diameter high speed fan due to lower rotational speed and consequently reduced mechanical noise.

Stang and Zeller in 1957 had shown the overall noise levels for axial flow fans to be a function of the fifth power of peripheral velocity. Further work by Zeller in 1959 indicated that fan noise was also a function of rotational frequency. The graph in Fig 8.2 taken from Eck shows this relationship.

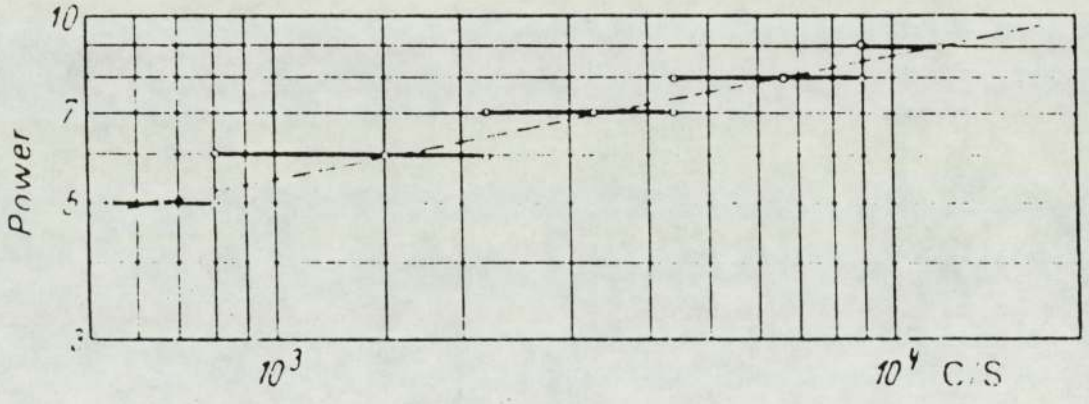

Figure 8.2 Graph showing variation of fan noise with tip speed

Hubner in 1959 showed that the noise levels for a centrifugal flow fan varies depending on the actual peripheral velocity: at slow tip speeds (under 50 m/s) the noise level was estimated as a function of velocity to the power 5.5; for higher tip speeds between 50 m/s and 100 m/s the

power was calculated as 8.7. In general the fifth power is used to give reasonable estimates of fan noise, but Hubners' results confirm that the power is dependant on the particular fan construction.

The aerodynamic factors of the fan: volume flow rate, pressure rise and efficiency also affect the noise levels. For most fans the sound level has its lowest value in the proximity of maximum efficiency. For axial flow fans Stang showed that in some cases maximum efficiency and lowest noise level may even coincide. For the centrifugal fan it is possible that minimum noise levels may occur at flow conditions distant from maximum efficiency. Without discussing details of fan aerodynamics, work by Riollet showed that any alteration from the optimum volume flow coefficient produced an increase in noise levels while research by Stang and Zeller showed the sound level to be clearly a function of the throttling condition of the fans.

Fan noise consists of both harmonic and broadband noise. The harmonic noise will be generated at frequencies related to the number of fan blades: the fundamental blade passage frequency is calculated as;

$$\text{Frequency (Hz)} = \frac{\text{Number of blades x rpm of fan}}{60}$$

Diehl (1972) showed that harmonic noise is also generated when fan blades pass close to any number of interruptions in the fan housing or obstructions to the air flow. The fundamental frequency generated is calculated as;

$$\text{Frequency (Hz)} = \frac{\text{No of blades x No of obstructions}}{\text{Highest common factor of integers above}} \times \frac{\text{rpm}}{60}$$

For the 10 fan blades and 4 housing obstructions in the Hydrovane cooling fan arrangement there are 20 distinct occasions per revolution when a blade "sees" an obstruction. On each of these occasions two

different blades see two separate obstructions therefore twice the amount of noise is generated. Diehl advises the use of prime number combinations as this increases the frequency and reduces the strength at which noise is generated and such noise is easier to attenuate.

The clearance between the blade tip and housing can be a particular problem. Tolerances in design will always introduce some eccentricity in this clearance which will produce tonal noise at blade passage frequency and also harmonics depending on the number of minima and maxima. While an increase in clearance is detrimental to fan efficiency, the effect that an increase in clearance has on noise is not fully understood. Fukano et al (1986) showed for an axial flow fan that an increase in noise levels occurred as tip clearance was increased. This occurred at both design and off-design flow conditions. For the centrifugal flow fan neither efficiency nor noise are particularly sensitive to a change in clearance. Diehl (1972) showed that with an initial increase in clearance, noise levels reduce more rapidly than efficiency: for futher increases in clearance efficiency continues to fall but noise levels are unpredictable. In this situation the clearance should be adjusted so that a satisfactory balance is achieved between noise and efficiency.

The broadband noise content of the spectrum obtained from a fan is generally attributed to turbulent air flow. According to Eck, the principal sources are the turbulence of the incoming air, the turbulent boundary layers and vortex shedding from blade edges. If flow distortions due to mainstream turbulence are significant, so that several blades pass through each eddy then pure tones can also be generated. Blade boundary layers produce high frequency noise whereas mainstream boundary layer variations give rise to low frequency noise.

Eck's summary draws the following conclusions. In general the design of a quiet fan involves the design of the most efficient fan for the

required flow conditions. Once the fan has been carefully designed and tolerances set to give satisfactory impeller to housing clearances, other factors that affect noise levels must also be considered. The inlet and outlet flow areas must be of sufficient size: Flow areas must not be too small as this can restict the efficient operation of the fan. However, large flow areas will introduce almost stationary air to blades travelling at relatively high speeds and the sudden change from low velocity to high velocity will introduce shock and turbulence, which increases noise. The flow conditions of the incoming air is another area that requires investigation: an increase in noise levels will occur if the fan injests turbulent air.

8.1 Cooling fan : Present arrangement

The arrangement of the cooling fan in the Hydrovane compressor is shown in Fig.8.3. The fan is surrounded by a lantern which acts as a housing and also supports the oil cooler and air-end. Air enters the cooler and flows radially inwards through the finned passages. The flow then turns through 90° and passes axially towards the fan. The air moving at the outer radius encounters the blade tip almost immediately after turning and receives a large radial impulse; the air at the inner radius continues axially and is turned gradually through 90° at the blade root after which it flows outwards along the radial blades. As air is discharged from the moving blade passages it encounters four obstructions. These have been cast in an aerofoil profile with respect to radial outlet flow but as the velocity diagrams in Fig.8.4 indicate, actual outlet flow is at 60° to radial. The blade tips also encounter four "gaps" in the housing which occur at the same angular positions as the obstructions mentioned above. The four obstructions to air flow and the four interruptions in housing continuity will both generate pure tones at the interference frequency and its harmonics and also give rise to substantial turbulence.

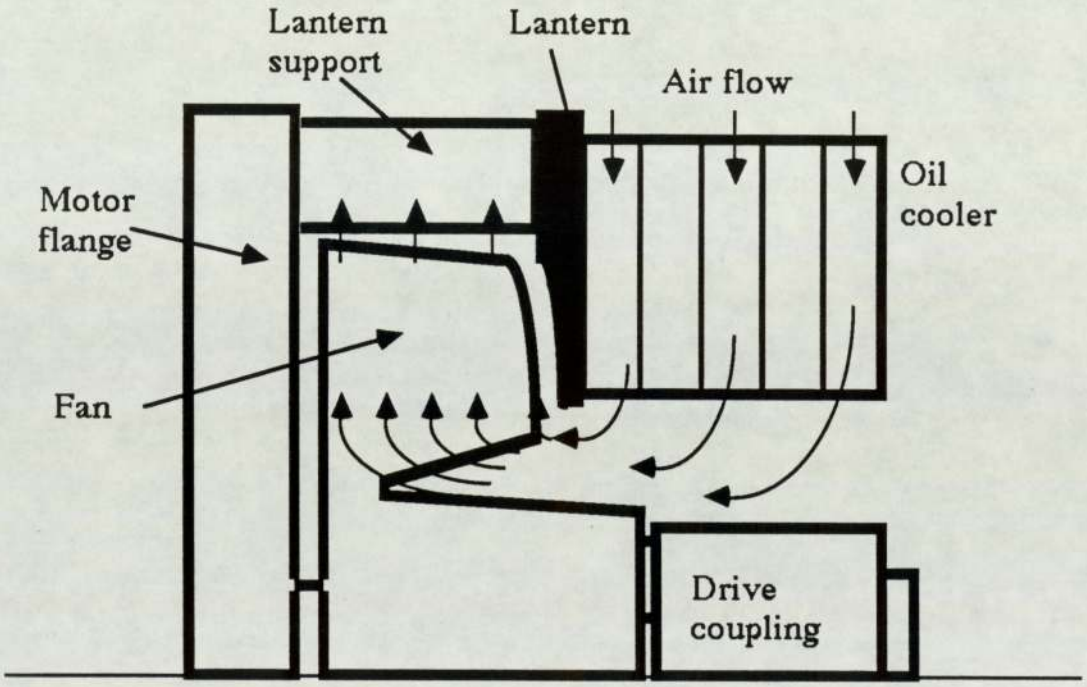

Figure 8.3 Schematic of air path through heat exchanger

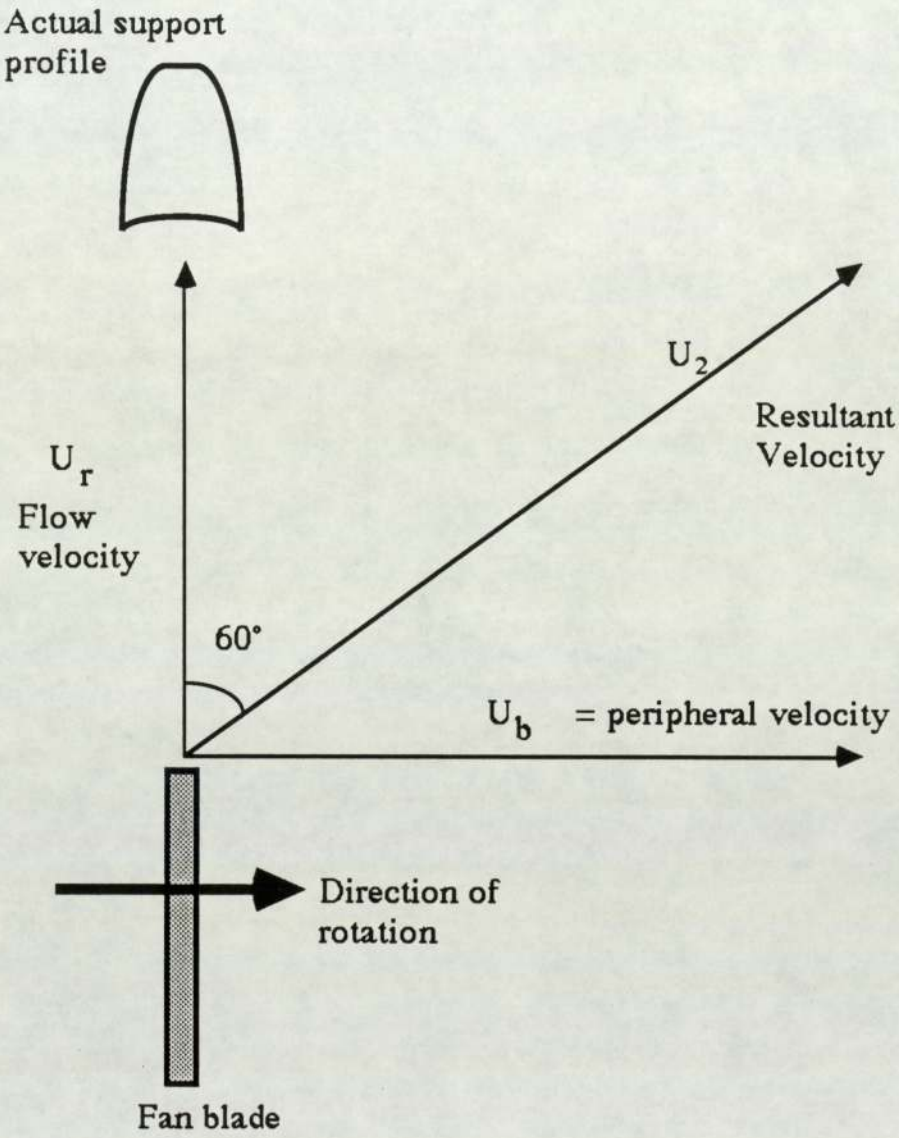

Figure 8.4 Fan outlet flow velocity triangle

8.2 Cooling fan noise : Experimental investigation

The following experiments were all concerned with noise generation from the combination of fan and lantern. SPL measurements were taken on the fan axis, as close as possible to the fan and avoiding interference from air flow (Fig.8.5).

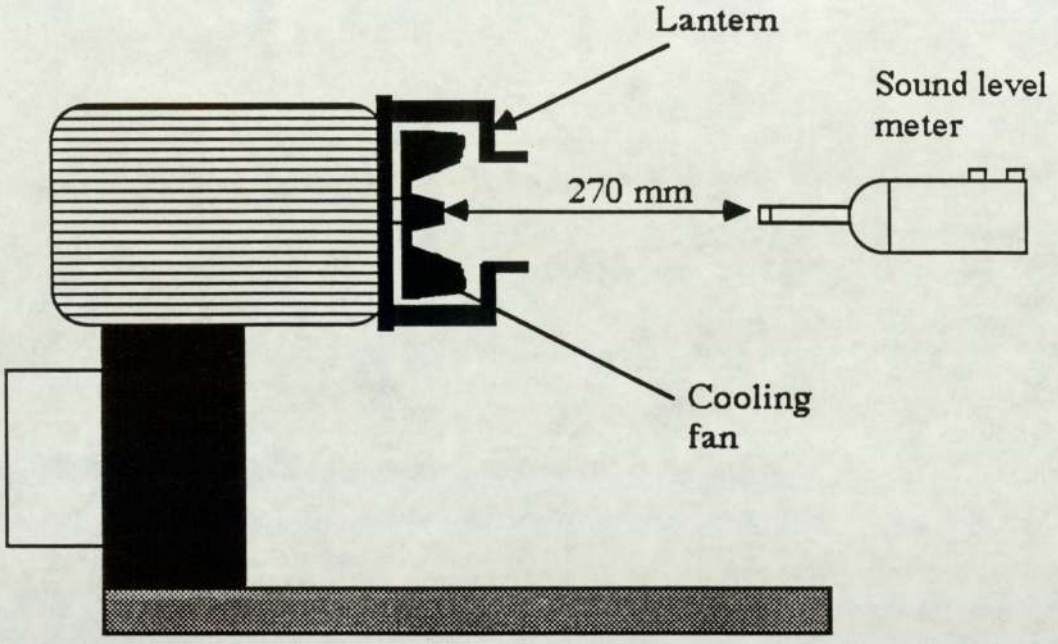

Figure 8.5 Cooling fan noise measurement location

8.2.1 Varying clearance of fan blade tips from lantern

To determine the effect of blade tip clearance on noise it was easier to vary and measure the distance between motor and fan (Fig.8.3), consequently the clearance between fan and lantern also altered. SPL measurements were recorded for each position. No measurement of flow rate was recorded. The results are shown overleaf in Table 8.1.

Table 8.1 Sound Pressure Levels for cooling fan position

Motor / fan gap (mm)	SPL dB(A)
2.0	89.5
2.5	87.2
3.5	86.5
4.0	88.0

It was observed that there is an optimum position for the fan between the motor and lantern with respect to noise. As Diehl had shown the increase in blade tip to housing clearance resulted in a reduction in noise level. However further increases in clearance actually increased the noise level. This was considered to be due to noise generated in a similar manner since a small clearance (2 mm) now existed between the back of the fan and the motor.

With no lantern in position and the fan at the specified 2 mm from the motor the SPL was measured as 82.5 dB(A); the corresponding spectrum is shown in Fig.8.6a. The spectrum shows a large peak at blade passage frequency and peaks reducing in magnitude at the first few harmonics. Introduction of the lantern had a considerable effect on the noise level, which was increased by 7 dB(A), by generating a large frequency component at 960 Hz (Fig.8.6b). This is due to the interference between the ten rotating blades and either the four lantern supports, the four discontinuities in the housing or a combination of both.

8.2.2 Varying fan blade inlet tip profile

It was noticed that the existing blade profile interfered with the air flow as it entered the fan, thus generating turbulence and noise. To reduce this effect the blade tip profile was altered on a lathe as shown in Fig.8.7.

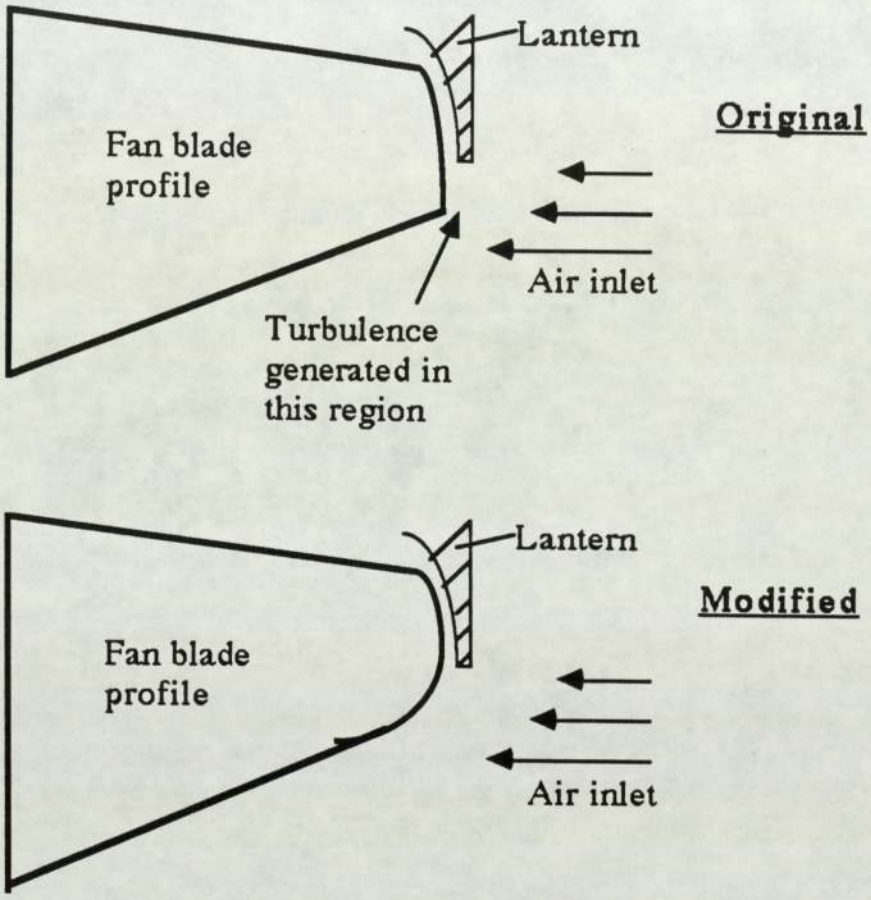

Figure 8.7 Original and modified blade tip profiles

The results are shown below in Table 8.2.

Table 8.2 SPL's for different tip and lantern arrangements

	No lantern	Lantern	
		2.0 mm	3.5 mm
Old profile	82.5 dB	89.5 dB	88.5 dB
New profile	82.5 dB	88.0 dB	85.8 dB

The new profile reduced the SPL by as much as 1.5 dB(A) and clearly reduced the possibility of turbulence occurring by reducing interaction between the low velocity air and high velocity blades.

8.2.3 Varying fan diameter

The above experiments were completed with a standard lantern in position but with no oil cooler attached. The oil cooler and drive coupling will affect the air flow so the results must be analysed in context. To enable more accurate measurements of fan noise to be made, the complete compressor was assembled with the exception of the drive coupling into the air-end since this arrangement simulated standard flow conditions. One further experiment was completed with the improved arrangement which compared noise levels for fans of three different diameters: 140mm (standard size), 135mm and 130mm. Noise measurements were made at two locations on a 1m arc from the fan as shown in Fig.8.8. No measurement of fan performance was recorded and the results are shown below in Table 8.3.

Table 8.3 SPL's for cooling fans of different diameters

Fan Diameter (mm)	SPL dB(A) Measurement location	
	1	2
140	74	73
135	73	72
130	72	71

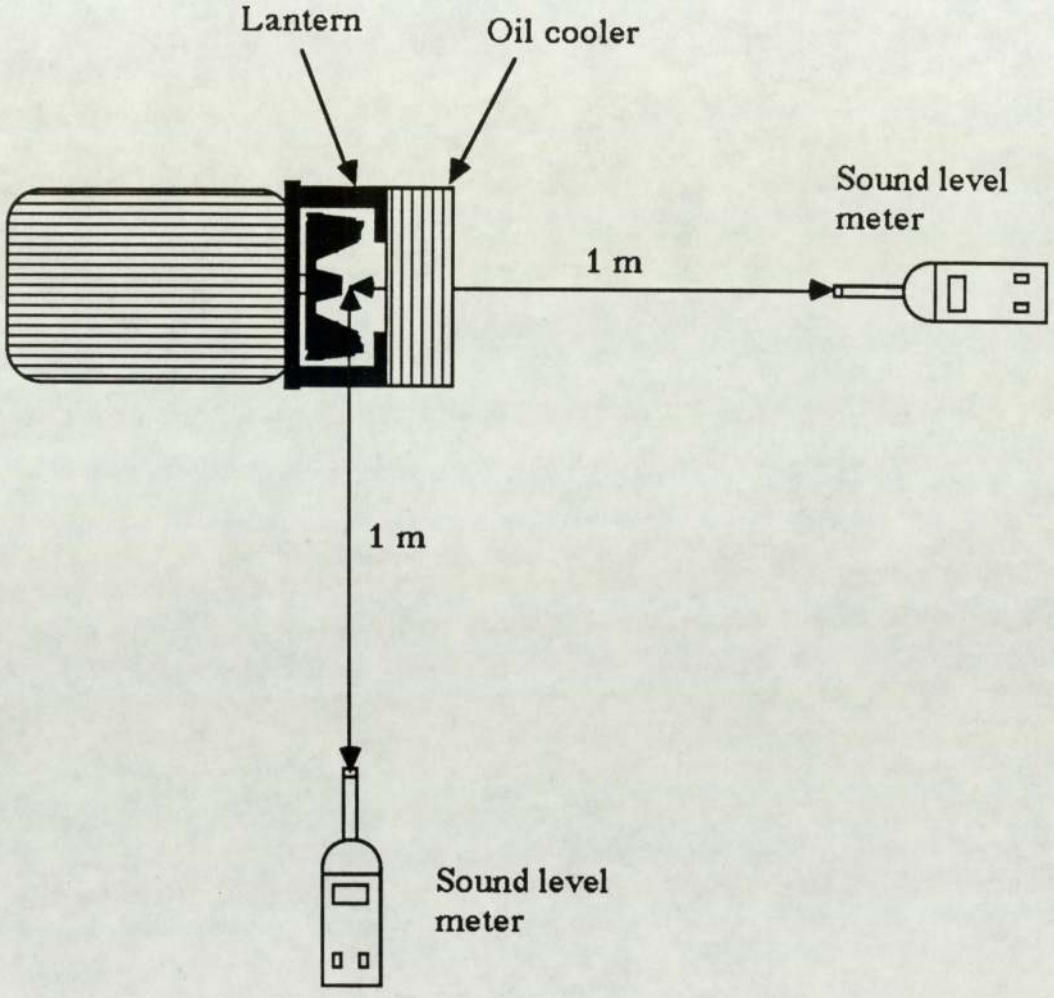

Figure 8.8 Cooling fan noise measurement locations

For a 5 mm reduction in fan diameter (3.6%) the overall noise level was reduced by 1 dB(A) at both microphone locations. For a 10 mm reduction in fan diameter (7.2%) the noise level was reduced by 2 dB(A). A calculation using the fifth power to approximate overall fan noise levels indicates that a 3.6% and a 7.2% reduction in fan diameter and therefore peripheral velocity would produce a 0.8 dB(A) and 1.6 dB(A) reduction in overall noise levels respectively. The difference between the calculated and measured results apart from experimental error is due to the increase in clearance between the fan blades and four lantern supports, not included in the calculation, which reduces both tonal and broadband noise. The spectrum for the reduced fan is shown in Fig.8.9: comparison with the standard fan (Fig.8.10) indicates only a small reduction in the peak at 960 Hz but a considerable reduction at 480 Hz. These results eliminate the combination of the blades and lantern supports as the cause of the peak at 960 Hz and confirms that it is the interference between the blade tips and the four discontinuities in the shaped part of the lantern housing (which remained unaltered).

8.3 Natural frequency of the cooling fan

It was noticed that the fan had a very prominant ring when excited. To determine the natural frequencies of the fan it was located on the motor shaft and then subjected to an impulse on the outer radius from the Bruel &Kjaer hammer discussed in Chapter 2. The decaying noise signal was measured with a sound level meter and also frequency analysis was performed. The frequency content of the spectrum was independant of the location at which the impulse was applied. A typical noise spectrum is shown in Fig.8.11. The spectrum contains peaks at 1560 Hz, 1940 Hz, 2520 Hz and 2800 Hz. These frequencies correspond to different modes of vibration, the natural frequencies.

It is significant that the first two peaks (1560 Hz and 1940Hz)

would coincide with the fourth and fifth harmonics of vane passage frequency given slight changes in running speeds. Under normal operating conditions the vibrations that exist in the drive shaft at these frequencies will be amplified by the fan resulting in some noise radiation from the fan.

The reduced diameter fan (130 mm) was tested in a similar manner and showed peaks at 1480 Hz, 1800 Hz, 2120 Hz and 2800 Hz (Fig. 8.12). None of these natural frequency peaks coincide with a forcing frequency and the cooling fan would not amplify any drive shaft vibration.

8.4 Cooling fan noise : Conclusions and recommendations

The cooling fan was designed to operate at four pole motor speeds and does not operate efficiently with respect to both thermodynamics and noise at the higher speeds of the two pole motor. Not only is there an increase in noise because the fan is not close to maximum efficiency but the fan diameter is greater than required for the necessary cooling. This induces higher flow velocities and tip speeds and increases the radiated noise since it is proportional to the fifth power of tip velocity. The present fan contributes the greatest proportion of total compressor noise and should therefore be redesigned

Altering the profile of the radial blades to blades with forward curved leading edges and backward curved trailing edges will improve efficiency and enable fan diameter to be reduced which in turn will lead to noise attenuation.

The number of fan blades and guide vanes should be altered to prime numbers to increase the frequency and reduce the intensity of noise generation.

The provision of guide vanes on the lantern. (The oil cooler supports are at present cast radially and could be altered to act as guide vanes) would induce rotary motion to the inlet flow in the direction of fan rotation: this would reduce turbulence at inlet.

The lantern housing should be void of discontinuities to prevent any interruption in flow pattern.

The radial clearance between fan blades and the lantern supports should be increased.

The axial clearance between the fan blade tip and the lantern should be set at an optimum position.

The blade tip should be profiled so as not to interfere with the inlet flow.

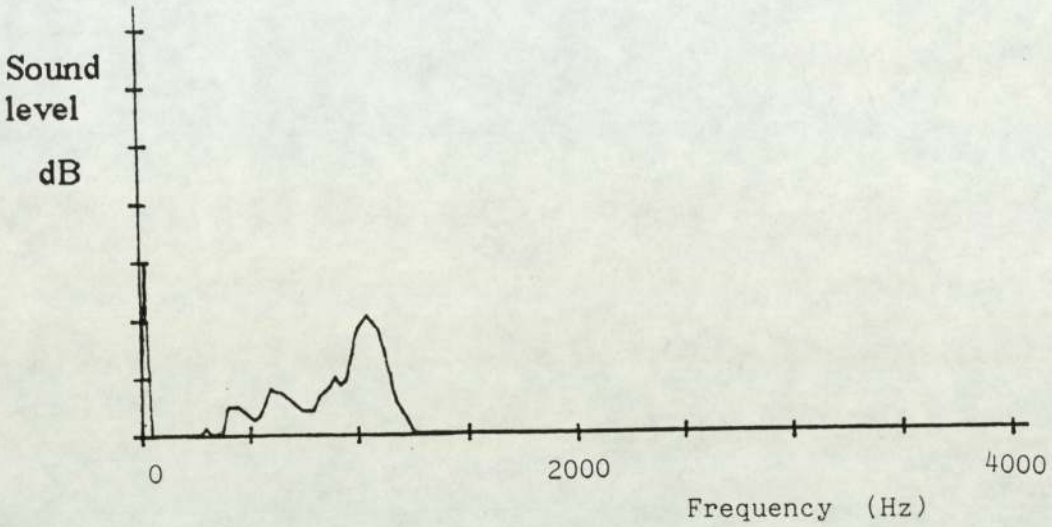

Figure 8.6a Noise spectrum from fan without lantern

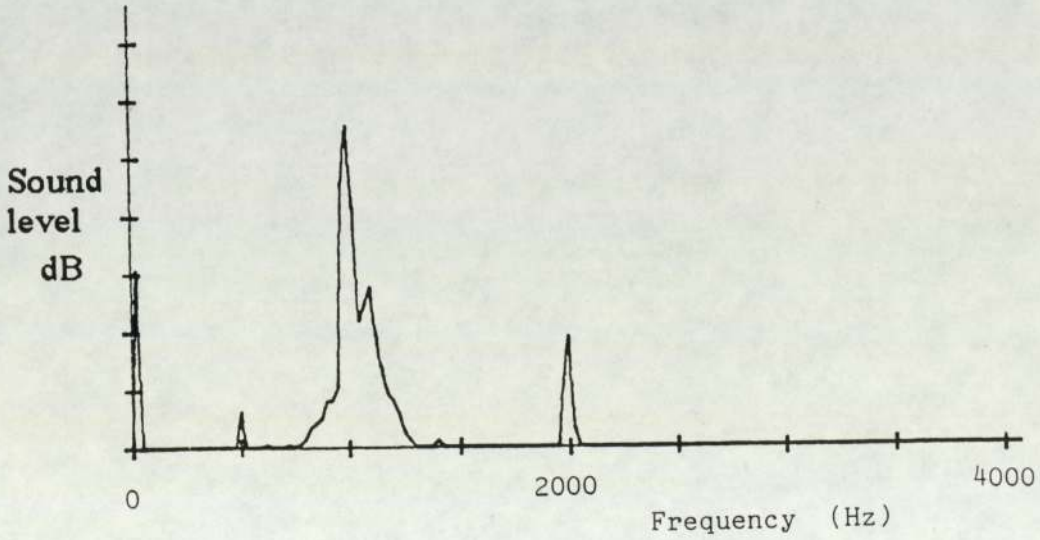

Figure 8.6b Noise spectrum from fan with lantern

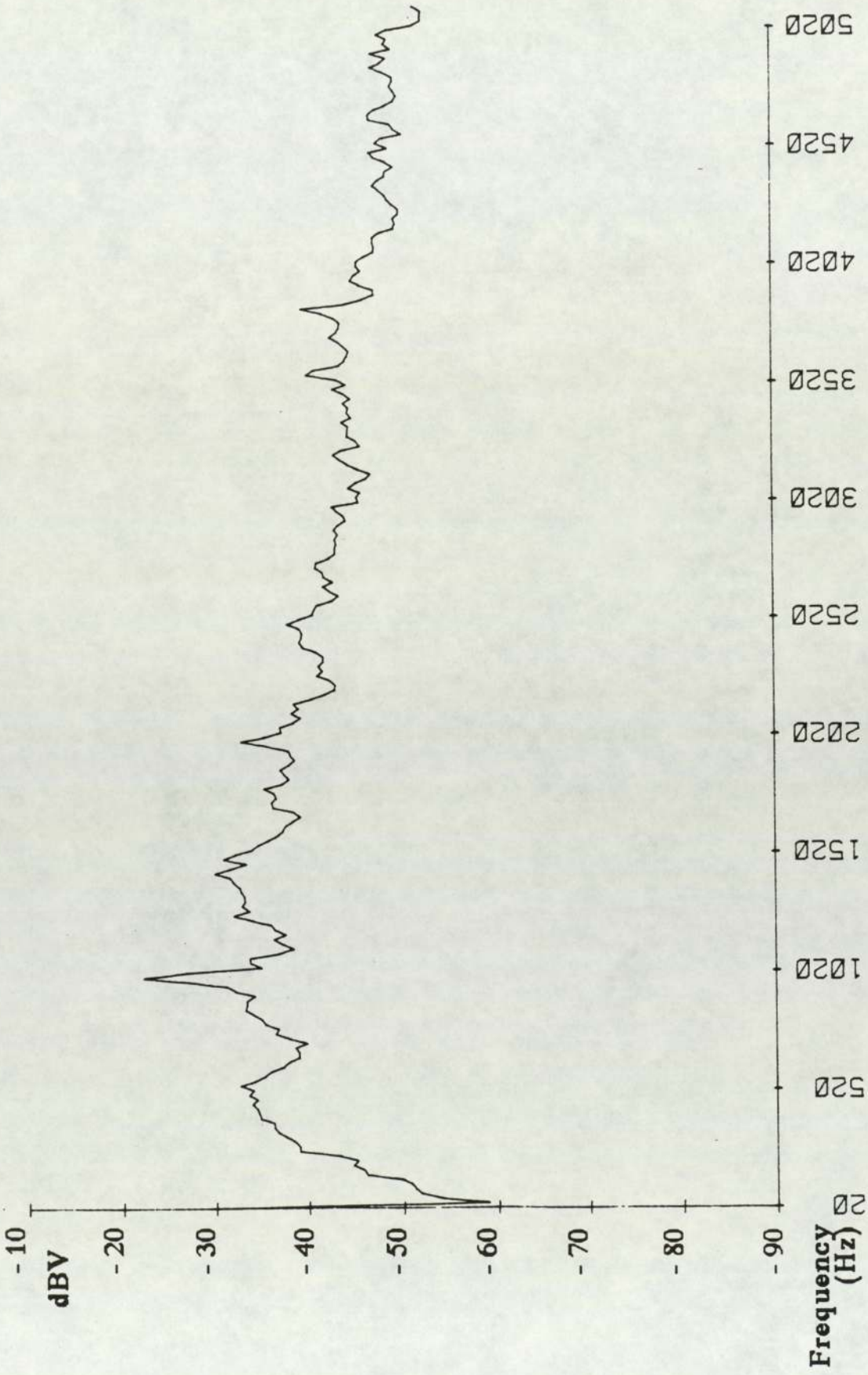

Figure 8.9 Noise spectrum reduced diameter fan

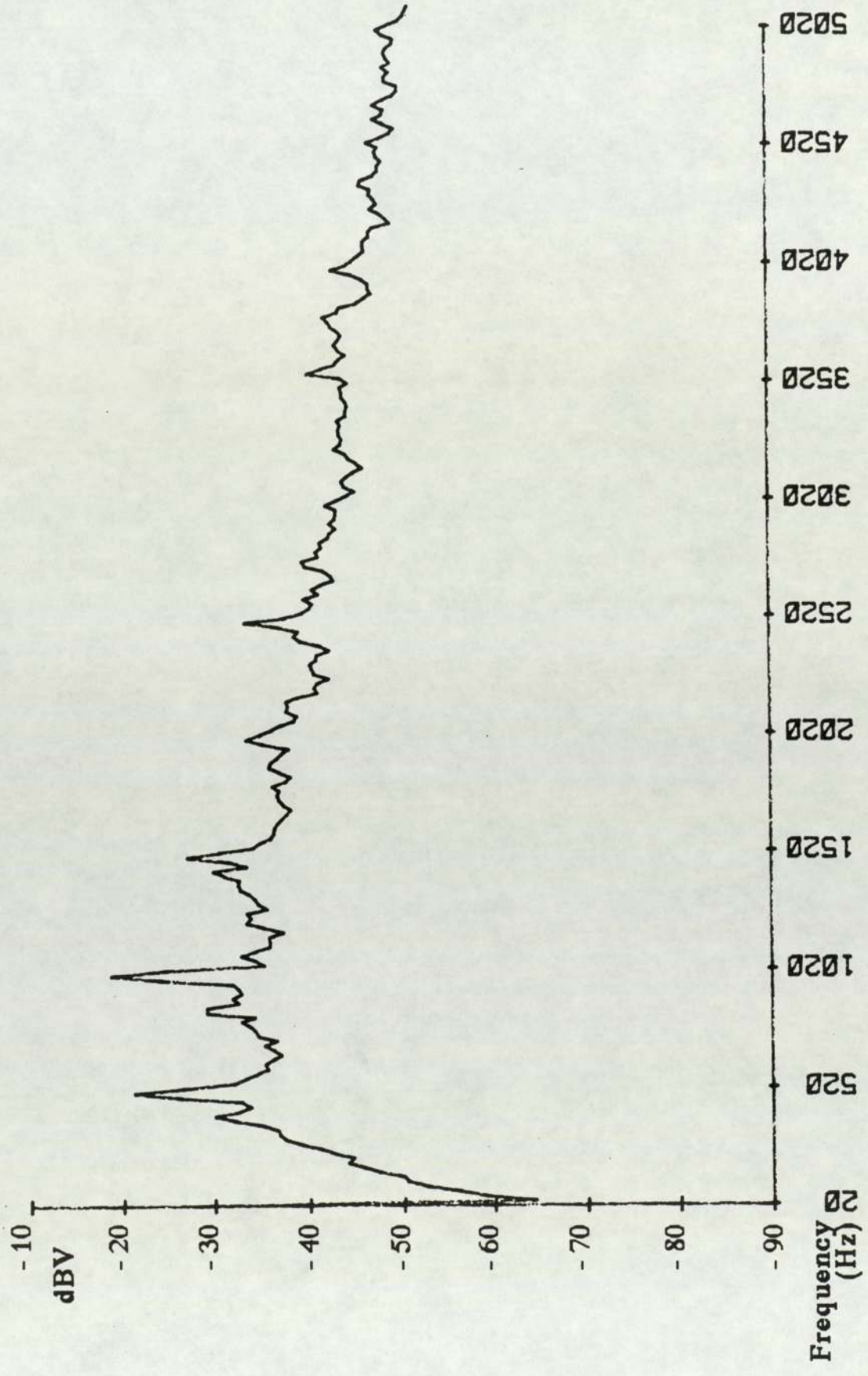

Figure 8.10 Noise spectrum standard diameter fan

Figure 8.11 Noise spectrum from hammer impulse to standard fan

Figure 8.12 Noise spectrum from hammer impulse to reduced fan

9.0 Project review, conclusions and future work

The present chapter aims to collate the essential details of the findings already described and to draw general conclusions, making recommendations for further work.

The introductory noise surveys conducted in an anechoic chamber to BS 4196 : Part 5, at two different speeds showed that the frequency spectra are dominated by peaks up to 8 kHz. The major peaks are all harmonics of the fundamental vane passage frequency: below 2.5 kHz the cooling fan blade passage frequency harmonics and rotational frequency harmonics also dominated. The casing vibration spectra are very similar to the noise spectra in terms of their strong harmonic content, showing that casing vibration is a major source of noise.

Separate investigation of the compressor motor, cooling fan and air-end showed the fan to be 2 dB(A) louder than either the motor or air-end at the higher of the two rotational speeds. To achieve any significant overall improvement fan noise would need to be reduced to at least the level of air-end noise before any action to reduce air-end noise becomes worthwhile. Modifications to the fan and housing showed a slight improvement in noise level, but it was apparent that complete redesign would be required. However, because the high rotational speed was not typical of Hydrovane compressors it was deemed more important to investigate and understand the sources of noise generation within the air-end.

Two sources of casing vibration have been considered: transmission via a solid path from the rotor / stator unit to the casing and noise / pressure fluctuations generated at the discharge port, transmitted via an airborne path. The transfer function between the rotor / stator unit and casing was determined experimentally, enabling casing vibration levels to be predicted accurately from measurements of stator

vibration in the absence of airborne sources. Comparision with the directly measured levels of casing vibration showed that this was principally structure-borne at frequencies up to 2.5 kHz and above 5 kHz. At this point it was inferred that airborne noise was responsible for the vibrations of the casing in the 2.5 - 5 kHz range. An auxiliary casing was excited by the normal pulsating delivery from an external rotor / stator unit and confirmed the contribution of the airborne noise.

A simple dynamic and thermodynamic analysis confirmed that rotor / stator unit vibration would be caused by acceleration of the vanes as they enter and leave the sealing arc and internal cell pressure variations. In addition, it was suspected that the sudden compression of a wedge of oil entering the sealing arc would generate some vibration. Elimination of these sources through the use of valve control of oil injection rates and a rotor / stator unit containing an endcover incorporating relief grooves revealed that both oil compression and air compression had minimal effect. The use of a stator with a purely circular bore showed that the sealing arc and corresponding vane accelerations are principally responsible for the mechanical vibration.

The aerodynamic source of noise was attributed to the discharge process. Experimental analysis of different discharge port configurations revealed that it is tonal noise generated at the port which is responsible rather than internal pressure fluctuations. The most efficient method of reducing tonal noise is a reactive silencer, the design of which requires knowledge of the speed of sound in the medium. A theoretical and experimental investigation confirmed the speed of sound in the air / oil environment and a reactive silencer was designed and tested. A 1 dB(A) improvement in overall noise levels was measured, but bearing in mind the contribution of the cooling fan it was estimated that air-end noise had been reduced by approximately 5 dB(A).

Finally cavity resonance was investigated and conditions were

generated for which this phenomenon occurred. However under normal operatimg conditions the annular cavity between stator and casing is blocked with oil and cavity resonance is not seen as a problem in this particular compressor arrangement.

9.1 Project conclusions

Both mechanical and aerodynamic sources of noise exist within the oil flooded sliding vane compressor. The principal forces causing vibration arise from the accelerations of the vanes as they enter and leave the sealing arc. These forces are transmitted very effectively via the solid path from stator to casing and the consequent vibration of the casing results in radiation of noise. They were eliminated through the use of a stator with a circular bore, leading to a marked reduction in the impulsive nature of the stator vibration spectra. The only remaining forces are then due to any rotor imbalance and the sliding of vanes within the slots and they do not contribute significantly to vibration or noise generation. However since the sealing arc is regarded as necessary to achieve high volumetric efficiency its complete removal is not feasable.

Oil flow rates also affect stator vibration through the volume which is compressed at entry to the sealing arc but the cooling, sealing and lubrication requirements are of greater significance. The oil flow rate should reflect the ideal compromise between noise and compressor performance.

Aerodynamic noise generated by each vane as it passes the discharge port excites the casing via the internal airborne path. A specially designed reactive silencer incorporated into the discharge system successfully reduced air-end noise levels by approximately 5 dB(A). This significant improvement could not be heard due to the

masking effect of cooling fan noise.

The foregoing conclusions relate to the air-end and would apply to any similar designs. The complete compressor requires an integral drive motor and cooling facility and it has been shown that the cooling fan can be the dominant noise source at high running speeds. It is essential that the fan is designed to operate at maximum efficiency at the normal running speed of the compressor. Prime number combinations of blades and unavoidable obstructions should be used to minimise tonal noise and any such obstructions in the air path should be removed as far as possible.

9.2 Suggestions for future work

Three main areas were identified which require further investigation.

1) A full examination on the effect on thermodynamic performance of eliminating the sealing arc should be undertaken. If results are unacceptable then the possibility of using suitable transition profiles to minimise vane accelerations at entry to and exit from the sealing arc becomes necessary. Such profiling may also alleviate the oil compression problem.

2) An extended theoretical and experimental investigation should be undertaken to quantify the dependance of aerodynamic noise on discharge port geometry. This might reveal that a silencer is not necessary or enable a more effective silencer to be designed.

3) The cooling fan used with the Hydrovane series 15 compressor must be redesigned before any overall improvement in noise is possible.

List of References

Asami K. and Ishijima K. (1982) "Improvements of noise and efficiency of rolling piston type rotary compressor for household refrigerators and freezers", Proceedings of the Purdue compressor technology conference. Sponsored by the Ray W. Herrick Laboratories in cooperation with ASHRAE, ASME and CAGI, July, West Lafayette, Indiana, edited by R. Cohen.

Bell L.W. (1982) "Industrial noise control", Marcel Dekker Inc, New York. Edited by L.L. Faulkner and S.B. Menkes

Beranek L.L. (1971) "Noise and vibration control", McGraw-Hill Inc, New York. Ch 18.

Blevins R.D. (1985) "Formulas for natural frequency and mode shape", Van Nostrand Reinhold Co, New York. Ch 12 pp 291 - 336.

Bovey E.C. (1983) "Development of an impact method to determine the vibration transfer characteristics of railway installations", Journal of sound and vibration, Vol 87 (2) pp 357 - 370

Bruel and Kjaer Laser velocity transducer set 3544 Application notes

Bruel and Kjaer (1982) "Measuring vibration handbook".

BS.4196 : Part 5 :1981: "Sound Power Levels of noise sources -: Precision methods for determination of sound power levels in anechoic and semi-anechoic rooms". British Standards Institute

Chang K.Y. (1983) "A theoretical and experimental study of an oil flooded rotary sliding vane compressor", PhD thesis Department of Thermodynamics and Fluid Mechanics, University of Strathclyde, Glasgow.

Diehl G.M (1972) "Compressor noise control" Proceedings of the Purdue compressor technology conference. Sponsored by the Ray W. Herrick Laboratories in cooperation with ASHRAE, ASME and CAGI, July, West Lafayette, Indiana, edited by W. Soedel.

Eck B. (1973) "Design and operation of Centrifugal, Axial-Flow and Cross-Flow Fans", Part F, Chapter 21,"Sound generation by fans" pp 485 - 499 Pergamon Press First English edition,Translated and edited by R.S Azad and D.R Scott.

Ewins D.J (1984) "Modal Testing: Theory and Practice", Research Studies Press Ltd, Letchworth ,England.

Fahy F.J. (1988) "Sound radiation" Institute of Sound and Vibration Research, Advanced noise and vibration course notes

Fujiwara A. et al (1986) "Experimental analysis of a screw compressor noise and vibration", Proceedings of the Purdue compressor technology conference. Sponsored by the Ray W. Herrick Laboratories in cooperation with ASHRAE, ASME and CAGI, August, West Lafayette, Indiana, edited by J. Hamilton and R. Cohen.

Fukano T. Takamatsu Y. and Kodama Y. (1986) "Effect of tip clearance on the noise of low pressure axial and mixed flow fans". Journal of sound and vibration, Vol 105 (2) pp 291 - 308.

Hamilton J. and Johnson C. (1972a) "Fractional horsepower study of a rotary vane refrigeration compressor", Proceedings of the Purdue compressor technology conference. Sponsored by the Ray W. Herrick Laboratories in cooperation with ASHRAE, ASME and CAGI, July, West Lafayette, Indiana, edited by W. Soedel

Hamilton J. and Johnson C. (1972b) "Cavity resonance in a fractional horsepower refrigeration compressor", Proceedings of the Purdue compressor technology conference. Sponsored by the Ray W. Herrick Laboratories in cooperation with ASHRAE, ASME and CAGI, July, West Lafayette, Indiana, edited by W. Soedel

Hamilton J. and Tree D. 1974 "A noise analysis of fractional horsepower compressors" Proceedings of the Purdue compressor technology conference. Sponsored by the Ray W. Herrick Laboratories in cooperation with ASHRAE, ASME and CAGI, July, West Lafayette, Indiana, edited by W. Soedel

Harris C.M. (1979) "Handbook of noise control", Mcgraw-Hill Inc, New York.

Imaichi K. et al (1980) "Noise reduction of rolling piston type rotary compressor for household refrigerators and freezers", Proceedings of the Purdue compressor technology conference. Sponsored by the Ray W. Herrick Laboratories in cooperation with ASHRAE, ASME and CAGI, July, West Lafayette, Indiana, edited by W. Soedel.

Institute of Sound and Vibration Research (1985) "Noise study of a prototype 25 hp compressor" Southampton, Report for Hydrovane No 289/81.

Kawaguchi S. et al (1986) "Noise reduction of a rolling piston type rotary compressor", Proceedings of the Purdue compressor technology conference. Sponsored by the Ray W. Herrick Laboratories in cooperation with ASHRAE, ASME and CAGI, August, West Lafayette, Indiana, edited by J. Hamilton and R. Cohen.

Kjeldson K. and Madsen P. (1978) "Reduction of compressor vibrations by optimising the location of counterweight and the internal springs", Proceedings of the Purdue compressor technology conference. Sponsored by the Ray W. Herrick Laboratories in cooperation with ASHRAE, ASME and CAGI, July, West Lafayette, Indiana, edited by J. Hamilton.

Lyon R.H. (1987) "Machinery noise and diagnostics" Ch 5, Butterworths, London.

McGary M.C. (1987) "Interaction of airborne and structure-borne noise radiated by plates", Journal of sound and vibration, Vol 115 (3) pp 387 - 404.

Mead D.J and Bardell N.S (1986) "Free vibration of a thin cylindrical shell with discrete axial stiffeners", Journal of sound and vibration, Vol 111 (2) pp 229 - 250

Mead D.J and Bardell N.S (1987) "Free vibration of a thin cylindrical shell with periodic circumferential stiffeners", Journal of sound and vibration, Vol 115 (3) pp 499 - 520.

Moody F. (1973) "Time dependant forces caused by blowdown and flow stoppage". Journal of Fluids Engineering, Trans. ASME. September 1973

Noguchi M. et al (1983) "Cavity resonance and noise reduction in a rotary compressor" IEEE transactions on industry applications vol 1A-19 Nov/Dec 1983 pp 1118 - 1123.

Saito F. et al (1980) "Noise reduction of a small hermetic compressor by improvement of its shell shape", Proceedings of the Purdue compressor technology conference. Sponsored by the Ray W. Herrick Laboratories in cooperation with ASHRAE, ASME and CAGI, July, West Lafayette, Indiana, edited by W. Soedel.

Sano K. and Mitsui K (1986) "Analysis of hermetic rolling piston type compressor noise and counter measures" Proceedings of the Purdue compressor technology conference. Sponsored by the Ray W. Herrick Laboratories in cooperation with ASHRAE, ASME and CAGI, August, West Lafayette, Indiana, edited by J. Hamilton and R. Cohen.

Saunders A. (1984) "Hydrovane internal report, photographic evidence".

Sharland I. (1972) "Woods practical guide to noise control" Waterlow (Dunstable)Ltd, England.

Sisson T. and Simpson F. (1984) "Analysis and control of hermetic compressors Sound Power Level", Proceedings of the Purdue compressor technology conference. Sponsored by the Ray W. Herrick Laboratories in cooperation with ASHRAE, ASME and CAGI, July, West Lafayette, Indiana, edited by R. Cohen.

Soedel W. (1980) "Simple mathematical model of the vibration and force transmission of discharge and suction tubes as a function of discharge and suction pressure", Proceedings of the Purdue compressor technology conference. Sponsored by the Ray W. Herrick Laboratories in cooperation with ASHRAE, ASME and CAGI, July, West Lafayette, Indiana, edited by W. Soedel.

Sound Research Laboratories, (1986) "Noise investigation of Hydrovane compressor" Sudbury, report for Hydrovane No C/6072/405

Tojo K. et al (1978) "Dynamic behaviour of a sliding vane in small rotary compressors", Proceedings of the Purdue compressor technology conference. Sponsored by the Ray W. Herrick Laboratories in cooperation with ASHRAE, ASME and CAGI, July, West Lafayette, Indiana, edited by J. Hamilton.

Tojo K. et al (1980) "Noise reduction of a refrigeration compressor", Proceedings of the Purdue compressor technology conference. Sponsored by the Ray W. Herrick Laboratories in cooperation with ASHRAE, ASME and CAGI, July, West Lafayette, Indiana, edited by W. Soedel.

Tree D. and Shryock R. (1976) "Effects of the suspension system and housing on the noise output of a rotating vane compressor", Proceedings of the Purdue compressor technology conference. Sponsored by the Ray W. Herrick Laboratories in cooperation with ASHRAE, ASME and CAGI, August, West Lafayette, Indiana, edited by J. Hamilton and R. Cohen.

Verma S.P. Singal R.K. and Williams K, (1987) "Vibration behaviour of stators of electrical machines" Journal of sound and vibration, Vol 115 (1) pp 1 - 23.

Waser M. and Hamilton J. (1984) "Noise reduction of hermetic refrigeration compressors by changing hermetic shell characteristics", Proceedings of the Purdue compressor technology conference. Sponsored by the Ray W. Herrick Laboratories in cooperation with ASHRAE, ASME and CAGI, July, West Lafayette, Indiana, edited by R. Cohen.

White R.G. and Walker J.G. (1982) "Noise and vibration", Ellis Horwood Ltd, Chichester, England.

Williams M. (1988) " Hydrovane private discussion"

Wilson R. (1974) "Compressor noise control and applications" Proceedings of the Purdue compressor technology conference. Sponsored by the Ray W. Herrick Laboratories in cooperation with ASHRAE, ASME and CAGI, July, West Lafayette, Indiana, edited by W. Soedel

Yee V.and Soedel W. (1980) "Comments on blade excited rigid body vibration of rotary vane compressors", Proceedings of the Purdue compressor technology conference. Sponsored by the Ray W. Herrick Laboratories in cooperation with ASHRAE, ASME and CAGI, July, West Lafayette, Indiana, edited by W. Soedel.

Yildiz I.E. (1988) "The attenuation of sound waves due to scattering from bubbles or liquid drops", Journal of sound and vibration, Vol 121 (1) pp 127 - 133.

APPENDIX A

Equipment, calibration and measurement techniques

A.1 Equipment list

Bruel & Kjaer	Half Inch Condenser Microphone	Type 4133
Bruel & Kjaer	Microphone power supply	Type 2801
Bruel & Kjaer	Impulse Hammer	Type 8202
Bruel & Kjaer	Force Transducer	Type 8200
Bruel & Kjaer	Conditioning Amplifier	Type 2626
C.E.L.	Precision Sound Level Meter	Type 314
C.E.L.	Half Inch Condenser Microphone	Type 186/3F
Racal	Four Channel Tape Recorder	Type Store 4
D J Birchall	Accelerometers	Type A04
D J Birchall	Charge Amplifiers	Type CA04
Hewlett Packard	2 Channel Spectrum Analyser	Type 3582A
Data Aquisition	2 Channel Spectrum Analyser and Digital Storage Oscilloscope	Type 9060
RDP	Pressure Transducer 0 - 200 psi	Type P6/200
Levell	A.C. Microvoltmeter	Type TM3B
Farnell	Sine-square Oscillator	Type LF1
Bruel & Kjaer	Calibration Exciter	Type 4209

A.2 Temperature sensitivity of accelerometers

The table below shows the amplification factor for charge sensitivity as a function of temperature.

Temperature (°C)	20	50	100	150	200
Amplification Factor	1.0	1.15	1.25	1.28	1.22

For early vibration experiments on the complete compressor the output from the charge amplifier was connected directly to the spectrum analyser. Subsequently, the output from the charge amplifier was connected to the magnetic tape recorder.

A.3 Calibration of accelerometers and spectrum analyser

A constant supply current of 100 mA was supplied to the vibrating table of the Calibration Exciter at a series of different frequencies between 50 Hz and 10 kHz. This ensured a constant force was applied to the vibrating table, resulting in a constant acceleration level. With the supply current set at 240 mA the force is quoted as 0.2 kgf and this varies linearly, therefore, at 100 mA the force is 0.083 kgf. The mass of the vibrating table and accelerometer is 197 grams and the resulting acceleration level is 0.42g.

The amplifier output voltage from the reference accelerometer was recorded at each frequency. This was then compared to the amplifier output for each accelerometer used in the experimental work. All accelerometers were measured to within 0.5 dB of the reference accelerometer between 10 Hz and 6.5 kHz.

A.4 Calibration of magnetic tape recorder

The calibration correction factor which determines the ratio of Output voltage to Input voltage is calcuated as

$$\text{Correction Factor} = \frac{\text{Output Voltage}}{\text{Input Voltage x Input attenuator setting}}$$

The table below shows the values recorded when a series of known input voltages were recorded and replayed. The accuracy of the Levell Microvoltmeter used to measure the voltages is specified as ± 1% of the reading.

Measured Input Voltage (mV)	Input setting	Measured Output voltage (mV)	Correction Factor
50	0.1	547	1.094
80	0.1	876	1.096
100	0.2	549	1.098
160	0.2	877	1.097
250	0.5	553	1.106
400	0.5	885	1.107
500	1.0	547	1.094
800	1.0	875	1.095

The average correction factor was calculated as 1.1 ± .008.

APPENDIX B

Computer model : Details of theoretical calculations

The mathematical model is split into four major sections: the first section analyses compressor geometry to enable cell volumes to be calculated, the second section is related to the compression process, the third section models the discharge process to predict pressure fluctuations and the fourth section combines information from all other sections to enable all the forces which act within the stator to be calculated. The calculations are detailed in the following sections.

B.1 Nomenclature

α	180 - vane angle
γ	Isentropic index
ω	Angular velocity
A_{CF}	Centrifugal component of acceleration
A_{GN}	Acceleration due to gravity
A_{ef}	Effective flow area of the discharge port
A_{surf}	Surface area of cell
ang	Trailing vane position
c_v	Specific heat capacity
celw	Cell width
dispres	Discharge pressure
disang	Trailing vane angle as cell starts to discharge
D_{hh}	Diameter of the half holes in trailing edge of slot
e	Eccentricity between stator and rotor
F_{root}	Force at vane root
F_{tip}	Force at vane tip
F_{CA}	Force due to viscous friction in slot
h	Heat transfer coefficient
m	mass flow rate
Q	Heat transfer to fluid
p	Pressure
n	Polytropic index
R	Gas constant
$R(\theta)$	Distance from rotor centre to stator
Rst	Stator radius

Rro	Rotor radius
SA	Half the sealing arc angle
TSA	Sealing arc angle
t	Time
T	Temperature
V	Volume
vana	Contact area between slot and vane
vanm	Vane mass
vanh	Vane height
vant	Vane thickness
W	Work done by fluid

B.2 Compressor Geometry

Figure B.1 is a schematic of the rotor stator and vanes. The purpose of the first section of the model was to determine the cell volume for each degree of rotation. Assuming the vane is in contact with the stator at all times the radial distance of the vane tip from the rotor centre can be defined as a function of angular position. This calculation is split into two sections due to the two bores of the stator, the main eccentric bore and the sealing arc bore. However, the first calculation necessary is to determine the angles each bore subtends with the rotor centre (Fig.B.2). For the half sealing arc angle (SA) using the cosine rule,

(1)

$$\cos SA = \frac{Rst^2 - Rro^2 - e^2}{2.Rro.e}$$

Due to symmetry the total sealing arc angle (TSA) is then calculated as

$$TSA = 2 \times SA$$

As the vane rotates through the sealing arc the radial distance of the vane tip is equal to the rotor radius. The radial velocity and radial acceleration of the vane in the sealing arc is therefore zero.

As the vane rotates through the eccentric bore for any angle (θ) the tip radius $R(\theta)$ is calculated using the cosine rule

(2)

$$Rst^2 = R(\theta)^2 + e^2 - 2.R(\theta).e.\cos\alpha$$

but $\theta = 180 - \alpha$ (Fig.B.2) therefore $\cos\theta = -\cos\alpha$ and

(3)

$$Rst^2 = R(\theta)^2 + E^2 + 2.R(\theta).E.\cos\theta$$

Now let

$$a = E/Rst \quad \text{and} \quad S = a^2(\sin\theta)^2$$

Substituting into equation (3) gives the vane tip radius as

(4)

$$R(\theta) = Rst\left(\sqrt{1-S} - a.\cos\theta\right)$$

The radial velocity of the vane by differentiation is calculated as

$$\frac{dR(\theta)}{dt} = \frac{dR(\theta)}{d\theta} \cdot \frac{d\theta}{dt}$$

which leads to

(5)

$$\dot{R}(\theta) = Rst \cdot \frac{a\sin\theta - a^2\sin 2\theta}{2(1-S)} \cdot \omega$$

Similarly the radial acceleration of the vane by further differentiation is calculated as

$$\frac{d\dot{R}(\theta)}{dt} = \frac{d\dot{R}(\theta)}{d\theta} \cdot \frac{d\theta}{dt}$$

which gives (6)

$$\ddot{R}(\theta) = Rst\left[\left(a\cos\theta - \frac{a^2}{(1-S)^{1.5}}\right).\cos 2\theta + a^2(\sin\theta)^4\right].\omega^2$$

The cell volume is now calculated by summing the individual volumes encompassed as a vane rotates through a 1° interval over the 45° range in which the cell is positioned. The individual volumes $dV(\theta)$ are calculated as the product of mean cell length and mean cell height (which are functions of tip radius calculated in equation 4) and also cell width as shown below.

(7)

$$dV(\theta) = \underbrace{\left(\frac{R(\theta)+R(\theta+1)}{2} - Rro\right)}_{\text{mean cell height}} \underbrace{\left(\left(\frac{R(\theta)+R(\theta+1)}{4} + \frac{Rro}{2}\right) \cdot \frac{\pi}{180}\right)}_{\text{mean cell length}} \underbrace{.celw}_{\text{cell width}}$$

rearranging gives

(8)

$$dV(\theta) = \frac{\left(\frac{R(\theta)+R(\theta+1)}{2}\right)^2 - Rro^2}{2} \cdot \frac{\pi}{180} \cdot celw$$

The values of $dV(\theta)$ are now summed for the 45° between vanes. However the volume occupied by the leading and trailing vane in this region must be subtracted from the total and the volume in the slot beneath the leading vane including the half holes must be added to the total. The cell volume for $\theta = i$ to $i+45$ is therefore

(9)

$$celvol = \sum_{\theta=i}^{\theta=i+45} dV(\theta) - \left(R(i) + R(i+45) - 2\,Rro\right)\frac{blt}{2}.celw + \left(R(i+45) - Rro\right) blt \,.\, celw + 2\,blh\left(\frac{p D_{hh}^2}{8}\right)$$

B.3 Compression process

The model assumes that at maximum cell volume the pressure within the cell is a function of discharge pressure: this is due to leakage through the sealing arc. This assumption is based on experimental results produced

by Chang 1983 which show that for a discharge pressure of 8.5 bar the inlet pressure is atmospheric i.e. 1 bar and for discharge pressures of 10.5 bar and 6.5 bar the inlet pressures are 1.1 bar and 0.95 bar respectively.

For the purpose of calculation it is assumed that no leakage occurs during the compression process and it is assumed to be a non flow process where pV^n is a constant. Leakage is accounted for at the end of this section.

From the second law of thermodynamics

(10)

$$Q - W = E_2 - E_1$$

The heat transfer is defined as

(11)

$$Q = h A_{surf} dT \, . \, dt$$

The work done by the fluid is defined as

(12)

$$W = \frac{p_1 V_1 - p_2 V_2}{n-1}$$

The change in internal energy is defined as

(13)

$$E_2 - E_1 = m c_v (T_2 - T_1)$$

Substituting equations 11, 12 &13 into equation 10 and reaaranging using pV^n is a constant gives

(14)

$$h A_{surf} dT \, dt - \frac{mR(T_1 - T_2)}{n-1} = \frac{mR(T_2 - T_1)}{\gamma - 1}$$

dividing by mR and rearranging gives

(15)

$$\frac{h A_{surf} dT\, dt}{m R} = (T_2 - T_1)\left[\frac{1}{n-1} - \frac{1}{\gamma - 1}\right]$$

and then substituting for T_2 from pV^n gives

(16)

$$\frac{h A_{surf} dT\, dt}{m R} = T_1\left\{\left(\frac{V_1}{V_2}\right)^{n-1} - 1\right\}\left[\frac{(n-1)-(\gamma-1)}{(n-1)(\gamma-1)}\right]$$

substituting from $p_1 V_1 = m R T_1$ gives

(17)

$$\frac{h A_{surf} dT\, dt\, T_1}{p_1 V_1} = T_1\left\{\left(\frac{V_1}{V_2}\right)^{n-1} - 1\right\}\left[\frac{(n-1)-(\gamma-1)}{(n-1)(\gamma-1)}\right]$$

Let $d = \frac{V_2 - V_1}{V_2}$ therefore $\left(\frac{V_1}{V_2}\right)^{n-1} = (1-d)^{n-1}$

and substituting into equation 17 gives

(18)

$$\frac{h A_{surf} dT\, dt}{p_1 V_1} = \left[(1-d)^{n-1} - 1\right]\left[\frac{(n-1)-(\gamma-1)}{(n-1)(\gamma-1)}\right]$$

Using the binomial expansion of $(1-d)^{n-1}$ gives

(19)

$$\frac{h A_{surf} dT\, dt}{p_1 V_1} = \left[-(n-1)d\right]\left[\frac{(n-1)-(\gamma-1)}{(n-1)(\gamma-1)}\right]$$

which leads to

$$\frac{h A_{surf} dT\, dt}{p_1 V_1} = d\left[\frac{(\gamma-1)-(n-1)}{(\gamma-1)}\right]$$

Rearranging gives

(20)

$$n = 1 + (\gamma - 1)\left[1 - \left(\frac{h\,A_{surf}\,dT\,dt}{p_1 V_1} \Big/ d\right)\right]$$

This value of n can then be used to calculate the new temperature and pressure in the cell. Now let

$$rat = \left(\frac{V_1}{V_2}\right)^{n-1}$$

Therefore the new temperature and pressure are calculated as

$$T_2 = T_1 \times rat \qquad \text{and} \qquad p_2 = p_1 \times rat^{\left(n/n-1\right)}$$

To allow for the effects of leakage on the calculated values of cell pressure during the compression process a leakage factor which was a function of discharge pressure and cell position was introduced into the model. To determine the actual factor various ratios were input into the model which contained the dimensions of Changs' compressor. The ratio which gave the best comparison to Changs' experimental results at three different discharge pressures is shown below

(21)

$$\text{leakage factor} = 1 + \frac{dispres - p_1}{7 \times 10^5 \left(disang + 1 - ang\right)^2}$$

where dispres is the nominal discharge pressure

disang is the angle at which the discharge port opens

The new cell pressure after each degree of rotation is therefore

$$p_{final} = p_2 \times \text{leakage factor}$$

B.4 Pressure fluctuations at discharge

The pressure calculation detailed above predicts the cell pressures as a function of angular position up to the angle that the discharge port opens. This section of the model then calculates the flow area between the cell and discharge manifold to enable the flow rates and pressure fluctuations to be calculated in the three chambers, namely the cell, manifold and receiver. The model assumes that a quasi-steady state flow exists. To obtain the necessary accuracy this section of the model is split into 390 intervals to represent the 39° of rotation during discharge. The two fundamental equations used are the nozzle equation and the first law of thermodynamics.

The nozzle equation determines the mass flow rate between two chambers of different pressures. For un-choked flow ($p_2/p_{01} < 1.893$) the equation is given as

(22)

$$\frac{\dot{m}\sqrt{RT_{01}}}{A_{ef}\,p_{01}} = \sqrt{\frac{2\gamma}{\gamma-1}\left(\frac{p_2}{p_{01}}\right)^{2/\gamma}\left[1-\left(\frac{p_2}{p_{01}}\right)^{\gamma-1/\gamma}\right]}$$

and for choked flow the equation is independant of downstream conditions and simplified as

(23)

$$\dot{m} = \frac{.6847\ A_{ef}\ x\ p_{01}}{\sqrt{R\,T_{01}}}$$

where in both equations

m is the mass flow rate

T_{01} and p_{01} refer to the upstream stagnation conditions

p_2 is the downstream pressure and

A_{ef} is the effective flow area of the nozzle

The first law of thermodynamics enables the new set of temperatures and pressures to be calculated for each chamber.

$$pV = mRT$$

The initial conditions required are the temperature, pressure and volume of all chambers and the areas of the various ports and slots connecting each chamber. The volumes of the manifold and receiver are fixed as are the flow areas between manifold and receiver and receiver and atmosphere. However there are two values which require input into the model before the calculation for each step change: these are the cell volume and the effective flow area between cell and manifold. The cell volume has already been calculated at 1° intervals in an earlier section of the model but for this section it is assumed that these 1° intervals are split further into ten equal divisions.

To calculate the effective flow area between cell and manifold for the various port configurations the actual port area was plotted against angle at 5° interval and then the best fit polynomial was calculated using standard Apple Macintosh computer software. The polynomial could then be used to calculate the actual port area (a_1) for any angular position.

The effective area is then calculated as follows

$$Aef = \frac{1}{\sqrt{\frac{1}{a_1^2} + \frac{1}{a_2^2}}}$$

where a_2 is the fixed area of the thin slot between stator and rotor whose dimensions are fixed (55 mm x 1.5 mm).

The temperature and pressure in the discharging cell have been calculated in the earlier section of the model and the initial conditions in all other chambers were based on actual measurements made by Hydrovane on an identical compressor.

Figure B.3 shows a graph of the variation of cell pressure against trailing vane angular position for the suction, compression and discharge processes for the three different nominal discharge pressures. Fig.B.4 shows the variation in manifold pressure for the standard port configuration at the three nominal discharge pressures.

B.5 Internal forces

The free body diagram of a vane in a slot is shown in Fig.B.5. It is necessary to calculate all the forces and that act radially on the vane and its resultant radial acceleration at any angular position. To maintain equilibrium there is an unknown contact force between the stator and vane tip and it is this force that induces vibration into the stator. The known radial forces include viscous friction in the slot and pressures acting at the vane root and tip. Radial, centrifugal and gravity components are all included in the calculation of resultant radial acceleration. The expressions are all functions of the vanes angular position: "vant" and "vanh" refer to the vane thickness and height respectively.

The force due to presssure at the vane root which is equal to the trailing cell pressure.

$$F_{root} = p(ANG - 45) \times vant \times celw$$

The force due to pressure at the vane tip whose area is is exposed to 60% trailing cell pressure and 40% leading cell pressure

$$F_{tip} = [p(ANG - 45) \times 0.6 + p(ANG) \times 0.4] \times vant \times celw$$

Force due to viscous friction in the slot where "vana" is the area over which a thin oil film exists between vane and slot

$$F_{CA} = \upsilon \times R(\theta) \times (2 \times celw \times vana) \times (slt - vant)/2$$

The total acceleration of the vane in a radial direction is comprised of three components, centrifugal, radial and gravitational.

In defining the compressor geometry an expression for the radial distance of the vane tip from the rotor centre $R(\theta)$ was generated. The radial acceleration is therefore given by $R(\theta)$

To calculate the radial distance of the vane centre of mass half the vane length must be subtracted. The centifugal acceleration at any angle is therefore calculated as

$$A_{CF} = \left(R(\theta) - \frac{vanh}{2}\right) \times \omega^2$$

The acceleration due to gravity

$$A_{GN} = g \times \cos(ANG + 30)$$

From Newtons Second law of motion the unknown contact force exerted by the stator on the vane must balance the various components listed above at each angle and it is calculated by the following equation.

Resolving in a radially outwards direction.

$$F_{ROOT} - F? - F_{TIP} - F_{CA} = vanm\,(R(\theta) - A_{GN} - A_{CF})$$

The variation of this contact force with vane position (ignoring cell pressures) is shown for one complete revolution in Fig.B.6. This clearly shows the abrubt change in force as a vane enters and leaves the sealing arc (20° and 340°).

Figure B.7 shows the fluctuation of the contact force for a nominal discharge pressure of 8.5 bar and the two abrubt changes still exist. However the graph also reveals that there are other regions in which sudden changes in force levels would be expected. These forces are due to the changes in pressure as the vane passes through different regions in the compression and discharge processes ie. one half of the vane will suddenly "see" a very high pressure while the other remains in a low pressure region. In the real situation it is expected that the effects of leakage in the vane tip region will reduce the sudden nature of these changes.

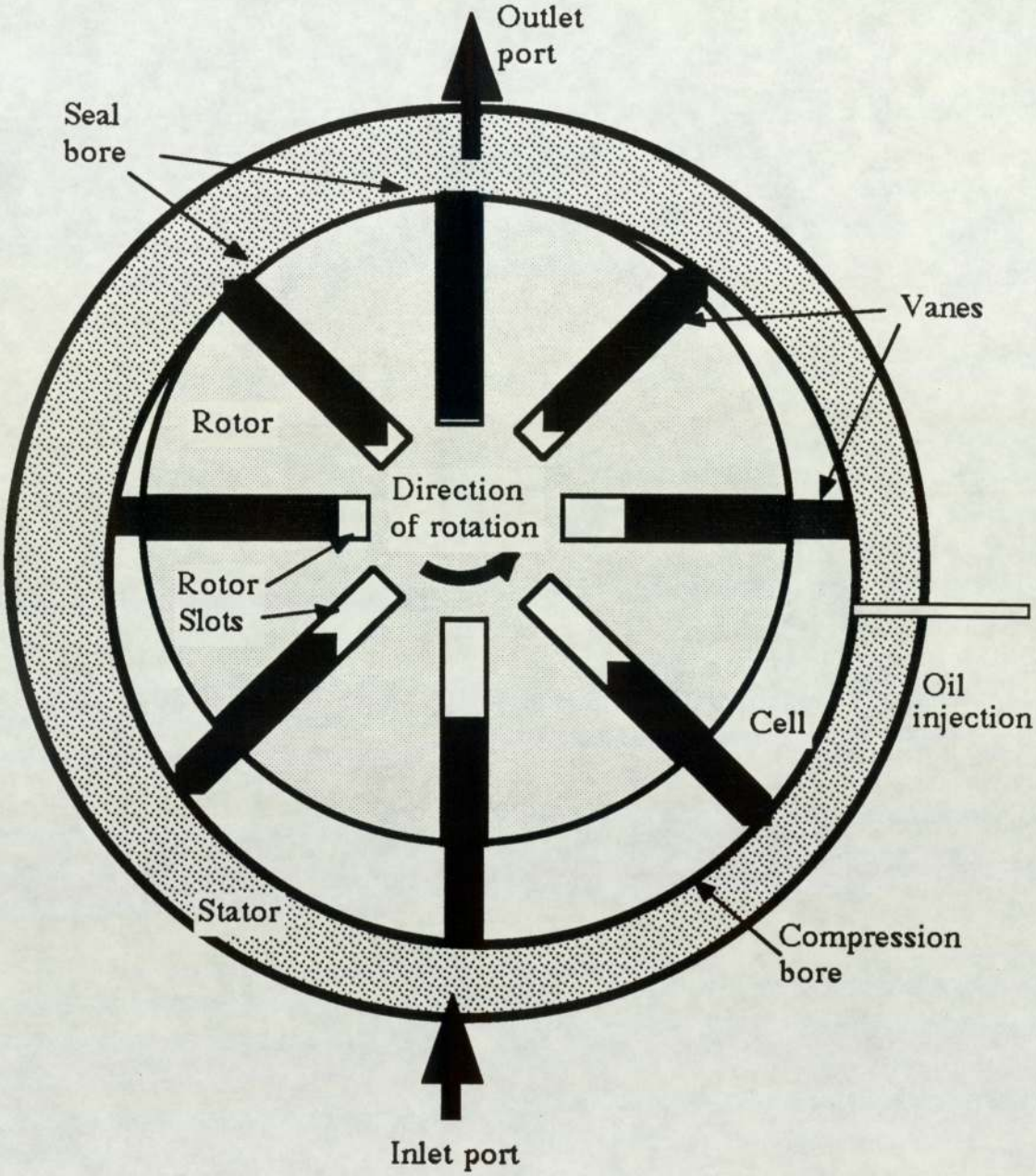

Figure B.1 General arrangement of rotor and stator

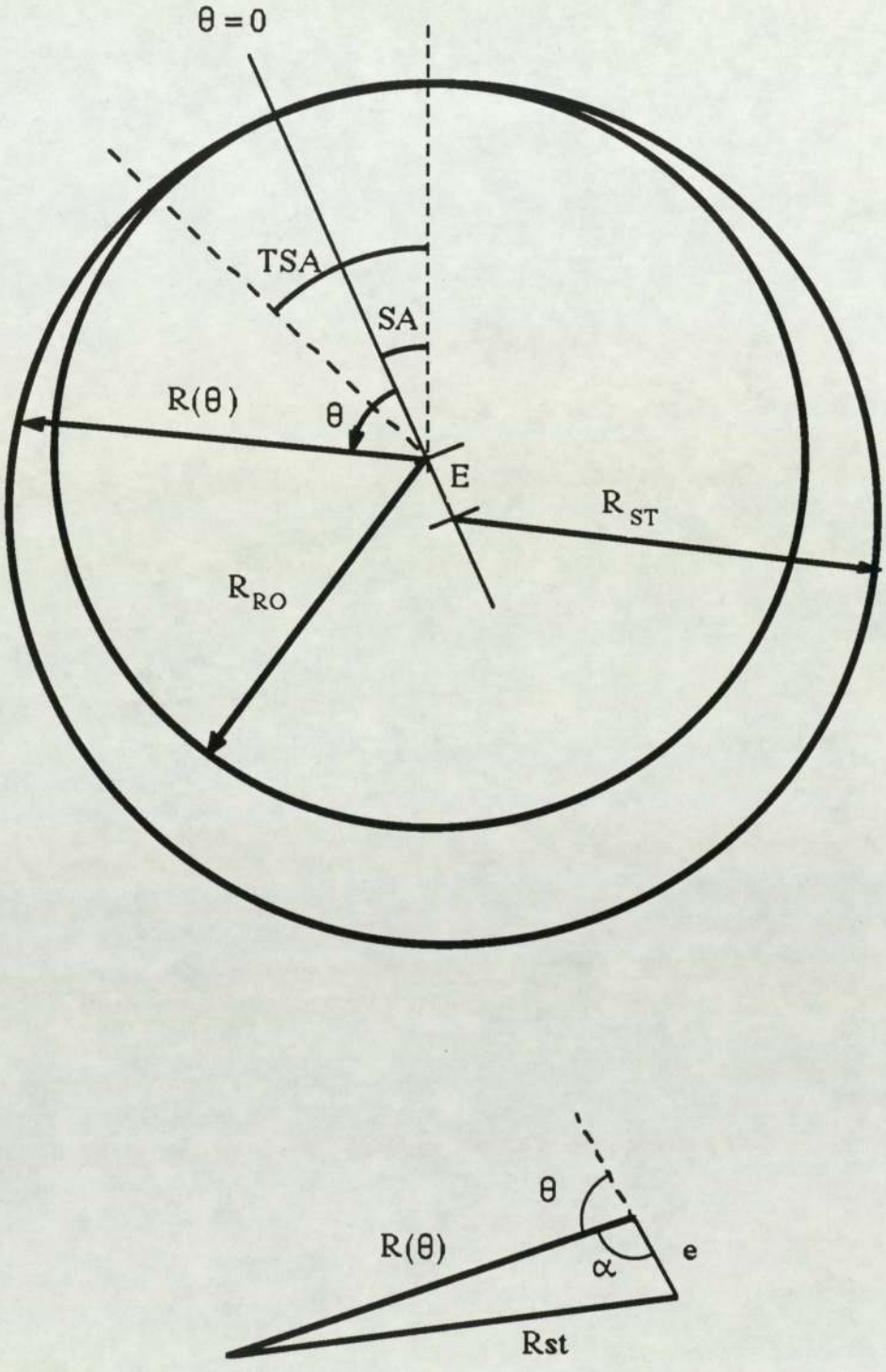

Figure B.2 Compressor geometry

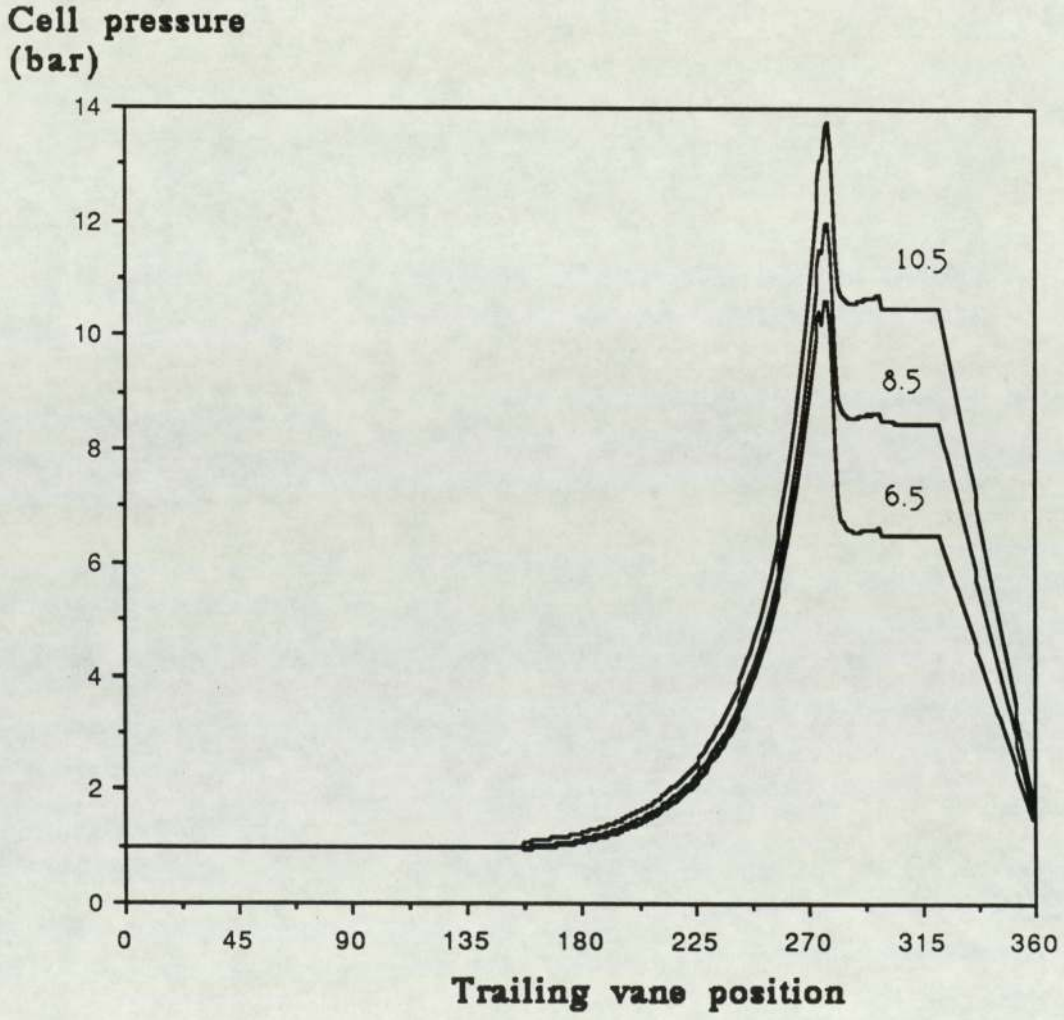

Figure B.3 Cell pressure against trailing vane position for three discharge pressure

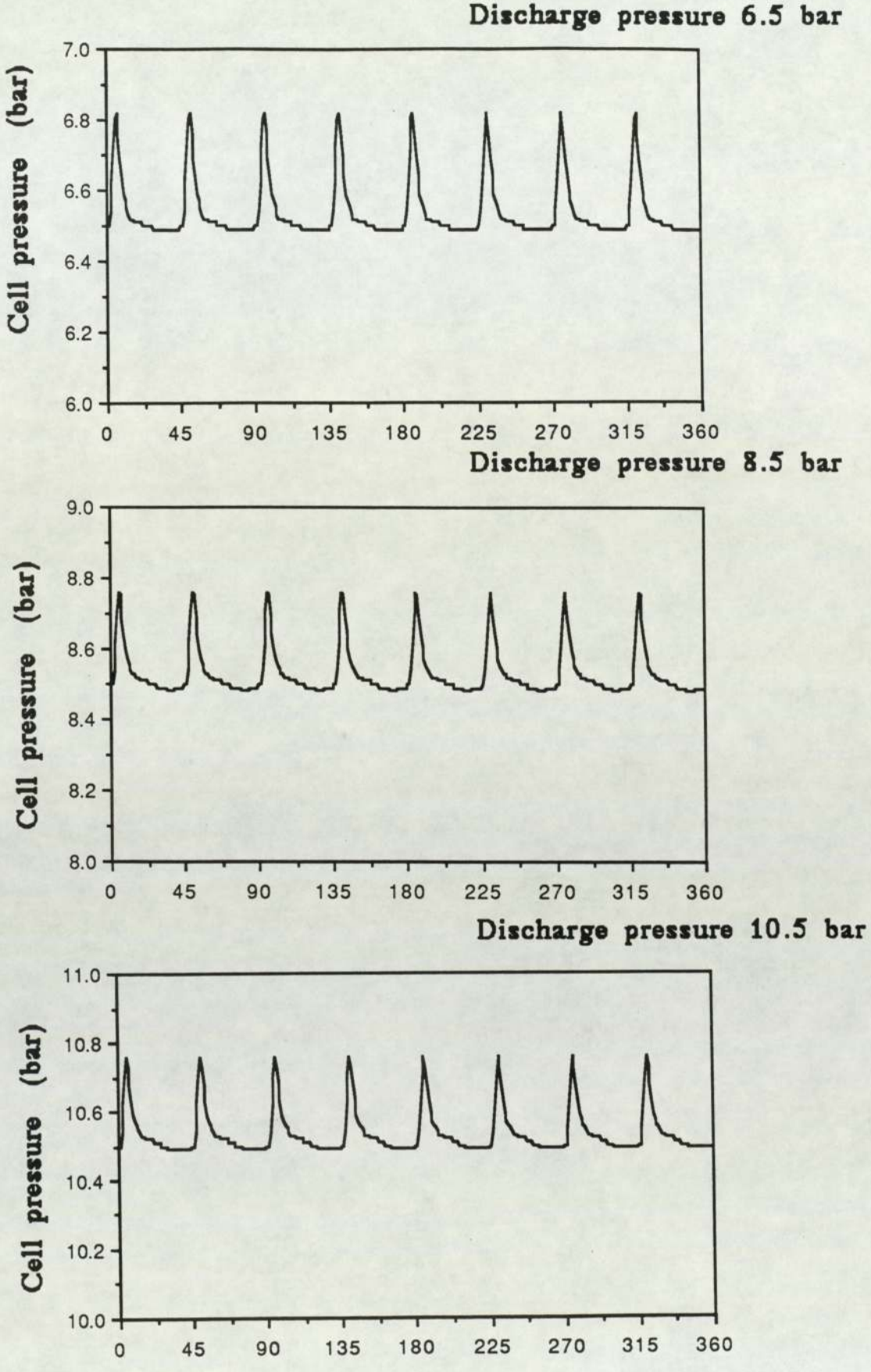

Figure B.4 Manifold pressure fluctuations over one rotor revolution for three discharge pressures

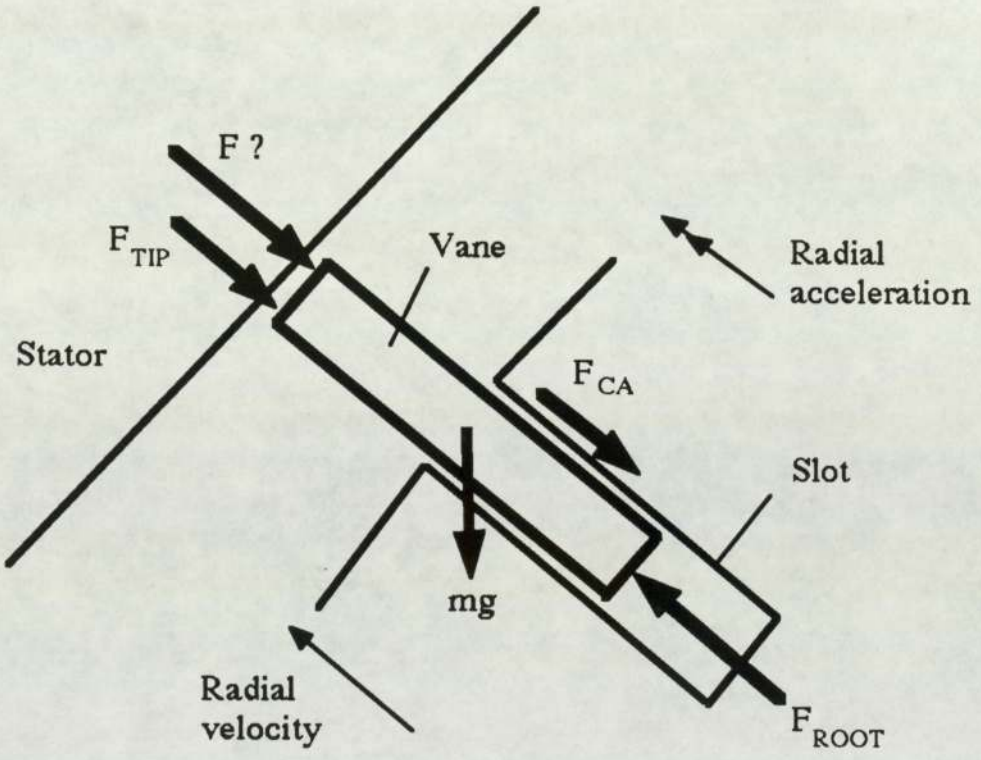

Figure B.5 Free body diagram showing vane forces

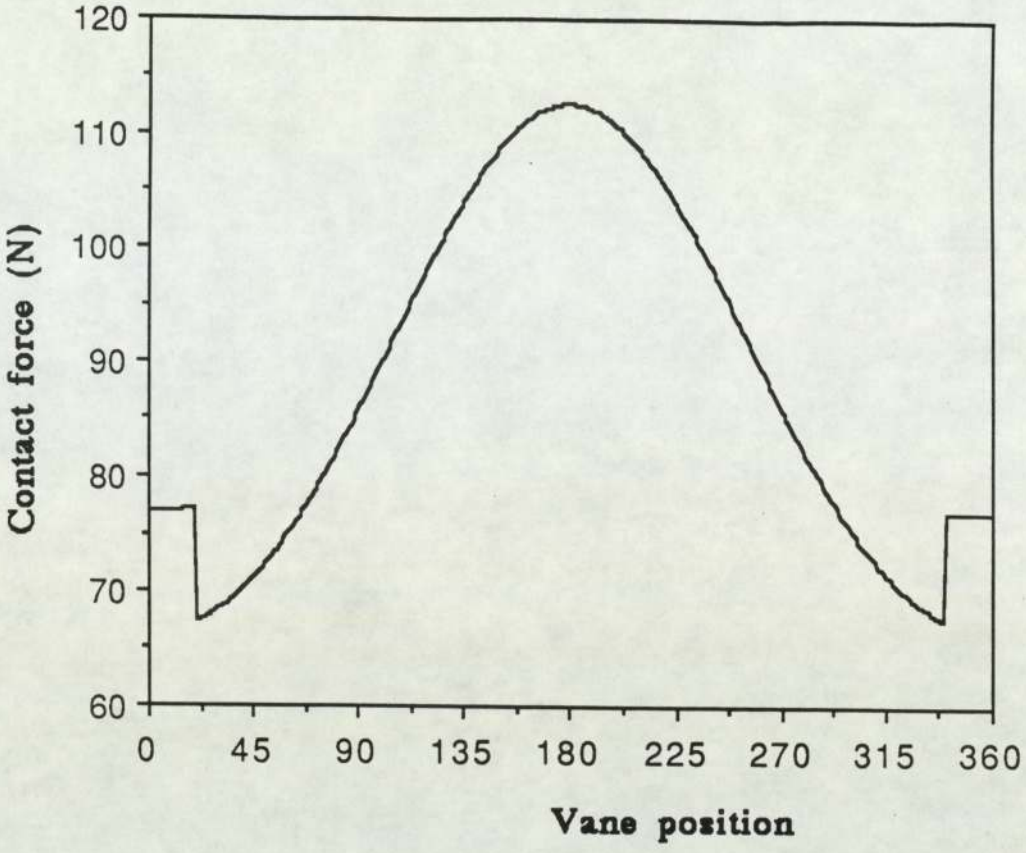

Figure B.6 Contact force against vane position (no pressure)

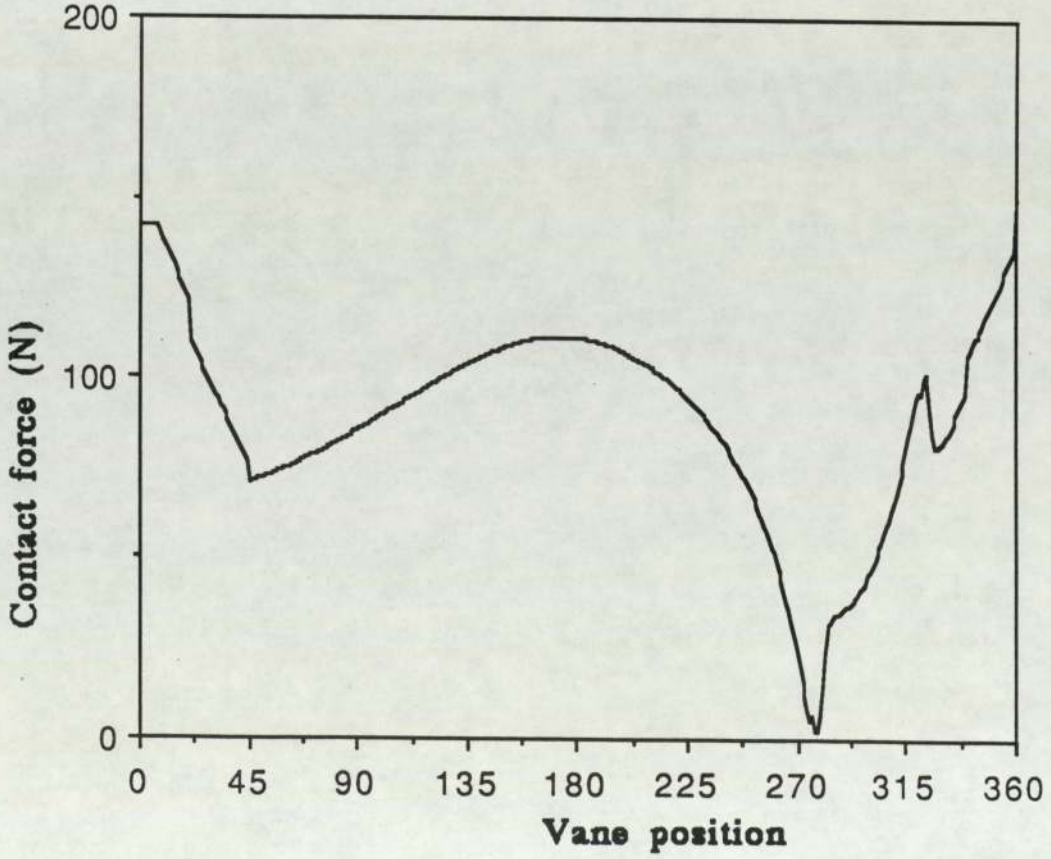

Figure B.7 Contact force against vane position (8.5 bar)